



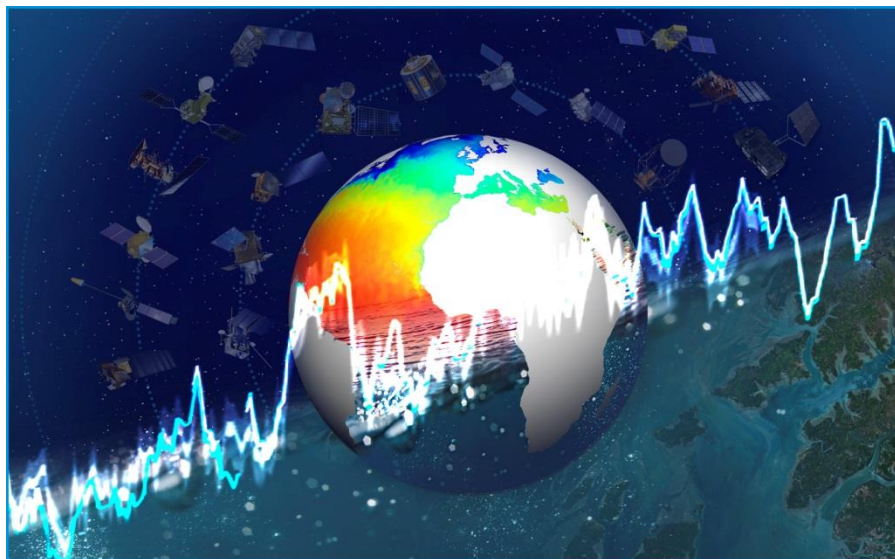
PROCEEDINGS OF THE GHRSSST XVI SCIENCE TEAM MEETING

ESA/ESTEC, Noordwijk, Netherlands
20th – 24th July 2015

ISSN 2049–2529

Issue 1.0

Edited by: The GHRSSST Project Office



Meeting hosted and sponsored by:



Copyright 2015© GHRSSST

This copyright notice applies only to the overall collection of papers: authors retain their individual rights and should be contacted directly for permission to use their material separately. Editorial correspondence and requests for permission to publish, reproduce or translate this publication in part or in whole should be addressed to the GHRSSST Project Office. The papers included comprise the proceedings of the meeting and reflect the authors' opinions and are published as presented. Their inclusion in this publication does not necessarily constitute endorsement by GHRSSST or the co-organisers.



GHRSSST International Project Office

Gary Corlett, Project Coordinator
gpc@ghrsst.org

Silvia Bragaglia-Pike, Project Administrator
gpa@ghrsst.org

www.ghrsst.org

Table of Contents

SECTION 1: AGENDA.....	6
MONDAY	7
TUESDAY	10
WEDNESDAY	11
THURSDAY	12
FRIDAY	14
SECTION 2: PLENARY SESSIONS SUMMARY REPORTS	16
PLENARY SESSION II: REVIEW OF ACTIVITIES I.....	17
SESSION REPORT.....	17
GHRSSST SYSTEM COMPONENTS: LTSRF.....	20
GHRSSST SYSTEM COMPONENTS: NOAA SQUAM AND IQUAM.....	25
GHRSSST SYSTEM COMPONENTS: RDAC UPDATE: CANADIAN METEOROLOGICAL CENTER.....	31
GHRSSST SYSTEM COMPONENTS: EUMETSAT REPORT FOR GHRSSST	34
GHRSSST SYSTEM COMPONENTS: EUMETSAT OSI SAF	37
REPORT TO GHRSSST XVI FROM JAXA	39
PLENARY SESSION II – REVIEW OF ACTIVITIES II	44
SESSION REPORT.....	44
RDAC UPDATE: JMA	48
RDAC UPDATE: UK MET OFFICE	52
ACSPO SST PRODUCTS AT NOAA: UPDATE FOR GHRSSST-XVI	55
NOAA NATIONAL CENTERS FOR ENVIRONMENTAL INFORMATION (NCEI) RDAC	59
PLENARY SESSION III: SPECIAL SESSION ON PASSIVE MICROWAVE SSTS	61
RECENT CAL/VAL UPDATES OF THE GCOM-W/AMSR2.....	61
OPTIMAL ESTIMATION OF SEA SURFACE TEMPERATURE FROM AMSR2	68
COMPARISON OF AMSR2 SEA SURFACE TEMPERATURE RETRIEVALS WITH IN-SITU DATA	74
PLENARY SESSION IV: NEW HORIZONS	81
SESSION REPORT.....	81
SEA SURFACE TEMPERATURE RETRIEVALS FROM INSAT-3D: INITIAL RESULTS AND VALIDATION.....	85
SEA SURFACE TEMPERATURE RETREIVAL FROM HIMAWARI-8.....	95
SEA SURFACE TEMPERATURE ESTIMATION IN UPWELLING AREA: ISSUES AND STRATEGIES	99
PLENARY SESSION V: DIURNAL VARIABILITY	103
AN ANALYSIS SYSTEM FOR DIURNAL SEA SURFACE TEMPERATURE	103
A FACILITY FOR NEAR-REAL TIME ESTIMATION AND EVALUATION OF DIURNAL WARMING.....	108
PLENARY SESSION VI: UNCERTAINTIES IN L2P PRODUCTS	114
SESSION REPORT.....	114
ROLES OF L2 SSES IN A L4 PRODUCTION CASE	118
REDESIGNED SINGLE SENSOR ERROR STATISTICS IN THE ADVANCED CLEAR-SKY PROCESSOR FOR OCEANS.....	121
MODELLED SST UNCERTAINTIES VS EMPIRICAL SSES	127

PLENARY SESSION VII: APPLICATIONS.....	131
SOLAR WARMING OF SOUTH CENTRAL AND NORTH WEST PACIFIC.....	131
PLENARY SESSION VIII: L4 ANALYSIS	135
THE NEW HIGH-RESOLUTION, OPTIMALLY INTERPOLATED SST DATASET (1982-2012) FOR THE MEDITERRANEAN SEA	135
ASSIMILATING RETRIEVALS OF SEA SURFACE TEMPERATURE FROM VIIRS AND AMSR2 IN THE EXPERIMENTAL HIGH RESOLUTION CMC SST ANALYSIS.....	140
SECTION 3: BREAKOUT SESSION REPORTS	147
BREAKOUT SESSION REPORTS	148
THE APPLICATIONS AND USER SUPPORT TECHNICAL ADVISORY GROUP (AUS-TAG) BREAKOUT MEETING REPORT	148
THE CLIMATE DATA RECORDS TECHNICAL ADVISORY GROUP (CDR-TAG) BREAKOUT MEETING REPORT..	151
RESCUE & REPROCESSING OF HISTORICAL AVHRR ARCHIVES WORKING GROUP (R2HA2-WG) BREAKOUT MEETING REPORT	154
THE ESTIMATION AND RETRIEVALS WORKING GROUP (EARWIG) BREAKOUT MEETING REPORT.....	156
THE SATELLITE SEA SURFACE TEMPERATURE VALIDATION GROUP (ST-VAL) BREAKOUT MEETING REPORT	159
SECTION 4: POSTERS AND POSTER ABSTRACTS.....	169
POSTERS	170
POSTER 1: IMPROVING APPLICATION OF DATA QUALITY INFORMATION IN ACCESSING AND USING SATELLITE DATA	170
POSTER 2: FORECAST OF SST: CALIBRATION OF OCEAN FORCING WITH SATELLITE FLUX ESTIMATES (COFFEE)	171
POSTER 3: IMOS AVHRR SST PRODUCTS SUITABLE FOR NEAR-COASTAL APPLICATIONS.....	172
POSTER 4: CLOUD DETECTION FOR SEA SURFACE TEMPERATURE FROM GLOBAL AREA COVERAGE PRODUCTS	173
POSTER 5: VALIDATION OF SATELLITE-DERIVED LAKE SURFACE TEMPERATURE	174
POSTER 6: VALIDATION OF SST AGAINST <i>IN SITU</i> DATA: EFFECT OF SPACE-TIME COLLOCATION CRITERIA	175
POSTER 7: SST CCI STATUS AND PROGRESS.....	176
POSTER 8: UNCERTAINTIES IN VALIDATION OF SST ANALYSES USING NEAR-SURFACE ARGO OBSERVATIONS.....	177
POSTER 9: FIDUCIAL REFERENCE MEASUREMENTS FOR CEOS (FRM4CEOS).....	178
POSTER 11: PATTERN RECOGNITION ENHANCEMENTS TO CLEAR SKY MASK FOR VIIRS SST.....	179
POSTER 14: IMPLICATIONS OF DIURNAL WARMING EVENTS ON ATMOSPHERIC MODELLING	180
POSTER 15: VALIDATION, ERROR ANALYSIS AND THE EFFECT OF CLOUD CONTAMINATION ON THE QUALITY OF VIIRS SST RETRIEVALS FOR VARIOUS ALGORITHMS	181
POSTER 16: EFFECTS OF LOW-FREQUENCY FRONTAL SCALE SEA SURFACE TEMPERATURE ON OCEAN- ATMOSPHERE COUPLING	182
POSTER 17: THE UNCERTAIN HIGH LATITUDE SST SAMPLING ERRORS AND THE REDUCED ERRORS IN SST SEASONAL ANOMALY	183
POSTER 18: VALIDATION OF MET OFFICE OSTIA DIURNAL ANALYSIS USING ARGO FLOATS.....	184
POSTER 20: BIAS AWARENESS IN OPTIMAL ESTIMATION OF SEA SURFACE TEMPERATURE	185

POSTER 21: INFRARED RADIOMETERS ON SHIPS OF OPPORTUNITY FOR SATELLITE-DERIVED SEA-SURFACE TEMPERATURE VALIDATION	186
POSTER 22: AN UPDATE ON MODIS AND VIIRS SEA-SURFACE TEMPERATURES	187
POSTER 23: FIDELITY AND UNCERTAINTY IN CLIMATE DATA RECORDS FROM EARTH OBSERVATION: THE FIDUCEO PROJECT.....	188
POSTER 25: SST USER WORKSHOP ON UNCERTAINTIES.....	189
POSTER 27: PREPARING OSI-SAF SEVIRI/MSG SST REPROCESSING 2004-2012.....	190
POSTER 28: EXPERIENCES WITH SENTINEL-3 OPTICAL SENSOR PRODUCTS.....	191
POSTER 29: UPWELLING CHARACTERISTICS FROM SST GRADIENTS IN THE PERU/CHILE COASTAL SYSTEM	192
POSTER 30: THE IMPACT OF THE OCEAN THERMAL SKIN LAYER ON AIR-SEA INTERFACIAL HEAT FLUXES .	193
POSTER 31: INVESTIGATING SEA SURFACE TEMPERATURE DIURNAL VARIATION OVER THE TROPICAL WARM POOL USING MTSAT-1R.....	194
POSTER 32: IN SITU SST QUALITY MONITOR VERSION2 (IQAM2).....	195
POSTER ABSTRACTS	196
POSTER 2: FORECAST OF SST: CALIBRATION OF OCEAN FORCING WITH SATELLITE FLUX ESTIMATES (COFFEE)	196
POSTER 17: THE UNCERTAIN HIGH LATITUDE SST SAMPLING ERRORS AND THE REDUCED ERRORS IN SST SEASONAL ANOMALY	202
POSTER 20: BIAS AWARENESS IN OPTIMAL ESTIMATION OF SEA SURFACE TEMPERATURE	205
POSTER 29: UPWELLING CHARACTERISTICS FROM SST GRADIENTS IN THE PERU/CHILE COASTAL SYSTEM	208
POSTER 30: THE IMPACT OF THE OCEAN THERMAL SKIN LAYER ON AIR-SEA INTERFACIAL HEAT FLUXES .	211
POSTER 31: INVESTIGATING SEA SURFACE TEMPERATURE DIURNAL VARIATION OVER THE TROPICAL WARM POOL USING MTSAT-1R.....	215
SECTION 5: APPENDICES.....	219
APPENDIX 1 – LIST OF PARTICIPANTS	220
APPENDIX 2 –PARTICIPANTS PHOTO	223
APPENDIX 3 – SCIENCE TEAM 2015/16.....	224

SECTION 1: AGENDA

MONDAY

Monday, 20th July 2015		
<u>Plenary Session I: Introduction</u>		
<u>Chair: Peter Minnett Rapporteur: Gary Corlett</u>		
09:00-10:30	Welcome and introductory talks	
09:00-09:05	<i>Welcome to GHRSSST XVI</i>	<i>Peter Minnett</i>
09:05-09:20	<i>Welcome address from ESA</i>	<i>Maurice Borgeaud</i>
09:20-09:30	<i>Overview of GHRSSST</i>	<i>Peter Minnett</i>
09:30-09:55	<i>SST, instrument development and applications at ESA</i>	<i>Craig Donlon</i>
09:55-10:05	<i>The sentinel 3 mission: mission management</i>	<i>Susanne Mecklenburg</i>
10:05-10:20	<i>SLSTR data and marine operations</i>	<i>Anne O'Carroll</i>
10:20-10:30	<i>Plans for the week ahead</i>	<i>Gary Corlett</i>
Tea/Coffee Break		
<u>Plenary Session II: Review of activities since G-XV (Part 1)</u>		
<u>Chair: Andy Harris Rapporteur: Owen Embury</u>		
11:00-11:10	<i>GHRSSST Connection with CEOS: SST-VC</i>	<i>Anne O'Carroll</i>
11:10-11:20	<i>GHRSSST system Components: GDAC</i>	<i>Ed Armstrong</i>
11:20-11:30	<i>GHRSSST system Components: EU GDAC</i>	<i>Jean-François Piollé</i>
11:30-11:40	<i>GHRSSST system Components: LTSRF</i>	<i>Ken Casey</i>
11:40-11:50	<i>GHRSSST system Components: SQUAM and iQUAM</i>	<i>Alexander Ignatov</i>
11:50-12:00	<i>GHRSSST system Components: Felyx</i>	<i>Jean-François Piollé</i>
12:00-12:10	<i>RDAC Update: ABoM</i>	<i>Helen Beggs</i>
12:10-12:20	<i>RDAC Update: CMEMS</i>	<i>Hervé Roquet</i>

Monday, 20th July 2015		
12:20-12:30	<i>RDAC Update: CMC</i>	<i>Dorina Surcel Colan</i>
12:30-12:40	<i>RDAC Update: EUMETSAT</i>	<i>Anne O'Carroll</i>
12:40-12:50	<i>RDAC Update: EUMETSAT OSI SAF</i>	<i>Stéphane Saux Picart</i>
12:50-13:00	<i>RDAC Update: JAXA</i>	<i>Misako Kachi</i>
Lunch		
<u>Plenary Session II: Review of activities since G-XV (Part 2)</u>		
<u>Chair: Anne O'Carroll Rapporteur: Ioanna Karagali</u>		
14:00-14:10	<i>RDAC Update: JMA</i>	<i>Masakazu Higaki</i>
14:10-14:20	<i>RDAC Update: Met Office</i>	<i>Simon Good</i>
14:20-14:30	<i>RDAC Update: NASA</i>	<i>Jorge Vazquez</i>
14:30-14:40	<i>RDAC Update: NAVO</i>	<i>Keith Willis</i>
14:40-14:50	<i>RDAC Update: NOAA/ACSP0</i>	<i>Alexander Ignatov</i>
14:50-15:00	<i>RDAC Update: NOAA/NESDIS/STAR</i>	<i>Eileen Maturi</i>
15:00-15:10	<i>RDAC Update: NOAA/NCEI</i>	<i>Ken Casey</i>
15:10-15:20	<i>RDAC Update: REMO</i>	<i>Gutemberg França</i>
15:20-15:30	<i>RDAC Update: RSS</i>	<i>Chelle Gentemann</i>
Tea/Coffee Break		
Posters		
1	<i>Improving application of data quality information in accessing and using satellite data</i>	<i>Ed Armstrong</i>
2	<i>Forecast of SST: calibration of ocean forcing with satellite flux estimates (COFFEE)</i>	<i>Charlie Barron</i>
3	<i>IMOS AVHRR SST products suitable for near-coastal applications</i>	<i>Helen Beggs</i>
4	<i>Cloud Detection for sea surface temperature from global area coverage products</i>	<i>Claire Bulgin</i>
5	<i>Validation of Satellite-derived Lake Surface Temperature</i>	<i>Erik Crosman</i>

Monday, 20th July 2015		
6	<i>SST validation: Effect of space-time collocation criteria and determination of product-specific internal errors - SQUAM Demo</i>	<i>Prasanjit Dash</i>
7	<i>SST CCI status and progress</i>	<i>Owen Embury</i>
8	<i>Uncertainties in validation of SST analyses using near-surface Argo observations</i>	<i>Emma Fiedler</i>
9	<i>Fiducial Reference Measurements for CEOS (FRM4CEOS)</i>	<i>Nigel Fox</i>
11	<i>Pattern recognition enhancements to clear sky mask for VIIRS SST</i>	<i>Irina Gladkova</i>
13	<i>Relative error in L4 products and “super-observations” as a function of grid resolution</i>	<i>Alexey Kaplan</i>
14	<i>Implications of diurnal warming events on atmospheric modelling</i>	<i>Ioanna Karagali</i>
15	<i>Validation, error analysis and the effect of cloud contamination on the quality of VIIRS SST retrievals for various algorithms</i>	<i>Prabhat Koner</i>
16	<i>Effects of low-frequency frontal scale sea surface temperature on ocean-atmosphere coupling</i>	<i>Tim Liu</i>
17	<i>The uncertain high latitude SST sampling errors and the reduced errors in SST seasonal anomaly</i>	<i>Yang Liu</i>
18	<i>Validation of met office OSTIA diurnal analysis using Argo floats</i>	<i>Chongyan Mao</i>
19	<i>NOAA/NESDIS Operational GHRSSST Sea Surface Temperature Products</i>	<i>Eileen Maturi</i>
20	<i>Bias awareness in optimal estimation of sea surface temperature</i>	<i>Chris Merchant</i>
21	<i>Infrared radiometers on ships of opportunity for satellite-derived sea-surface temperature validation</i>	<i>Peter Minnett</i>
22	<i>An update on MODIS and VIIRS Sea-surface Temperatures</i>	<i>Peter Minnett</i>
23	<i>Fidelity and Uncertainty in Climate Data Records from Earth Observation: The FIDUCEO project</i>	<i>Jon Mittaz</i>
24	<i>Felyx demo</i>	<i>Jean-François Piollé</i>
25	<i>SST user workshop on uncertainties</i>	<i>Nick Rayner</i>
26	<i>CMEMS OSI TAC progress report</i>	<i>Hervé Roquet</i>
27	<i>Preparing OSI-SAF SEVIRI/MSG SST reprocessing 2004-2012</i>	<i>Stéphane Saux Picart</i>
28	<i>Experiences with Sentinel-3 Optical Sensor Products</i>	<i>Anne O’Carroll</i>
29	<i>Upwelling characteristics from SST gradients in the Peru/Chile coastal system</i>	<i>Jorge Vazquez</i>
30	<i>The impact of the ocean thermal skin layer on air-sea interfacial heat fluxes</i>	<i>Elizabeth Wong</i>
31	<i>Investigating Sea surface temperature diurnal variation over the tropical warm pool using MTSAT-1R</i>	<i>Helen Beggs</i>
32	<i>In situ SST Quality Monitor version2 (iQuam2) iQUAM Demo</i>	<i>Xinjia Zhou</i>
33	<i>Evaluating SST capability to capture coastal thermal features and diurnal warming on the Great Barrier Reef</i>	<i>Xiaofang Zhu</i>

Monday, 20th July 2015

Welcome reception

TUESDAY

Tuesday, 21st July 2015

Plenary Session III: Special session on Passive Microwave SSTs

Chair: Craig Donlon Rapporteur: Tim Nightingale

09:30-10:00	<i>Recent Cal/Val Updates of the GCOM-W/AMSR2</i>	<i>Misako Kachi</i>
10:00-10:30	<i>Optimal Estimation of Sea Surface Temperature FROM AMSR2</i>	<i>Kevin Pearson</i>
10:30-11:00	<i>In situ validation of sea surface temperatures from the GCOM-W1 AMSR2 RSS calibrated brightness temperatures</i>	<i>Chelle Gentemann</i>
Tea/Coffee Break		
11:30-12:00	<i>Comparison of AMSR2 Sea Surface Temperature retrievals with in-situ data</i>	<i>Kevin Pearson/Chelle Gentemann/Misako Kachi</i>
12:00-13:00	<i>Open discussion led by session chair</i>	
Lunch		
<u>Plenary Session IV: New horizons</u>		
<u>Chair: Alexander Ignatov Rapporteur: Prasanjit Dash</u>		
14:00-14:20	<i>Sea surface temperature retrievals from INSAT-3D: Initial results</i>	<i>Rishi Kumar Gangwar</i>
14:20-14:40	<i>SST retrieval from HIMAWARI-8</i>	<i>Yukio Kurihara</i>
14:40-15:00	<i>SST estimation in upwelling area: issues and strategies</i>	<i>Gutemberg França</i>
15:00-15:30	<i>Open discussion led by session chair</i>	
Tea/Coffee Break		
<u>Plenary Session V: Diurnal Variability</u>		
<u>Chair : Carol Anne Clayson Rapporteur: Sandra Castro</u>		
16:00-16:20	<i>SST diurnal cycle and heat budget estimates in the Mediterranean Sea</i>	<i>Salvatore Marullo</i>
16:20-16:40	<i>New analysis system for diurnal Sea Surface Temperature</i>	<i>James While</i>
16:40-17:00	<i>A facility for near-real time estimation and evaluation of diurnal warming</i>	<i>Gary Wick</i>

Tuesday, 21st July 2015

17:00-17:30	<i>Open discussion led by session chair</i>
-------------	---

WEDNESDAY

Wednesday, 22nd July 2015

Plenary Session VI: Uncertainties in L2P products

Chair: Helen Beggs Rapporteur: Werenfrid Wimmer

08:30-08:50	<i>Roles of L2 SSES in a L4 production case</i>	<i>Mike Chin</i>
08:50-09:10	<i>Redesigned SSES for ACSPO SST</i>	<i>Boris Petrenko</i>
09:10-09:30	<i>Modelled SST Uncertainties vs. Empirical SSES</i>	<i>Claire Bulgin</i>
09:30-10:00	<i>Open discussion led by session chair</i>	

Tea/Coffee Break

Plenary Session VII: Applications

Chair: Peter Cornillon Rapporteur: Gary Corlett

10:30-10:50	<i>SST developments needed in support of climate services</i>	<i>Nick Rayner</i>
10:50-11:10	<i>Solar warming of south central Pacific</i>	<i>Tim Liu</i>
11:10-11:30	<i>Northeast Pacific SST anomaly</i>	<i>Chelle Gentemann</i>
11:30-12:00	<i>Open discussion led by session chair</i>	

Lunch

Afternoon Team Building

GHR SST Dinner

THURSDAY

Thursday, 23rd July 2015

GHRSSST Parallel Breakouts for TAGs/WGs

08:30-10:30	DVWG	CDRTAG
<p>Discussion of the following items:</p> <ul style="list-style-type: none"> • <i>Future DVWG workshop</i> • <i>Comparison of models with data sets with a focus on their ability to reproduce observed diurnal variability.</i> • <i>Comparisons of parameterizations</i> • <i>New Argo possibilities</i> 		<ol style="list-style-type: none"> 1) <i>Vote for new Vice-Chair</i> 2) <i>Review International Project Status slides</i> 3) <i>Talk by Helen Beggs on "23 year data record from IMOS AVHRR SST HRPT data"</i> 4) <i>Talk by Eileen Maturi on "NOAA/NESDIS/STAR Reprocessing 5km Sea Surface Temperature Analysis"</i> 5) <i>Presentation by me on Uncertainties in CDR products and where the CDR-TAG may go in the future</i> 6) <i>Discussion</i>
Tea/Coffee Break		
11:00-13:00	STVAL	AUSTAG
<ol style="list-style-type: none"> 1) <i>Overview of ST-VAL activities since GHRSSST-XV (10 mins)</i> 2) <i>Action arising from 2014 ST-VAL Meeting: Where to host the ship-borne radiometer L21 data? (5 mins)</i> 3) <i>Discuss issues relating to satellite SST validation (20 mins)</i> 4) <i>Discuss SSES and Quality Level methodologies (60 mins)</i> <p>Some outcomes from the G15 STVAL session were:</p> <ul style="list-style-type: none"> • <i>SSES and QL need to be de-coupled</i> • <i>QL should be more continuous rather than a step function</i> <p>Open Questions:</p> <ol style="list-style-type: none"> <i>How should Quality Level be defined?</i> <i>How to create consistency in QL across different sensors?</i> <i>How to create continuous uncertainties across QL?</i> <i>How to incorporate "Modelled Uncertainties" per pixel?</i> <i>Do we still need SSES if we have Modelled Uncertainties?</i> <i>Other questions ...</i> <i>Next steps.</i> <p>5) <i>Terms of Reference of ST-VAL Technical Advisory Group (10 mins).</i></p>		<ol style="list-style-type: none"> 1) <i>Terms of reference (overall direction of AUS TAG): Jorge Vazquez facilitating discussion</i> 2) <i>Presentation of new web site and discussion: Gary Corlett and all participating in discussion</i> 3) <i>Discussion on</i> <ol style="list-style-type: none"> <i>user survey discussion;</i> <i>quick start guide</i> 4) <i>Discussion on identifying any gaps (knowledge gap, e.g., not knowing what is desired (user comes in with no knowledge of SST. How well do we know what products users want? Current search capabilities don't really account for such a user; communication gap, e.g., not providing clear instructions on which products to choose, delivery gap, e.g., data interruptions): Prasanjit Dash</i> 5) <i>User support (roles of GDAC and LTSRF): Jorge Vazquez/Ken Casey</i> 6) <i>Review of trends of user statistics: Jorge Vazquez</i> 7) <i>Future of AUS-TAG membership. Jorge and Prash</i>
Lunch		

Thursday, 23 rd July 2015		
14:00-16:00	EaRWiG	DASTAG
		<ul style="list-style-type: none"> • <i>NOAA Big Data Partnership with Amazon, Google, Microsoft, IBM, and the Open Cloud Consortium., Ken Casey, NODC</i> • <i>New technology development and infusion at the JPL PO.DAAC, Edward Armstrong, Thomas Huang, Vardis Tsontos. NASA JPL</i> <p><i>Working with increasingly larger oceanographic data and datasets presents some unique challenges as well as opportunities to improve the user experience and productivity. We will review current technology efforts at the NASA Jet Propulsion Lab that address the topics of :</i></p> <ul style="list-style-type: none"> • <i>On demand data processing, mining, visualization and data interrogation</i> • <i>Data quality screening service</i> • <i>Improved data discovery and search relevancy</i> • <i>Satellite to in situ data matchup services.</i> <p><i>Many of these efforts are directly using and targeting GHRSSST data and some sample uses cases will be presented.</i></p> <ul style="list-style-type: none"> • <i>initiatives for virtual research platforms in Europe, usage of big data technologies (hadoop, spark) at Ifremer, JF Piollé - IFREMER</i> <p><i>Other points of discussion :</i></p> <ul style="list-style-type: none"> • <i>DOIs: how should we use them in GHRSSST, who is responsible for attributing a DOI?</i> • <i>GHRSSST GDACs/RDACs model in coming years, Ken's proposal for a new GHRSSST R/GTS framework</i> • <i>I am leaving out L2i format discussion as it is addressed in ST-VAL and both sessions are not in conflict in the agenda</i>
Tea/Coffee Break		
16:30-18:30	ICTAG	R2HA2
	<ul style="list-style-type: none"> • <i>16:30-16:50: Updates</i> • <i>16:50-17:40: Discussion "Impact of SSES on L4 SST Products"</i> 	

Thursday, 23rd July 2015

<ul style="list-style-type: none"> • Including reserved contributions (≤ 5 min & ≤ 2 slides each, no movies) from: <ul style="list-style-type: none"> ▪ Nick Rayner, ▪ Emma Fiedler, ▪ Mike Chin, ▪ Boris Petrenko • 17:40-18:10: Discussion "L4 SST Error in Coastal Zones" • Including a kick-off contribution by <ul style="list-style-type: none"> ▪ Gutemberg França • 18:10-18:30: General discussion and plans for the next year 	
--	--

FRIDAY

Friday, 24th July 2015

<p><u>Plenary Session VIII: L4 analysis</u> <u>Chair: Alexey Kaplan Rapporteur: Mike Chin</u></p>		
08:30-08:50	<i>The new high-resolution, optimally interpolated SST dataset (1982-2012) for the Mediterranean Sea</i>	<i>Andrea Pisano</i>
08:50-09:10	<i>Assimilating retrievals of sea surface temperature from VIIRS and AMSR2 in the experimental high resolution CMC SST analysis</i>	<i>Dorina Surcel Colon</i>
09:10-09:30	<i>Open discussion led by session chair</i>	
<p><u>Closing Session</u> <u>Chair: Peter Minnett Rapporteur: Gary Corlett</u></p>		
09:30-10:00	<i>Future activities of GHRSSST</i>	<i>Gary Corlett</i>
Tea/Coffee Break		
10:30-10:45	<i>Report from Advisory Council</i>	<i>Craig Donlon</i>
10:40-11:30	Summary of breakout groups	
1	<i>AUS-TAG</i>	<i>Jorge Vazquez</i>
2	<i>CDR-TAG</i>	<i>Jon Mittaz</i>
3	<i>DAS-TAG</i>	<i>Jean-François Piollé</i>
4	<i>DVWG</i>	<i>Carol-Anne Clayson</i>
5	<i>R2HA2</i>	<i>Hervé Roquet</i>
6	<i>EaRWiG</i>	<i>Andy Harris</i>

Friday, 24th July 2015		
7	<i>IC-TAG</i>	<i>Alexey Kaplan</i>
8	<i>ST-VAL</i>	<i>Helen Beggs</i>
11:30- 12:15	<i>Review of action items</i>	
12:15- 12:45	<i>Identification of priorities for following 12 months</i>	
12:45- 13:00	<i>Wrap-up/closing remarks</i>	
Close of GHRSSST XVI		

SECTION 2: PLENARY SESSIONS SUMMARY REPORTS

PLENARY SESSION II: REVIEW OF ACTIVITIES I

SESSION REPORT

Chair: Andy Harris⁽¹⁾, Rapporteur: Owen Embury⁽²⁾

(1) University of Maryland, College Park, MD, U.S.A., Email: andy.harris@noaa.gov

(2) University of Reading, UK, Email: o.embury@reading.ac.uk

ABSTRACT

The second plenary session of the 16th GHRSSST Science Team Meeting covered the review of GHRSSST activities since the previous Science Team Meeting. This report provides a brief overview of the 12 presentations given by the various agencies and organizations. Two of the common themes across many talks were the use of DOIs for datasets and move towards providing uncertainty information rather than SSES.

1. Schedule

The list of presentations and speakers is shown below in Table 1.

Presentation	Speaker
GHRSSST Connection with CEOS: SST-VC	Anne O'Carroll
GHRSSST system Components: GDAC	Ed Armstrong
GHRSSST system Components: EU GDAC	Jean-François Piollé
GHRSSST system Components: LTSRF	Ken Casey
GHRSSST system Components: SQUAM and iQUAM	Alexander Ignatov
GHRSSST system Components: Felyx	Jean-François Piollé
RDAC Update: ABoM	Helen Beggs
RDAC Update: CMEMS	Hervé Roquet
RDAC Update: CMC	Dorina Surcel Colan
RDAC Update: EUMETSAT	Anne O'Carroll
RDAC Update: EUMETSAT OSI SAF	Stéphane Saux Picart
RDAC Update: JAXA	Misako Kachi

Table 1: The schedule of presentations and speakers during the Monday morning plenary session.

2. Summary of Presentations

2.1. CEOS: SST-VC, Anne O'Carroll

O'Carroll summarized the activities of the SST Virtual Constellations which facilitates interactions between the international SST community, GHRSSST and the coalition of national space agencies Committee on Earth Observing Satellites (CEOS).

2.2. GDAC, Ed Armstrong

Armstrong presented the report from the Global Data Assembly Centre (GDAC). 28 new GDS2.0 datasets have been added and FTP continues to be the most popular data access mechanism. The GDAC has developed a Metadata Compliance Checker (MCC) which performs granule levels metadata checks to ensure all products conform to the relevant standards (CF, ACDD, GDS2.0, *etc.*). Issues for consideration include improving dataset lifecycle quality descriptions and dataset provider documentation such as ATBDs.

2.3. EU GDAC, Jean-François Piollé

Piollé presented the EU-GDAC report which covered the products collected at the EU-GDAC (primarily OSI SAF, MyOcean, and Medspiration products), communication and collaboration between the US-GDAC and EU-GDACs. Two tools discussed were a Python based tools for Data search and access (Naiad) and Felyx. Issues raised were the difficulty in tracking down the usage of data – particularly when the dataset does not have an associated scientific publication. The use of DOIs for datasets could improve this.

2.4. LTSRF, Ken Casey

Casey presented the status of the Long Term Stewardship and Reanalysis Facility (LTSRF) that is now operated by the National Centers for Environmental Information (NCEI), which replaces the former individual NOAA Data Centers. The LTSRF dataset list is now dynamically generated from the metadata of archived datasets so it is always up-to-date, and the LTSRF has the ability to mint DOIs for hosted datasets. Work on Pathfinder v5.3 continues with numerous improvements over v5.2. Processing is now done in the cloud using Amazon Web Services (AWS).

2.5. SQUAM and iQUAM, Alexander Ignatov

Ignatov presented reports on the SST Quality Monitor (SQUAM) and *in situ* SST Quality Monitor (iQUAM). In order to add new SST products into SQUAM they are considering retiring older products which are not actively used. The iQUAM system is now using a netCDF4 format based on the “GDS2i” proposal made at the last science meeting.

2.6. Felyx, Jean-François Piollé

Piollé presented the current development status of the Felyx system. It is now in demonstration and testing phase, with a full public release expected in early 2016.

2.7. ABoM, Helen Beggs

Beggs presented news from the Australian Bureau of Meteorology (BoM) RDAC. IMOS/BoM have now processed their Australian and Antarctic region HRPT AVHRR SST archive back to 1992 and validated against IMOS data. Other BoM work includes ingestion of JAXA AMSR-2 SST into the BoM L4 analyses, further IMOS ships of opportunity, and preparation for Himawari-8 SSTs.

2.8. CMEMS, Hervé Roquet

Roquet presented the Copernicus Marine Environment Monitoring Service (CMEMS) a new European Commission core service. The OSI TAC contract for satellite SST was awarded to the same consortium as MyOcean. CMEMS satellite SST products include global and regional NRT multi-sensor L3/L4, with a focus on high-resolution products. Issues raised were the NRT access mechanisms that GDAC/PODAAC cannot provide; instead users should get NRT data directly from the data provider (NOAA/NASA). Secondly the issues of Single Sensor Error Statistics (SSES) vs uncertainty information, as all OSI TAC L4 producers need reliable uncertainty estimates (ideally separated into uncorrelated and correlated components), current SSES standard deviation estimates are not suitable.

2.9. CMC, Dorina Surcel Colan

Colan presented the report from the Canadian Meteorological Centre (CMC) RDAC. The CMC is producing a new higher resolution L4 analyses at 0.1 degree resolution. Future plans include use of CMC 3DVAR ice assimilation for the analysis, and addition of lake surface temperatures.

2.10. EUMETSAT, Anne O'Carroll

O'Carroll presented the news from the EUMETSAT RDAC, this included the recent launch of MSG-4, the imminent launch of Sentinel-3 and future missions. Ongoing work at EUMETSAT includes a 1D-VAR retrieval from IASI which includes uncertainty estimates, and preparation for Sentinel-3 SLSTR SST products.

2.11. EUMETSAT OSI SAF, Stéphane Saux Picart

Saux Picart presented the OSI SAF RDAC report that covered real-time SST products from Metop AVHRR and SEVIRI, and the current SEVIRI reprocessing. Issues raised were the use of DOIs for real-time products and definition of SSES as many users ignore SSES as they are inconsistent between products.

2.12. JAXA, Misako Kachi

Kachi presented the report from JAXA covering: AMSR-E which is now in slow rotation mode (2 rpm) with L1 data available on request; AMSR-2 on board GCOM-W; and Himawari-8. AMSR-E data will be reprocessed using consistent algorithms and output formats to AMSR-2. AMSR-2 includes a new research product based on the 10 GHz channel, this provides higher resolution than the standard 6 GHz products but is much less sensitive to SSTs below ~10 degrees C. Issues raised included the definition of SSES.

GHR SST SYSTEM COMPONENTS: LTSRF

Kenneth S. Casey, Korak Saha, Ajay Krishnan, Yuanjie Li, John Relph, Dexin Zhang, Yongsheng Zhang, and Sheekela Baker-Yeboah⁽¹⁾

(1) NOAA National Centers for Environmental Information, USA, Email: Kenneth.Casey@noaa.gov

ABSTRACT

Since the 15th GHR SST Science Team Meeting, the Long Term Stewardship and Reanalysis Facility (LTSRF) at the NOAA National Centers for Environmental Information (NCEI) has made significant progress in the long-term stewardship of all GHR SST datasets. NCEI is the merger of the previous three separate NOAA National Data Centers. Operational services were maintained and incrementally improved, with better management of multiple versions of GHR SST data products. New services this year include the minting of DOIs for GHR SST products on request, deployment of a dynamic data table, and the real-time ingest and archive of selected products. This report summarizes these accomplishments and provides an overview of NCEI’s contribution to the international SST community.

1. Introduction

The NOAA National Centers for Environmental Information (NCEI) was formed this year as the merger of the three, previously distinct National Climatic Data Center (NCDC), National Geophysical Data Center (NGDC), and National Oceanographic Data Center (NODC). NCEI continues in NODC’s place, providing long-term stewardship for all GHR SST products provided to the Regional Global Task Sharing (R/GTS) Framework, illustrated in in Figure 1.

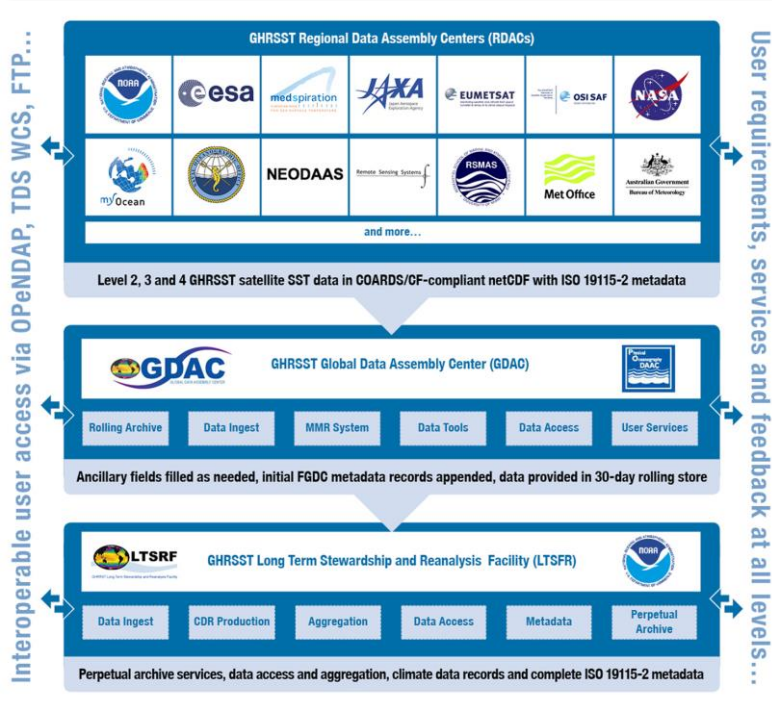


Figure 1: The GHR SST Regional Global Task Sharing Framework.

In addition to providing long-term archival services, the NCEI also serves as a Regional Data Assembly Center (RDAC) for the Pathfinder SST climate data record and the Daily OISST products. Those RDAC activities are reported in a separate extended abstract.

2. Operational Progress Since GHR SST 15

Table 1 summarizes the progress made by the LTSRF since 2007. Each year, as the volume of the archive has grown the number of services available to these data has grown as well. At the time of this report, the NCEI LTSRF is capable of providing all GHR SST products through FTP, HTTP (<http://data.nodc.noaa.gov/ghrsst>), OPeNDAP (<http://data.nodc.noaa.gov/opendap>), and the THREDDS Data Server (TDS). Gridded products are additionally made available through the Live Access Server (LAS, <http://data.nodc.noaa.gov/las>) and a wide range of discovery services are enabled through the NCEI-MD (formerly NODC) Geoportal Server (<http://data.nodc.noaa.gov/geoportal>). MCEI also ensures that GHR SST meets the expectations of the Committee on Earth Observing Satellites (CEOS) by providing both collection and granule level discovery to the CEOS WGISS Integrated Catalog (CWIC) system.

	2007	2008	2009	2010	2011	2012	2013	2014	2015*
Products		22	26	27	40	59	60	62	77
Accessions		39,048	49,957	59,982	67,906	92,282	105,046	112,182	123,325
Files		679,000	993,580	1,352,901	1,662,004	2,459,724	3,290,806	3,971,657	4,894,891
Volumes (TB)		13	20	28	34	57	60	81	92
Services	ftp http	ftp http	ftp http DAP	ftp http DAP WMS WCS	ftp http DAP WMS WCS LAS	ftp http DAP WMS WCS LAS Geoportal	ftp http DAP WMS WCS LAS Geoportal Granules CWIC	ftp http DAP WMS WCS LAS Geoportal Granules CWIC	ftp http DAP WMS WCS LAS Geoportal Granules CWIC

Table 1: Summary of LTSRF progress since 2007. * - data for 2015 are through 17 July 2015.

	2006	2007	2008	2009	2010	2011	2012	2013	2014
Files served per day	85	1130	1734	3413	21,956	14,896	28,807	20,056	21,196
GB served per day	0.2	1.8	3.9	18.8	66.3	115	73	145	156
Users served per day	3	7	8	8	11	19	19	24	36

Table 2: User accesses from the LTSRF.

Table 2 summarizes the user accesses to the GHRSSST LTSRF at NCEI through 2014. Overall growth has been seen every year since the LTSRF began serving GHRSSST data in 2005.

Operational services continued to be maintained and sustained since GHRSSST-15. NCEI continues supporting that seamless linkage between collection and granules, so that once a user discovers a GHRSSST collection, they can jump directly to a granule (or file) level discovery process using a common look and feel interface. The LTSRF also still maintains automated status reporting and provides browse graphics for all ingested data files. Incremental improvements were also made to the LTSRF's ability to seamlessly manage multiple versions of incoming GHRSSST products. As directed by the RDACs, new versions of an existing product are shown first and foremost to users through what is known as a "best copy" directory hierarchy. In those folders, the most recent version of a dataset is always shown. If users truly want an older version they can access that through the NCEI archive systems. In addition, a GDS1-only and a GDS2-only directory hierarchy also exist, for users who specifically want access to only one GDS version. Metadata in the discovery systems reflect when a product line is either GDS1, GDS2, or contains both versions.

3. Dynamic Data Table

In the last year, NCEI implemented a dynamically generated data table that lists all of the archived GHRSSST products and some key information about each. Figure 2 below shows a screenshot of the top of the table.

GHRSSST Products in the LTSRF									
RDAC	Product	Product Level	Start Date	End Date	GDS Version	Grid / Pixel Resolution	Metadata	Access	Disk Volume · Number of Days · Number of Files
ABOM	GAMSSA_28km GLOB	L4	2008-08-24	2015-05-30	1.5	28 km	Details · Granule Search · Live Access Server	FTP · HTTP · OPeNDAP · THREDDS	2.4GB · 2468 days · 2468 files
	RAMSSA_09km AUS	L4	2008-04-01	2015-05-30	1.5	9 km	Details · Granule Search · Live Access Server	FTP · HTTP · OPeNDAP · THREDDS	4.1GB · 2593 days · 2597 files
CMC	CMC0.2deg GLOB	L4	2013-06-27	2015-05-04	2.0	0.2°	Details · Granule Search · Live Access Server	FTP · HTTP · OPeNDAP · THREDDS	0.9GB · 448 days · 448 files
DMI	DMI_OI GLOB	L4	2013-12-11	2015-04-23	2.0	0.05°	Details · Granule Search	FTP · HTTP · OPeNDAP · THREDDS	20.4GB · 123 days · 136 files
	DMI_OI NSEABALTIC	L4	2007-06-04	2015-05-31	1.5	3 km	Details · Granule Search · Live Access Server	FTP · HTTP · OPeNDAP · THREDDS	1.5GB · 2887 days · 2887 files
EUR	AMSRE	L2P	2004-12-19	2007-02-26	1.5	25 km	Details · Granule Search · Live Access Server	FTP · HTTP · OPeNDAP · THREDDS	3.0GB · 744 days · 8995 files
	ATS_NR_2P	L2P	2004-12-30	2009-09-29	1.5	1 km	Details · Granule Search	FTP · HTTP · OPeNDAP · THREDDS	315.4GB · 1643 days · 22303 files

Figure 2: Dynamic data table showing GHRSSST products available at LTSRF and key characteristics.

The table is generated automatically from the product and system metadata, so it always reflects the most accurate information available from the LTSRF.

4. Digital Object Identifiers

In the last year, NCEI also minted its first DOIs for GHRSSST data sets. The LTSRF will mint a DOI for GHRSSST products when requested by the RDAC. An example for OSPO ACSPO VIIRS L2P is doi:10.7289/V5PR7SX5 and the landing page is shown below in Figure 3.

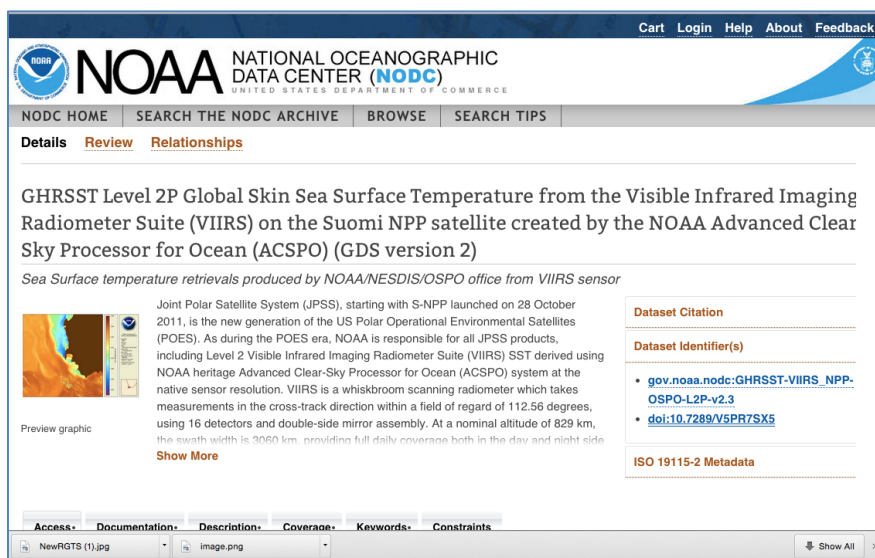


Figure 3: Landing page for OSPO's ACSPO VIIRS L2P product, with its DOI, [doi:10.7289/V5PR7SX5](https://doi.org/10.7289/V5PR7SX5).

5. Real Time Ingest and Archive

To better meet the specific requirements of certain RDACs, NCEI also implemented the capability of archiving data directly from an RDAC or the GDAC in near real time, without the standard 30-day delay imposed by the GDAC interface. In this approach, NCEI archives the data right away, but still performs a check against the GDAC data 30 days after observation to ensure the LTSRF is receiving the best available version of a data set. This system was implemented for the OSPO VIIRS ACSPO L2P product.

6. Conclusion

The period since GHRSSST-15 has been another successful one for the former NODC, now NCEI, LTSRF. In addition to maintaining all operations during the significant merger of the three previously separate NOAA National Data Centers, NCEI was able to improve service delivery to GHRSSST through the provision of a dynamic data table, the minting of DOIs, and the successful operation of a real-time archive ingest for the OSPO ACSPO VIIRS L2P SST product.

GHRSSST SYSTEM COMPONENTS: NOAA SQUAM AND IQUAM

Alexander Ignatov⁽¹⁾, Prasanjit Dash⁽²⁾, Xinjia Zhou⁽³⁾, Feng Xu⁽⁴⁾

(1) NOAA STAR, USA, Email: Alex.Ignatov@noaa.gov

(2) NOAA STAR and CSU CIRA, USA, Email: Prasanjit.Dash@noaa.gov

(3) NOAA STAR and CSU CIRA, Inc, USA, Email: Xinjia.Zhou@noaa.gov

(4) NOAA STAR, Fudan Univ. and GST Inc, USA/China, Email: Feng.Xu@noaa.gov

ABSTRACT

The SST Quality Monitor (SQUAM; www.star.nesdis.noaa.gov/sod/sst/squam/; Dash et al., 2010, 2012) and the *in situ* SST Quality Monitor (*iQuam*; www.star.nesdis.noaa.gov/sod/sst/iquam/; Xu and Ignatov, 2014) are two NOAA online near-real time SST monitoring systems. The SQUAM monitors satellite (L2/3) and analysis (L4) SST products, produced both at NOAA and by partner organizations, and consistently validates them against uniformly quality controlled (QC) *in situ* SSTs produced by *iQuam*. The *iQuam* performs QC of *in situ* data, monitors QCed SSTs online, and serves to NOAA (including SQUAM) as well as external users, for the use in satellite Cal/Val. This abstract summarizes the progress made since GHRSSST-15, and future work.

1. Summary of major developments in SQUAM and *iQuam*

In SQUAM, two previously tested products are now fully implemented (NAVO VIIRS and ARC); two new NOAA ACSP0 products added to testing – operational VIIRS L3U and experimental Himawari-8 AHI L2; ,ore consistent handling of outliers implemented (maps and histograms are now generated with and without outliers); *in situ* Val uniform regenerated for all products and their monthly statistics added; the gridding code optimized; and the previously used RTG replaced with CMC L4 reference, due to improved diagnostic skill.

In *iQuam*, v1 is being upgraded to the v2 (temporary placed at www.star.nesdis.noaa.gov/sod/sst/iquam/v2/, eventually to be moved to the permanent address www.star.nesdis.noaa.gov/sod/sst/iquam/, once testing is complete). The v2 includes several enhancements. First, v2 now covers period from 1981-pr (cf. with 1991-pr in *iQuam*1). The extension was done using ICOADS data. Also, QC in v2 has improved, through adding: the 2nd reference (CMC L4 SST, in addition to the Reynolds L4 previously available in *iQuam*1); individual QFs from external data products (OSI/SAF CMS black list, ICOADS and ARGO floats, etc); and the new “performance history” check (which serves as a more graceful and continuous version of the black list). Four new *in situ* data types were included in v2 (ARGO floats, high-resolution GHRSSST drifters, IMOS ships from Australian BoM, and moored buoys from the NOAA Coral Reef Watch). The web interface has improved, through adding daily statistics, enhancing the web graphics, and redesigning and optimizing the code. Finally, the output format has changed from pervious hdf4 in v1, to NetCDF4 in v2, and now better complies with the GHRSSST data specification version 2, GDS2 for satellite data.

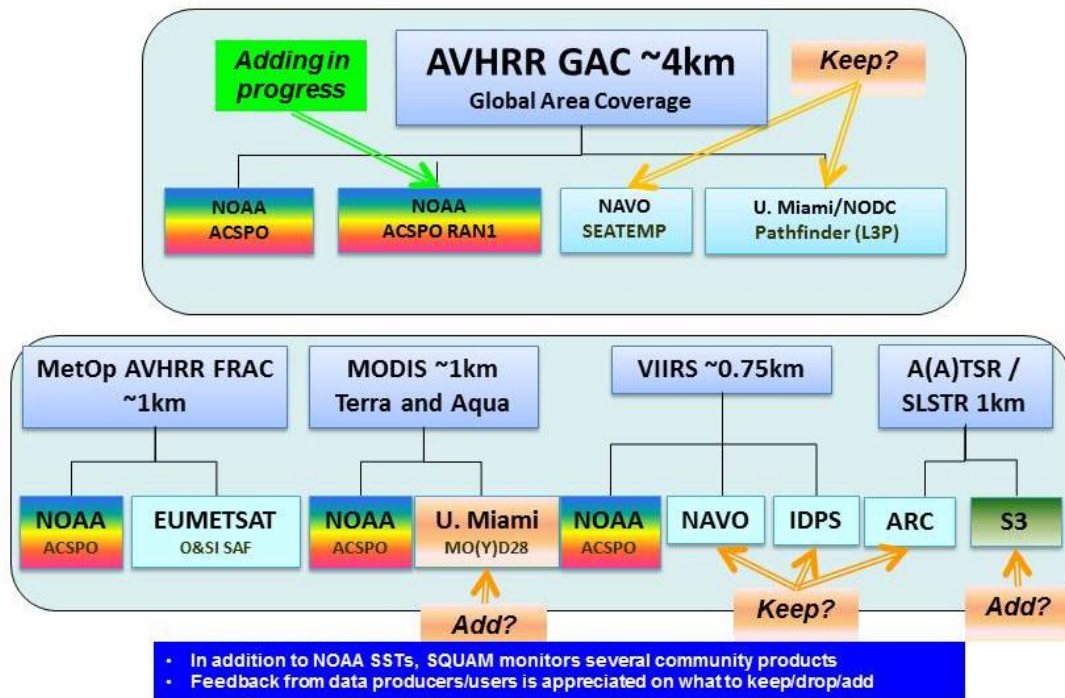


Figure 1: Data currently monitored in SQUAM. Top: low resolution (~4km); Bottom: high resolution data (~1km).

2. SST Quality Monitor (SQUAM)

The L2/3 SQUAM comprises two modules – low and high resolution (Figure 1). The initial objective of SQUAM was to evaluate the NOAA ACSPO SST products from AVHRRs onboard NOAA/Metop and from VIIRS onboard S-NPP (Ignatov, et al., 2015, this meeting). Several other NOAA and partners’ polar IR SST products were also included in SQUAM, to evaluate the ACSPO SSTs in the appropriate context. Since then, the scope of NOAA SST has grown and now includes the new line of ACSPO geo products, from Himawari-8 (H8; launched in October 2014) and from GOES-R (to be launched in 2016). Preparations are also underway for the two new polar launches – JPSS-1 in early 2017 and Metop-C in 2018. As a result, the SQUAM priorities are being revisited.

In the coming year, partners’ products currently included (e.g., NAVO, IDPS and ARC, Pathfinder) or planned to be included in SQUAM (e.g., the SLSTR onboard Sentinel-3, and MOD28/MYD28 products produced by NASA/U. Miami) will be reviewed, in the interest of redirecting NOAA resources towards monitoring ACSPO polar and geo products. Comparisons with other products may still be occasionally conducted using SQUAM functionality, to ensure ACSPO consistency with other community SST products. Non-NOAA data producers and users are encouraged to explicitly express their interest, to ensure continuous and systematic data processing and display in SQUAM.

Below, shown are several examples of initial monitoring of the two new ACSPO products in SQUAM – operational JPSS L3U (Figures 2-3) and experimental H8 L2P (Figures 4-5).

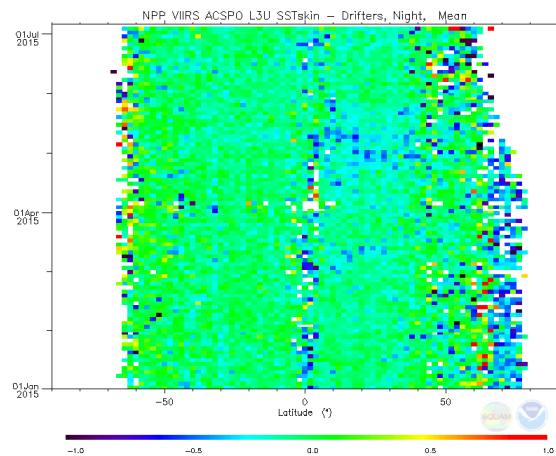


Figure 2: Hovmoller diagram of ACSP0 VIIRS L3U minus *iQuam* drifters SSTs (at night).

The biases in ACSP0 VIIRS retrievals in Figure 2 are mostly seen in the high latitudes and to a lesser degree in the tropics, which are predominantly cold (note however increased noise in these areas, due to reduced density of *in situ* data and therefore fewer match-ups; as a result, spots with warm biases are often interleaved with cold biases). These systematic patterns may be due to a combination of residual cloud and biases in the multi-channel SST retrieval algorithms. Work is underway to understand and minimize those.

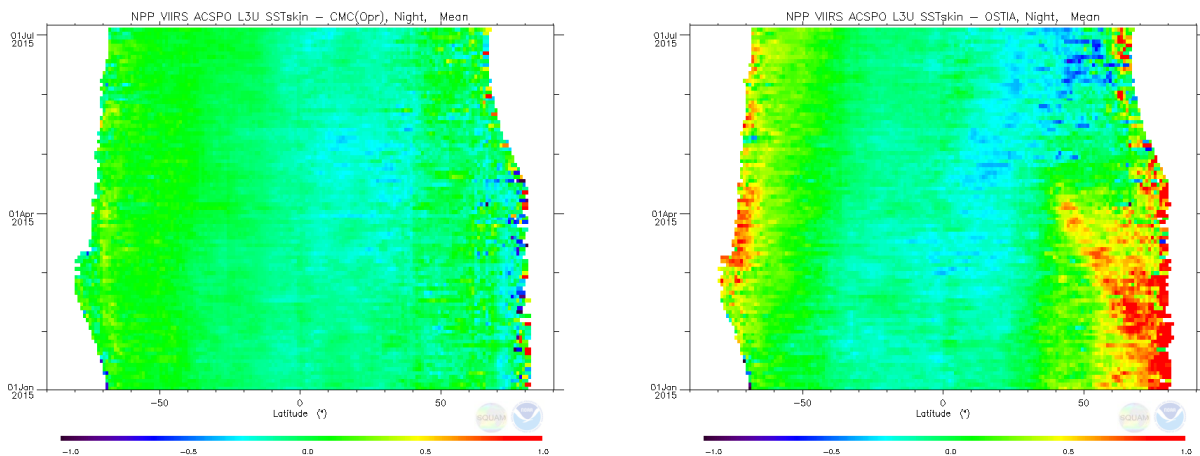


Figure 3: Night time Hovmoller diagrams of ACSP0 VIIRS L3U minus wrt to (left) CMC and (right) OSTIA L4 fields.

Figure 3 shows corresponding Hovmoller diagrams with respect to two L4 products widely used in the SST community, CMC and OSTIA. The ACSP0 SST generally agrees well with both L4s, over most global ocean. The largest differences with the OSTIA L4 SST are found in the high latitudes, where the OSTIA SST appears much colder than ACSP0 which in turn shows cold biases relative to *in situ* SSTs (cf. Figure 2). Recall that OSTIA is currently “anchored” to the OSI SAF Metop-A AVHRR L2 SST, and a similar cold bias is seen in the OSI SAF L2 SST relative to CMC L4 and *in situ* SSTs, whereas OSTIA and OSI SAF products are in close agreement (these results are not shown here but available in SQUAM). On the other hand, the CMC SST agrees well with the ACSP0 VIIRS SST which is assimilated in CMC L4, whereas the OSTIA L4 SST is anchored to the OSI SAF AVHRR L2 SST. Both L2/L4 pairs are biased cold in the Northern high latitudes, although biases are larger in the OSTIA/OSI SAF tandem. Work is currently underway to explore assimilation of the ACSP0 VIIRS L3U in OSTIA L4, and to better understand and minimize these cross-product biases seen in SQUAM.

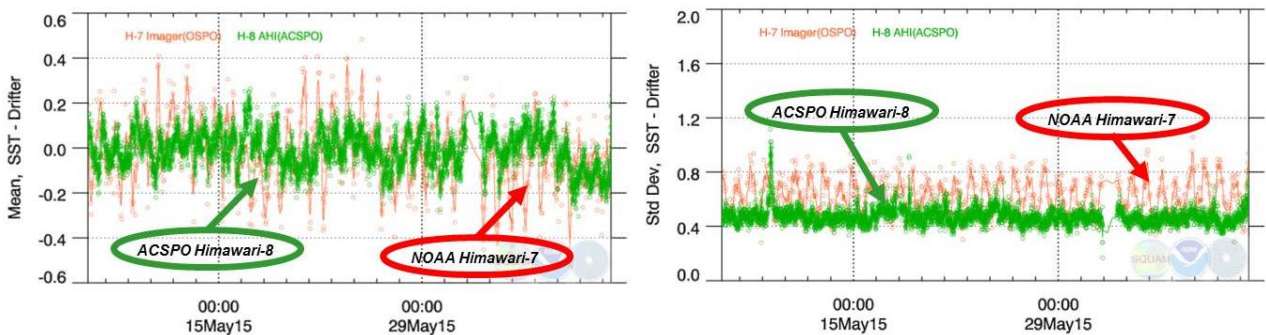


Figure 4: Validation of NOAA ACSP0 H8 and heritage H7 SSTs wrt iQuam drifters in May 2015, before experimental production of H8 commenced: (Left) Biases; (right) Standard deviations. Each data point represents: 10min FD for H8; 1 hr product file for H7.

Figure 4 shows results of validation of the H8 ACSP0 SST (for more information on ACSP0 SST, see Ignatov et al., this meeting). For comparison, the current operational NOAA SST product produced from MTSAT-2 (H7) using the NOAA heritage (pre-ACSP0) geo SST processing system is also shown. Typical biases in H8 ACSP0 SST are within ± 0.2 K. There is a ~ 0.10 - 0.15 K diurnal cycle in the *in situ* validation results, due to differences between ACSP0 skin and *in situ* bulk SSTs. These performance statistics are typically a factor of 2 better than for the heritage H7 SSTs. The corresponding H8 ACSP0 standard deviations range from 0.4-0.6 K, smaller numbers being representative of local nights and larger of local days. The H7 standard deviations are comparable with the corresponding H8 counterparts at night. However, during the daytime, the H8 ACSP0 SST shows a significant improvement, from 0.8-1 K for H7 to ~ 0.6 K. Part of the improvement in the H8 SST is due to using AHI sensor onboard H8, with a significantly improved spatial resolution and radiometric performance. On the other hand, the initial implementation of the H8 ACSP0 SST is expected to evolve, and performance of H8 SST will improve in the future development.

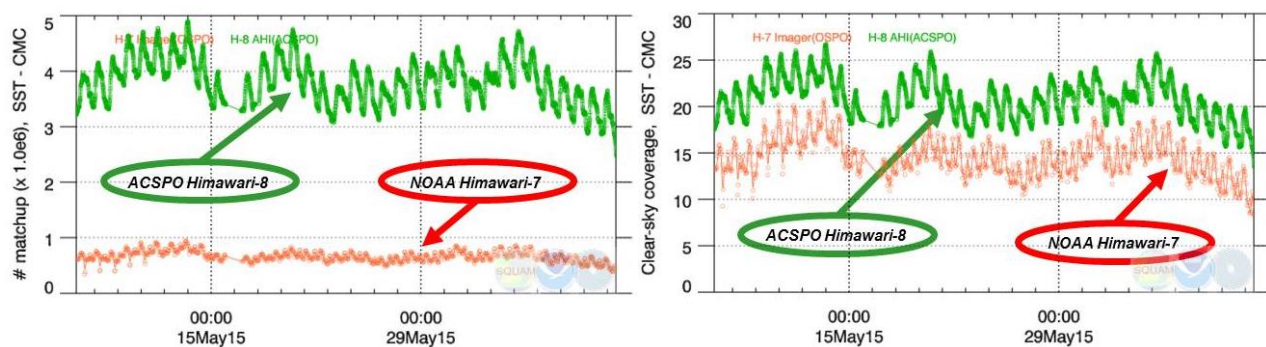


Figure 5: (left) Number of clear-sky ocean pixels for H8/7. (Right): Clear-sky fraction (ratio of clear-sky to total pixels).

Figure 5 shows that H8 product not only has superior performance (cf. Figure 4), but does it in a larger retrieval domain. Larger number of clear-sky pixels in H8 is expected, due to its 2km spatial resolution which results in larger total number of pixels than for H7 (4km resolution). The ratio of clear pixels to the total number of pixels is therefore more representative. It is also shown in Figure 5. In H8 product, the clear-sky fraction ranges from 15-27%, whereas in the heritage H7 product it ranges from 8-20%. Larger fraction in H8 is expected, due to the finer spatial resolution of AHI sensor. Our initial analyses also suggest that initial settings of the ACSP0 clear-sky mask may be overly conservative, and can be improved. Work is currently underway to explore improved clear-sky mask for AHI.

3. *In situ* SST Quality Monitor version 2 (iQuam2)

Figure 5 shows the interface of the new iQuam2 system.

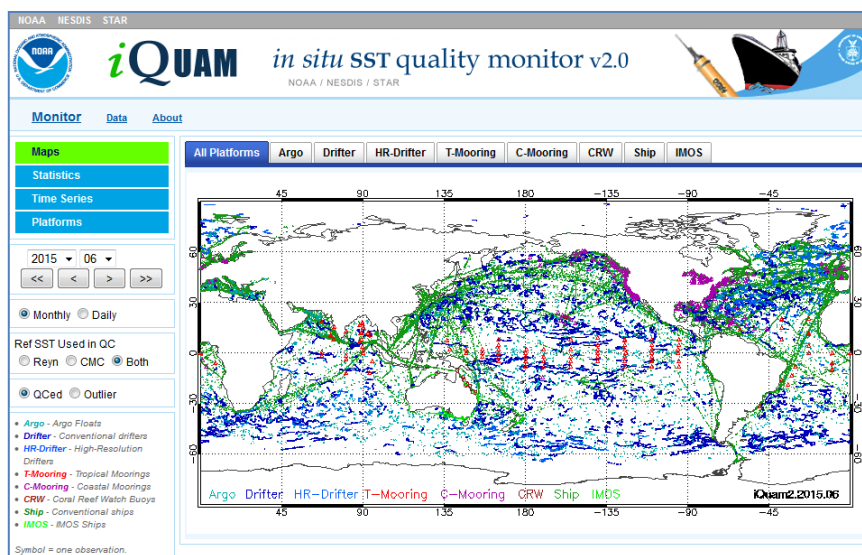


Figure 6: The interface of iQuam2. New data added in iQuam2 are ARGO floats, HR drifters, IMOS shops, CRW buoys.

Complete documentation of iQuam2 is currently underway (Ignatov, et al, 2016). Examples below illustrate new data added in iQuam2, including the GHRSSST high-resolution (HR) drifters (DBCP-GHRSSST, 2010). Figure 7 shows that the HR-drifters are mostly found in the N. Atlantic and S. Indian and S. Pacific.

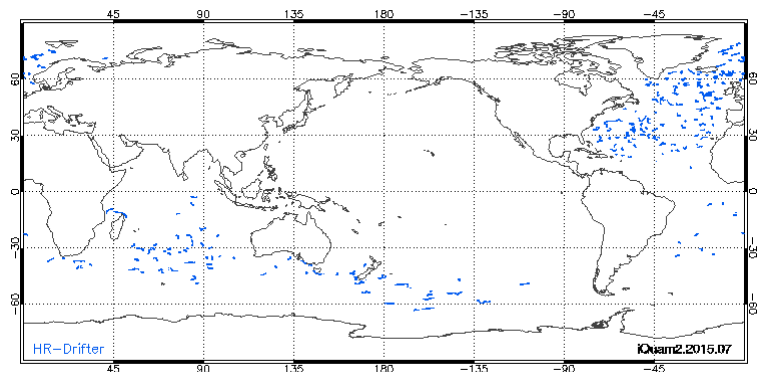


Figure 7: The HR drifters are mostly found in the N. Atlantic, S. Indian and S. Pacific Oceans.

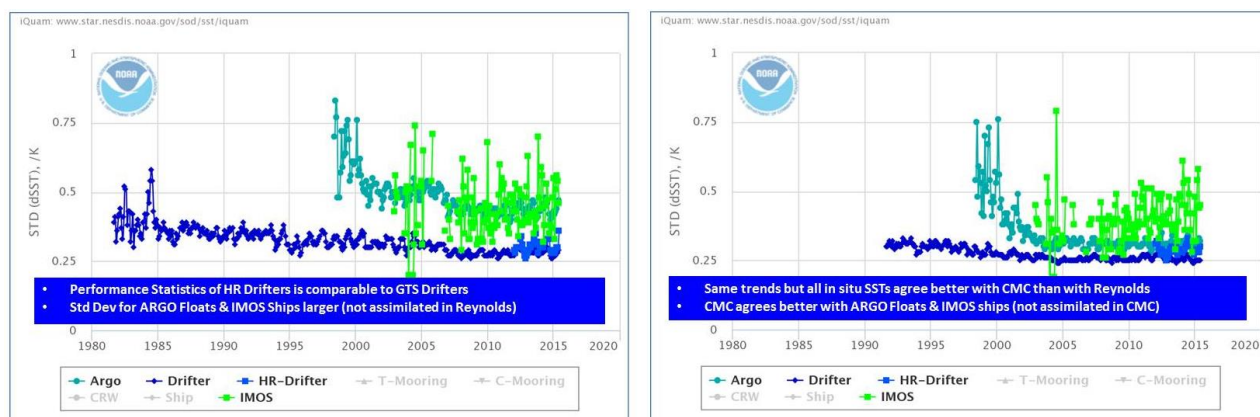


Figure 8: Standard deviations of in situ minus reference SST, for two references (left) Reynolds L4; and (b) CMC L4.

Figure 8 shows that out of the 4 *in situ* data plotted here, the drifters agree best with both Reynolds and CMC L4 analyses. Recall that both analyses assimilate drifter data. The better agreement with CMC than with Reynolds may be deceiving as it depends on how strongly one or another analysis is “forced” into *in situ* drifter data. Validation of both L4s against ARGO floats and IMOS ships provides an independent validation, as these *in situ* data have not been assimilated in both L4s. To that end, the agreement with both is closer and more stable in time for CMC than for Reynolds, suggesting the improved quality of the CMC analysis. Interestingly, the HR drifters do not show improved agreement with either CMC or Reynolds, compared to the conventional drifters. (In fact, the agreement with the CMC is even degraded.) This is likely due to the fact that statistics of highly regional HR drifters is compared with the global statistics for conventional drifters. Analyses are currently underway to compare the regional statistics of the two types of drifters.

4. Conclusion and Future Work

Significant progress was made since the GHRSSST-15 with both NOAA SST monitoring systems. Major SQUAM priorities for the coming year will be: reduced monitoring of the community products for which no feedback is received from either data producers or users; adding complete geo capability; redesigning the low resolution L2-SQUAM page, to monitor the reprocessed AVHRR GAC products from 2002 – pr; and improvement and completion of SQUAM functionality as deemed appropriate. The current *iQuam1* will be retired and replaced with *iQuam2*; archival with GHRSSST (PO.DAAC, NCEI) will be explored; and *iQuam2* will be documented. Work towards *iQuam3* will include adding the remaining *in situ* data (SAMOS ships, World Ocean Database) and exploring the 3-way error analysis, to determine errors in individual *in situ* data.

5. References

- Dash, P., A. Ignatov, Y. Kihai, and J. Sapper, The SST Quality Monitor (SQUAM), *JTech*, **27**, 1899-1917, doi:10.1175/2010JTECHO756.1, 2010.
- Dash, P., A. Ignatov, M. Martin, et al, GHRSSST analysis fields inter-comparisons—Part 2: L4-SQUAM, *Deep Sea Research Part II: Topical Studies in Oceanography*, **77**, 31-43, 2012.
- DBCP-GHRSSST, 2010: Proposal for a joint DBCP-GHRSSST Pilot Project to upgrade elements of the global drifting buoy fleet to allow the reporting of higher resolution SST and position, www.ghrsst.org/ghrsst/tags-and-wgs/stval-wg/dbcp-ghrsst-pilot-project/.
- Ignatov, A., F. Xu, and X. Zhou, Redesigned *in situ* SST Quality Monitor: *iQuam* version 2, *JTech*, 2016 (in preparation).
- Ignatov, et al., ACSPO SST Products at NOAA: Update for GHRSSST-16, *this meeting*.
- Xu, F., and A. Ignatov, In situ SST Quality Monitor (*iQuam*), *JTech*, **31**, 164-180, doi:10.1175/JTECH-D-13-00121.1, 2014.

GHRSSST SYSTEM COMPONENTS: RDAC UPDATE: CANADIAN METEOROLOGICAL CENTER

Dorina Surcel Colan

Numerical Environmental Prediction Section, National Prediction Development Division, Meteorological Service of Canada, Environment Canada, Email: dorina.surcel-colan@ec.gc.ca

ABSTRACT

The Canadian Meteorological Centre (CMC) produces one Level 4 SST analysis in the operational cycle. In the last year a new higher resolution product has been developed, using an improved methodology and new satellite retrievals datasets. This paper presents details about CMC products and how these products are used in the atmospheric and oceanic forecasting systems.

1. Introduction

CMC participates in GHRSSST with an L4 0.2° SST analysis produced in real time. The release in 2014 of two new SST datasets from VIIRS instrument onboard the Suomi National Polar-Orbiting Partnerships (S-NPP) satellite and AMSR2 instrument onboard the Global Change Observing Mission-Water (GCOM-W) satellite, raised the question of the potential contribution of these datasets to SST analyses. Tests have been done to include these datasets into an experimental 0.1° version of the CMC analysis.

2. L4 CMC SST analyses

The SST analyses produced at CMC are based on the statistical interpolation method as described in Brasnett (2008). This method is also used for the quality control of observations and the bias correction of satellite retrievals. The CMC analysis represents SST at a depth where no diurnal variability is present. The assimilation methodology uses anomaly from climatology as the analysis variable. The background is based on simple persistence.

The 0.2° SST analysis produced in the operational cycle assimilates data from 4 AVHRR instruments together with in situ data from moored and drifting buoys and ships and ice information.

The new 0.1° SST analysis has been recently implemented in experimental mode. Data from VIIRS and AMSR2 instruments are assimilated in addition of data used in the operational analysis. Along with increasing the resolution of the analysis grid, additional changes were needed to fully benefit from the improved resolution. More details about this new product are included in a separate paper by Brasnett and Surcel.

Table 1 contains details about each data set used in these analyses. Both analyses are produced in GDS2 format. Since 2014, the 0.2° SST delivered to GHRSSST via PO.DAAC website assimilates also data from VIIRS and AMSR2. Reanalysis back to Sept. 1, 1991 using this version are available in GDS2 format. No SSES bias or standard deviation errors are used in these analyses.

Data set	Data type	Source
NOAA18 AVHRR	L2P	NAVOCEANO
NOAA19 AVHRR	L2P	NAVOCEANO
Metop A AVHRR	L2P	NAVOCEANO
Metop B AVHRR	L2P	NAVOCEANO
AMSR2	L3	RSS
VIIRS-NPP	L2P	NOAA/NESDIS/OSPO
In situ		GTS
Sea-ice concentration	L4	CMC ice analysis

Table 1: Data sets uses in CMC SST analyses

3. Use of SST analysis in the operational cycle at CMC

At the Canadian Meteorological Centre, forecast models use the SST analysis from the micro scale to the global scale. Among these systems, the Global and Regional Deterministic Prediction Systems (GDPS, RDPS) and the Global and Regional Ensemble Prediction Systems (GEPS, REPS) use the SST in the initialization process. SST values are updated once per day and the field is kept constant during the integration.

Recently, environmental systems have been implemented to produce ocean and ice forecasts. The Global Ice Ocean Prediction System (GIOPS) (Smith et al, 2015) provides daily global ice and ocean analyses and 10-day forecasts on a 1/4°-resolution grid. GIOPS includes a full multivariate ocean data assimilation system that combines satellite observations of sea level anomaly and sea surface temperature together with in situ observations of temperature and salinity. The CMC SST analysis is interpolated onto GIOPS grid and assimilated directly with a constant error of 0.3°C. This error corresponds closely to the estimated error from the CMC SST analysis (Brasnett, 2008) and also provides a good constraint for SST to reduce initialization shock when using GIOPS analyses in coupled medium-range forecasts with the GDPS (Smith et al., 2013).

GIOPS participates in GODAE OceanView Inter-comparison project (Ryan et al, 2015). Evaluations of ocean forecasts at different lead times against in situ data show good performance of GIOPS especially for the SST. Figure 1 shows the performance of GIOPS compared with other oceanic systems during 2014 for 120h forecast of SST.

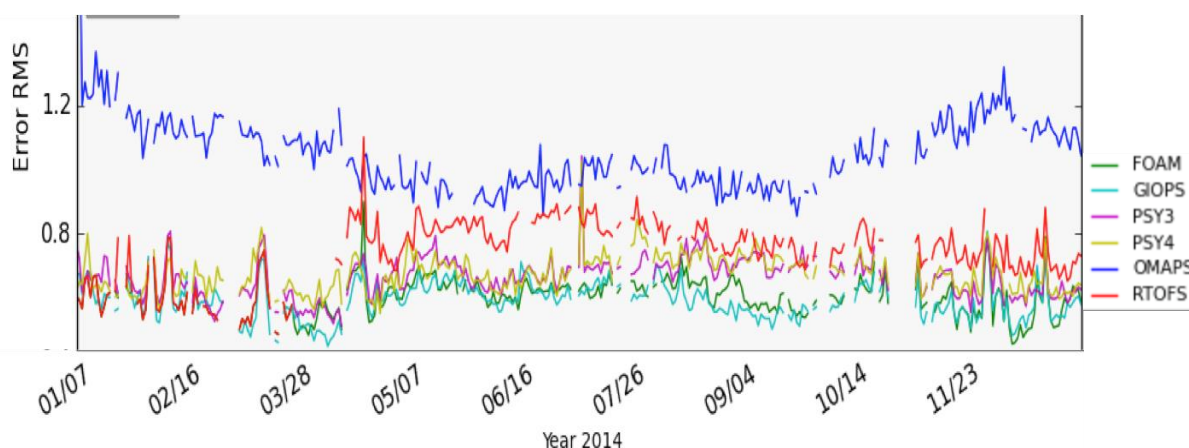


Figure1: 2014 time series of RMSE error for 120h forecast of SST; the forecast is compared with USGODAE in-situ drifting buoys. The oceanic forecasting systems participating in GODAE Oceanview intercomparison project are described in Ryan et al. (2015). This figure was provided by Jinshan Xu and Fraser Davidson.

4. Future plans

With the implementation in the operational cycle of the new higher resolution analysis and the availability of reprocessed satellite datasets back to 1981 it is an interest to produce reanalysis of SST for the last 30 years.

The performance of GIOPS model encourages us to review the methodology of SST analysis in order to introduce GIOPS information into the background field. Interests are also to produce a regional surface water temperature analysis to include the large number of Canadian lakes.

5. References

Brasnett, B., The impact of satellite retrievals in a global sea-surface-temperature analysis. *Quart. J. Roy. Met. Soc.*, **134**, 1745-1760, 2008.

Ryan, A.G., C. Regnier, P. Divakaran, T. Spindler, A. Mehra, G.C. Smith, F. Davidson, F. Hernandez, J. Maksymczuk, and Y. Liu, GODAE OceanView Class 4 forecast verification framework: global ocean inter-comparison, *Journal of Operational Oceanography*, **8.1**, 2015.

Smith GC, Roy F, Mann P, Dupont F, Brasnett B, Lemieux J-F, Laroche S, Bélair S. A new atmospheric dataset for forcing ice–ocean models: Evaluation of reforecasts using the Canadian global deterministic prediction system, *Quart. J. Roy. Met. Soc.*, 2013, doi: 10.1002/qj.2194.

Smith, G.C., and Coauthors, Sea ice Forecast Verification in the Canadian Global Ice Ocean Prediction System. *Quart. J. Roy. Met. Soc.*, 2015, DOI:10.1002/qj.2555.

GHRSSST SYSTEM COMPONENTS: EUMETSAT REPORT FOR GHRSSST

Anne O'Carroll⁽¹⁾, Igor Tomazic, Hans Bonekamp⁾

(1) EUMETSAT, Eumetsat-Allee 1, 64295 Darmstadt, Email: Anne.Ocarroll@eumetsat.int

ABSTRACT

The European Organisation for the Exploitation of Meteorological Satellites (EUMETSAT) delivers operational weather and climate-related satellite data, images and products throughout all day and year. EUMETSAT also has commitments to operational oceanography and atmospheric composition monitoring. Activities over the next twenty years include the continuation of the Mandatory Programmes (MSG, EPS) and future (MTG, EPS-SG), which all include ocean observations of SST and sea surface winds. Other oceanography activities include with and towards sea-ice products, radiative fluxes, significant wave height, sea surface topography, sea-ice surface temperature, ocean colour products, turbidity, and aerosol optical depth over water.

1. Sea Surface Temperature activities

EUMETSAT operational services from Metop-B (AVHRR, IASI) and Meteosat-10 (SEVIRI) continue. Launches related to oceanography for 2015 include MSG-4 (SEVIRI) on 15th July 2015; and the 3rd party/optional programmes of Copernicus Sentinel-3A SLSTR in October/November 2015 (Sentinel-3B expected 18months later); and Jason-3. Further ahead, Metop-C is planned for 2018; EPS-SG (MetImage, IAS) around 2020; and MTG-I1 (FCI) in 2018 and MTG-S1 (IRS) in 2020.

EUMETSAT supervises and coordinates its Satellite Application Facility (SAF) network. The EUMETSAT Ocean and Sea-ice SAF is lead by Meteo-France with a consortium of institutes from EUMETSAT member states, and provides reliable and timely operational services related to meteorology, oceanography and the marine environment.

In addition to mandatory programme activities the oceanography group at EUMETSAT collaborates and interacts and/or supports the Copernicus programme, OSI-SAF, GSICS, Felyx, Horizon 2020 Fiduceo plus others.

IASI SSTs have been available since April 2008, contained within the EUMETSAT IASI Level 2 product. These data are available via EUMETCast, together with vertical temperature and humidity profiles in the BUFR product called IASI L2 TWT. The Metop-A IASI L2Pcore SST product follows the GDS2r5 and has been available via ftp from the Data Centre since March 2011, with Metop-B available since January 2014. The SSTs are based on those available from the IASI L2 product.

The IASI SST L2Pcore contains skin SSTs from the IASI PPF, flags, quality information and SSES, plus an auxiliary wind-speed field, but no further auxiliary data required for the complete GHRSSST specification. Within the Continuous Development and Operations Phase 2 (CDOP-2) of the EUMETSAT Ocean and Sea-Ice Satellite Application Facility (OSI SAF) a full GHRSSST specified Metop-A IASI L2P SST is produced based on the Metop-A IASI L2Pcore SST from the central facilities. The full L2P product has extra auxiliary data, such as sea-ice fraction and aerosol information, which is necessary to fulfil the complete GHRSSST specification. The SST retrieval from IASI is based on the 1D-VAR Optimal Estimation Method, recently updated with the Version 6 of the IASI Level-2 Product Processing Facility (PPF) from 30 September 2014. OSI-SAF IASI SST L2P product (OSI-208) has been declared operational and is available from the OSI SAF ftp site at Ifremer or via EUMETcast. OSI-208 has been pre-operational since 20 November 2014, and available from the OSI SAF ftp site at Ifremer since the end of 2014. The OSI-208 has been available via EUMETcast since 8 January 2015.

IASI SSTs have been collocated to in situ drifting and moored buoy measurements, and additionally compared with AVHRR SST observations (O'Carroll and Marsouin, 2015). The IASI SSTs from version 6 of the IASI L2 PPF show a slight cool bias against drifting buoys with the highest quality results (Quality Level 5) displaying a cool bias of -0.06 K (standard deviation 0.38 K). The impact of the newly implemented Version 6 of the PPF

is to reduce a previously observed IASI cool bias significantly for the higher quality results. For all quality levels the cool bias has been reduced by the new version by 0.1–0.2 K. Plans for 2016 include improved aerosol detection and flagging for IASI SSTs; and validation of uncertainties and improvements in product uncertainties.

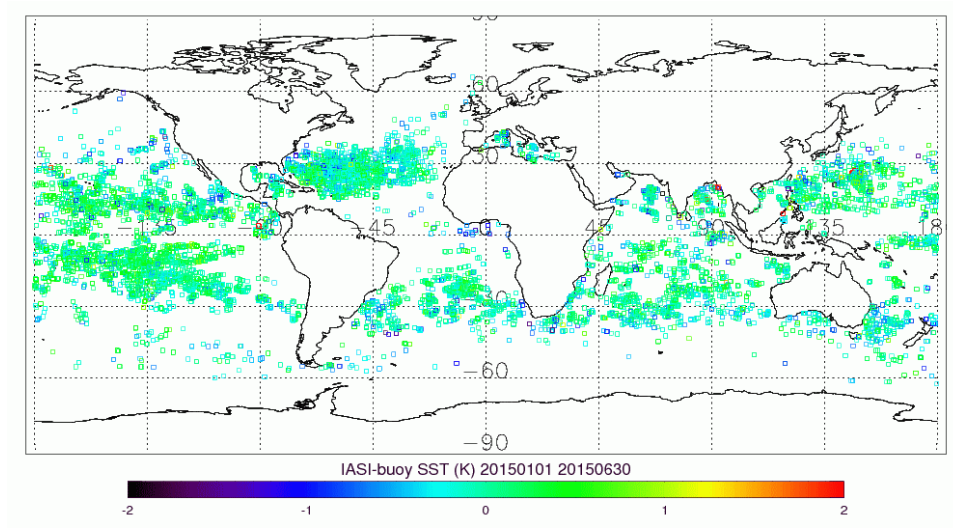


Figure 1: IASI buoy SST January to June 2015

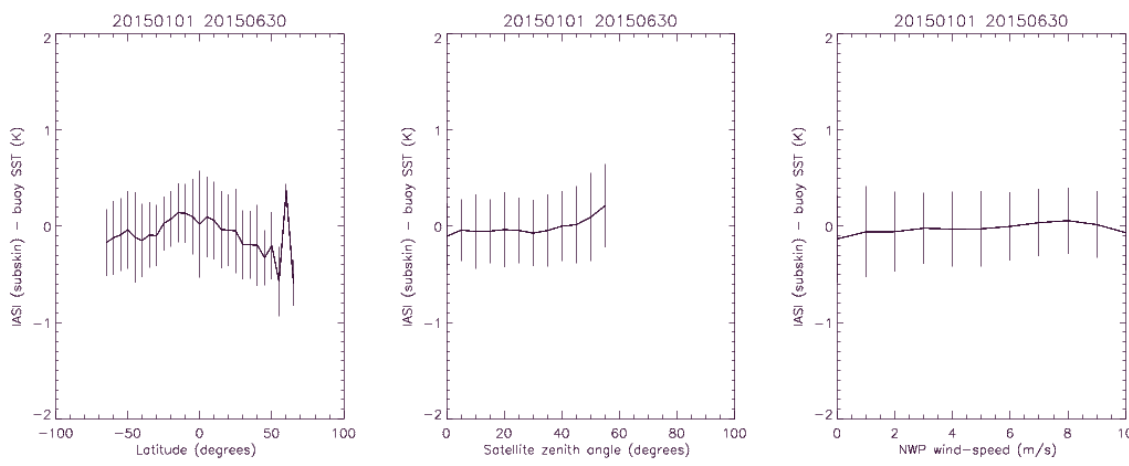


Figure 2: Binned plots showing the IASI SST minus drifting buoy SST versus latitude, satellite zenith angle, and wind-speed over the period January to June 2015.

2. Sea-ice surface temperature activities

Activities are underway at EUMETSAT towards research and development needed for Copernicus Sentinel-3 SLSTR sea-ice cloud detection. Further Copernicus activities are planned to follow on algorithm development and validation for sea-ice surface temperature and marginal ice zone temperature retrievals.

3. Copernicus Sentinel-3 SLSTR

EUMETSAT is participating in the European Commission's Copernicus Sentinel-3 programme in partnership with ESA, where EUMETSAT will operate the satellite and will serve the marine user community. ESA is responsible for the development of the Sentinel-3 space and ground components and will serve the land user community. The Sentinel-3 launch is planned for October/November 2015.

The satellite will have on board the Sea and Land Surface Temperature radiometer (SLSTR), a dual-view sensor, and is a successor to the ATSR series but with a wider swath and updated instrument characteristics. Information on the products can be found in O'Carroll et al, 2015.

Level 0 and Level 1 data and products will be generated at and L1 distributed by both EUMETSAT and ESA. EUMETSAT will be the Sentinel-3 marine centre and are responsible for the production and distribution of the level-2 marine products. Data will be distributed through EUMETCast and the EUMETSAT data centre. Further information, including data access, data format, products and (soon) sample Test Data Sets (e.g. Tomazic et al, 2015), can be found from:

<http://www.eumetsat.int/website/home/TechnicalBulletins/CopernicusUserPreparation/index.html>.

Preparations towards the EUMETSAT Mission Performance Implementation Plan for Sentinel-3 Calibration and Validation activities continue, in coordination with the ESA Mission Performance Centre. Activities include the OSI-SAF Federated Activity on the SLSTR Matchup Database, in coordination with ESA Felyx. Activities are planned towards a pilot project for better calibrated drifting buoys for satellite validation, in coordination with the Data Buoy Cooperation Panel and ESA.

Preparation activities by the Sentinel-3 Validation Team continue. Further participation is welcome, please contact Anne.Ocarroll@eumetsat.int or Craig.Donlon@esa.int for more information.

4. Third party data activities

Work towards access to relevant sea surface temperature data from third-parties continues including the agreements with NOAA, ISRO, SOA, NSOAS and JAXA. S-NPP VIIRS ACSPO (v2.4) L3U are available through EUMETCast. GCOM W2 AMSR2 L2P SSTs are available as a demonstrational service to EUMETSAT member states in NRT. An operational service for INSAT-3D is going through approval for a proposed dedicated service (L2 SST in HDF format). EUMETSAT also receives a continuous data stream of HY-2a L2 data.

5. References

O'Carroll, A.G. and A. Marsouin, 2015: OSI-SAF Metop-A IASI Sea Surface Temperature L2P (OSI-208) Validation report, Version 1.4, April 2015, SAF/OSI/CDOP2/M-F/TEC/RP/210 (<http://www.osi-saf.org>).

O'Carroll, A.G., H. Bonekamp, F. Montagner, V. Santacesaria, I. Tomazic, 2015: Sea Surface Temperature from EUMETSAT including Sentinel-3 SLSTR, Proceedings of ESA Sentinel-3 for Science Workshop, Venice, June 2015.

Tomazic, I., H. Bonekamp, E. Kwiatkowska, F. Montagner, A. O'Carroll, V. Santacesaria, 2015: Experiences with Sentinel-3 Optical Sensor L1 and L2 products, Proceedings of ESA Sentinel-3 for Science Workshop, Venice, June 2015.

GHRSSST SYSTEM COMPONENTS: EUMETSAT OSI SAF

Stéphane Saux-Picart⁽¹⁾ & OSI SAF team

(1) OSI/SAF/Météo France, France, Email: stephane.sauxpicart@meteo.fr

ABSTRACT

The OSI SAF objective is to provide users with operational data of the ocean surface derived from meteorological satellites. As far as Sea Surface Temperature is concerned, the OSI-SAF is currently delivering a suite of products in near real time mode (see table below).

Product ID	Instrument	Coverage
OSI-201	METOP-A/AVHRR	Global on a 0.05° grid/12 hourly
OSI-202	METOP-A/AVHRR and NPP/VIIRS	North Atlantic Region/6 hourly
OSI-203	METOP-A/AVHRR	Atlantic High Latitudes/12 hourly
OSI-204	METOP-A/AVHRR	Global full resolution in satellite projection
OSI-206	METEOSAT10/SEVIRI	Covering 60S-60N and 60W-60E on a 0.05° grid/hourly
OSI-207	GOES13-East	Covering 60S-60N and 135W-15W on a 0.05° grid/hourly
OSI-208	METOP-A/IASI	Global full resolution in satellite projection

These products are disseminated through various means:

Ifremer FTP server http://www.osi-saf.org	All OSI SAF SST products (except high latitudes) in near real time in GHRSSST format
NAIAD: http://naiad.ifremer.fr/	Same as above
PO.DAAC: http://podaac.jpl.nasa.gov/	Same as above
GHRSSST Long Term Stewardship and Reanalysis Facility	Same as PO.DAAC (archive)
EUMETCast (Satellite broadcast system)	All products (in GRIB2 format) & METOP/AVHRR L2P in GHRSSST format. Planning to distribute other data in GHRSSST format.
EUMETSAT Data Center	Global or regional products (in GRIB2 or GHRSSST format depending on product)

In 2014-2015, OSI-SAF has been finishing and testing the implementation of the new polar orbiter processing chain which will deliver operational SST products derived from METOP-B/AVHRR. This chain includes the algorithm correction scheme (Le Borgne et al., 2011) using NWP model outputs to perform brightness temperature simulations for each clear sky pixels. The products of this chain will replace METOP-B/AVHRR products OSI-201, OSI-202 and OSI-204. The EUMETSAT Operational Readiness Review is planned for the end of 2015 and will result in the beginning of the operational delivery of these products.

OSI-SAF is also working on the reprocessing of MSG/SEVIRI archive. This reprocessing will cover 2004 to 2012 and the dataset resulting is planned to be delivered mid-2016. It will consist in hourly fields projected onto a regular 0.05°x0.05° lat/lon grid. It is envisaged that two datasets will be delivered: one using the

algorithm correction method (Le Borgne et al., 2011), and one using the optimal estimation method (Merchant et al., 2013). In the coming months, most of the effort at Météo-France/CMS will be directed towards the elaboration of these datasets.

As far as high latitude is concerned, sea-ice surface temperature has been included in SST OSI-203 high latitudes regional product and OSI-205 full resolution in satellite projection (granules) product. The operational delivery of these products is planned for the next few months.

REPORT TO GHTSST XVI FROM JAXA

Misako Kachi

Japan Aerospace Exploration Agency (JAXA), Tsukuba (Japan), Email : kachi.misako@jaxa.jp

ABSTRACT

Recent Japan Aerospace Exploration Agency (JAXA) activities are summarized and reported.

All AMSR2 standard products have been updated to version 2 in March 2015. In addition to standard products, eight research products including 10-GHz SST and All-weather Sea Surface Wind Speed are defined. GCOM-C, which carrying SGLI instrument, is currently scheduled to be launched in Japanese Fiscal Year of 2016. AMSR-E has restarted but in slow rotation of 2-rpm since December 2012 to implement cross-calibration between AMSR2. TRMM satellite, which was JAXA-NASA joint mission, completed its mission operation in April 2015, and satellite re-entered to the Earth's atmosphere over the Southern Indian Ocean on 16 June 2015 (UTC). JAXA-NASA joint mission Global Precipitation Measurement (GPM) Core Observatory was launched on 28 February 2014 (JST) and all data are released to public.

New SST products produced from GPM-Core/GMI in GDS 2.0 format is added to the JAXA GHRSSST server (<http://suzaku.eorc.jaxa.jp/GHRSSST/>) in addition to AMSR2, AMSR-E, WindSat and VIRS in GDS 2.0 format. JAXA also prepares to distribute SST of the JMA' geostationary satellite Himawari-8 in GDS 2.0 format in August 2015 (<http://www.eorc.jaxa.jp/ptree/>).

JAXA data policy regarding environmental satellite data, including GCOM and GPM, was changed and accepts free distribution to third parties and commercial use without restriction, and products in JAXA GHRSSST server can be provided to GDAC and LTSRF, except Himawari-8 SST that follows JMA's data policy.

1. Introduction

JAXA developed the Advanced Microwave Scanning Radiometer (AMSR) as passive microwave imagers to observe SST, onboard the ADEOS-II, AMSR for EOS (AMSR-E) onboard NASA's EOS Aqua satellite, which has been operating since 2002, and launched AMSR2 onboard the GCOM - Water (GCOM-W) in May 2012. C-band (6.9-GHz/7.3 -GHz) channels on AMSR, AMSR-E and AMSR2 are indispensable for retrieving global sea surface temperature and soil moisture. All-weather and frequent measurements enables analyses of rapid changes of SST.

JAXA is currently developing the Second generation Global Imager (SGLI), which will be carried by the Global Change Observation Mission (GCOM) - Climate (GCOM-C) scheduled to be launched in Japanese Fiscal Year (JFY) 2016.

Two JAXA-NASA joint missions, the Tropical Rainfall Measuring Mission (TRMM) and the GPM Core Observatory, carry SST instruments provided by NASA. TRMM has the TRMM Microwave Imager (TMI), which has 10-GHz channels, and Visible Infrared Scanner (VIRS). The GPM Core Observatory carries GPM Microwave Imager, which has 10-GHz channels.

JAXA exchanged agreement between Japan Meteorological Agency (JMA) to distribute their geostationary satellite Himawari-8 Level 1 data from the JAXA server to non-commercial users in NRT basis. JAXA Himawari Monitor web site opens to public in August 2015 (<http://www.eorc.jaxa.jp/ptree/>), and some Level 2 products, including SST, produced by JAXA are also released in this server.

2. Current status of JAXA missions

2.1. AMSR-E

AMSR-E was launched in May 4, 2002, and halted its observation in 4 October 2011. AMSR-E has restarted observation at 2-rpm (in slow rotation) since December 2012 to implement cross-calibration with AMSR2. Details about slow rotation AMSR-E operation are available from the AMSR-E web site (http://sharaku.eorc.jaxa.jp/AMSR/products/amsre_slowdata.html).

Currently, AMSR-E L1B data in 2-rpm mode is distributed to public through the GCOM-W Research Product web page (http://suzaku.eorc.jaxa.jp/GCOM_W/research/terms.html).

We are preparing new AMSR-E products, which are processed with new calibrated L1, AMSR2 L2 algorithms and output in AMSR2 formats, to produce continuous and coherent dataset between AMSR-E and AMSR2.

2.2. AMSR2 on GCOM-W

AMSR2 is multi-frequency, total-power microwave radiometer system with dual polarization channels for all frequency bands. The instrument is a successor of AMSR and AMSR-E. The frequency bands include 6.925, 7.3, 10.65, 18.7, 23.8, 36.5, and 89.0-GHz.

AMSR2 onboard the GCOM-W satellite was launched on 18 May 2012 (JST) from Tanegashima Space Center, Japan. The GCOM-W satellite has joined A-train orbit since 29 June. After GCOM-W was inserted into the planned position on the A-Train orbit, AMSR2 was spun up to 40-rpm, and then set to "science mode" to start observation in 3 July. Initial checkout of the satellite and the instrument has completed in 10 August without major problem. The GCOM-W satellite was installed in front of the Aqua satellite to keep continuity of AMSR-E observations and provide synergy with the other A-Train instruments for new Earth science researches.

AMSR2 standard products are distributed through the GCOM-W1 Data Distribution Service system (<http://gcom-w1.jaxa.jp>) as well as AMSR-E and AMSR standard products. The first public release version 1 of AMSR2 standard products were released in 2013.

On 26 March 2015, JAXA updated L1 and L2 algorithms from Ver.1 to Ver.2.0, and on 3 April 2015, updated again to Ver.2.1 to correct inappropriate parameter settings in L1 processing system. Reprocessing of L1 Ver.2.1 for the past period was completed, and that of L2 is planned to be completed in autumn 2015.

AMSR2 SST product version 2 was validated by comparing with the quality controlled buoy SST observations of the iQUAM version 1 provided by NOAA/NESDIS. Each match-up data will include AMSR2 footprints around buoy stations within radius of 30 km and 2 hours. Root mean square error (RMSE) between AMSR2 and buoy SSTs from August 1, 2012 to July 31, 2014 is 0.58 °C, which is including both ascending (noon) and descending (night). Detailed results are shown in Kachi et al. (2015) in GHRSSST XVI. We also opens AMSR2 Validation Monitoring web (http://suzaku.eorc.jaxa.jp/GCOM_W) to check variability of the products.

Eight research products were defined for AMSR2 in Mar. 2015, including 10-GHz SST and all-weather sea surface wind speed. 10-GHz SST (research product) has been included in standard SST product from Ver.2, but not distributed in GDS2.0 format from the JAXA GHRSSST server.

AMSR2 standard SST algorithm uses 6.9-GHz channels to retrieve SST, but has a weak point that horizontal resolution of 6.9-GHz is the worst in the AMSR2 channel set. The 10-GHz channel also has sensitivity to SST higher than 10-12 °C, and can provide SST with finer horizontal resolution, and less missing areas along the coast lines (Figure 1). RMSE of AMSR2 10-GHz SST versus buoy observation is 0.61 °C for SST higher than 9 °C. 10-GHz SST under 9 °C is set as missing in the current version.

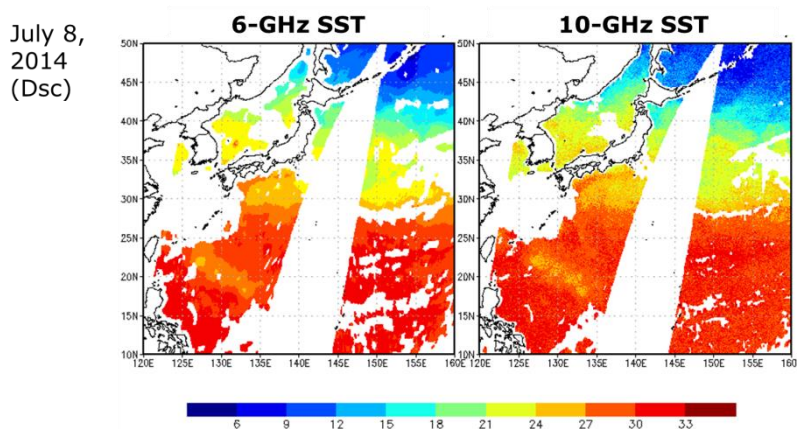


Figure 1. Comparison of AMSR2 standard (6-GHz) SST (left) and 10-GHz SST (right) in descending orbit on July 8, 2014.

2.3. VIRS on TRMM

TRMM is a joint mission between JAXA and NASA, which was launched in November 1997 and completed its mission operation on April 8, 2015. The Visible Infrared Scanner (VIRS), which was developed by NASA, on board the TRMM satellite turned off on 21 March, 2014, due to satellite bus battery anomalies and considering operational priority within the mission. TMI completed its operation on April 8, 2015. The satellite re-entered to the Earth's atmosphere over the Southern Indian Ocean on 16 June 2015 (UTC).

TRMM Version 8 products, which will be the products applying GPM algorithms to TRMM data, plan to use GPM V05 algorithms but not next GPM V04 algorithms due to waiting results of cross-calibration between the Precipitation Radar (PR) and Dual-frequency Precipitation Radar (DPR) L1 products.

2.4. GMI on GPM Core Observatory

The GPM Core Observatory, a joint mission between JAXA and NASA, was launched from JAXA Tanegashima Space Center on 28 February, 2014 (JST). GPM Microwave Imager (GMI) was developed by NASA as a successor of TMI on board the TRMM satellite. GPM V03 for DPR, GMI, combined products (standard) and JAXA global rainfall map GSMaP (national), have been released in Sep. 2014. NASA global rainfall map IMERG (national) V03 has been released in Mar. 2015. Standard products are available from JAXA G-Portal (<http://www.gportal.jaxa.jp/>) and also from NASA PPS.

Next major algorithm version up (V04) is scheduled in January 2016 for DPR, GMI, DPR/GMI combined, and the first GPM latent heating products.

JAXA has developed the GMI 10GHz SST, GMI sea ice concentration (SIC), and DPR SIC products as JAXA's GPM research products. GMI 10-GHz SST is already available at JAXA GHRSSST server in GDS 2.0 format. Its accuracy is almost same or slightly worse than AMSR2 10-GHz SST product. Next version up of GMI 10-GHz SST is scheduled in January 2016, following update of GMI L1 products to V04.

2.5. SGLI on GCOM-C

SGLI is a versatile, general purpose optical and infrared radiometer system covering the wavelength region from near ultraviolet to infrared. SGLI system consists of two components; SGLI-VNR (Visible & Near infrared push-broom Radiometer); and SGLI-IRS (shortwave & thermal InfraRed Scanner) to optimize optics for each wavelength range. Two major new features are added to SGLI, they are 250 m spatial resolution for 11 channels and polarization/multidirectional observation capabilities. The GCOM-C satellite is currently scheduled to be launched in Japanese Fiscal Year of 2016.

The 250m resolution data of SGLI-VNR will enable to detect more fine structure in the coastal area such as river outflows, regional blooms, and small currents SST and ocean color products derived from SGLI will provide additional information to AMSR2 SST.

2.6. AHI on Himawari-8

JMA's new geostationary satellite Himawari-8 (means sunflower) was launched in October 2014, and has replaced observation by MTSAT-2 since July 7, 2015. Himawari-8 carries the Advanced Himawari Imager (AHI). The functions and specifications are notably improved from those of the imagers on board MTSATs (see more details at JMA's web site: <http://www.jma-net.go.jp/msc/en/support/index.html>).

JAXA exchanged agreement with JMA to receive the AHI L1 products provided by JMA in near-real-time basis in order to distribute them to user community of non-profit purposes. In addition, JAXA produces own L2 products from AHI L1 data, seeking synergy with JAXA's other Earth Observation missions.

JAXA has started operation of the web site "JAXA Himawari Monitor" and ftp server called as the P-Tree system (<http://www.eorc.jaxa.jp/ptree>) since August 31, 2015. L1 products are in Himawari Standard Data (HSD) format, and consist of Full-disk data in 10-minute intervals, Japan area (region 1 & 2) in 2.5-minute intervals, and Target area (region 3) in 2.5-minute intervals. We also provide Color Image Data in png format. JAXA's L2 products are in netCDF format, and currently Aerosol Properties including optical thickness and angstrom exposition, and SST including day/night SST and nighttime SST are provided. SST algorithm is same as that is developing for SGLI on GCOM-C. Users also can look at browse images of Himawari-8 SSTs from the above web site (Figure 2).

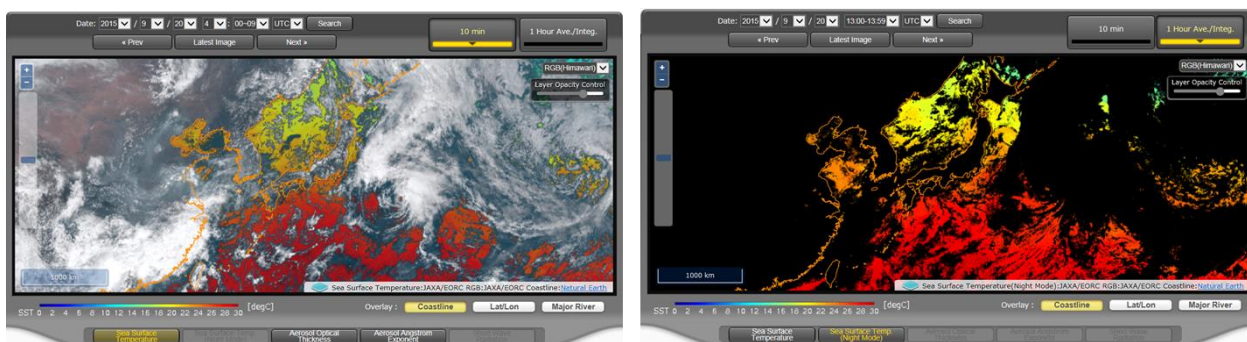


Figure 2. Sample of JAXA Himawari-8 Monitor web with day/night SST (10-minute) at 04:00UTC on September 20, 2015 (left) and nighttime SST (1-hour average) at 13UTC on September 20, 2015 (right).

3. Current status of JAXA GHRSSST Server

The JAXA GHRSSST server (<http://suzaku.eorc.jaxa.jp/GHRSSST/>) has been operating. Web site shows information of available SST products produced by JAXA, registration form to download data, and near-real-time monitor of products.

Simple registration is needed to access to password protected ftp site to download data. Several passive microwave imagers, such as AMSR2, AMSR-E, and NOAA's WindSat onboard the Coloris, and the Visible Infrared Scanner (VIRS) onboard the Tropical Rainfall Measuring Mission (TRMM) satellite are available. GMI 10-GHz SST was newly added since March 2015. L2P and L3C SST products of those instruments will be available in GDS 2.0 format. AMSR2, GMI and Windsat SSTs are provided both in near-real-time and standard (late) modes.

JAXA data policy regarding environmental satellite data, including GCOM and GPM, was changed in 2013 and accepts free distribution to third parties and commercial use without restriction, and products in JAXA GHRSSST server, except Himawari-8 products that follows JMA's data policy, can be provided to GDAC and LTSRF. Currently, we are working with GDAC how to establish data flow.

Himawari-8 SSTs are provided to users not from the JAXA GHRSSST server but from the JAXA's P-Tree system (<http://www.eorc.jaxa.jp/ptree>) along with the other Himawari-8 products. Himawari-8 SST products follow GDS2.0 format and in 2km resolution in Full Disk area. Day/night SST has both L2P (10-minute intervals) and L3C (1-hour average) products. Nighttime SST has only L3C (1-hour average) product. Utilization of Himawari-8 products including SSTs are limited to non-profit purposes only due to the JMA's data policy.

4. Activities and Plan for 2015-2019

Currently, we're planning following activities during 2015 and 2019 as shown in Table 4.

Year	Activities and plans
2015	Update of AMSR2 SST algorithm Release of GMI SST data to public Release of Himawari-8 SST data to public Release of AMSR2 10-GHz SST data to public Establish connection between JAXA GHRSSST server and GDAC
2016	Release of AMSR-E SST processed by AMSR2 algorithm Update of GMI SST algorithm
2017	Launch of GCOM-C satellite Update of AMSR2 SST algorithm Update of Himawari-8 SST algorithm
2018	Release of SGLI data products to public (TBD) Addition of SGLI SST to JAXA GHRSSST server (TBD)
2019 or later	Launch of AMSR2 follow-on (TBD)

Table 4. List of JAXA activities and plans from 2015 to 2019

Conclusion

Activities and future plans of JAXA are described. Both of GCOM-W satellite and AMSR2 instruments are in good condition after the launch in May 2012, and their performances are excellent. All AMSR2 standard products were updated to Version 2 in March 2015 and distributed through the GCOM-W Data Providing Service System (<https://gcom-w1.jaxa.jp>). AMSR2 10-GHz SST is accepted as one of eight research products in March 2015, and included in the AMSR2 standard SST product as complementary information.

The GPM Core Observatory and its instruments are also in good condition after the launch in February 2014. All GPM standard products are released to public in September 2014 through the JAXA G-Portal (<http://www.gportal.jaxa.jp/>) and also from NASA PPS. JAXA has developed GMI SST algorithm applying AMSR2 10-GHz SST algorithm, and distributed data through the JAXA GHRSSST server since March 2015.

Himawari-8 SST products produced by JAXA as well as JMA's Himawari-8 L1 products and other JAXA-produced L2 products have been distributed from the JAXA P-Tree system (<http://www.eorc.jaxa.jp/ptree>) since August 31, 2015, based on agreement between JAXA and JMA. Himawari-8 SST L2P product is distributed in GDS2.0 format with 2km resolution and 10-minute intervals. We also produce L3C products in 1-hour average for day/night SST and nighttime SST.

JAXA GHRSSST server (<http://suzaku.eorc.jaxa.jp/GHRSSST/>) currently distributes SST data from AMSR2, Windsat, VIRS and GMI in GDS 2.0 format. In corresponding to change of JAXA data policy accepting distribution of JAXA products, except Himawari-8 products, from GDAC and LTSRF, we started coordination with GDAC to establish data flow.

PLENARY SESSION II – REVIEW OF ACTIVITIES II

SESSION REPORT

Chair: Anne O'Carroll⁽¹⁾, Rapporteur: Ioanna Karagali⁽²⁾

(1) EUMETSAT, Darmstadt, Germany, Email: Anne.Ocarroll@eumetsat.int
(2) DTU Wind Energy, Risø Campus, Roskilde, Denmark, Email: ioka@dtu.dk

1. RDAC JMA: Masakazu Higaki

Main activities

- *MGDSST in GDS2 in preparation, expected release date 2015*
- *Improvement of MGDSST: plan for new sat data VIIRS and MetOp-B, shorter timescale AMSR2*
- *Regional analysis development using MTSAT SST, plan to use HIMAWARI 8*
- *HIMAWARI 8 L3 being prepared*

MGDSST specs:

- *Global, 0.25 deg, daily, L4*
- *Input data NOAA18,19, METOPA, AMSR2, windsat, in situ*
- *Prompt and delayed analysis and reanalysis*

Regional SST analysis

- *Western pacific, 1/10 deg, daily (MTSAT, AMSR2, in situ)*
- *Comparison with MGDSST shows that SST analysis has sharper SST gradient*

Transition from MTSAT to HIMAWARI8 (more frequent obs, better resolution), HIM8 is operational, will observe 15 years

MTSAT1/HIM8 L3 SST > MTSAT2 produced, planning for HIM8 L3 SST

2. RDAC Met Office: Simon Good

NRT products with full operational support (OSTIA L4, GMPE, diurnal analysis, seasonal and monthly OSTIA)

Reprocessing products (ESA SST CCI, HadISST, HadSST, HadIOD, reanalysis using OSTIA)

Dissemination of GHRSSST products (to GDAC via ftp, Copernicus Marine Environment Monitoring Service, CMEMS for GMPE, diurnal, OSTIA bias and anomaly)

Reprocessing of products (ESA SST CCI L4, OSTIA reanalysis, HADISST1, HADIOD)

GHRSSST data inputs (NRT feeds for OSTIA from PODAAC and data producers, for GMPE from PODAAC)

Main activities since GHRSSST XV:

- *Diurnal SST analysis operational: hourly SST_{skin}*
- *Validation of diurnal analysis using Argo*
- *Assess Argo network for validation of SST analyses*
- *Workshop on Uncertainties*
- *Update SST CCI User Requirements Doc*
- *Currently: Climate Assessment Report for CCI*
- *Update assimilation code used by OSTIA*
- *NRT GMPE operational*
- *Operational activities in super computer*
- *Efficiency of sat data pre processing*
- *Testing new sat data in OSTIA*
- *HadSST uses buoys as reference*
- *Update method of uncertainty calculation in HadSST*
- *New version of HadISST (CCI AVHRR, ARC ATSR): larger analysis ensemble*
- *New version HadIOD (1850-2014)*

3. RDAC NASA: Jorge Vasquez

Physical Oceanography main focus: support PO missions in orbit and in development, studies related to missions

NASA GHRSSST support: all GDAC activities, MISST, funded datasets

Current missions (MODIS, VIIRS, AMSR2, GMI) and future (HYSPIRI)

Support and Overview (evolution of GHRSSST)

- *MUR users/volume GB by month about 200 users/month but increasing trend)*
- *MODIS2: stable trend, lower amount of users*
- *Increase of users for AVHRR_OI but less volume GB due to lower resolution*

Messages

- *Use such statistics for maintained GHRSSST products, MUR most popular*
- *Continuous support of NASA to GHRSSST*

4. RDAC NAVO: Keith Willis

L2P production (NOAA, MetOp A/B, VIIRS) in GDS2

L2P Input data, output file content (new version VIIRSS has land/sea flag using method of Sasa)

List of statistics for L2P

10 km L4 NAVOCEANO (updated 4 times/daily)

User statistics (people still get v1 data even though are turned off)

VIIRS SST v2 (upgrades: 10km from 100km in daily climatology, improved cloud mask, full swath processing, etc), v2 shows improved coverage

Accomplishments: update NAVO cloud mask, etc

Future Plans

- *Improvements to cloud mask*
- *Use Pathfinder SST climatology*
- *Ice data in 10km L4*
- *Obtain Sentinel 3 L2P*
- *10km L4 SST in GDS2*

5. RDAC NOAA/ACSP0: Alexander Ignatov

Update on processing system: 2 regional data assembly centers (OSPO-operational and STAR-research). Most of processing at STAR

List of products (operational, reanalysis, experimental)

Progress since GHRSSST XV: VIIRS in GDS2, AVHRR (transition to GDS2), HIMAWARI-8 (experimental), GOES-R (plan for cal/val support and experimental products)

VIIRS: 2 ACSP0 versions, underway a reanalysis, new versions next year (use pattern recognition where there is deviation from L4 but L4 is also wrong, rely on SST). L2P and L3U validation show same standard deviation

HIMAWARI 8: experimental product, diagnostics in SQUAM. Next year: improve clear sky mask, experimental L3 product. More conservative cloud mask

AVHRR: 2 versions, new SSES, only 2 sensors at a time (1 day, 1 night)

Topics for discussion: help with archival of ACSP0 within GHRSSST, discuss with users testing ACSP0 in L4 analyses, Users feedback on future ACSP0 development, Annual JPSS meeting

6. RDAC NOAA/NESDIS/STAR: Eileen Maturi

Operational GHRSSST products in GDS2 (MSG-3 to be replaced by 4)

Geostationary Improvements: in Radiative Transfer, Bayesian Cloud mask, matchup data in netCDF

SST retrievals using Physical Retrieval Methodology

5 km Blended Analysis: 1/20 deg, paper in BAMS, with polar and geo, improvements (replace reference NCEP RTG with OSTIA). Product accuracy, mean bias -0.03 K

Reprocessing geo-polar blended SST (from 1994-when GOES/A started to 2015)

Applications:

- *Coral reef watch product originally depended on AVHRR only. Now based on the 5km SST analysis: much greater precision but climatology is not derived from the same dataset.*
 - *Oceanic Heat Content for various basins*
-

7. RDAC NOAA/NCEI: Ken Casey

NCEI RDAC Update: Summary of datasets (Pathfinder 5.2, working on 5.3 L2P, CoRTAD version 5), processing on Amazon Web Services. Planning on quarterly updates.

Improvements of Pathfinder V5.3 (identify anomalous periods in different regions)

Daily OISST L2 v2 (working towards higher resolution OI mapped to same grid as Pathfinder), match-ups and coefficients from Bob Evans.

Collect statistics for L2P

Service Level Agreement for delivery of Pathfinder within Copernicus could be discussed.

8. RDAC REMO: Gutemberg França

SST analysis 0.05deg, August 2002-March 2015, for a specific area (oil producing): validation with buoys

New SST product from March 2015 up to now, bias correction processing

Observing System Experiments: SST, SLA and Argo assimilation and impact of SST in HYCOM

- *High impact of SST in specific regions: Malvinas and Newfoundland*

9. RDAC RSS: Chelle Gentemann

In GDS2 (NRT and reprocessed)

WindSAT: indications that is failing

Issues: should optional variables be removed from GHRSSST files?

Validation of GPM GMI: good statistics of v7GMI despite it is not fine-tuned (but no temperature below 12 degrees used), statistics get bad under 12 degrees, how to flag bad data?

Helen Beggs pointed out that producers maybe should not decide to remove flagged data, because users not always care about accuracy (example SST quality flag 2 used for mapping currents from users)

RDAC UPDATE: JMA

**Masakazu Higaki⁽¹⁾, Shiro Ishizaki⁽²⁾, Toshiyuki Sakurai⁽¹⁾, Mika Kimura⁽¹⁾, Akiko Shoji⁽¹⁾,
 and Yoshiaki Kanno⁽¹⁾**

(1) *Office of Marine Prediction, Japan Meteorological Agency, Tokyo (Japan),
 Email: m-higaki@naps.kishou.go.jp*
 (2) *Sapporo District Meteorological Observatory, JMA, Sapporo (Japan)*

ABSTRACT

This report describes the recent activities of Japan Meteorological Agency (JMA) related to GHRSSST. The highlights include: (1) JMA launched its new-generation geostationary meteorological satellite, Himawari-8, in October 2014, and started its operation in July 2015. The L3 SST product of Himawari-8 is being prepared. (2) JMA continues the improvement of its global L4 SST analysis, MGDSST, and the development of a new regional SST analysis by utilizing MTSAT/Himawari SST products. (3) The GDS 2.0 implementation of MGDSST is ongoing.

1. Introduction

Japan Meteorological Agency (JMA) is the National Hydrological-Meteorological Service (NHMS) of Japan, and focuses its efforts on monitoring the earth's environment and forecasting natural phenomena related to the atmosphere, the oceans and the earth. In this line, it has operated a series of meteorological geostationary satellites, and also provides oceanographic information including SST. In this report, we describe the main activities related to SST since GHRSSST XV.

2. Himawari-8 and its SST product

JMA has operated a series of geostationary meteorological satellites that observe the East Asia and Western Pacific Region, contributing to the space-based global observation system. Himawari-8 is the latest satellite of the series and the world's first next-generation geostationary meteorological satellite. It was launched on 7 October 2014, and started operation at 02 UTC on 7 July 2015, replacing its predecessor, MTSAT-2. In addition, Himawari-9 is scheduled to be launched in JFY2016. These two satellites, Himawari-8 and -9 will observe the East Asia and Western Pacific regions for a period of 15 years (Figure 1).

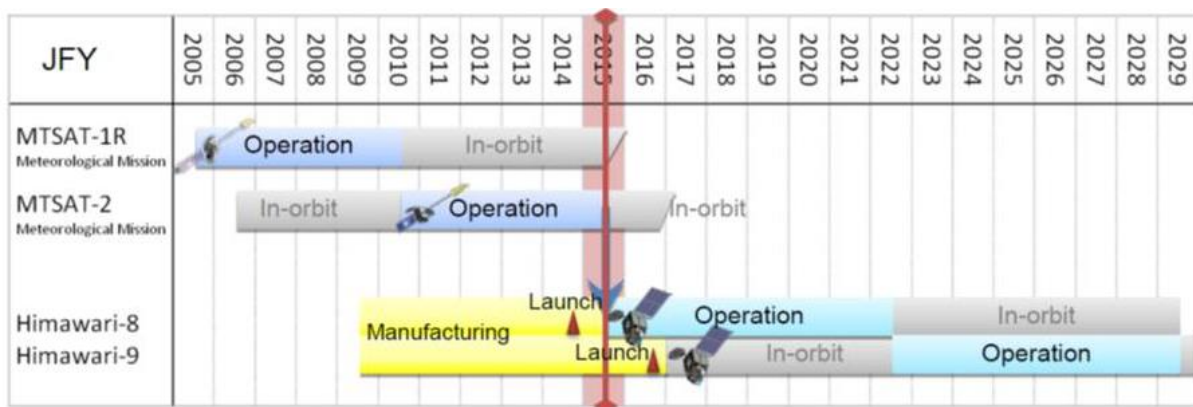


Figure 1: Schedule of JMA's geostationary meteorological satellites: MTSAT-1R/2 and Himawari-8/9.

Himawari-8 and -9 are equipped with highly improved Advanced Himawari Imagers (AHI), which have 16 observation bands (3 for visible, 3 for near-infrared, and 10 for infrared), while the MTSAT series have five bands. The horizontal resolution of Himawari-8/9 is also enhanced to 0.5 – 1 km for VIS, and 1 – 2 km for IR,

approximately twice those of its predecessor. Furthermore, Himawari-8 observes the full disk of the Earth with a repeat cycle of 10 minutes, while MTSAT does with a cycle of 30 minutes. Those enhancements enable Himawari-8 to provide more detailed information on atmosphere, ocean, and land than MTSAT did.

3. L3 SST products of MTSAT-2 and Himawari-8

Meteorological Satellite Center (MSC) of JMA produces L3 SST by using the observation of MTSAT-2 on a routine basis, at this writing. It is based on 1D-VAR retrieval algorithm of Kurihara (2012), which includes single layer radiative transfer calculation in order to take into account effects of water vapor absorption and sea surface emissivity. The L3 SST is produced hourly with 0.04-degree horizontal resolution, and the coverage of 60S – 60N, 80E – 160W. Following the commencement of the Himawari-8 operation, MSC/JMA is now preparing a new L3 SST product derived from Himawari-8 observation. The horizontal resolution of Himawari-8 L3 SST will be enhanced by 0.02-degree, by taking advantage of the enhanced horizontal resolution of Himawari-8 AMI. The other specifications such as spatial coverage and data frequency are identical to those of MTSAT L3 SST. The production of Himawari-8 L3 SST is planned to start soon.

4. Current Status of MGDSST

JMA has operated an SST analysis system to generate global daily SST data (Merged satellite and in-situ data Global Daily Sea Surface Temperature: MGDSST) on a routine basis since 2005. The system adopts an optimal interpolation (OI) method which considers not only spatial correlation but also temporal correlation. It produces 0.25° resolution, daily global SST analysis, using both satellite and in-situ SST observation. The satellite data currently ingested to MGDSST are: AVHRR SST (NOAA-18, NOAA-19 and MetOp-A), WindSat SST and AMSR2 SST. MGDSST is used in various operational systems in JMA. In the regional ocean data assimilation system (MOVE/MRI.COM-WNP; Usui et al., 2006), MGDSST is used as observation data. It is also used as lower boundary conditions in numerical weather prediction (NWP) models at JMA. Since long term, consistent time series of the SST analysis is needed for climate research, JMA also conducted the reanalysis of MGDSST for the 1982 – 2006 period using AVHRR Pathfinder Version 5.0/5.1 SST and AQUA/AMSR-E SST.

Those data are available through the North-East Asian Regional GOOS (NEAR-GOOS) Regional Real Time Database (RRTDB): <http://ds.data.jma.go.jp/gmd/goos/data/database.html>. Note that the URL of the website has been changed since October 2014. Currently, the data come with text format, not GDS 2.0. However, we are preparing the GDS 2.0 implementation of MGDSST, to facilitate the use of JMA's SST products in GHRSSST activities. Recently, we have made a program to convert MGDSST into GDS2.0 and sample data files. The metadata parameters like center name and product name, and the file name of the data set (which would be "201509010600-JMA-L4_GHRSSST-SSTfnd-MGDSST-GLOB-v02.0-fv01.0.nc") need to be determined and registered to GDS 2.0 Specification. JMA will take procedures needed to release the data set during the intersessional period of GHRSSST ST.

To improve MGDSST, several developments are planned in JMA. One is introducing new satellite data such as ACSPO VIIRS and MetOp-B. Recently we started the routine data acquisition of ACSPO VIIRS, and are accumulating the data in order to calculate the statistics required for the OI in MGDSST analysis. We are also considering the use of the shorter timescale (10- to 27-day) components from AMSR2 observation for better temporal response in MGDSST.

5. Regional SST analysis with MTSAT/Himawari-8 SST

Although MGDSST meets various kinds of needs such as the boundary condition for ocean data assimilation system and NWP models, SST analyses with a higher resolution are expected to provide better information to such applications. Therefore, JMA is now developing a regional high resolution (0.1°) SST analysis system for the western North Pacific region. Its analysis framework is based on that of MGDSST. In addition to the satellite data used in MGDSST, the components of smaller spatio-temporal scale derived from MTSAT L3 SST product are ingested to the regional analysis (Figure 2).

The regional SST analysis is still under development and we are examining its performance by conducting several kinds of verifications. Figure 3 is an example of such verifications, and shows the SST gradients calculated from MGDSST (left) and the regional analysis (right) in the same manner as in Martin et al (2012). The regional SST analysis shows sharper SST gradients than those of MGDSST because of its higher grid resolution and the use of short wavelength components from MTSAT.

6. Conclusion

The recent activities of JMA related to GHRSSST are summarized. Himawari-8, JMA's new geostationary meteorological satellite, is now operational, and its L3 SST product is being prepared. JMA plans to improve MGDSST by introducing new satellite data, and is also developing a regional SST analysis by taking advantage of MTSAT/Himawari L3 SST. The GDS 2.0 implementation of MGDSST is also ongoing.

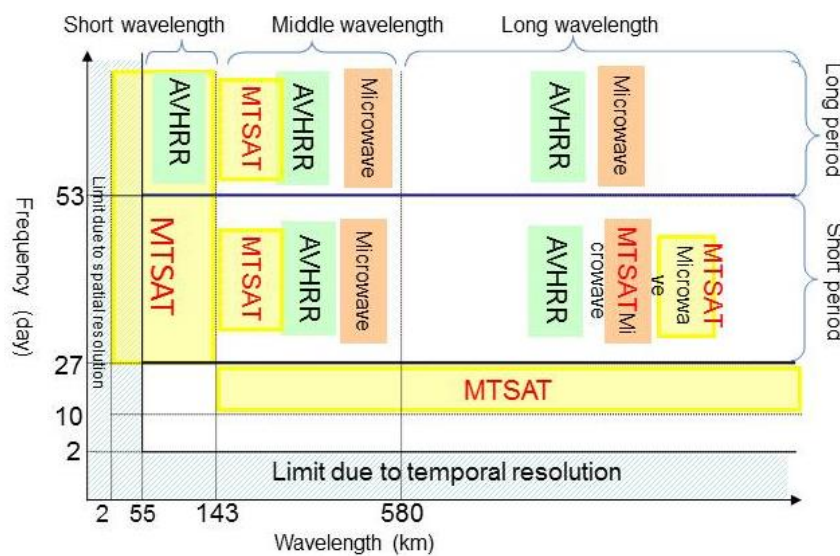


Figure 2: Spacio-temporal decomposition in JMA's SST analysis. Yellow boxes indicate the components which are derived from MTSAT observation and to be added to the regional SST analysis.

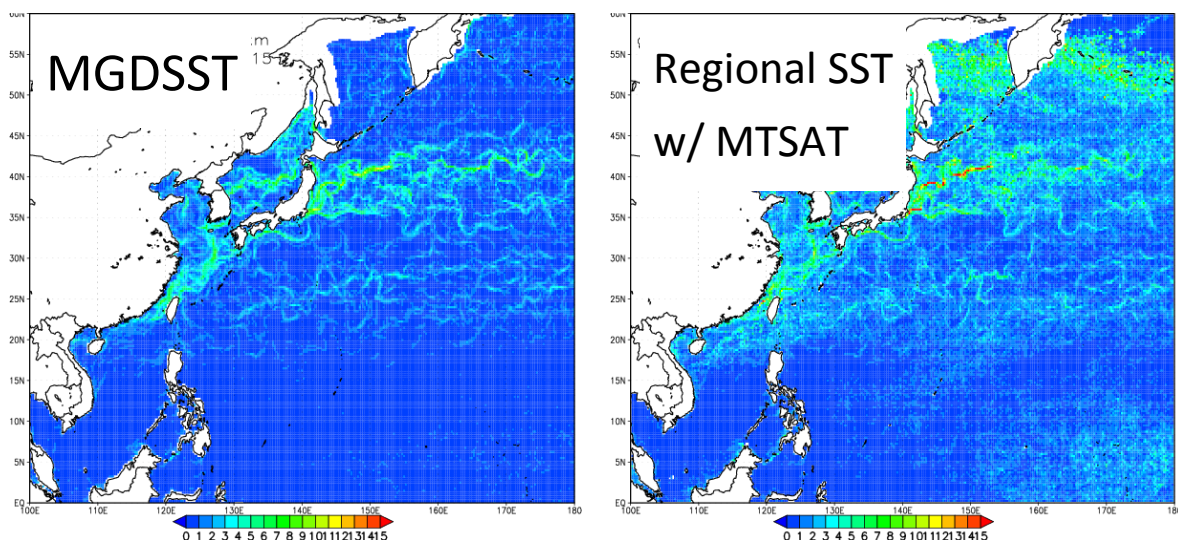


Figure 4: Comparison of SST gradients (left: MGDSST, right: regional analysis).

7. References

- Kurihara, Y., Optimal estimation technique for SST from MTSAT-2, Presented to the 13th GHRSSST science team meeting, Tokyo, Japan, 5-8th July, 2012.
- Martin, M., P. Dash, A. Ignatov, V. Banzon, H. Beggs, B. Brasnett, JF Cayula, J. Cummings, C. Donlon, C. Gentemann, R. Grumbine, S. Ishizaki, E. Maturi, R. Reynolds and J. Roberts-Jones, Group for High Resolution Sea Surface temperature (GHRSSST) analysis fields inter-comparisons. Part 1: A GHRSSST multi-product ensemble (GMPE), *Deep Sea Research Part II: Topical Studies in Oceanography*, 77–80, 21–30, doi:10.1016/j.dsr2.2012.04.013. 2012.
- Usui, N., S. Ishizaki, Y. Fujii, H. Tsujino, T. Yasuda and M. Kamachi, Meteorological Research Institute multivariate ocean variational estimation (MOVE) system : Some early results. *Advances in Space Research*, 37, 806-822, 2006.

RDAC UPDATE: UK MET OFFICE

Simon Good, Jonah Roberts-Jones, Emma Fiedler, Chongyuan Mao, John Kennedy, Chris Atkinson, Nick Rayner, James While

Met Office, Exeter, UK, Email: simon.good@metoffice.gov.uk

ABSTRACT

Met Office products related to GHRSSST include: the Operational Sea Surface Temperature and Sea Ice Analysis (OSTIA) foundation SST analyses; the OSTIA diurnal hourly average skin SSTs; the GHRSSST Multi-Product Ensemble (GMPE) and climate datasets such HadSST, HadISST and HadIOD (the Met Office Hadley Centre's SST, interpolated Ice and SST and Integrated Ocean Database).

Activities since the last GHRSSST science team meeting have included transitioning the GMPE and OSTIA diurnal systems to operational production, porting of the suites to a new supercomputer, assessment and use of Argo data to validate SST analyses and improvements to the Met Office Hadley Centre's climate datasets.

1. Introduction

At the Met Office, a range of products are produced that are relevant to GHRSSST. In near real time the Operational Sea Surface Temperature and Sea Ice Analysis (OSTIA) is produced. This is a gap-free global gridded foundation SST product on a 0.05° grid and is produced daily (Donlon et al., 2012). Associated products include estimates of biases relative to reference instruments and monthly and seasonal averages. Also produced daily are hourly average skin SSTs produced by combining the OSTIA foundation SST with a 'warm layer' model (which assimilates satellite SSTs) and a cool skin model. This was described in a separate presentation at the GHRSSST meeting by James While. The GHRSSST Multi-Product Ensemble (Martin et al., 2012) takes various level 4 analyses as its input, places them on a common grid and produces files containing, amongst other things, the median and standard deviation of the ensemble. All these products are available through the Copernicus Marine Environment Monitoring Service (CMEMS; <http://marine.copernicus.eu/>). The OSTIA foundation analyses are also available via the GHRSSST GDAC.

Reprocessed/climate dataset are also produced at the Met Office. There is a reprocessed version of OSTIA covering 1985-2007 (Roberts-Jones et al., 2012) available from CMEMS. More recently, analyses produced as part of the ESA SST Climate Change Initiative project (Merchant et al., 2014) have been made available via the UK's NERC (Natural Environment Research Council (NERC) Earth Observation Data Centre (NEODC) (<http://neodc.nerc.ac.uk>). Long (>100 year) climate datasets are produced by the Met Office Hadley Centre: HadISST (the Hadley Centre Sea Ice and SST reconstructions; Rayner et al., 2003), HadSST (non-interpolated gridded data which uses an ensemble to represent uncertainty; Kennedy et al. 2011 a and b) and HadIOD (the Hadley Centre Integrated Ocean Database which includes both surface and subsurface observations; Atkinson et al. 2014). Data are available from www.metoffice.gov.uk/hadobs except HadIOD (which can be made available on request). Note also that a more recent version of HadISST is also available on request.

2. Activities since GHRSSST-XV

A brief summary of the activities at the Met Office since the last science team meeting relevant to GHRSSST is given below. Where indicated more detail is available in other talks and posters.

A variety of technical developments have taken place at the Met Office over the past year. Progress has been made towards updating the data assimilation code used to produce the OSTIA foundation SST analysis. The aim is to move to using a variational data assimilation scheme (NEMOVAR) in place of the current optimal-interpolation-like scheme. A demonstration system is running operationally but is not yet ready to disseminate products.

Over the summer the Met Office transitioned to using a new Cray supercomputer. This necessitated work to port the processing suites used to produce the GHRSSST products onto the new system. Work is also underway

to improve the efficiency of our code to pre-process incoming satellite data in preparation for new data streams such as from the Sea and Land Surface Temperature Radiometer (SLSTR).

The GMPE and OSTIA diurnal SST analyses are now running within operational suites at the Met Office, which means that they enjoy 24 hour per day support. Products are delivered daily to users via CMEMS. A description of the diurnal system was given in the talk by James While at the science team meeting. Validation of the diurnal analyses is being performed using near surface Argo data, as described in the poster by Chongyuan Mao.

Under the E-AIMS (Euro-Argo Improvements for the Marine Service) project, the Argo network has been assessed for its suitability in validating SST analyses. This was described in the poster 'Uncertainties in validation of SST analyses using near-surface Argo observations' by Emma Fiedler. Plots of validation statistics for the GMPE system using Argo data can be viewed at http://ghrsst-pp.metoffice.com/pages/latest_analysis/sst_monitor/argo/.

Evaluation has been taking place of data types with the aim of including these within OSTIA. This evaluation yields various statistics that may be of interest to data providers.

As part of the ESA SST CCI project a user workshop on uncertainties was hosted at the Met Office in November 2014. This was described at the science team meeting in a poster by Nick Rayner; more information can be found at <https://eos.org/meeting-reports/communicating-uncertainties-in-sea-surface-temperature> (for a summary) or <http://www.esa-sst-cci.org/PUG/workshop.htm> (for a full report).

Work has also progressed on the Met Office Hadley Centre's climate datasets. HadSST was updated to use buoys as its reference, which required an update to the method to calculate the uncertainty in the dataset. There is ongoing work to calculate biases for individual ships while retaining independence of the dataset from satellite data. There is a new version of HadISST2 based on ESA SST CCI AVHRR data and ARC (ATSR Reprocessing for Climate) ATSR data. Improvements to HadISST's interpolation scheme and the use of the new HadSST ensemble will allow the generation of a larger HadISST2 ensemble to represent uncertainty. HadIOD was updated to cover 1850-2014 and a monthly update cycle is planned.

3. Conclusion

GHRSSST related activities at the Met Office since the last science team meeting have included:

- Technical developments aimed at transitioning the OSTIA system to use the NEMOVAR data assimilation scheme.
- Porting of our operational systems to a new Cray supercomputer.
- Work on improving the efficiency of our code to pre-process satellite observations.
- Transition of GMPE and the OSTIA diurnal system into operational suites.
- Assessment and use of Argo data for validating SST analyses.
- Evaluation of new data to include in OSTIA.
- Hosting of a user workshop on uncertainties in SST data as part of the ESA SST CCI project.
- Improvements to the Met Office Hadley Centre's marine climate datasets.

4. References

Atkinson, C. P., N. A. Rayner, J. J. Kennedy, and S. A. Good (2014), An integrated database of ocean temperature and salinity observations, *J. Geophys. Res. Oceans*, **119**, 7139–7163, doi:10.1002/2014JC010053.

Donlon, C. J., M. Martin, J. Stark, J. Roberts-Jones, E. Fiedler and W. Wimmer, (2012), The Operational Sea Surface Temperature and Sea Ice Analysis (OSTIA) system, *Remote Sensing of Environment* **116**, 140-158

Kennedy J.J., Rayner, N.A., Smith, R.O., Saunby, M. and Parker, D.E. (2011a). Reassessing biases and other uncertainties in sea-surface temperature observations since 1850 part 1: measurement and sampling errors. *J. Geophys. Res.*, **116**, D14103, doi:10.1029/2010JD015218 (PDF 1Mb)

Kennedy J.J., Rayner, N.A., Smith, R.O., Saunby, M. and Parker, D.E. (2011b). Reassessing biases and other uncertainties in sea-surface temperature observations since 1850 part 2: biases and homogenisation. *J. Geophys. Res.*, **116**, D14104, doi:10.1029/2010JD015220 (PDF 1Mb) Martin, M. et al., (2012), Group for High Resolution Sea Surface temperature (GHRSSST) analysis fields inter-comparisons. Part 1: A GHRSSST multi-product ensemble (GMPE), *Deep Sea Research II*, **77-80**, 21-30

Merchant, C. J., O. Embury, J. Roberts-Jones, E. Fiedler., C. E. Bulgin, G. K. Corlett, S. Good, A. McLaren, N. Rayner, S. Morak-Bozzo, and C. Donlon, (2014), Sea surface temperature datasets for climate applications from Phase 1 of the European Space Agency Climate Change Initiative (SST CCI). *Geoscience Data Journal*, **1**: 179–191. doi: 10.1002/gdj3.20

Rayner, N. A.; Parker, D. E.; Horton, E. B.; Folland, C. K.; Alexander, L. V.; Rowell, D. P.; Kent, E. C.; Kaplan, A. (2003) Global analyses of sea surface temperature, sea ice, and night marine air temperature since the late nineteenth century *J. Geophys. Res.* Vol. **108**, No. D14, 4407 10.1029/2002JD002670

Roberts-Jones, J., E. K. Fiedler, M. J. Martin, (2012), Daily, global, high-resolution SST and sea ice reanalysis for 1985-2007 using the OSTIA system, *Journal of Climate*, **25**, 6215-6232.

ACSPO SST PRODUCTS AT NOAA: UPDATE FOR GHRSSST-XVI

Alexander Ignatov⁽¹⁾, John Stroup⁽²⁾, Yury Kihai⁽³⁾, Boris Petrenko⁽⁴⁾, Prasanjit Dash⁽⁵⁾,
Irina Gladkova⁽⁶⁾, Maxim Kramar⁽⁷⁾, Xinjia Zhou⁽⁸⁾, Xingming Liang⁽⁹⁾, John Sapper⁽¹⁰⁾,
Yaoxian Huang⁽¹¹⁾, Yanni Ding⁽¹²⁾, Feng Xu⁽¹³⁾, Kai He⁽¹⁴⁾, Marouan Bouali⁽¹⁵⁾, Karlis Mikelsons⁽¹⁶⁾

(1) NOAA STAR, USA, Email: Alex.Ignatov@noaa.gov

(2) NOAA STAR and STG, Inc, USA, Email: John.Stroup@noaa.gov

(3) NOAA STAR and GST, Inc, USA, Email: Yury.Kihai@noaa.gov

(4) NOAA STAR and GST, Inc, USA, Email: Boris.Petrenko@noaa.gov

(5) NOAA STAR and CSU CIRA, USA, Email: Prasanjit.Dash@noaa.gov

(6) NOAA STAR, CUNY and GST, Inc, USA, Email: Irina.Gladkova@gmail.com

(7) NOAA STAR and GST, Inc, USA, Email: Maxim.Kramar@noaa.gov

(8) NOAA STAR and CSU CIRA, Inc, USA, Email: Xinjia.Zhou@noaa.gov

(9) NOAA STAR and CSU CIRA, USA, Email: Xingming.Liang@noaa.gov

(10) NOAA OSPO, USA, Email: John.Sapper@noaa.gov

(11) NOAA STAR and CSU CIRA, USA, Email: Yaoxian.Huang@noaa.gov

(12) NOAA STAR and CSU CIRA, USA, Email: Yanni.Ding@noaa.gov

(13) NOAA STAR, Fudan Univ. and GST Inc, USA/China, Email: Feng.Xu@noaa.gov

(14) NOAA STAR and GST, Inc, USA, Email: Kai.He@noaa.gov

(15) NOAA STAR, CSU CIRA and San Paolo Univ., USA and Brazil, Email: Marouan.Bouali@noaa.gov

(16) NOAA STAR and GST Inc, USA, Email: Karlis.Mikelsons@noaa.gov

ABSTRACT

The Advanced Clear Sky Processor for Ocean (ACSPO) is the NOAA enterprise SST retrieval system. ACSPO is currently used to generate operational AVHRR products from NOAA GAC and Metop FRAC, and from S-NPP VIIRS. Experimental L2 SSTs are produced from Himawari-8 AHI and from two MODISs onboard Terra and Aqua. Preparations are made for two new launches – GOES-R in 2016 and JPSS-1 in 2017. Two reprocessing efforts are underway: S-NPP VIIRS (from Jan 2012 – pr) and AVHRR GAC (from 2002 – pr).

Two ACSPO versions were implemented since GHRSSST-15, v2.31 and v2.40. V2.31 fixed cloud leakages from low stratus, particularly noticeable in the high latitudes. V2.40: 1) introduced a new SSES in ACSPO (see Petrenko et al., this meeting); 2) implemented destriping of VIIRS and MODIS BTs; and 3) generated a new Level 3 uncollated (L3U) product. Work toward v2.50 and v2.60 is underway. V2.50 will improve VIIRS and MODIS SST imagery, and v2.60 will explore it to enhance the ACSPO clear-sky mask (particularly, in the dynamic, coastal, and high latitude regions), and to generate a new SST frontal product.

The ACSPO VIIRS SST product is used in the NOAA geo-polar blended and in the Canadian Met Centre L4 analyses. It is also explored at UK MO, Australian BoM, and JMA as input in the corresponding OSTIA, GAMSSA and MGDSSST L4 analyses. ACSPO AVHRR GAC data from 2013-2015 were requested by U. Maryland ocean analysis group, for the use in their assimilation.

1. Two NOAA RDACs: OSPO and STAR

This report discusses the status of ACSPO products at the two Regional Data Assembly Centers (RDACs) at NOAA NESDIS: the Center for Satellite Applications and Research (STAR; research arm of NESDIS), and the Office of Satellite Products and Operations (OSPO; operational arm of NESDIS). Operational ACSPO products are produced at OSPO whereas experimental and reprocessed products are produced at STAR.

Typical file names produced by the ACSPO system look like this

20150712000000-OSPO-L3U_GHRSSST-SSTskin-VIIRS_NPP-ACSPO_V2.40_0.02-v02.0-fv01.0.nc

20150711000000-STAR-L2P_GHRSSST-SSTskin-AHI_H08-ACSPO_V2.41b02-v02.0-fv01.0.nc

The 1st file is a 10min L3U VIIRS granule operationally produced by ACSPO v2.40 at OSPO. The 2nd file is a full disk L2P file experimentally produced at STAR by ACSPO 2.41b02 (beta02 of the ACSPO v2.41, which is currently under development and testing).

2. S-NPP VIIRS

Figure 1 shows a time series of ACSPO VIIRS validation statistics, against *i*Quam drifters (see Ignatov et al., this meeting). The retrievals are generally well within specs (shown by horizontal lines superimposed on the graphs), excepting very early in the mission. Also, regular periodic outliers are observed once a quarter caused by the warm-up cool-down (WUCD) exercises performed by the NASA VIIRS Calibration Team. Time series are more stable and regular in the last year, due to ACSPO processing improvements. Reprocessing is underway to generate a consistent time series from 20 Jan 2012 (the beginning of SST record) up to the present. Work is also in progress with the VIIRS calibration team to improve sensor performance during the WUCD events.

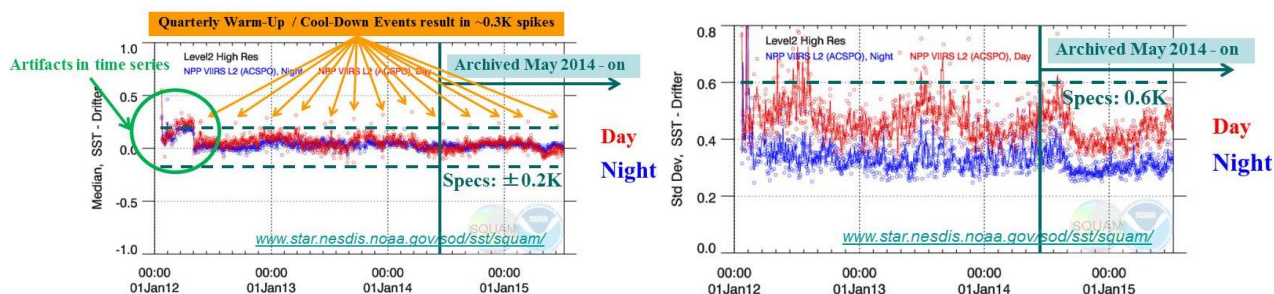


Figure 1: Time series of ACSPO VIIRS L2 SST minus *i*Quam drifters: (left) median bias, and (right) standard deviation.

Performance of the L3U product is comparable to that of L2P.

Note that the v2.30 L2P product has been archived at the PO.DAAC and at the NOAA Center for Environmental Information (NCEI) since May 2014, whereas the L3U product is only available from May 2015 (with implementation of v2.40). The links to ACSPO VIIRS SST are as follows

PO.DAAC

- http://podaac.jpl.nasa.gov/dataset/VIIRS_NPP-OSPO-L2P-v2.4 - L2P v2.40 (5/19/2015 - pr)
- http://podaac.jpl.nasa.gov/dataset/VIIRS_NPP-OSPO-L3U-v2.4 - L3U v2.40 (5/19/2015 - pr)
- http://podaac.jpl.nasa.gov/dataset/VIIRS_NPP-OSPO-L2P-v2.3 - L2P v2.30 (5/20/204 - 5/19/2015)

NCEI

- http://data.nodc.noaa.gov/cgi-bin/iso?id=gov.noaa.nodc:GHRSSST-VIIRS_NPP-OSPO-L2P - L2P
- http://data.nodc.noaa.gov/cgi-bin/iso?id=gov.noaa.nodc:GHRSSST-VIIRS_NPP-OSPO-L3U - L3U

Reprocessing of the full VIIRS SST record with ACSPO v2.40 is currently underway in conjunction with U. Wisconsin (Liam Gumley's group). Once reprocessed data are available, the corresponding directories will be populated and the community will be notified.

Work is also in progress on two new ACSPO versions, v2.50 and v2.60. The 1st one will improve the VIIRS SST imagery, by filling in bow-tie deleted areas and correcting the bow-tie distortions which become significant at the swath edges (Gladkova, et al., 2015a). The 2nd one will explore the new imagery to improve the ACSPO clear-sky mask and derive a new SST frontal product (Gladkova, et al., 2015b).

3. Himawari-8 (H8) AHI and preparation for GOES-R launch in 2016

An experimental H8 ACSPO L2P SST product has been generated at NOAA STAR beginning on 11 June 2015, in the original swath projection (2km at nadir; degrading towards swath edges) and at 10 minute intervals. The data are processed in near-real time in STAR using automated scripts, and posted at ftp://ftp.star.nesdis.noaa.gov/pub/sod/sst/acsपो_data/l2/ahi/. There are a total of 142 files per 24hr period (full disks at 0240 and 1440 UTC are missing due to service performed on AHI), with a total volume of ~45 GB/day. This data volume is challenging to archive and use for various applications. Work is underway to produce a smaller size L3 or L2C (collated in time) product.

Corresponding composite imagery including comparisons with VIIRS are also routinely generated and posted in the same directory, along with global and regional movies. Example of AHI vs. VIIRS nighttime composite is shown in Figure 2. The SST distribution is similar. Note that only 1-2 images per day contribute to the VIIRS composite, whereas in case of AHI, it may be up to 70 full-disk images. As a result, the coverage is somewhat superior in the AHI composite, due to multiple looks. Work is also underway to continuously monitor AHI SST in SQUAM (see Ignatov, et al, 2015).

Once reduced volume L3/L2C data is produced, the efforts will be directed at improving each element of the processing chain, including the ACSPO clear-sky mask and SST algorithms (currently, the regression SST is based on 8.6, 10.4, 11.2, and 12.3 μm , for consistency between day and night, and for smooth reproduction of the diurnal cycle). We will also explore improved L3/L2C compositing approaches, to best reduce the data while preserving the information content of the high spatial and temporal resolution of AHI SST.

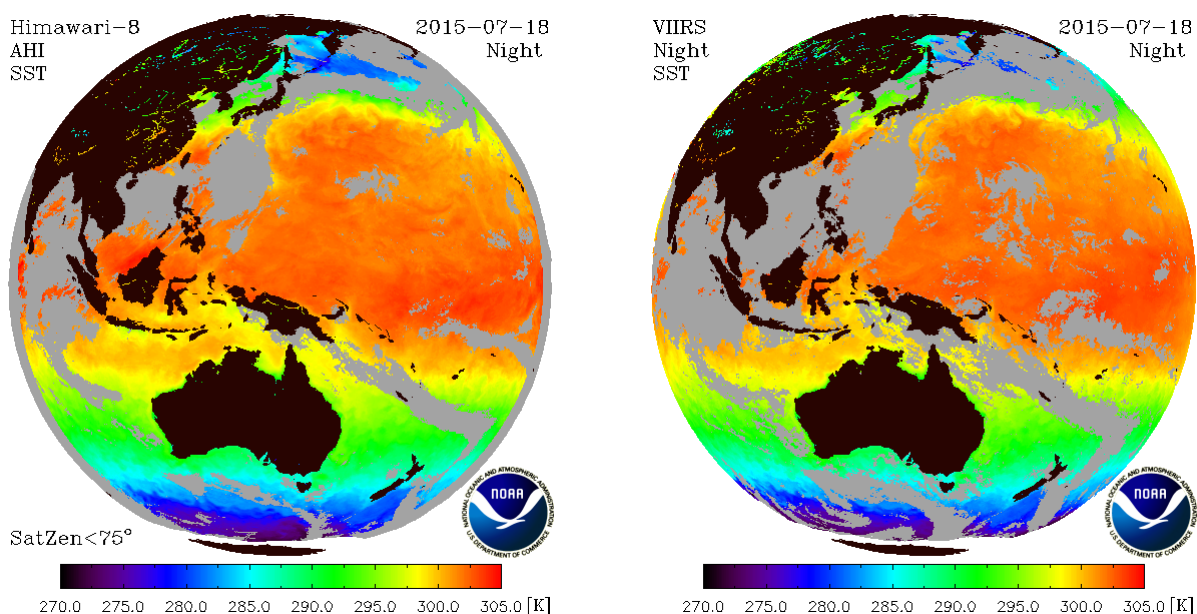


Figure 2: Night time composite SST images on 18 July 2015: (left) H8 AHI; (right) S-NPP VIIRS.

Work with Himawari-8 is directed at (1) replacement of the MTSAT2 product at NOAA which will be discontinued in December 2015, and (2) preparation for the late 2016 launch of GOES-R, which will carry the ABI onboard, an instrument nearly identical to the AHI aboard Himawari-8.

4. NOAA and METOP AVHRR

NOAA currently produces ACSPO SST products from several NOAA and Metop AVHRRs (in case of Metop for both GAC and FRAC). However, the product is generated in a heritage hdf4 format and is stored and accessed at NOAA CLASS. Work is underway to switch to GDS2 netcdf format, and start storing with

PO.DAAC and archiving at NCEI. Once that occurs, reprocessed GAC data from 2002-pr will be backfilled with AVHRR Reanalysis-1 (RAN1) reprocessed data, and the GHRSSST community notified.

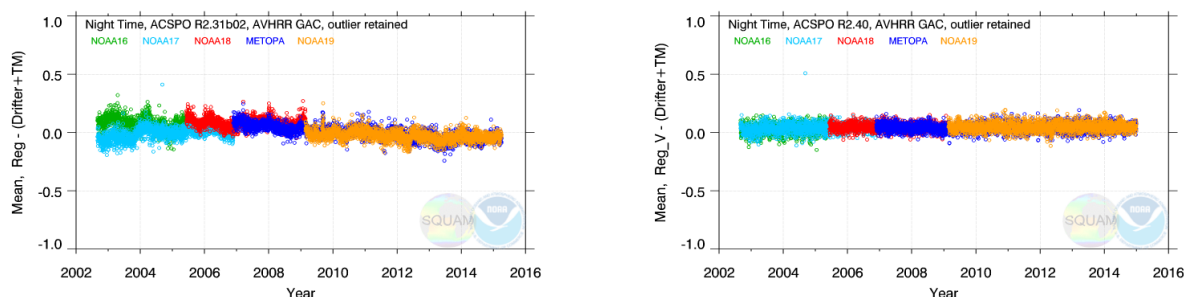


Figure 3: Time series of night time SST from ACSP0 RAN1 (left) fixed regression coefficients (right) variable coefficients.

Time series of ACSP0 RAN1 minus *i*Quam drifters is shown in Figure 3, using two methods of calculating the regression coefficients in the MCSST equation: fixed coefficients (calculated once and used for the mission of a satellite), and variable coefficients (calculated on each day using a 3-month moving window) (for more details, see Petrenko, et al., 2014a,b). Each data point represents a daily match-up statistic. Every day, the data from two platforms will be reported: one PM (a combination of NOAA16, 18 and 19), and one AM (a combination of NOAA17 and Metop-A). Work is underway with users at the U. Maryland to test out the data and perform sensitivity study to evaluate its information content.

5. Conclusion and Future Work

Progress is being made with the NOAA ACSP0 SST system, along several major priorities. First, new products requested by users (L3U) and functionalities (new SSES, producing of destriped imagery) are being added. Active efforts are being made to comprehensively test the Himawari-8 retrieval system, produce reduced size L3/L2C product from AHI/ABI with minimal information losses, and get ready for the GOES-R launch in 2016. Two reprocessing efforts, with VIIRS and AVHRR GAC, are underway. The ACSP0 AVHRR product is being converted to GDS2 format. Near-future ACSP0 work will be mostly directed at the improved SST imagery and its use to open up a larger SST domain, through using an improved clear-sky mask based on pattern recognition approaches. The improvements are expected to be most noticeable in the dynamic, coastal, and high-latitude areas of the ocean. A byproduct of the pattern recognition processing, SST fronts will be also produced and reported in the ACSP0 files. These improvements should be in place by the time the JPSS-1 satellite is up in 2017. As part of the US-European Joint Polar System agreement, NOAA will continue producing ACSP0 SST products from Metop-A and -B, and generate a new product from Metop-C following its planned launch in 2018.

6. References

- Gladkova, et al., Improved SST Imagery from VIIRS and MODIS, *Remote Sensing*, 2015a (in submission).
- Gladkova, et al., SST Pattern Test in ACSP0 clear-sky mask for VIIRS, *RSE*, **160**, 87-98, 2015b.
- Ignatov, et al., SQUAM and *i*Quam at NOAA: Update for GHRSSST-16, *this meeting*.
- Petrenko, et al., Redesigned SSES in ACSP0, *this meeting*.
- Petrenko, B., et al. (2014a), SST algorithms in ACSP0 reanalysis of AVHRR GAC data from 2002-2013, *Proc. SPIE911, Ocean Sensing and Monitoring VI*, 91110E (May 23, 2014); doi:10.1117/12.2053008.
- Petrenko, B., et al. (2014b), SST algorithms in ACSP0 reanalysis of AVHRR GAC data from 2002-2013, *Proc. GHRSSST-XV, Capetown, South Africa* (June 2-6, 2014), pp. 156-160

NOAA NATIONAL CENTERS FOR ENVIRONMENTAL INFORMATION (NCEI) RDAC

**Kenneth S. Casey, Viva Banzon, Korak Saha, Ajay Krishnan, Yuanjie Li, John Relph,
Dexin Zhang, Yongsheng Zhang, and Sheekela Baker-Yeboah⁽¹⁾**

(1) NOAA National Centers for Environmental Information, USA Email: Kenneth.Casey@noaa.gov

ABSTRACT

The NOAA National Centers for Environmental Information (NCEI) was formed this year as the merger of the three, previously distinct National Data Centers and continues to provide extensive contributions to the GHRSSST community. In addition to providing GHRSSST with science team members, the co-Chair of the SST Virtual Constellation, and GHRSSST archive services, NCEI provides the AVHRR Pathfinder climate data record product and the Daily Optimally-Interpolated SST (OISST) product. Pathfinder is currently available in L3C for Version 5.2, but a release later this year will make several improvements to Version 5.3 and will include L2P and L3U as well. The AVHRR-only Daily OISST product continues to be updated in real time and provided to GHRSSST, and work is underway to revitalize the microwave OISST, modernize the code base, and create a high resolution OISST at the same 4 km resolution of Pathfinder.

1. Introduction

The NOAA National Centers for Environmental Information (NCEI) was formed this year as the merger of the three, previously distinct National Climatic Data Center (NCDC), National Geophysical Data Center (NGDC), and National Oceanographic Data Center (NODC). Both NCDC and NGDC previously served as independent RDACs, and their existing products still utilize those RDAC codes. Future products will bear the NCEI RDAC name, however. As an organization, NCEI provides to the GHRSSST community two science team members, a member of the GHRSSST Advisory Council, the co-chair of the CEOS SST Virtual Constellation (VC), the archive of the Level 0/Level 1 AVHRR, GOES, and NPP data sets used by many other RDACs, the GHRSSST Long Term Stewardship and Reanalysis Facility (LTSRF) where all current GHRSSST products are archived, and two sets of GHRSSST datasets. The LTSRF and SST-VC activities are detailed in other reports, and this report focuses on NCEI's datasets.

2. AVHRR Pathfinder

Currently, NCEI continues to provide the AVHRR Pathfinder climate data record for SST to the GHRSSST community. Version 5.2 is available now twice-daily at ~4 km resolution and spans 1981 through 2013 in GHRSSST L3C format, though `sst_dtime` and the bias and uncertainty values are currently empty. Pathfinder Version 5.2 has a Digital Object Identifier (DOI), which can be used to formally cite the data set (<http://dx.doi.org/10.7289/V5WD3XHB>). Figure 1 shows a subset of the Pathfinder Version 5.2 dataset.

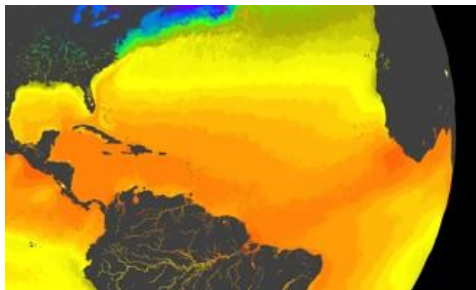


Figure 1: Browse-graphic subset of the AVHRR Pathfinder Version 5.2 dataset.

In the near future, NCEI will provide a substantial new update to Pathfinder, bringing the dataset up to Version 5.3. This new version, scheduled for release in October of 2015 corrects several shortcomings in V5.2:

- In addition to L3C products, Pathfinder Version 5.3 for the first time will include L2P and L3U products

- SSTs will be available for all quality levels, including quality of 0 which was left out of V5.2 due to memory issues in the production code
- Sun glint regions will be better included in the data
- Cloud tree tests for NOAA-7 and NOAA-19 will be consistent now with the rest of the sensors. In Version 5.2 they were not
- The L2P and L3U will now include SST_dtime, though L3C still will not
- SSES bias and standard deviation still won't be available until the release of Version 6, planned for late 2016
- Anomalous hot-spots at land-water boundaries are better identified and flagged than in Version 5.2
- The land mask has been updated (based on Global Lakes and Wetlands Database: Lakes and Wetlands Grid Level 3, 2015)
- Sea ice data over the Antarctic ice shelves are marked as ice
- The output netCDF is netCDF version 4 in classic mode. In Version 5.2 the netCDF-4 files were not explicitly identified as "classic".

The current plan calls for the future Version 6.0 to include uncertainty estimates and be fully processed by NCEI in fiscal year 2016.

3. Daily Optimally Interpolated SST

NCEI also continues to produce and provide in near-real time to the GDAC and LTSRF the Daily AVHRR_OI dataset, at 25 km resolution back to 1981. The AVHRR_AMSR_OI remains available but with the demise of the AMSR-E instrument the dataset is no longer produced in near real time. It is available for 1981 through September 03, 2013. A major effort to revitalize and modernize the Daily OI SST software base is underway and is expected to be complete by the end of the year. Other development work includes revitalizing the microwave OISST product with the newly available microwave data from JAXA, and creating a 4 km resolution OI product that matches the Pathfinder gridding scheme. Once complete, NCEI will have a comprehensive and consistent set of L2P, L3U, L3C, and L4 products all available globally at the 4 km resolution.

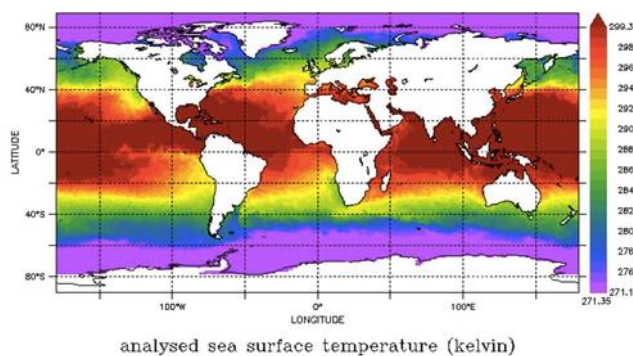


Figure 2: Browse-graphic of the Daily AVHRR-only OISST v2 dataset.

4. Conclusion

NCEI continues to make substantial contributions as an RDAC to the GHRSSST community, combining the efforts of the once separate NCDC and NODC.

PLENARY SESSION III: SPECIAL SESSION ON PASSIVE MICROWAVE SSTS

RECENT CAL/VAL UPDATES OF THE GCOM-W/AMSR2

Misako Kachi ⁽¹⁾, **Keiji Imaoka** ⁽¹⁾, **Takashi Maeda** ⁽¹⁾, **Hiroyuki Tsutsui** ⁽¹⁾,
Haruhisa Shimoda ⁽²⁾, **Taikan Oki** ⁽¹⁾⁽³⁾

(1) Japan Aerospace Exploration Agency (JAXA), Tsukuba (Japan), Email : kachi.misako@jaxa.jp

(2) Tokai University Research and Information Center (TRIC), Tokai University, Tokyo (Japan)

(3) Institute of Industrial Science (IIS), The University of Tokyo, Tokyo (Japan)

ABSTRACT

AMSR2 onboard the GCOM-W satellite has started its continuous scientific observation since July 3, 2012, and released the first public distribution products (version 1) in January 2013 for Level1 brightness temperature and in May 2013 for Level 2 geophysical parameters through the GCOM-W1 Data Providing Service (DPSS, <https://gcom-w1.jaxa.jp/>).

On March 26, 2015, JAXA has released new version (version 2) of AMSR2 Level 1-3 products to public through DPSS. In Level 1, geolocation accuracy is improved and partial error in brightness temperature of low frequency channels (7-18GHz) is reduced. In Level 2, several improvements are applied to each algorithm. Regarding SST product, effects of RFI and sea surface wind speed are reduced. Evaluation of AMSR2 SST with NOAA's iQuam buoy dataset indicates RMSE of 0.58 degC for new version (version 2) for the period from August 2012 to July 2014, while current version (version 1) shows that of 0.59 degC for the same period.

From version 2, AMSR2 SST product includes high spatial resolution SST using 10GHz channel as the second layer of geophysical parameters. While standard SST algorithm uses 6GHz channel for retrieval, 10GHz channel also sensitivity to SST higher than 10-12 degC and has finer spatial resolution about (30km) than 6GHz channel (about 50km). 10GHz observed SST is defined as one of the AMSR2 standard products in March 2015, and added to the product file in addition to standard 6GHz SST in order to provide complementary information to users. In version 2 product, 10GHz SST that is less than 9 degC is set to missing value, since 10GHz channel has poor sensitivity to low temperature range. Evaluation of AMSR2 10GHz SST with iQuam buoy dataset indicates RMSE of 0.94 degC, but 10GHz SST higher than 12 degC shows almost equal performance to that of 6GHz SST.

1. Introduction

The Advanced Microwave Scanning Radiometer 2 (AMSR2) is multi-frequency, total-power microwave radiometer system with dual polarization channels for all frequency bands. The instrument is a successor of AMSR-E on the NASA's EOS Aqua satellite.

AMSR2 onboard the GCOM-W satellite was launched on 18 May 2012 (JST) from Tanegashima Space Center, Japan. The GCOM-W satellite has joined A-train orbit since 29 June. After GCOM-W was inserted into the planned position on the A-Train orbit, AMSR2 was spun up to 40-rpm, and then set to "science mode" to start observation in 3 July. Initial checkout of the satellite and the instrument has completed in 10 August without major problem. The GCOM-W satellite was installed in front of the Aqua satellite to keep continuity of AMSR-E observations and provide synergy with the other A-Train instruments for new Earth science researches.

2. Overview of the AMSR2

Observation targets of the GCOM-W satellite and AMSR2 are water-energy cycle. AMSR2 is designed to continue AMSR-E observations, and basic concept of AMSR2 is almost identical to that of AMSR-E. Major differences between AMSR2 and AMSR-E are; 1) deployable main reflector system with 2.0m diameter while that of AMSR-E is 1.6m; 2) addition of 7.3GHz channel for RFI mitigation; 3) two-point external calibration with improved HTS (hot-load); and 4) addition of a redundant momentum wheel to increase reliability. Table 1 is a summary of frequency channels of AMSR2 and their resolutions.

Table 2 is a list of the AMSR2 standard products. Brightness temperature (Level-1B, -1R) and eight geophysical parameters (Level-2) are provided. Release accuracy should be achieved when data is released to general users. Standard accuracy should be satisfied when AMSR2 completes its designed mission life, and goal accuracy is target as an extra success of the mission. Note that those accuracies are defined as root mean square error (RMSE) except precipitation, snow depth, and soil moisture products. Accuracy of precipitation product is defined as relative error (RMSE/Mean in percent), and that of snow depth and soil moisture content products is defined as Absolute Mean Error (AME).

Center Freq.[GHz]	Band width [MHz]	Pol.	Beam width [deg] (Ground res. [km])	Sampling interval [km]
6.925/7.3	350	V and H	1.8 (35 x 62)	10
10.65	100		1.2 (24 x 42)	
18.7	200		0.65 (14 x 22)	
23.8	400		0.75 (15 x 26)	
36.5	1000		0.35 (7 x 12)	
89.0	3000		0.15 (3 x 5)	5

Table 1: AMSR2 Channel Set

Products	Areas	Resolution	Release accuracy	Standard accuracy	Goal Accuracy	Range
Brightness Temperature	Global	5-50km	± 1.5 K	± 1.5 K	±1.0K (systematic) ±0.3K (random)	2.7 - 340K
Integrated Water Vapor	Global, over ocean	15km	± 3.5 kg/m ²	± 3.5 kg/m ²	±2.0 kg/m ²	0 - 70kg/m ²
Integrated Cloud Liquid Water	Global, over ocean	15km	± 0.10 kg/m ²	± 0.05 kg/m ²	±0.02kg/m ²	0- 1.0kg/m ²
Precipitation	Global, except cold latitude	15km	Ocean ± 50 % Land ± 120 %	Ocean ± 50 % Land ± 120 %	Ocean ±20% Land ±80%	0 - 20mm/h
Sea Surface Temperature	Global, over ocean	50km	± 0.8 °C	± 0.5 °C	±0.2 C (zonal mean)	-2 - 35 C
Sea Surface Wind Speed	Global, over ocean	15km	± 1.5 m/s	± 1.0 m/s	±1.0m/s	0 - 30m/s
Sea Ice Concentration	Polar region, over ocean	15km	± 10 %	± 10 %	±5%	0 - 100%
Snow Depth	Land	30km	± 20 cm	± 20 cm	±10cm	0 - 100 cm
Soil Moisture Content	Land	50km	± 10 %	± 10 %	±5%	0 - 40%

Table 2: List of AMSR2 standard products

3. Update of Level 1 Products

The AMSR2 Level 1 algorithms and parameters were updated to Version 2.1 on April 3, 2015 based on the validation results of previous Ver.1.1 products. There is almost no variation in brightness temperatures between Ver. 2 and Ver. 1.1 under normal situation. Highlights of updates of Level 1 are; 1) correction of the antenna temperature of the cold calibration target (CSM) that leads maximum 0.2K differences for 6.9 V/H, 7.3 V/H; 2) removal of radio frequency interference (RFI) included in the CSM that leads maximum 3K differences for 10.65 V and maximum 0.1K for 18.7 V; 3) removal of RFI included the hot calibration target (HTS); 4) optimization of scan-bias correction that leads maximum 2.5K differences for 6.9 V/H, 7.3 V/H and 10.65 V/H but only at the scan-edge; 5) optimization of geometric calibration; and 6) modification of weighting coefficients to calculate brightness temperatures in L1R products from those in L1B products.

4. Update of Level 2 Standard Ocean Products

AMSR2 Version 2.1 products were released to public on April 3, 2015, at the same timing with Level 1.

Major updates of the AMSR2 SST version 2 are; 1) addition of RFI removal method; 2) refining 6GHz Vertical polarization brightness temperature correction table; 3) refining sea surface wind speed correction method; and 4) addition of 10GHz observed SST (research product, missing values stores SST less than 9 °C) to the second layer in the SST product. By those updates, there were improvements in RFI error removal, brightness temperature error correction, and sea surface wind speed error removal.

AMSR2 SST product is validated by comparing with the iQuam buoy dataset, which is compiled and quality controlled by NOAA, and obtain monthly root mean square error (RMSE). Each match-up data includes AMSR2 footprints around buoy stations within radius of 30 km and 2 hours. RMSE between AMSR2 Version 2 and iQuam buoy SSTs from August 1, 2012 to July 31, 2014 is 0.58 °C and correlation coefficient (R) is 0.998 (Figure 1, left). New version shows smaller error compared to old Version 1 (Figure 1, right). This value also satisfied release accuracy of 0.8 °C.

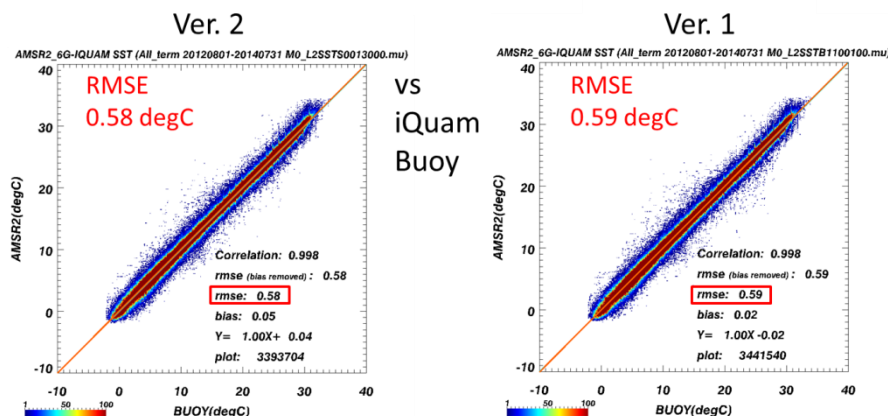


Figure 1: Scatter plots of AMSR2 SST and buoy SST (iQUAM V1) data from August 1, 2012 to July 31, 2014 for both ascending and descending orbits. Left: Version 2.1. Right: Version 1.1.

Major updates of AMSR2 sea surface wind speed product(4) are; 1) improvements in wind direction correction; and 2) improvements in wind speed conversion table. Improvements in positive biases of AMSR2 in weak wind speed range. By those updates, there were improvements in positive biases of AMSR2 in both strong and weak wind speed ranges.

AMSR2 sea surface wind speed product is validated by comparing with quality controlled buoy wind speed observations. We have applied several quality control checks to buoy data, such as moving speed check, time continuity, and comparison with numerical models. Condition of match-up data is same as SST. RMSE between AMSR2 and buoy sea surface wind speed from July 23, 2012 to July 31, 2014 is 1.11 m/s and is

0.920 (Figure 2, left). New version shows smaller error compared to old version (Figure 2, right). This value also satisfied release accuracy of 1.5 m/s.

5. Research Products

The AMSR2 research products were defined in March 2015 in order to provide new and challenging products obtained from AMSR2 data. Eight new products are defined and summarized in Table 3. There are two ocean related products, All-weather sea surface wind speed and 10-GHz SST.

Products	Area	Resolution	Target accuracy	Range
All-weather sea surface wind speed	Ocean	60 km	± 7 m/s (at 15-40 m/s range)	0 - 70 m/s
10-GHz Sea Surface Temperature	Ocean	30 km	± 0.8 °C	9 – 35 °C
Soil moisture and vegetation water content based on the land data assimilation	Africa, Australia	25 km	soil moisture: $\pm 8\%$ vegetation water: ± 1 kg/m ²	0 – 100 % 0 - 2 kg/m ²
Land surface temperature	Land	15 km	forest area: ± 3 °C nondense vegetation: ± 4 °C	0-50 °C
Vegetation water content	Land	10 km	± 1 kg/m ²	0 – 4 kg/m ²
High resolution sea ice concentration	Ocean in high latitude	5 km	± 1 %	0 – 100 %
Thin ice detection	Okhotsk sea	15 km	± 80 %	N/A
Sea ice moving vector	Ocean in high latitude	50 km	2 components: 3 cm/s	0 - 40 cm/s

Table 3: List of AMSR2 Research Products

The All-weather sea surface wind speed (AWS) can estimate wind speed under tropical cyclones or heavy rainfall regions by using both 6-GHz and 10-GHz channels. Figure 2 is comparison of AMSR2 standard sea surface wind speed and all-weather sea surface wind speed for the same observation on July 9, 2015, descending orbits. Typhoons No.9 and No.11 in 2015 (within red dashed circles) were located in the south of Japan.

JAXA has been processing All-weather sea surface wind speed from AMSR-E and Windsat as research product, and same algorithm was applied to AMSR2. Test processing of All-weather sea surface wind speed was implemented in near-real-time basis, and the Japan Meteorological Agency (JMA) uses this research product in their operational typhoon analysis.

Validation of all-weather sea surface wind speed is not simple because of lack of available in-situ observations in strong wind speed area. Currently we are working on evaluation of ASW accuracy for future data release that is scheduled in autumn 2015. Figure 3 is early validation results using match-up data with GPS-dropsonde data provided by NOAA. Present version shows RMSE of 6.52 m/s for all wind speed ranges. Although it satisfied target accuracy defined in Table 3, which is RMSE should be within 7m/s at 15-40m/s ranges, we plan to refine the algorithm further before the release.

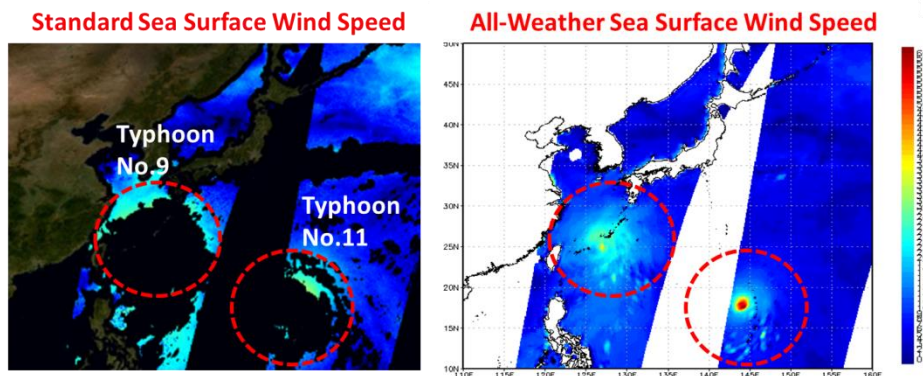


Figure 2: Comparison of AMSR2 sea surface wind speed on July 9, 2015, in descending orbit. Left: Standard product: Sea Surface Wind Speed. Right: Research product: All-Weather Sea Surface Wind Speed.

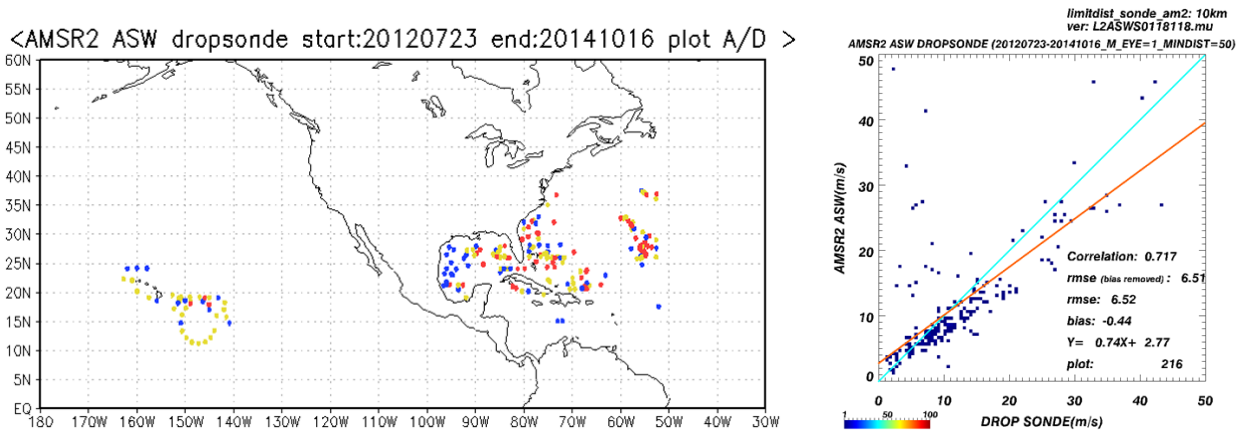


Figure 3: Early validation results of AMSR2 All-weather Sea Surface Wind Speed (AWS) in comparison with GPS-dropsonde data. Left: Location of match-ups from July 23, 2012 to October 16, 2014. Right: Scatter plot of AMSR2 AWS and dropsonde. GPS-dropsonde data are provided courtesy of the NOAA/AOML/Hurricane Research Division in Miami, FL (USA).

The standard AMSR2 SST algorithm uses 6.9-GHz channels to retrieve SST, but it has a weak point that horizontal resolution of 6.9-GHz is the worst in the AMSR2 channel set. 0-GHz channel, however, also has sensitivity to SST higher than 10-12 °C, and has finer spatial resolution (about 30km) than 6-GHz channel (about 50km) as shown in Figure 4. From Version 2 product, 10-GHz observed SST is included in the AMSR2 SST product file in addition to standard 6-GHz SST, in order to provide complementary information to users.

Figure 5 is validation result of 10-GHz SST, and that of 6-GHz SST is also shown for reference (same as Figure 1. Left). Validation of 10-GHz SST uses same method and data to those of 6-GHz SST. RMSE of 10GHz SST to iQuam buoy SST from August 1, 2012 to July 31, 2014 is 0.61 °C, and 10-GHz SST more than 10 °C shows almost equal performance to that of 6-GHz SST. In the current product, 10-GHz SST that is less than 9 °C is set to missing value since 10-GHz channel has poor sensitivity to low temperature range.

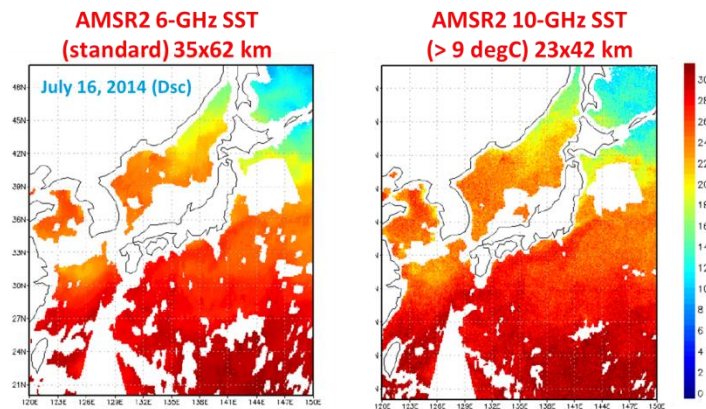


Figure 4: Comparison of AMSR2 standard (6-GHz) SST (left) and 10-GHz SST (right) for the descending orbit on July 16, 2014.

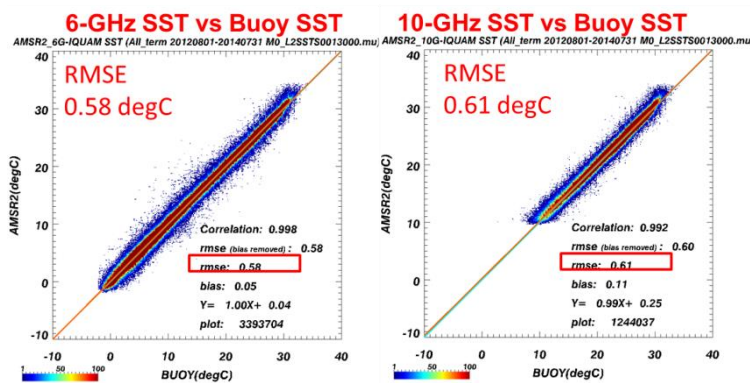


Figure 5: Scatter plots of AMSR2 SST and buoy SST (iQUAM V1) data from August 1, 2012 to 31 July 2014 for both ascending and descending orbits. Left: Standard product: 6-GHz SST. Right: Research Product: 10-GHz SST.

The 250m resolution data of SGLI-VNR will enable to detect more fine structure in the coastal area such as river outflows, regional blooms, and small currents SST and ocean color products derived from SGLI will provide additional information to AMSR2 SST.

6. Collaboration with the Global Precipitation Measurement (GPM)

The GPM Core Observatory, a joint mission between JAXA and NASA, was launched from JAXA Tanegashima Space Center on 28 February, 2014 (JST). The GPM Microwave Imager (GMI) was developed by NASA as a successor of the TRMM Microwave Imager (TMI) on board the Tropical Rainfall Measuring Mission (TRMM) satellite, which completed its operation on April 8, 2015.

Since GMI has 10-GHz channels same as TMI and has a capability to measure SST higher than 10-12 °C, we have applied the AMSR2 10-GHz SST algorithm to GMI to retrieve SST. Figure 6 is validation result of GMI SST comparing with buoy SST. RMSE of GMI SST to iQuam buoy SST from March 4, 2014 to April 10, 2015 is 0.63 °C, and shows almost equal performance to that of AMSR2 10-GHz SST. In the current product, GMI SST that is less than 10 °C is set to missing value since 10-GHz channel has poor sensitivity to low temperature range, but we plan to update the algorithm and retrieve SST more than 9 °C same as AMSR2 10-GHz SST.

We also collaborate with the GPM to produce the Sea Ice Concentration data retrieved from the Dual-frequency Precipitation Radar (DPR) as well as GMI. DPR Sea ice concentration was produced by comparing

noise power of DPR Ku-band (13.6-GHz) and AMSR2 SIC. Finer resolution SIC maps (5 km) can be obtained although the coverage is smaller.

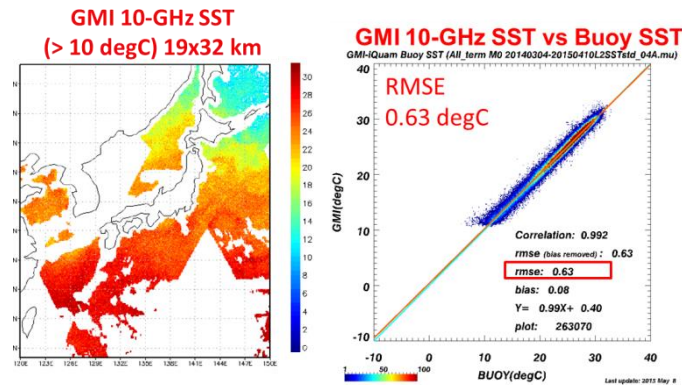


Figure 6: SST retrieved from the GPM Microwave Imager (GMI) (left), and scatter plots of GMI SST and buoy SST (iQUAM V1) data from March 4, 2014 to April 10, 2015.

7. Conclusion

Both of GCOM-W satellite and AMSR2 instruments are in good shape after the launch in May 2012, and their performances are excellent.

AMSR2 standard products are distributed through the GCOM-W Data Providing Service (<https://gcom-w1.jaxa.jp/>). The latest version of the products are version 2.1. The system also distributes AMSR and AMSR-E standard products. Also, registered users can obtain near-real-time data by applying special user form.

AMSR2 6-GHz SST and GMI SST data are also provided in GDS 2.0 format through the JAXA GHRSSST server (<http://suzaku.eorc.jaxa.jp/GHRSSST/>) as well as Windsat, AMSR-E and TRMM/VIRS SSTs. We also plan to distribute AMSR2 10-GHz SST from the server in near future as well as the JMA's new geostationary satellite "Himawari-8" SST.

OPTIMAL ESTIMATION OF SEA SURFACE TEMPERATURE FROM AMSR2

Kevin Pearson⁽¹⁾, Chris Merchant⁽²⁾, Owen Embury⁽³⁾

(1) Department of Meteorology, University of Reading, UK, Email: k.j.pearson@reading.ac.uk

(2) Department of Meteorology, University of Reading, UK, Email: c.j.merchant@reading.ac.uk

(3) Department of Meteorology, University of Reading, UK, Email: o.embury@reading.ac.uk

ABSTRACT

We present ongoing work to apply the method of optimal estimation to the AMSR2 microwave instrument particularly aimed at the retrieval of Sea Surface Temperatures (SST). An information content analysis is described that results in a prioritized channel order and a prediction, under idealised circumstances, of a mean uncertainty in retrieved SST of 0.38K using all 14 channels. These are compared to simulated retrievals over the same profile set which produce a mean error of 0.06K with standard deviation of 0.39K. Application to real AMSR2 data is also shown, highlighting the need to characterize biases between the forward model and observations.

1. Introduction

Remote sensing measurements of SST are often carried out at infrared frequencies given that the location of the peak in the thermal blackbody emission from the ocean lies in this region. Despite poorer signal to noise and a larger spatial footprint, microwave instruments also have a potentially useful role to play as they can make SST measurements in regions that would be obscured by cloud in the infrared. The method of optimal estimation (Rodgers, 2000) has been applied to retrievals from infrared instruments under the ESA SST CCI project in similar way to that of Merchant et al. (2008). As part of the same project, we are investigating the potential for applying an optimal estimation scheme to data from the microwave radiometer AMSR2.

Optimal estimation provides a best estimate of the geophysical parameters in the vector \mathbf{x} , given an initial estimate \mathbf{x}_a with corresponding modelled observations \mathbf{y}_a and new (real) observations \mathbf{y} as

$$\hat{\mathbf{x}} = \mathbf{x}_a + \mathbf{S}_a \mathbf{K}^T [\mathbf{K} \mathbf{S}_a \mathbf{K}^T + \mathbf{S}_\varepsilon]^{-1} (\mathbf{y} - \mathbf{y}_a).$$

Here \mathbf{S}_a is the covariance matrix of the *a priori* information contained in \mathbf{x}_a and \mathbf{S}_ε is the covariance matrix of the observation vector \mathbf{y} . \mathbf{K} is the Jacobian matrix $\frac{\partial y_i}{\partial x_j}$ expressing the sensitivity of each of the observations to each of the geophysical variables. For this application, the observation vector contains the brightness temperature in each of the 14 AMSR2 channels and the state vector contains SST, the logarithm of the total column water vapour (TCWV), the two horizontal wind components and the logarithm of the total cloud liquid water (TCLW). Forward modelling to calculate \mathbf{y}_a and to generate the terms for the Jacobian matrix is carried out using RTTOV (Hocking, 2013).

The expected uncertainty in a retrieval scheme can be found using an information content analysis. This is expressed in a retrieval uncertainty covariance matrix \mathbf{S} given by

$$\mathbf{S} = [\mathbf{K}^T \mathbf{S}_\varepsilon^{-1} \mathbf{K} + \mathbf{S}_a^{-1}].$$

In practice, this will always be a somewhat idealised estimate as it assumes perfect characterization of the observation system in order to generate the matrices on the right hand side of the equation.

2. Application to AMSR2

An information content study was carried out using profiles (approximately 2700) from the NWP SAF q-sampled dataset (Chevallier, 2006) to calculate the predicted retrieval uncertainty across a range of conditions although in the absence of any rain. Both \mathbf{S}_a and \mathbf{S}_ε were assumed to be diagonal. Values for the

a priori uncertainties followed the precedent of Prigent et al. (2013) by using 3.31K for SST and 0.92 m/s for each of the two wind components. An uncertainty of 10% was used for TCWV and TCLW. The mean expected SST uncertainty from the retrievals when all 14 channels are used is plotted in Figure 1. This shows a strong peak but long tail. The mean uncertainties across the profiles are $S_{SST}=0.38K$, $S_{ln(TCWV)}=0.11$, $S_u=0.64m/s$, $S_v=0.71m/s$, $S_{ln(TCLW)}=0.078$. By considering all the possible channel combinations it is possible to rank the channels in order of which are most effective in reducing the expected uncertainty in SST. Figure 2 shows the predicted uncertainty for the best single channel and then for each subsequent additional channel, in turn, that is most usefully added.

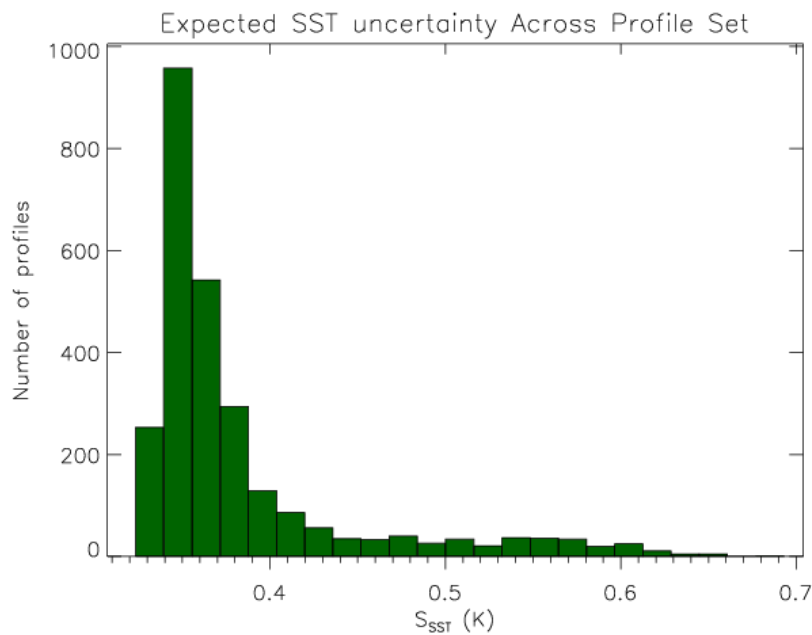


Figure 1: Predicted retrieved SST uncertainty distribution from an information content analysis using all 14 AMSR2 channels.

Simulated retrievals were carried out using the same profile set as above. Noise was added according to the assumed uncertainties to produce a synthetic “true” state with “true” observations using RTTOV to which the retrieval equation was then applied. The error distribution across the profile set between the retrieved and “true” value of SST is plotted in Figure 3. The standard deviation of the retrieval error is plotted in ranked channel order in Figure 4. Using all channels, the standard deviation of the retrieval error for each of the state variables was $\sigma_{SST}=0.39K$, $\sigma_{ln(TCWV)}=0.14$, $\sigma_u=0.71m/s$, $\sigma_v=0.77m/s$, $\sigma_{ln(TCLW)}=0.083$. The mean error in SST across the profile set SST was 0.06K.

The retrieval scheme has been applied to a day of AMSR2 orbit data from 15 December 2012 in the form of the L1R product where the brightness temperature from each of the channels is resampled onto a common footprint. ECMWF analysis data was interpolated to the observed location and used as the *a priori* information. A consistency check between the observed and modelled brightness temperature was also applied by calculating

$$\chi^2 = \delta \mathbf{y}^T \mathbf{S}_y^{-1} \delta \mathbf{y}$$

where

$$\delta \mathbf{y} = \mathbf{y} - \mathbf{y}_a$$

and

$$\mathbf{S}_y = \mathbf{K} \mathbf{S}_y \mathbf{K}^T + \mathbf{S}_\varepsilon.$$

A map of retrieved SST with overlying χ^2 mask is shown in Figure 5. This masking scheme provides a means of detecting factors that have not been included in the forward model such as rain or RFI. However, it does not provide a means to be able to discriminate between the causes of such bad retrievals. The values of χ^2 generated by the retrieval are much larger than would be expected for a system with 14 channels of measurements. This reflects the effect of a bias between the forward model and observed brightness temperature. We have implemented a form of 'bias-aware' optimal estimation (Merchant, this volume) that retrieves the bias value for each channel along with the physical variables. It is possible to trace out the form of the brightness temperature dependence of this bias by carrying out the retrievals in order of increasing brightness temperature. This is shown in Figure 6. Such a dependency suggests it arises from instrument calibration effects. This form of bias adjustment significantly improves the χ^2 distribution but additional sources of bias remain, particularly those related to wind-speed effects, that are due to limitations in the forward model. Work to incorporate these into the bias-aware scheme is ongoing.

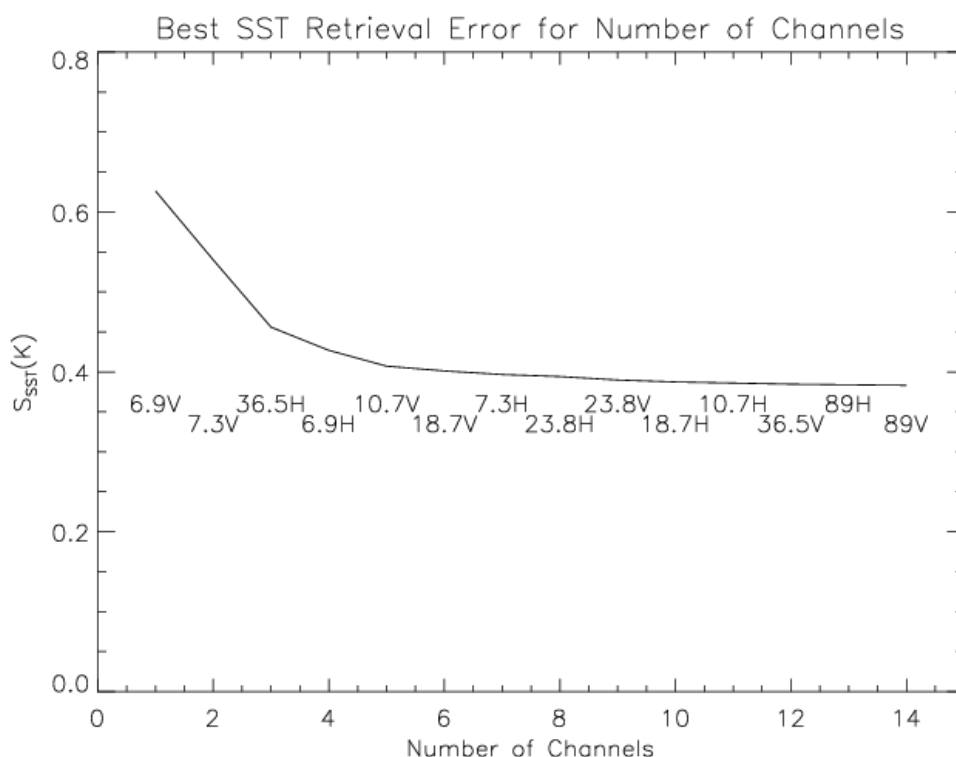


Figure 2: The predicted uncertainty in the retrieved SST from the information content analysis plotted against the number of channels included in the retrieval scheme. The best additional channel to include in the scheme is indicated.

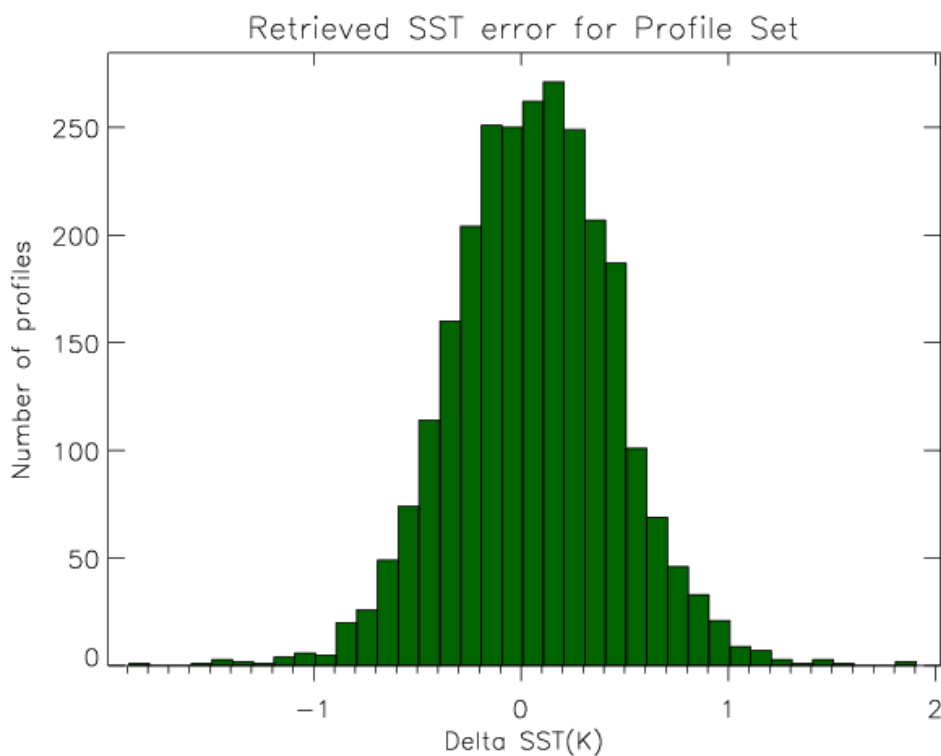


Figure 3: The retrieved SST error distribution from a simulated retrieval scheme using all 14 AMSR2 channels.

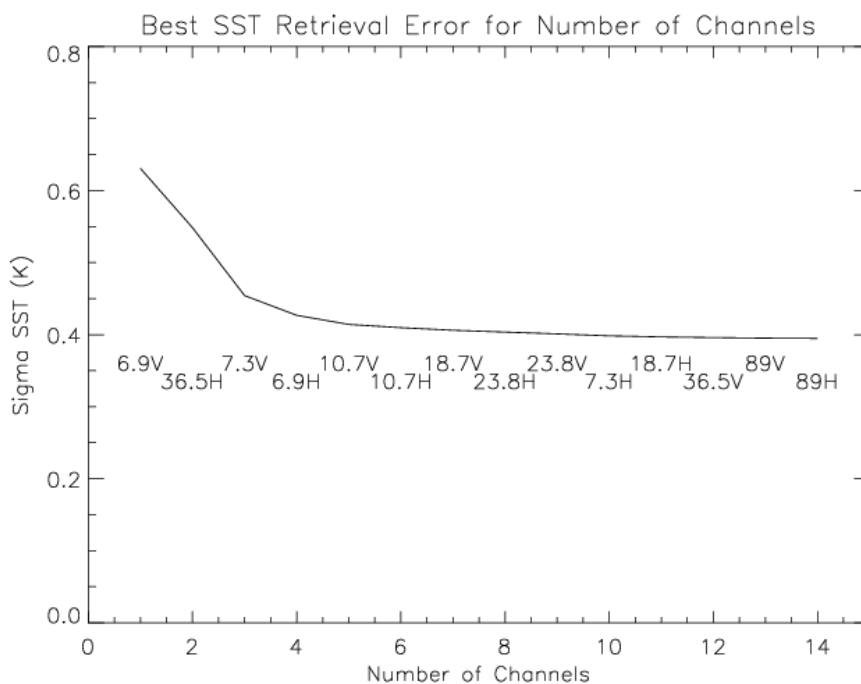


Figure 4: Standard deviation of the retrieved SST error distribution for the simulated retrieval plotted against the number of channels included in the retrieval scheme. The best additional channel to include in the scheme is indicated.

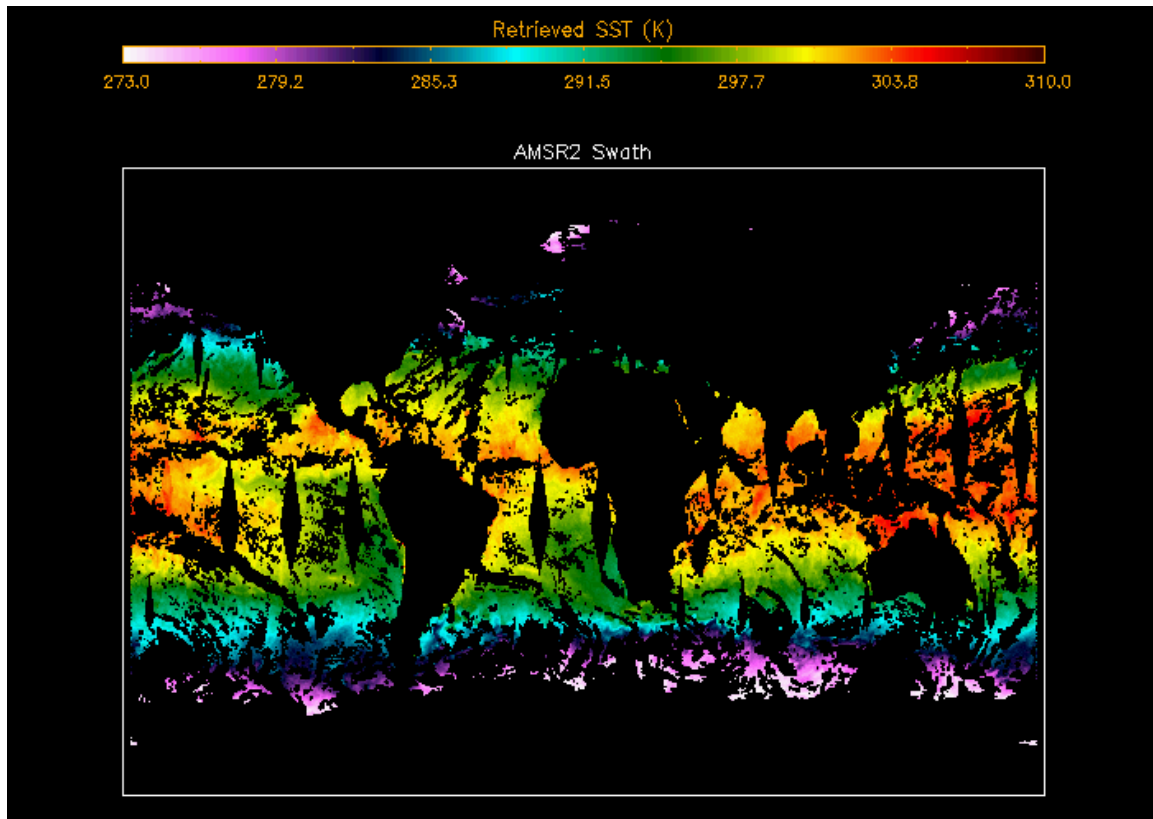


Figure 5: Map of retrieved SST, using all 14 AMSR2 channels, from 15 December 2012. A mask based on χ^2 between the observed and modelled brightness temperatures has been applied to exclude regions with unreliable retrievals due to rain, RFI etc.

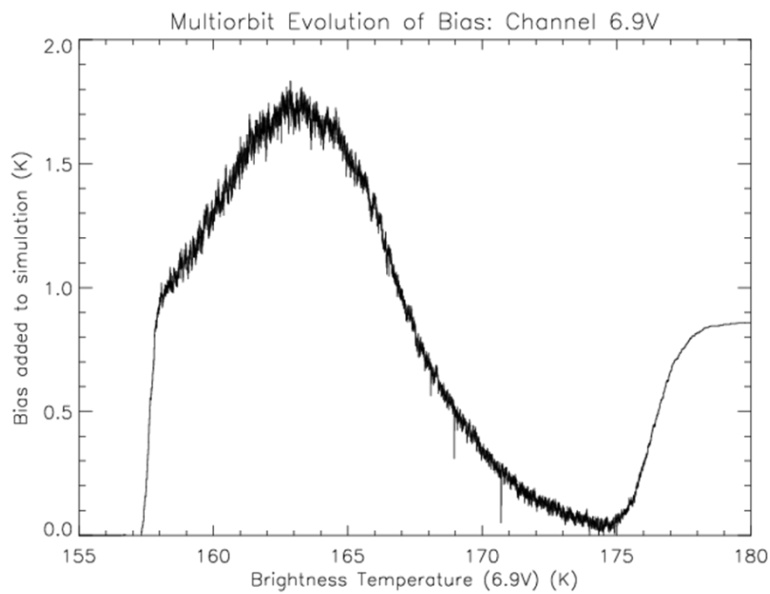


Figure 6: Brightness temperature dependence of the bias between the forward model and measured brightness temperature in the 6V channel.

3. Conclusion

The information content and simulated retrievals show that an optimal estimation approach has the potential to derive SST with sufficient accuracy to contribute to the climate record. Practical application to real data shows the importance of proper representation of the biases between the forward model being used and the instrument. Work is ongoing to incorporate this into the retrieval scheme.

4. References

- Chevallier, F., S. Di Michele and A. P. McNally, Diverse profile datasets from the ECMWF 91-level short-range forecasts, v1, 2006. https://nwpsaf.eu/downloads/profiles/profiles_91L.pdf
- Hocking, J., P. Rayer, D. Rundle, R. Saunders, M. Matricardi, A. Geer, P. Brunel and J. Vidot, RTTOV v11 Users Guide, v1.3, 2013. https://nwpsaf.eu/deliverables/rtm/docs_rtov11/users_guide_11_v1.3.pdf
- Merchant, C.J., F. Le Borgne, A. Marsouin and H. Roquet, Optimal estimation of sea surface temperature from split-window observations, *Remote Sensing of Environment* 112, 2469-2484, 2008. doi: 10.1016/j.rse.2007.11.011
- Prigent, C., F. Aires, F. Bernardo, J.-C. Goutoule, H. Roquet and C. Donlon, Analysis of the potential and limitations of microwave radiometry for the retrieval of sea surface temperature: Definition of MICROWAT, a new mission concept, *JGR:O*, **118**, 3074-3086, 2013. doi: 10.1002/jgrc.20222
- Rodgers, C.D., *Inverse Methods for Atmospheric Sounding: Theory and Practice*, *World Scientific Publishing Co. Pte. Ltd.*, 2000.
- Ingleby, N. B. and A. C. Lorenc, Bayesian Quality-Control Using Multivariate Normal-Distributions, *Quart. J. Roy. Met. Soc.* **119** (513), 1195-1225 Part B, 1993.

COMPARISON OF AMSR2 SEA SURFACE TEMPERATURE RETRIEVALS WITH IN-SITU DATA

Kevin Pearson⁽¹⁾, Chelle Gentemann⁽²⁾, Misako Kachi⁽³⁾

(1) Department of Meteorology, University of Reading, UK, Email: k.j.pearson@reading.ac.uk

(2) Remote Sensing Systems, USA, Email: gentemann@remss.com

(3) JAXA, Japan, Email: kachi.misako@jaxa.jp

ABSTRACT

Retrieval schemes for Sea Surface Temperature, using data from the GCOM-W1 AMSR2 microwave instrument, from Remote Sensing Systems (RSS), the Japan Aerospace Exploration Agency (JAXA), and the University of Reading (UoR) were compared using simultaneous collocations with in situ observations. Overall, at the commonly agreed locations for good retrievals, the RSS and JAXA schemes gave very similar results with mean differences from the *in situ* values of -0.039 K and 0.033 K with standard deviations 0.55 K and 0.54 K for the RSS and JAXA retrievals respectively. The recently developed UoR scheme produced a mean difference of -0.26 K with a standard deviation 0.71 K and showed the effects of under-corrected, wind-dependent biases in the forward model brightness temperatures. This method of validation primarily examines the actual algorithm accuracy and does not test the accuracy of each institutions data flagging.

1. Introduction

We have carried out a comparison between three retrieval schemes for Sea Surface Temperature (SST) from the AMSR2 microwave instrument used by the Japan Aerospace Exploration Agency (JAXA), Remote Sensing Systems (RSS) and the University of Reading (UoR). The JAXA and UoR algorithms use version 2 of the JAXA calibrated AMSR2 brightness temperatures (see http://suzaku.eorc.jaxa.jp/GCOM_W/materials/product/AMSR2_L1_2.pdf). The RSS algorithm uses the RSS calibrated AMSR2 brightness temperatures (Hilburn and Gentemann, submitted). The standard JAXA retrieval scheme (Shibata 2013) is based on the brightness temperature in the 6V channel. Corrections are applied for the atmospheric effects of water vapour and cloud liquid water using the 23V and 36V channels respectively. A further correction for the effect of wind speed is applied based on the 6H channel and both 36 GHz channels. In this comparison, we have used a new research product for the JAXA retrieval that follows the same approach but is based on the 10V channel rather than 6V.

The RSS scheme (Wentz and Meissner, 2000, 2007) uses weighting coefficients derived from the RSS physical radiative transfer model to combine together the brightness temperatures in all of the channels to produce an initial estimate of SST and wind speed. A second stage uses the appropriate set of coefficients from a set trained across the range of SST-wind speed pairs to provide an improved SST retrieval.

The UoR scheme uses an optimal estimation technique based on that currently used in the SST CCI project for infrared instruments that is similar to that of Merchant et al. (2008). This uses *a priori* information from ECMWF analysis fields to simulate AMSR2 brightness temperature using the forward model RTTOV. This information is combined using the sensitivity of each channel to each of the retrieved physical variables and the covariance matrices of both the *a priori* information and the measurements to derive an updated estimate of the physical state.

Retrievals from each of the schemes over the period 1 July 2012 to 30 June 2014 were compared to a collocated set of *in situ* observations. These came from the Hadley Centre Integrated Ocean Database (HadIOD, Atkinson et al., 2014) that merges data taken from the latest versions of the International Comprehensive Ocean-Atmosphere Data Set (ICOADS) for surface observations and the Met Office Hadley Centre EN dataset (EN4) for subsurface observations. Further data from the Global Tropical Moored Array (GT MBA) was downloaded directly and added to the database. Additional quality control was carried out to eliminate any remaining unreliable measurements and a final set of collocated matches to satellite overpasses

was extracted that contained 803 991 drifting buoys, 12 910 Global Tropical Moored Array and 63 024 Argo float measurements. The full time window between the *in situ* measurement and the satellite overpass extended ± 4 hours but 88% of observations were within 1 hour.

The RSS retrievals have associated quality information distinguishing between those that are bad (eg. due to rain or high wind), those useable but with potential caveats (eg. showing strong diurnal warming or nearby rain) and those of best quality. For this inter-comparison, only the best quality data was used. The other two retrieval schemes made no distinction between quality levels for successfully retrieved values. Thus, for these two schemes, all of the “good” retrievals were used in the comparison. The JAXA scheme does include a flag indicating the origin of “bad” retrievals. The UoR scheme, however, eliminates retrievals on the basis of a χ^2 value and therefore does not distinguish between the potential causes of bad retrievals.

The distribution of the difference between the retrieved SST and the *in situ* value for each of the schemes is shown in Figures 1 to 3 with summary statistics listed in Table 1. The equivalent statistics including only those locations where all of the schemes generated a valid retrieval are shown in Table 2. The results from JAXA and RSS schemes are very similar both in the mean and standard deviation of the difference. The UoR scheme also produces small values of the mean and standard deviation but these are somewhat larger than the other two schemes reflecting that it is still under development.

A summary list of the JAXA and RSS flags for the commonly agreed locations of excluded data is given in Table 3. A direct comparison of the numbers is difficult due to a difference in flagging philosophy. The JAXA data only includes a single flag for any given observation but the RSS retrievals can be flagged as bad for multiple reasons at once.

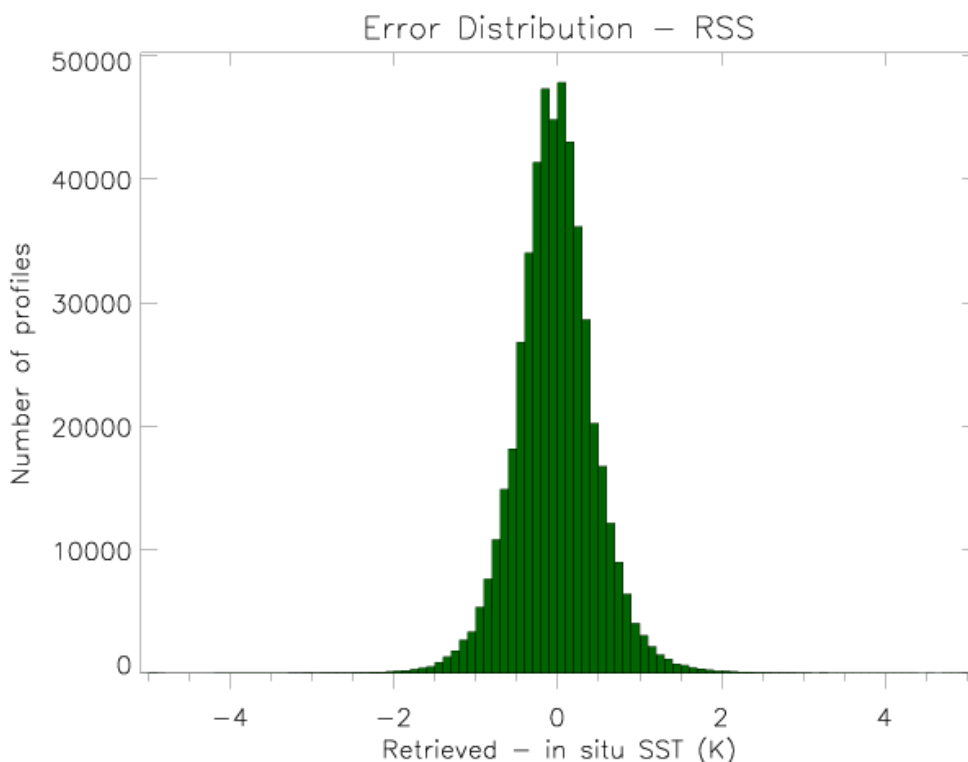


Figure 4: RSS error distribution

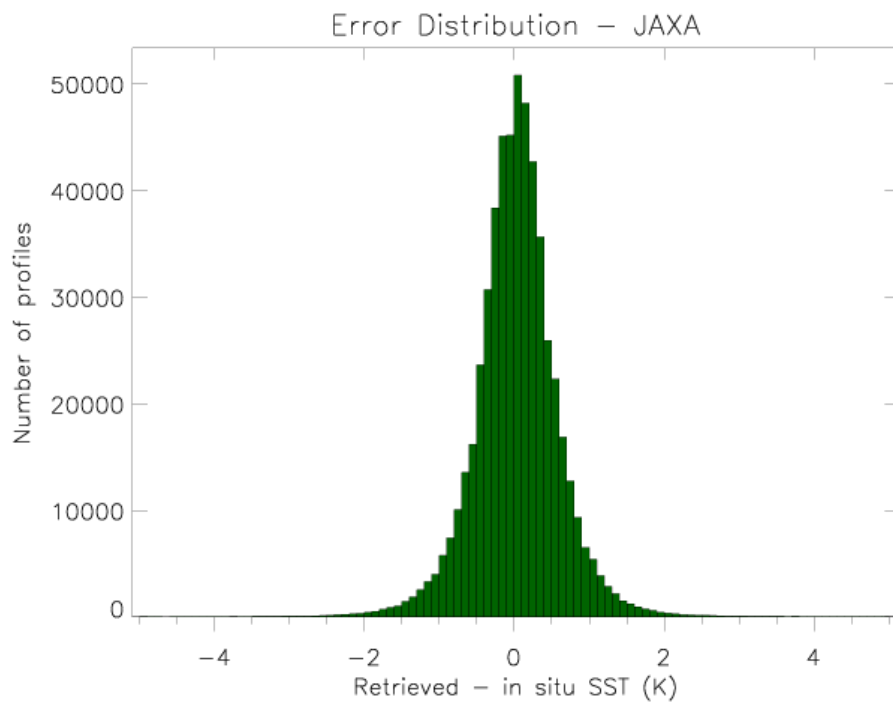


Figure 2: JAXA error distribution

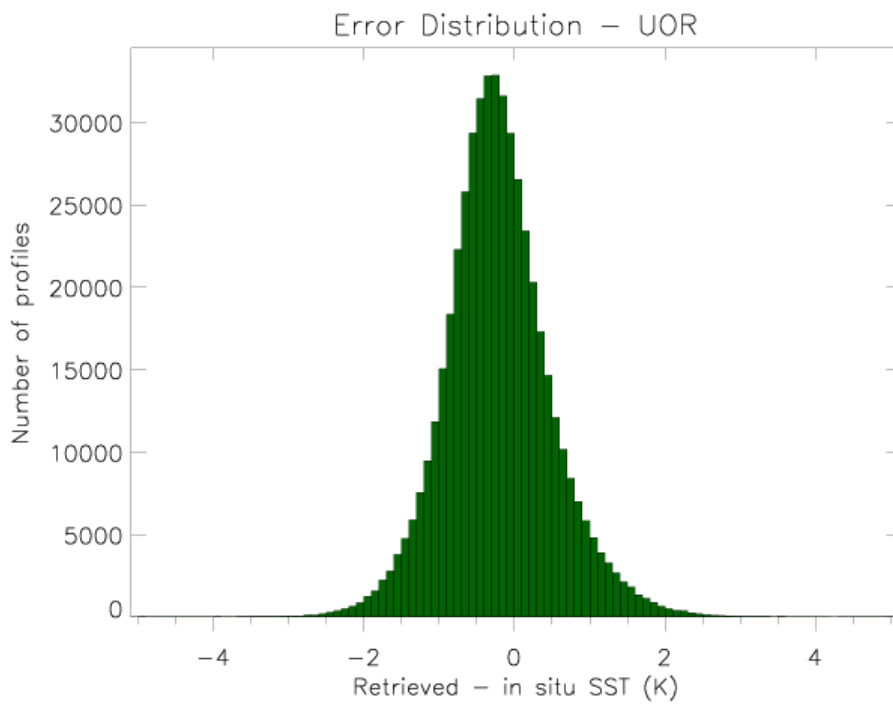


Figure 3: UoR error distribution

	JAXA	RSS	UoR
Good Retrievals	568 761	517 671	511 716
Matching Good Buoys	549 864	501 304	495 506
Mean Error	0.035	-0.028	-0.21
Std. Dev.	0.63	0.59	0.75
MAD (equiv. Std. Dev.)	0.31 (0.45)	0.29 (0.43)	0.42 (0.62)

Table 1: Error statistics summary, using all the good retrievals from each scheme:

	JAXA	RSS	UoR
Good Retrievals	365 997	365 997	365 997
Matching Good Buoys	355 394	355 394	355 394
Mean Error	0.033	-0.039	-0.26
Std. Dev.	0.54	0.55	0.71
MAD (equiv. Std. Dev.)	0.28 (0.41)	0.26 (0.39)	0.40 (0.59)

Table 2: Error statistics summary, using the common set of good retrievals

	JAXA	RSS	Common
Total Excluded Retrievals	337 556	400 056	301 760
Land	66 142	31 465	30 844
Ice	55 184	49 111	39 117
Rain	146 106	222 814	118 937
Wind	16 987	-	-
Other	48 225	162 352	-
Sunlint	-	42 681	-
RFI	-	1 938	-
Missing	4 912	1	-
Warnings	-	204 502	-

Table 3: Origin of the bad data flag in the JAXA and RSS retrievals. JAXA data is flagged for only one cause, whereas the RSS data can be flagged for several causes.

Mean differences, with their standard errors, for retrievals binned by various geophysical variables are shown in Figures 4 to 7. These include only the commonly retrieved locations. Figure 4 shows the retrievals plotted against wind speed. The UoR scheme shows the effect of a bias between the RTTOV forward model and the observations. The UoR retrieval scheme includes a method to automatically compensate for a fixed bias or linear bias-windspeed dependency but non-linear effects still remain. Work to incorporate an enhanced form of this bias-aware scheme to include higher order terms is ongoing. Both the RSS and JAXA schemes are reasonably robust to wind speed although the RSS data does show a small increase in the size of the bias with wind speed above 10 m/s.

Figure 5 shows the retrievals plotted against *in situ* SST. The UoR retrieval again shows the residual effect of a forward model bias. Both the JAXA and RSS retrievals appear approximately constant for temperatures above 285K although there is a small trend below this value in the RSS data. The results are plotted against latitude in Figure 6. All of the retrievals show no trend for lower latitudes. Above about 40°N the UoR results show an increased offset probably reflecting the trends at higher wind speed and cooler temperatures in the previous two figures. Figure 7 shows the results as a function of Total Column Water Vapour (TCWV). The RSS retrievals are flat across the whole range of values. The JAXA scheme, however, shows a steady trend with increasing water vapour. The UoR scheme is also relatively unaffected by TCWV except at the highest values.

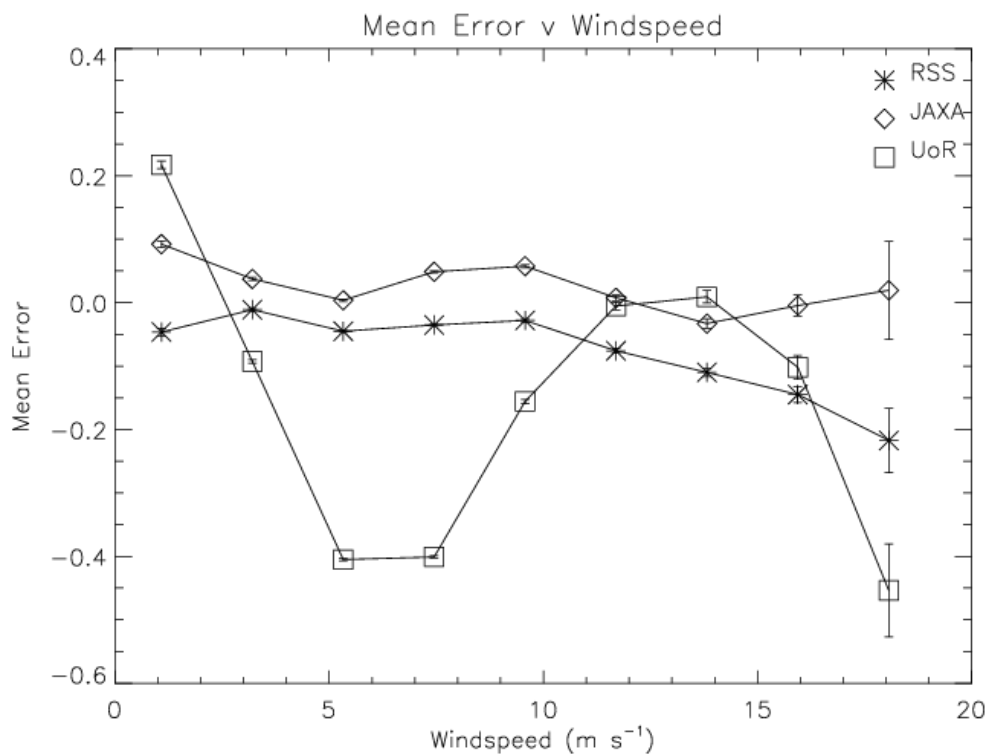


Figure 4: Mean Error comparison against windspeed. (The UoR retrievals include a linear windspeed-dependent bias correction)

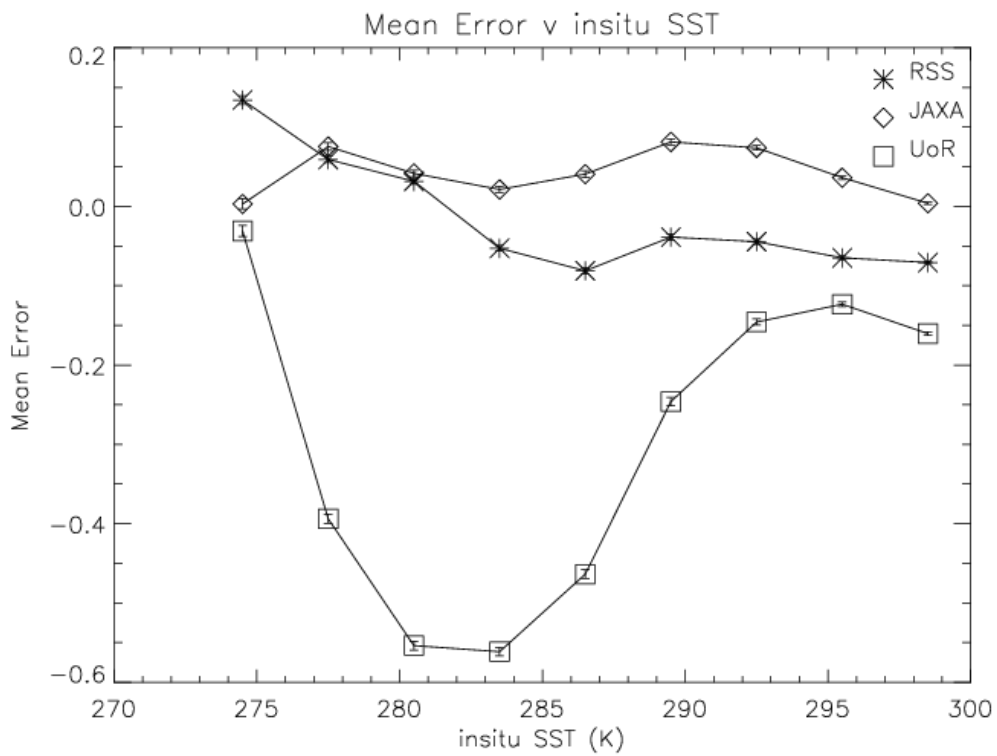


Figure 5: Mean Error Comparison against in situ SST

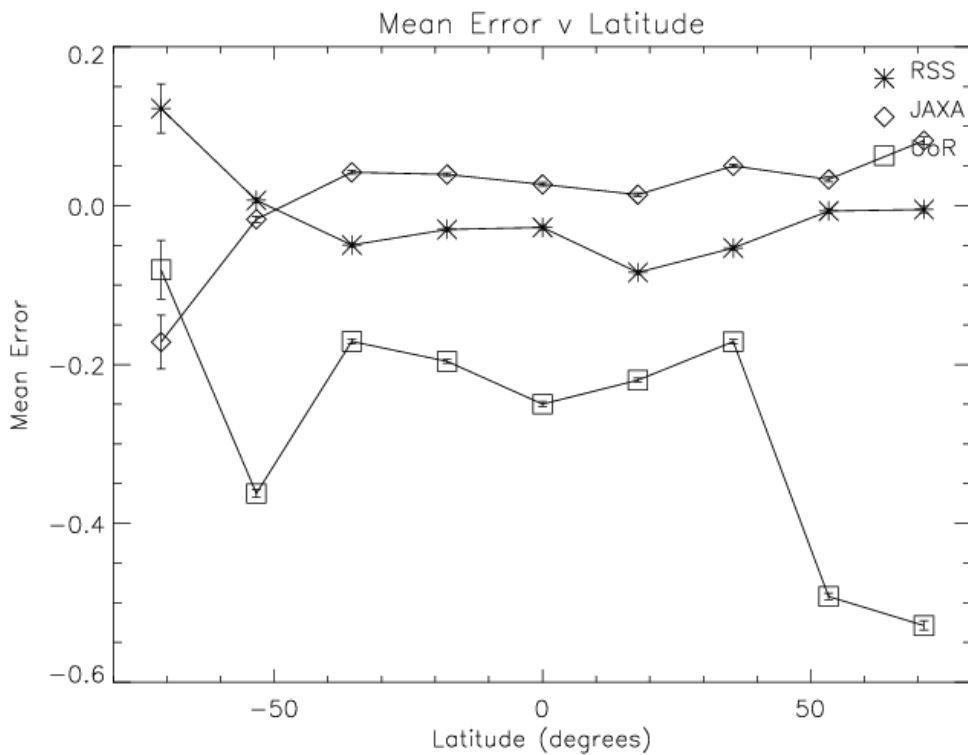


Figure 6: Mean Error Comparison against Latitude

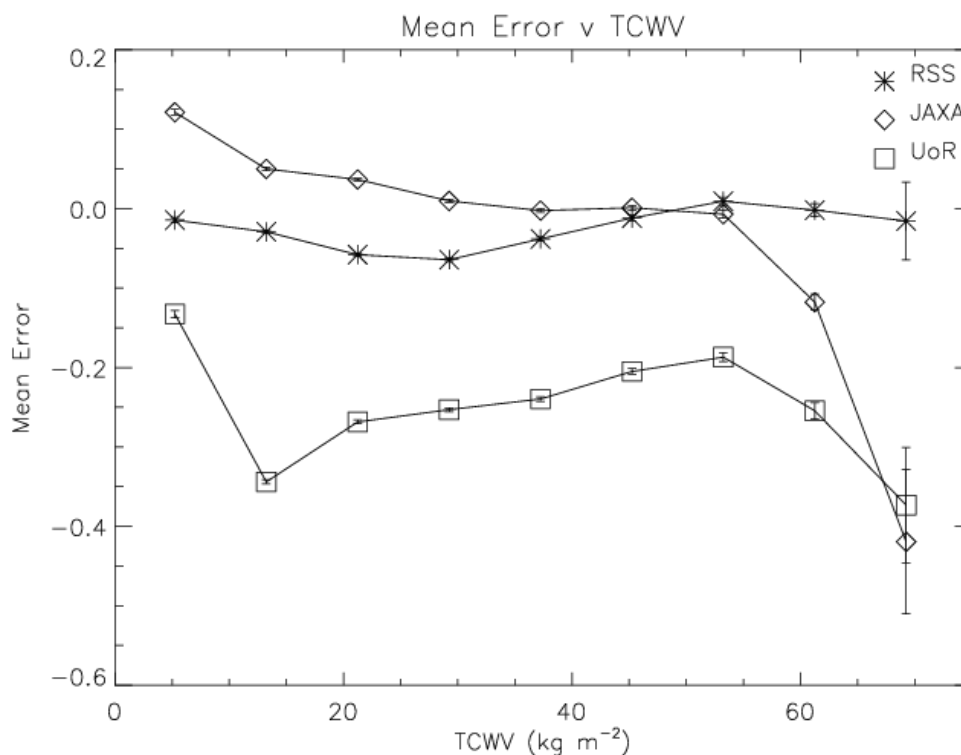


Figure 7: Mean Error Comparison against TCWV

2. Conclusion

The RSS and JAXA retrieval algorithms show similar results in terms of their overall error distributions. There are some differences between the two relating to trends with different geophysical variables but overall the two schemes are comparable. The UoR scheme shows a larger mean error and broader distribution with some noticeable structure when plotted against geophysical variables. This reflects some as yet under-corrected biases between the forward model and the observations.

3. References

- Atkinson, C.P., N.A. Rayner, J.J. Kennedy and S.A. Good, An integrated Database of Ocean Temperature and Salinity Observations, *JGR-Oceans* **119**, 7139-7163, 2014. doi:10.1002/2014HCO10053.
- Merchant, C.J., F. Le Borgne, A. Marsouin and H. Roquet, Optimal estimation of sea surface temperature from split-window observations, *Remote Sensing of Environment* **112**, 2469-2484, 2008. doi: 10.1016/j.rse.2007.11.011.
- Shibata, A., Description of GCOM-W1 AMSR2 Sea Surface Temperature Algorithm, *Japan Aerospace Exploration Agency*, 2013. http://suzaku.eorc.jaxa.jp/GCOM_W/materials/product/AMSR2_L2.pdf
- Wentz, F.J. and T. Meissner, Algorithm Theoretical Basis Document (ATBD) for AMSR Ocean Algorithm, version 2, RSS Tech. Proposal 121599A-1, *Remote Sensing Systems, USA.*, 2013.
- Wentz, F.J. and T. Meissner, Supplement 1, Algorithm Theoretical Basis Document for AMSR-E Ocean Algorithm, RSS Tech. Rep. 051707, *Remote Sensing Systems, USA.*, 2007.

PLENARY SESSION IV: NEW HORIZONS

SESSION REPORT

Chair: Alexander Ignatov⁽¹⁾, Rapporteur: Prasanjit Dash⁽²⁾

(1)NOAA STAR, Email: Alex.Ignatov@noaa.gov

(2)NOAA STAR and CSU CIRA, Email: Prasanjit.Dash@noaa.gov

ABSTRACT

The session featured three speakers representing three organizations, and an open floor discussion.

Summary of Speakers and Organizations

SST from INSAT-3D: Initial Results (20min) – Rishi Kumar Gangwar

SST from Himawari-8 (20min) – Yukio Kurihara

SST in upwelling areas: Issues and Strategies (20min) – Gutemberg França

Open floor discussion (30min)

1. Summary of presentations

The highlights for each talk and floor discussion are given below.

1.1. SST from INSAT-3D – Rishi Kumar Gangwar

This presentation was made on behalf of the Satellite Application Center (SAC) of the ISRO, in Ahmedabad. Geo SST is important for India which has a long coastline (Arabian Sea, Bay of Bengal, and Indian Ocean) and needs support Fisheries, NWP for monsoon, acoustic propagation, and climate change studies. Atmosphere is very opaque in the tropics and the top-of-atmosphere signal mostly originates from the water vapor rather than from SST. AVHRR and ATSR SSTs may be subject to errors over the Indian Ocean due to high water vapor load. India launched Kalpana-1 geostationary satellite in Sep 2002, which had only one thermal IR – wide band from 10.5-12.5. Using a single channel SST algorithm resulted in >2K RMSE. Including water vapor term as an explicit predictor reduced RMSE to ~1K. The water vapor information was obtained from TMI when available, or ICOADS. In April 2003, INSAT-3A was launched, with the same single channel set up. In May 1999, Oceansat-1 with a microwave scanning Microwave Radiometer (MSMR) was launched, with 6.6, 10.6, 18, and 21 GHz (V & H). It provided SST retrievals with RMSE ~1K, and was used in conjunction with the Ocean Color Monitor also onboard Oceansat-1, to map potential fisheries zones. ISRO also worked with other satellites and sensors on SST retrievals using split-window bands, including AVHRR/HIRS onboard NOAA satellites, ATSR onboard ERS1, TMI onboard TRMM, and MODIS onboard Aqua and Terra. Validation against pyrometer skin temperature suggests RMSEs~0.6-0.8K. INSAT-3D was launched in July 2013. Onboard are imager (with pretty much AVHRR bands for SST retrievals, one centered at 3.9 μm , and two split-window long wave bands, centered at 10.8 and 12 μm), and sounder which also has window bands. Several geophysical products are derived, including SST. In pre-launch period, RTM modeling was performed, using MODTRAN code with the TIGR database. Simulations were performed for the SST imager's bands and several representative NEdTs and view zenith angles (VZA). A quadratic split window SST equation was derived, and it was proposed to derive the regression coefficients using collocated buoy SSTs. During the daytime, only split-window bands are used; at night, the 3.9 μm is additionally employed. In case of failure of one of the split-window bands, the graceful degradation assumes using a Kalpana/INSAT-3A single channel algorithm, with a water vapor predictor. Cloud screening is performed using a cloud flag from an external cloud mask routine, plus VIS/IR thresholds, spatial coherence, and split-window brightness temperature difference. Additional QC is performed by comparing the retrieved SST to the previous cycle SST and Reynolds 1^o SST. Validation is

performed against ARGO floats, Triton moorings, research vessels, and other available SST fields (MODIS, other GHRSSST products). The processing chain was tested by applying to data of GOES-11. Post-launch, GSICS bias correction (derived against IASI) would be applied, and validation performed against buoys and other satellite SSTs. Operational SST production from split-window bands commenced on Oct 1, 2013. The product is generated every 30min, at 4km resolution. Daily, weekly and monthly composites are also produced. Validation against drifters in Oct-Nov 2013, suggests a bias from -0.5-0.7K, and RMSE ~1.3-1.6K. Comparisons with MODIS SST shows ~-0.6K bias and RMSE~1-2 K. SST gradients are also produced and analyzed, to identify potential fishing zones. Evolution of SST fronts can be monitored from geo platforms. Overall, the daytime accuracy of SST is better than at night, when sun light may be impinging on the black body. Suitable GSICS calibration is not available for such anomalies. Several issues which are being addressed, include filtering the warm low clouds, degraded performance of the SST algorithm at the swath edges, different geolocation errors in different band leading collocation errors (which may be also scan angle dependent), destriping, and generating a degraded resolution (10km) SST product for better cloud filtering. Future SST missions at ISRO include planned launch of INSAT-3DR in 2016, INSAT-3DS in 2017, and Oceansat-3 series, tentatively planned for launch in 2017, 2019, and 2020.

1.2. SST from Himawari-8 – Yukio Kurihara

Himawari-8 (H8) was launched in October 2014. It stays at 36,000 km above 140E and observes SE Asia, W. Pacific, and Australia every 10min. Advanced Himawari Imager (AHI) is onboard. H8 became operational on 7 July 2015 replacing the MTSAT-2. Spatial resolution in IR bands has improved to 2km (from 4km on MTSAT-2). AHI has more SST bands, better radiometric performance, and provides full disk every 10min (compared with 30min on MTSAT-2). Skin SST algorithm was developed which uses bands centered at 10.4 and 11.2 μm , whereas bands at 12.4, 8.6 and 3.9 bands are used optionally. Coefficients and parameters used in retrievals were calculated with RTTOV/NWP simulations in advance. Bayesian method is used to detect cloud. Data in 10.4, 12.4, and 3.9 μm bands, angles (view, solar, and relative azimuth), and MGDSST analysis are used in the Bayesian algorithm (Merchant et al, 2005; Embury, Merchant, 2014). Preliminary validation of the experimental SST product against buoy data was performed using 3hourly data in May 2015 data, using cloud probability <0.3 which was shown to provide a reasonable spatial coverage. Base "split" algorithm (10.4+11.2 μm)+12.4, split+8.6, and split+3.9 were tested. Drifting buoys were taken from NOAA iQuam system. Matchups were created within 3km, 3hrs. Nighttime validation shows that Split+12.4 gives bias~+0.1K and RMSE~0.7 K; Split+8.6 results in bias~-0.17 and RMSE~0.52 K; Split+3.9 gives bias~-0.30 and RMSE~0.46 K. During the daytime, Split+12.4 gives bias~-0.2 and RMSE~0.60 K; Split+8.6 results in bias~0 and RMSE~0.48 K. The dependencies on the VZA of all retrieval algorithms are relatively stable, up to ~65°. Future plans include making H8 L2 SST available via JAXA ftp server, and including monitoring and validation in SQUAM at NOAA. GCOM-C SST will be retrieved using the H8 algorithm.

1.3. SST in upwelling areas: Issues and Strategies – Gutemberg França

A regional L4 SST 0.05° daily analysis product is produced at the Oceanographic Modeling and Observation Network (REMO) of the Applied Meteorology Laboratory at the Federal University of Rio de Janeiro (LMA/UFRJ) and archived at http://podaac.jpl.nasa.gov/dataset/REMO_OI_SST_5km-UFRJ-L4-SAMERICA-v1.0. This presentation provided an update of the recent changes to this product, and issues and challenges the team is facing. Up until recently, REMO used NAVO AVHRR L2 products from NOAA-18 and -19 and from the microwave imager onboard TRMM, to produce analysis from 45°S-15°N, and from 15-70°W. NAVO discontinued NOAA-18 processing in Mar 2015, and TRMM data quality has been questionable since Nov 2014. In the new version of the product which became operational on Dec 1, 2014, NOAA-18 AVHRR data have been replaced with Metop-A data, and TRMM with AMSR2 and Windsat. The REMO L4 SST has been continuously validated against moored and drifting buoys and against some other GHRSSST SST products. The agreement is generally good. At the same time, the domain covered by the product was extended and now covers from 78°S-60°N, and from 100°W-45°E. The REMO Data Assimilation System (RODAS) now uses HYCOM-1/4. Comparisons with OSTIA L4 suggest generally a good agreement, except in some dynamic and coastal areas where the two products may significantly differ. The resolution in the full domain is same at 0.05°, but in the close vicinity to Brazil, in the Campos and Santos basins, higher resolution product was requested

by users. Two 0.01° resolution products are currently generated from 12-34°S, 30-54°W, one from observations only (NOAA-19 LAC 1.1km, Metop-A global 1.1km, and VIIRS 1.1km). The plan is also to include GOES-13 and microwave in the assimilation. The largest challenge is producing high-quality SST analysis in the Campos and Santos basin areas during the upwelling events. The problem was illustrated with a buoy launched by the Instituto de Estudos do Mar Almirante Paulo Moreira (IEAPM) in Jul 2013, in the immediate vicinity of Brazilian coast. During upwelling events, this buoy shows a strong vertical stratification of the ocean. Comparison of REMO and OSTIA analyses during the upwelling events suggest that REMO is a little closer to the SST measured by the buoy, and a little more realistically reproduces the spatial structure of the SST distribution around the buoy. However, all analyses including REMO, OSTIA and MUR overestimate the SST measured by the buoy, sometimes by >4°C. Moreover, analyses of all satellite data in the area also suggest that they all “don’t see” the upwelling, and measure SSTs >4°C warmer than what the buoy reads. Moreover, the top-of-atmosphere brightness temperatures measured by AVHRRs appear to be warmer than SST measured by the buoy. Additional analyses have shown that during the upwelling period, monthly mean values of the air temperature measured by the IEAPM buoy maybe warmer than SST by as much as 4°C. Approaches to work around this issue were discussed, including calculation of local coefficients in the standard MCSST/NLSST algorithms, or development of alternative atmospheric correction algorithms. These results and proposed approach have stirred a live discussion (see below).

2. Summary of Floor Discussion (discussion/suggestions/action)

2.1. SST from INSAT-3D

- *The presentation showed ‘ship – sat’ vs. Water Vapor and question was raised “why ship” and concerns were shown due to a low number of matchups.*
- *Comment: GSICS cal correction is not adequate (Andy H)*
- *Is scene dependent bias (GSICS) implemented (Andy H)*
- *Comment: how do we capture the questions raised by Rishi and others and respond (Craig D.). (Peter M.: after the meeting, offline). Craig also urged all to give support to Rishi/ISRO, if requested.*
- *Catch up on mid-night calibration (Eileen M.)*

2.2. SST from Himawari-8

- *Q: Night time validation against buoys? How it compares to ACSPO (Helen B.)
A: We are between 0.4-0.6K general (Sasha I.)*
- *Chris M. asked to explain more about the retrieval algorithm (p13 the ppt) and commented that SST derived at each IR band should have the same value, at least theoretically.*
- *Comment: The observed nighttime negative bias, e.g., -0.30 K in Split+3.9, could be because of cloud leakage. Using 3.9 micron channel, you see a bit more (Andy H.)*

2.3. SST in upwelling areas: Issues and Strategies

- *During upwelling, BT was seen to be more than Buoy temperature (a series of Questions by Peter M.)
Comments/Q: very thought provoking presentation. Show the time-series of air temperature (air-sea tempt) time-series: very unusual. Which direction is the wind flowing? (Peter M.)
A: from the East (Gutenberg F.)*

- Q: Do you know relative humidity? Do you have fog? (Peter M)
A: No (Gutemberg F.)
Comment: then RH is not high, you got to have a stable boundary layer. These are unusual phenomena and could be very well a failure in the algorithms.
 - Q: What you call Winter in the Southern Hemisphere (Sasha I)
A: OK, this is actually local summer (Gutemberg F.)
 - Q: is the upwelling ever identified as clouds? Is it ever rejected? There is a lot of cold temperature (Charlie)
Comment: I was thinking the same thing. This is one of the things we should take into account. What Peter said is impressive. Because you have strange air-sea T difference (audience)
Comment: We see some problem in CA and is a broader problem we should consider (Charlie)
 - Q: what are the wind speeds? (Peter M)
A: Not sure (Gutemberg F.)
Comment: when you have large air-sea T, fluxes go down to zero. You got a stable boundary layer in the ocean and atmosphere. The air-sea will tend to move heat to ocean (latent heat) (Peter M)
Response: I was told buoys are wrong and got technicians to check. Another problem is cloud (Gutemberg F)
 - Q: Do you have this plot for daytime (BT comparison against buoys)? Because its hard to identify for nighttime (Andy H)
A: I do not have daytime plot, here (Gutemberg F.)
Comment: You need to show that there is no cloud there, really important. My gut reaction is, it (satellite) is not able to see surface; that is why it is negative. You should check for daytime (Andy H)
 - Comment: If you have subsidence, surface RH will be low (Peter M)
Comment: look the difference between ch4 and ch5 is low, means no water vapor (Andy H., Charlie)
Comment: so for me, cold sea (Craig D.)
Response: yes, if we have WV, difference between ch4 and ch5 should be high (Gutemberg F)
 - Q: is it possible to have more than one buoy? (Irina G)
A: Yes, but we need more money (Gutemberg F.)
 - Comments: we did some comparisons, between off Chile. We did not necessarily see any of these biases. It might be interesting to see how conditions differ between these geographical areas. There must be some regional differences. Will be interesting to see this. (Jorge V.)
 - Comments: this is one of those areas, GHRSSST should look at, may be using Felyx. Make a box and keep monitoring. Fascinating area. (Craig D.)
 - Q: What is the depth of the buoy? (Peter M)
A: My God!, 2mts (Gutemberg F.)
Comment: What you might have is a very large T-gradient just above that, may be very strong diurnal heating that is not eroded in night (Peter M.)
 - Close: provocative presentation & lots of comments. Any other comments before closing (Sasha I)
 - Closing comments: we heard the importance of MW today. Also, Geostationary is very important. May be we should focus on consolidating Geo products. The 3rd thing is coastal thing. For those who are interested to lead it and present next year. (Gary C.)
 - Comments: quick follow up on Gary's comment. Ocean RS 2016 just sent out the agenda; we might want to look at it and GHRSSST can participate (Jorge V.)
-

SEA SURFACE TEMPERATURE RETRIEVALS FROM INSAT-3D: INITIAL RESULTS AND VALIDATION

Rishi Kumar Gangwar⁽¹⁾ and Alope Kumar Mathur⁽²⁾

(1) GRD/AOSG/EPESA, Space Applications Centre (ISRO), Ahmedabad, India,
Email: rgbly1986@sac.isro.gov.in

(2) CVD/ADVG/EPESA, Space Applications Centre (ISRO), Ahmedabad, India,
Email: alokemathur@sac.isro.gov.in

ABSTRACT

India on 26th July 2013 successfully launched its advanced meteorological spacecraft INSAT-3D by Ariane-5 launch vehicle from the spaceport of Kourou in French Guiana and parked at 82°E. INSAT-3D is designed for enhanced meteorological observations, monitoring of land and ocean surfaces, generating vertical profile of the atmosphere in terms of temperature and humidity for weather forecasting and disaster warning. It carries four payloads viz. 6 channel multi-spectral Imager, 19 channel Sounder, Data Relay Transponder (DRT) and Search and Rescue Transponder. For sea surface temperature (SST) measurement, Imager has two split window channels (10.3-11.3 μm and 11.5-12.5 μm) and a mid-IR channel (3.8-4.0 μm) with 4 km ground resolution. Post-launch operations included characterization of various payload instruments for first few months. Thermal Imager level-1B data was available in October, 2013 after first level of commissioning phase. After correcting for initial bias in INSAT-3D Imager channels with reference instrument as IASI onboard METOP-A and METOP-B following the standard procedure of Global Space-based Inter-Calibration System (GSICS), INSAT-3D level-1B and geophysical parameters data has been released for internal users. Sea Surface temperature (SST) product has also routinely generated using Imager thermal split window channels on half hourly, daily, weekly and monthly time scale. Various near simultaneous satellite SST products like GHRSSST from NPP and swath product from MODIS as well as quality controlled in-situ SST observations like ARGO drifter/moored buoy have been used to monitor the quality and accuracy of SST retrievals from INSAT-3D generated for each half-an-hourly acquisition. Initial results of validation for six months duration from July to December 2014 with MODIS SST shows root mean square deviation of $\sim 1\text{K}$. However, during certain time-window (around 11hrs -2000hrs GMT) anomaly in TIR-1 and TIR-2 are observed resulting in sudden drop and then rise in brightness temperatures. The most likely reason for this phenomenon may be the switching-off and switching-on of 'onboard-heaters' during 'Sun-intrusion' into the payload and blackbody housing of the spacecraft.

1. Introduction

Tropical Indian oceans are distinctively characterized with respect to mid and high latitude oceans due to prevailing higher sea surface temperatures as well as higher atmospheric water vapor loading above them. Satellite SST retrievals through infrared sensors for these regions are therefore required to account for the atmospheric correction arising out of such water vapor loading and its vertical distribution. Low clouds formation due to convective systems activity also poses a challenge in delineating such clouds during SST retrievals. Understanding of diurnal SST variations requires more accurate and frequent observations over these oceans. Ever since India's space program's conception, such a requirement was pending. Considering the importance of the SST over the Indian oceans in understanding the regional meteorological phenomenon like monsoon as well as its tele-connection with other global weather and climate processes, India launched its advance weather satellite INSAT-3D on 26th July 2013 from Kourou, French Guiana. Table 1 and 2 respectively are showing the channel characteristics as well as instrument specifications of INSAT-3D Imager.

Table-1: Imager channels' characteristics

Channel no.	Spectrum (µm)	Resolution (Km)	S/N or NEDT (K)
1	0.52 – 0.72	1	150:1
2	1.55 – 1.70	1	150:1
3	3.80 – 4.00	4	0.27
4	6.50 – 7.00	8	0.18
5	10.3 – 11.2	4	0.10
6	11.5 – 12.5	4	0.25

Table-2: Imager specifications

Telescope Aperture	310 MMΦ
Number of channels	Six
Channel separation	Beam splitter
Channel definition	Interference Filters
IFOV	28µrad VIS and SWIR (1km)
	112µrad MIR, TIR1 & TIR2 (4km)
	224µrad WV (8km)
Sampling interval	1.75 samples/IFOV for VIS, SWIR, MIR & TIR-1 and TIR-2
	3.5 samples/IFOV for WV
Scan step angle	Linear in E-W direction (8 µR step size)
	Line step 224 µrad N-S
Scan rate	20°/sec + 0.2 sec turn around
Scan linearity	56 µR (peak-peak)
In-flight calibration	Full aperture blackbody and spaceview
Scan modes	Full, normal and programmable sector
Frame time	25 minutes for normal mode
Radiometric performance	See Table-2
Signal quantization	10bits/sec
Down link data rate	4.0MB/sec
System power	140Watts
System weight	98Kg (without cooler)

INSAT-3D IR camera was switched on 7 August 2013, first IR image corresponding to 1658 GMT is shown in Figure-1. Subsequently all the cameras were switched-on successfully. After commissioning phase operations of different sensors and payload, geophysical parameters from INSAT-3D Imager viz. Sea surface temperature, rainfall, Outgoing longwave radiation, Upper tropospheric humidity and atmospheric motion vector winds etc. were generated operationally for all the half hourly acquisitions since 1st October 2013. These products are available from Meteorological and Oceanographic Satellite Data Analysis Centre (www.mosdac.gov.in) after registration. Real time products from INSAT-3D are also displayed through India Meteorological Department website (www.imd.gov.in). Every SST image, developed at sensor resolution of 4 km, consists of 2816 scan lines and 2805 pixels. SST data products (half hourly, daily, weekly, monthly, seasonally and annually) are being generated in HDF-5 format.

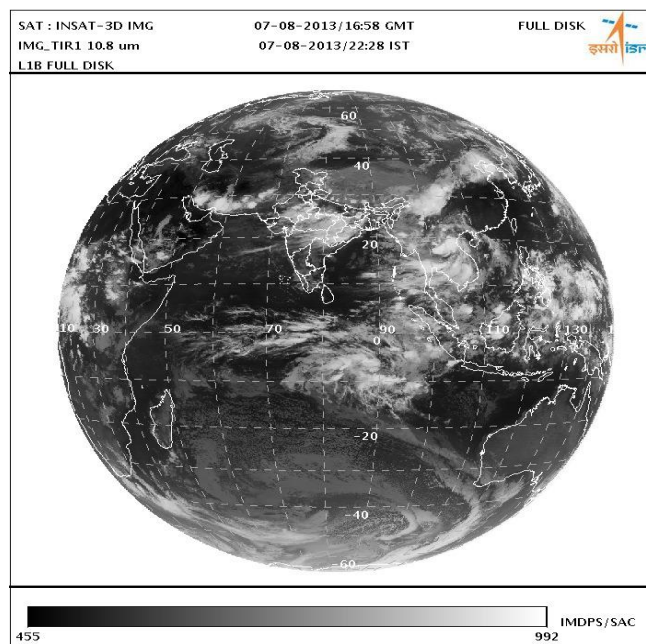


Figure 1

2. Retrieval algorithm

Radiance from Earth's terrestrial emission peaks at around 9.6 μm and it has minimum absorption by atmospheric gases, hence in order to measure earth's temperature, space borne sensors are designed around this band (8-12 μm). Still this band is not completely transparent. Atmospheric water vapour and CO₂ are the major components that attenuate the IR signal reaching at the top of the atmosphere. Since CO₂ is a uniformly mixed gas, its effect can be taken care, but water vapour being highly variable its effect can only be removed by its measurement (directly or indirectly). Retrieval of sea surface temperature (SST) from thermal infrared window channels (10-12 μm) requires atmospheric corrections arising due to attenuation of signal by intervening moisture. This correction is more in tropics during summers due to higher amount of atmospheric moisture (Barton 1983, Anding and Kauth 1970, Gohil et al 1994, Mathur and Agarwal 1991, 2002, Shenoy 1999). Our radiative transfer simulations studies have shown that with proper characterization of tropical marine conditions in the atmosphere, a suitable algorithm can be developed for accurate SST retrieval (<0.7K) using split thermal window and mid IR thermal channels provided the sensor noise is of the order of 0.1K. The SST retrieval uses IMDPS's pre-launch satellite zenith angle based retrieval coefficient sets, for both day and night (Mathur et al, 2006). SST at each cloud-free pixel is retrieved using the equation

$$SST = A_0 + A_1 T_{11} + A_2 dT + A_3 dT^2 \quad (1)$$

Where A_0 , A_1 , A_2 and A_3 are coefficients determined by simulation and may have satellite zenith angle dependence.

$$dT = T_{11} - T_{12} \quad (2)$$

where T_{11} and T_{12} are brightness temperatures for the split-window channels.

To determine the regression coefficients in the above equation, radiative transfer simulations to generate INSAT-3D channels' brightness temperatures for Indian marine tropical environmental conditions have been carried out. The important step in regression is to ensure that the sample dataset is fully and solely representative of the population for which the SST is to be derived. Instrument noise in simulated data for INSAT-3D channels have been introduced in the simulated dataset.

A typical example of half hourly, daily, weekly and monthly SST products generated operationally is shown in figure 2(a, b, c, d).

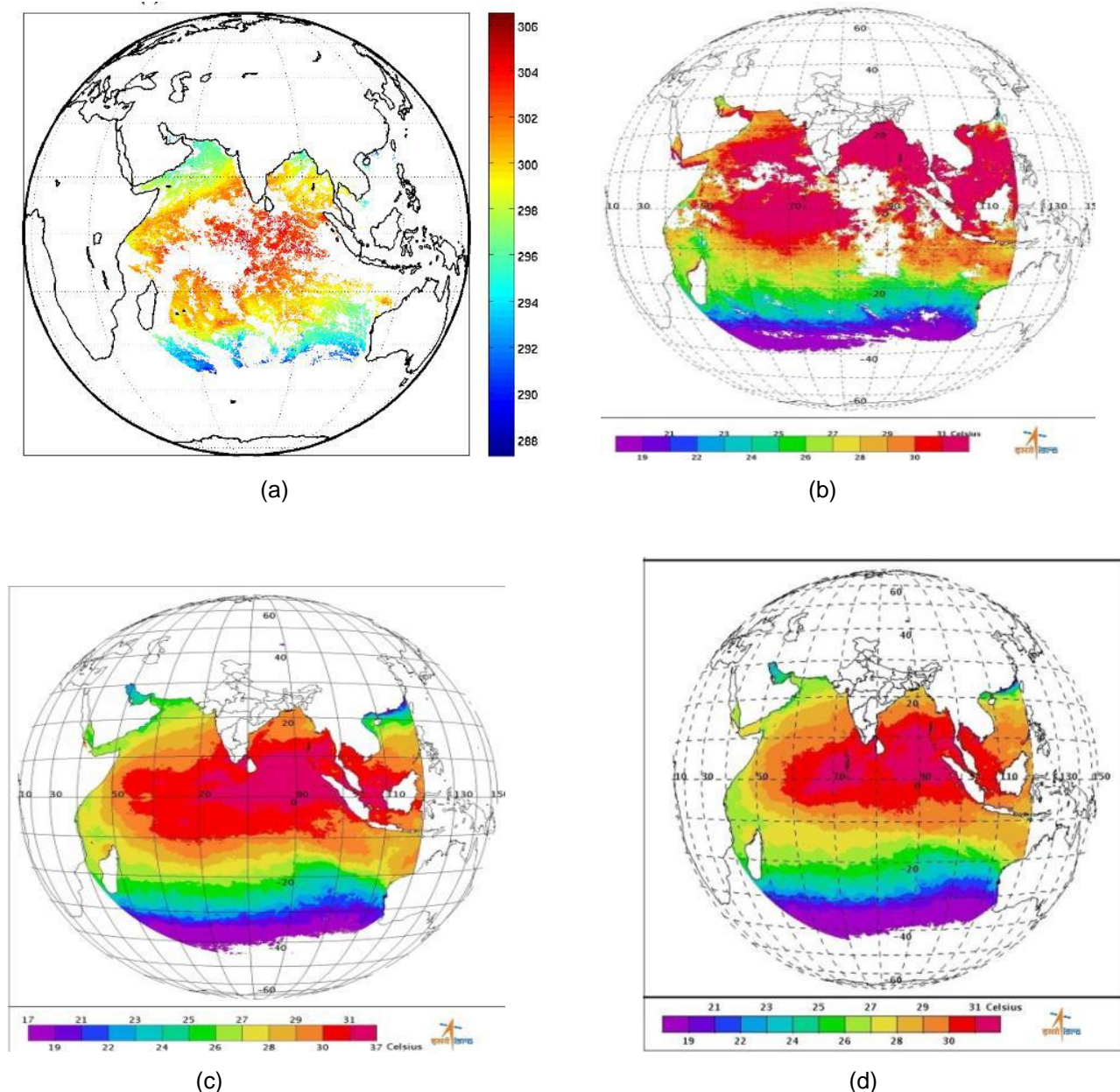


Figure 2 (a) Half-hourly (b) Daily (c) Weekly (d) Monthly SST products

3. Validation of retrieved SST

Before retrieval of SST over any pixel, INSAT-3D brightness temperature data for both the split thermal window channels are checked for land/ocean mask, cloud detection, upper and lower thresholds, differential check, satellite zenith angle. SST thus retrieved undergoes a climatological SST check. The climatological SST dataset is prepared from NOAA-AVHRR and buoy observations of 1981-2001 and is known as Reynolds SST climatology. Since MODIS SST has been very well validated for global oceans and represent best as far as

satellite derived ocean skin temperature is concerned, this product was chosen to validate INSAT-3D derived SST. Moreover, the validation of the retrieved SST from INSAT-3D has also been performed with GHRSTT from NPP satellite and in-situ drifter buoy measurements of SST.

MODIS provides sea surface temperature at 1-km (Level 2) and 4.6 km, 36 km, and 1° (Level 3) resolutions over the global oceans. This product consists of four global SST fields: daytime (D1) and nighttime (N1) SST derived from the 11-micron channel and daytime (D2) and nighttime (N2) SST derived from the 4-micron channel. In addition, a quality-assessment parameter is included for each pixel. The Level 2 product is produced daily and used to generate the gridded Level 3 products daily, 8-day, monthly, and yearly for day and night conditions. A quality parameter is provided for each data set. In the present validation exercise MODIS swath data with 1 km resolution has been used and re-gridded to 0.04 X 0.04 degree to match INSAT-3D pixel resolution.

The spatial and temporal collocation criterion for INSAT-3D derived SST at pixel resolution with respect to MODIS-SST and NPP-GHRSSST was 0.04° and ±30 minutes. Accordingly, MODIS-SST swath data and NPP-GHRSSST data were re-gridded to 0.04°. For validation with ARGO drifter buoys we have taken 0.1° as spatial resolution and ±30 minutes as temporal resolution.

The errors in SST retrieved from INSAT-3D has been quantified in terms of bias and root mean squared difference (RMSD). Bias and RMSD were calculated as per the following expressions:

$$Bias = \frac{1}{N} \sum_{i=1}^N (SST_a(i) - SST_b(i)) \quad (3)$$

$$RMSD = \sqrt{\frac{1}{N} \sum_{i=1}^N (SST_a(i) - SST_b(i))^2} \quad (4)$$

Where, SST_a and SST_b are the SST from INSAT-3D and from in-situ or other satellite like MODIS and NPP, respectively. N is the number of matchup points.

4. Results and discussions

The validation of the retrieved SST from INSAT-3D has been performed with GHRSSST from NPP, drifter buoys SST from ARGO and SST from MODIS swath based data. The following sections describes the validation results.

4.1. Comparison with GHRSTT from NPP:

Figure 3 shows the spatial distribution of retrieved SST as well as concurrent SST fields from NPP GHRSSST while figure 4 is showing the bias and RMSD in the retrieved SST with respect to NPP GHRSSST for the period 02-08 November, 2013. From the figure 3 it can be seen that the retrieved SST matches well with the GHRSSST except over north Arabian Sea where the retrieved SST is showing less values as compared to GHRSSST. This behavior can be attributed to the fact that over north Arabian Sea the aerosol dust affects the satellite measurements and we have not accounted this correction in our retrieval algorithm.

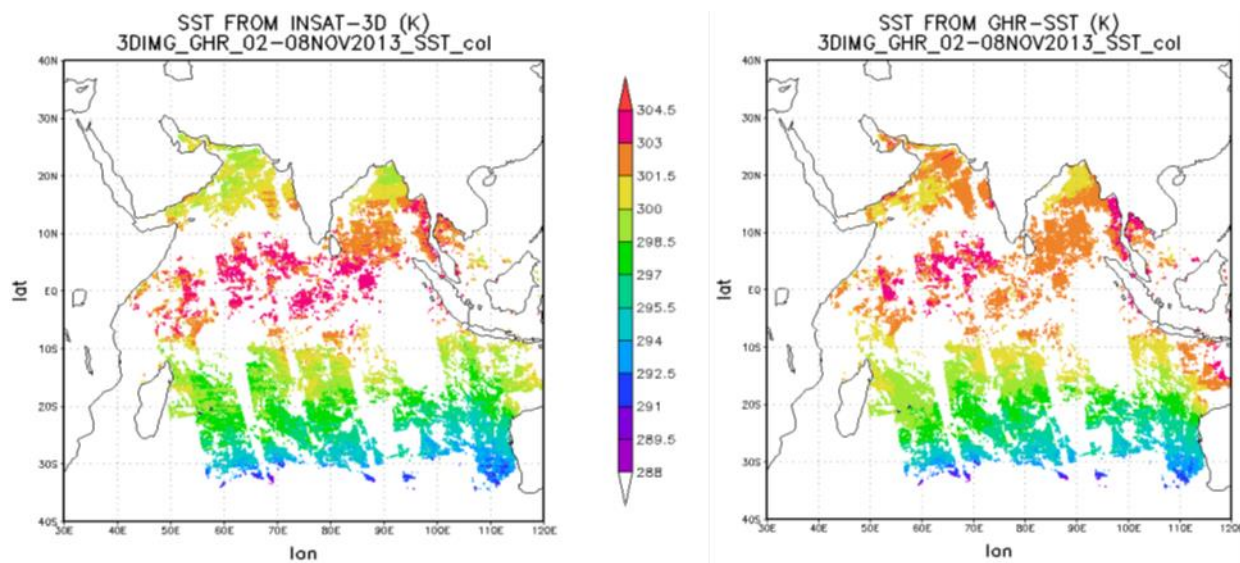


Figure 3: Spatial distribution of SST from INSAT-3D and NPP GHRSSST

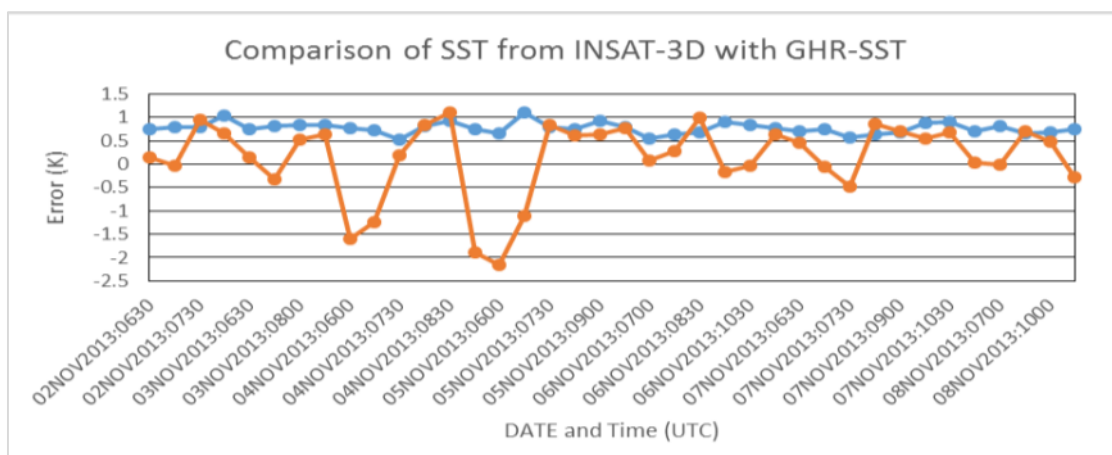


Figure 4: Bias (orange) and RMSD (blue) in retrieved SST with respect to NPP GHRSSST

We can point out from figure 4 that bias is variable with respect to time and RMSD is less than 1K for almost all the time.

4.2. Comparison with ARGO drifter buoys:

We have validated retrieved SST with in-situ SST from ARGO drifter buoys. The following figure 5 shows the locations of ARGO buoys for the period Oct-Nov 2013 for which the validation exercise has been carried out.

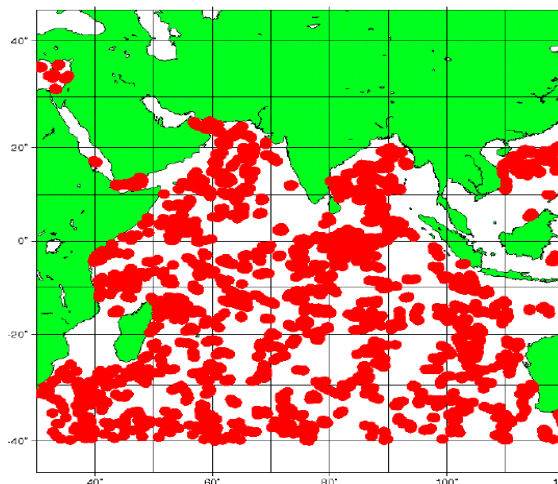


Figure 5: Coverage of ARGO drifter buoys for Oct-Nov 2013

Table 3 is showing the mean (bias) and standard deviation (Std) of the difference between retrieved SST and buoy SST for October and November 2013. We can see that for both the months INSAT-3D is underestimating the SST values. Also the higher standard deviation can be explained by the fact that the buoys measure bulk SST while satellite measures the skin SST, therefore for appropriate comparison of satellite SST we should first convert skin SST into bulk SST and then perform the validation exercise. In this exercise we haven't conducted the conversion process therefore getting the higher errors in SST with respect to buoy SST.

Table3: Statistics of comparison of retrieved SST with buoy SST

Data Used	BIAS (K)	Std (K)	No. of collocated points
Oct 2013	-0.68	1.57	15463
Nov 2013	-0.47	1.33	5970

4.3. Comparison with MODIS swath SST

To compare the retrieved SST from INSAT-3D with MODIS-AQUA swath based SST products we have collocated both the products as per collocation criterion given in the above section for the period of July to November 2014. Figure 6 shows the retrieved as well MODIS SST for 01 June 2014. It can be seen from the figure that the trends are well captured by the retrieved SST i.e. showing high SST at equatorial region and decreasing gradually towards higher latitudes on both the sides. One more thing can be pointed out that over north Arabian Sea the retrieved SST is showing less values as compared to MODIS SST. Similar kind of behavior was observed in the retrieved SST while comparing with buoy SST.

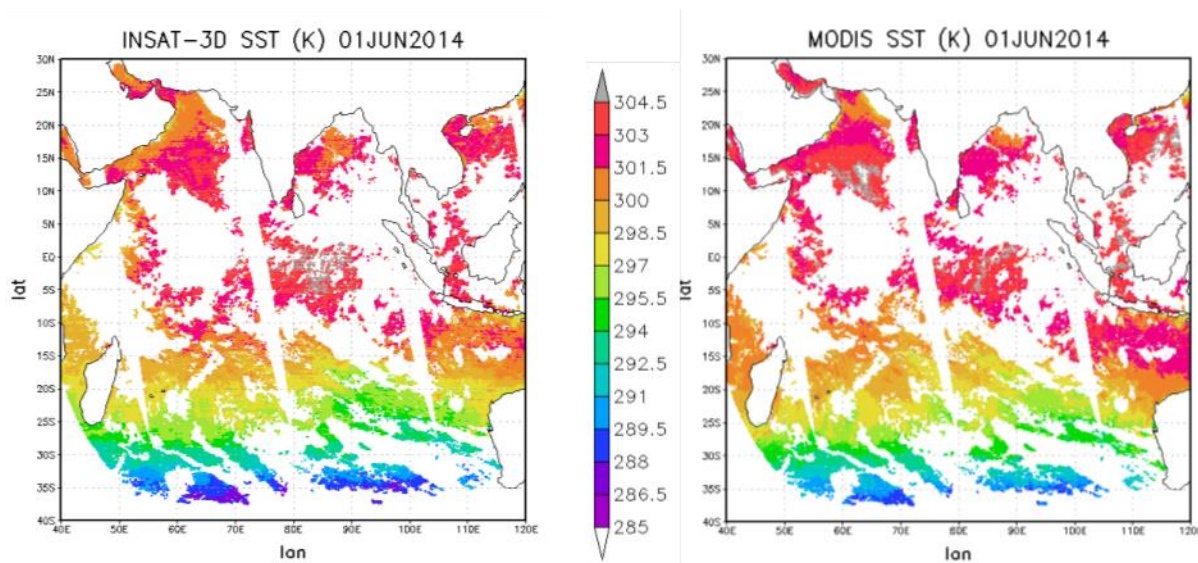


Figure 6: Spatial distribution of SST retrieved (left) and concurrent SST from MODIS (right)

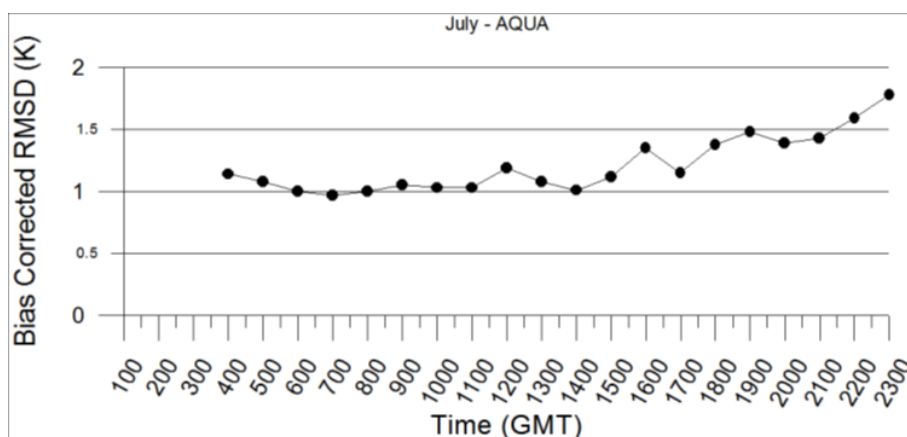


Figure 7(a)

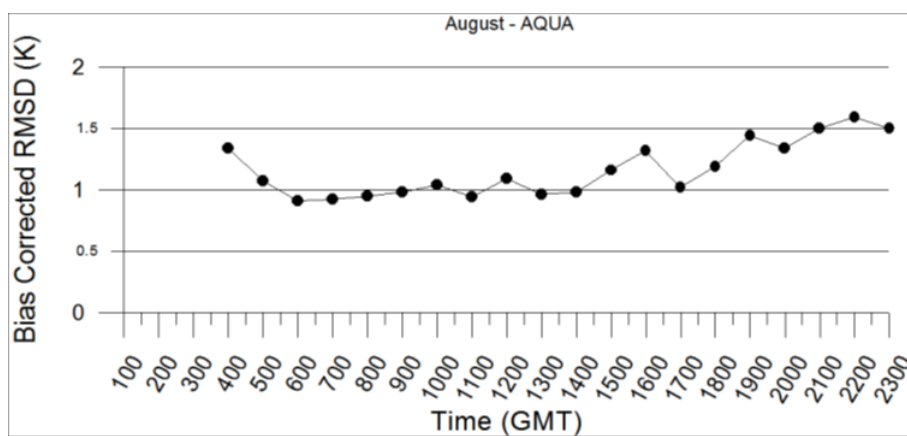


Figure 7(b)

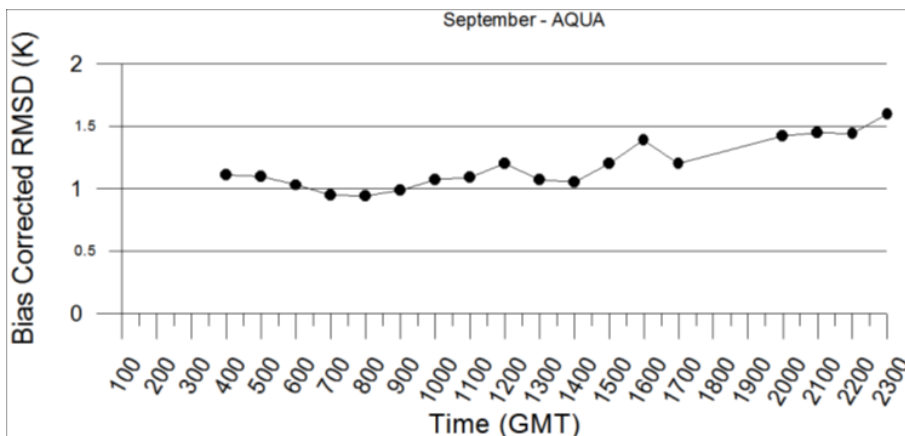


Figure 7(c)

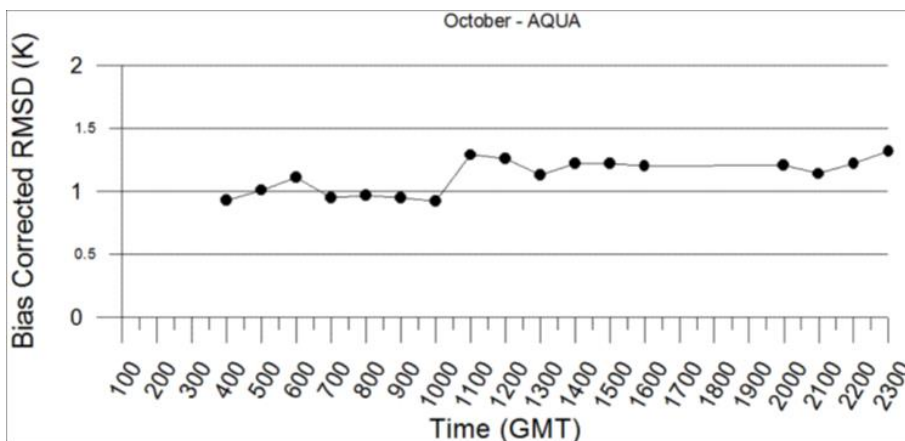


Figure 7(d)

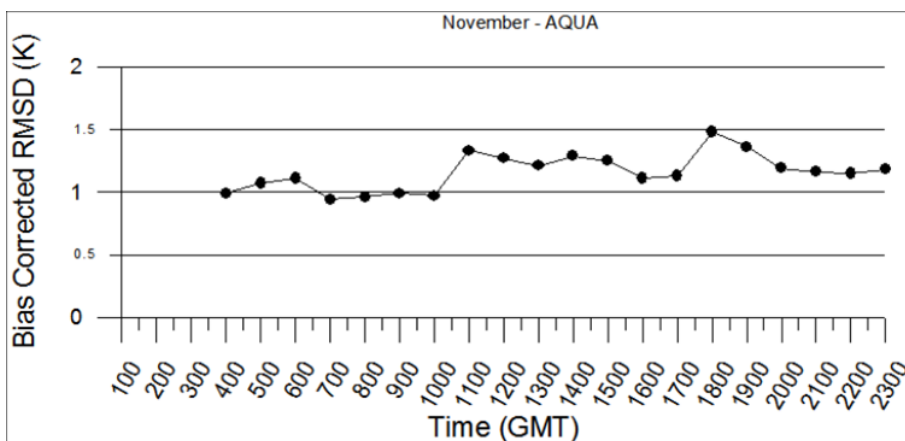


Figure 7(e)

Figures 7(a, b, c, d, e) are showing the bias corrected RMSD for hourly comparison of the retrieved SST with MODIS SST for July to November 2014. We can see from these figures that in all the months the RMSD increases after 1100 GMT. This can be partially attributed to sun intrusion impact on onboard blackbodies and payload lack of suitable GSICS calibration for conversion of radiance. We have also performed the same validation exercise with MODIS-TERRA SST data and got similar error trends in the retrieved SST.

5. Conclusion

SST products for every half hourly acquisition, daily, weekly and monthly from INSAT-3D are operationally generated. Half hourly and daily products are available from MOSDAC site (www.mosdac.gov.in) after registration. Validation of the SST products of INSAT-3D have been carried out on instantaneous basis for one year with three different sources i.e. ARGO buoys, GHRSSST from NPP and SST from MODIS. Initial validation with MODIS skin SST and GHRSSST from NPP shows that the accuracy of INSAT-3D SST is ~1K. An accuracy of ~1.5 K has been found in comparison with buoy SST. The sensitivity of diurnal sensor response and onboard calibration is being studied in detail to improve the accuracy. Furthermore, incorporation of first guess SST from general circulation models is also attempted to improve the results.

6. References

- Anding D. and R. Kauth (1970), Estimation of sea surface temperature from space, *Remote Sensing of Environment*, 1, 217-220, 1970.
- Barton I. J., Dual channel satellite measurements of sea surface temperature, *Quarterly journal of Royal Meteorological Society*, 109,365-378, 1983.
- Gohil B. S., A. K. Mathur and P. C. Pandey, An algorithm for sea surface temperature estimation from ERS-1 ATSR using moisture dependent coefficients: a simulation study, *International Journal of Remote Sensing*, Vol. 15, No.5, 1161-1167, 1994.
- Mathur A. K. and V. K. Agarwal, A quantitative study on the effect of water vapour on estimation of sea surface temperature using satellite IR observations, *Oceanography of the Indian Ocean*, B. N. Desai, Ed., Oxford & IBH publishing Co. Pvt. Ltd., 673-680,1991.
- Shenoy S. C., On the suitability of global algorithms for the retrieval of SST from the north Indian Ocean using NOAA/AVHRR data, *International Journal of Remote Sensing*, 20, 1, 11-29, 1999.

SEA SURFACE TEMPERATURE RETREIVAL FROM HIMAWARI-8

Yukio Kurihara ⁽¹⁾, Akira Shibata ⁽²⁾, Takahito Imai ⁽³⁾, Hiroshi Murakami ⁽¹⁾, Misako Kachi ⁽¹⁾

(1) Japan Aerospace Exploration Agency, Tsukuba, Ibaraki, Japan, Email: kurihara.yukio@jaxa.jp

(2) Remote Sensing Technology Center of Japan, Tsukuba, Ibaraki, Japan

(3) Japan Meteorological Agency, Tokyo, Japan

ABSTRACT

We developed a new SST algorithm which estimates SST from multi-band infrared data. The algorithm calculates SSTs by solving a parameterized simple form of the radiative transfer equation inversely. We applied the algorithm to Himawari-8 data and validated retrieved SSTs by comparing with BUOY data. Comparison result shows 0.54 ~ 0.57 of root mean square difference (RMSD) and -0.16 ~ -0.17 K of bias. In this paper, brief outline of the algorithm and validation result is presented.

1. Introduction

The Himawari-8 is a Japanese meteorological satellite operated by the Japan Meteorological Agency (JMA). Himawari-8 was launched on 7 October 2014 and located at 140.7 degrees east. It observes eastern Asia and the western Pacific region every 10 minutes. The Advanced Himawari Imager (AHI) onboard Himawari-8 carries 16 bands (3 for visible, 3 for near-infrared and 10 for infrared). Bands centered at 3.9, 8.6, 10.4, 11.2 and 12.4 microns are available for SST. Spatial resolution of these bands is 2 Km at nadir. Quality of retrieved SST is expected to be improved with these advanced observation functions of Himawari-8.

We developed a new SST algorithm which calculates skin SST by taking infrared radiative transfer processes approximately into account. With this algorithm, SST can be calculated from any combination of two or more than two IR data. JAXA is preparing L2P Himawari-8 SST product. SSTs calculated from 10.4, 11.2 and 8.6 micron data and those from 10.4, 11.2 and 3.9 micron data are provided via JAXA's FTP server [1].

Cloud areas are detected by the Bayesian inference method. Cloud mask and quality level based on the calculated cloud probability is provided with the retrieved SSTs. Bias and standard deviations against BUOY data is also calculated as a function of the probability and will also be provided as SSES information.

JAXA's Himawari-8 SST is going to be monitored and compared with other Himawari-8 SSTs at SQUAM by NOAA. Our new SST algorithm is introduced by the Meteorological Satellite Center (MSC) of JMA. JMA will generate another Himawari-8 SST product by using this SST algorithm and their original cloud mask.

This paper presents a brief outline of the algorithm and validation results.

2. Algorithm

The (1) is the basic infrared radiative transfer equation under clear sky condition. Note that each parameter is decomposed into a mean part and the difference part from the mean part.

$$\begin{aligned} \bar{I}_\lambda + \Delta I_\lambda &= \varepsilon_\lambda (\bar{I}_\lambda^s + \Delta I_\lambda^s) (\bar{\tau}_\lambda + \Delta \tau_\lambda) + \\ &(1 - \varepsilon_\lambda) (\bar{I}_\lambda^\downarrow + \Delta I_\lambda^\downarrow) (\bar{\tau}_\lambda + \Delta \tau_\lambda) + (\bar{I}_\lambda^\uparrow + \Delta I_\lambda^\uparrow) \end{aligned} \quad (1)$$

$$\begin{pmatrix} \Delta I_{\lambda_0} \\ \Delta I_{\lambda_0}^s \\ \Delta \tau_{\lambda_0} \\ \Delta I_{\lambda_0}^\uparrow \\ \Delta I_{\lambda_0}^\downarrow \end{pmatrix} \simeq \begin{pmatrix} 1 & 0 & 0 \\ a_{21} & 1 & 0 \\ a_{31} & a_{32} & 1 \\ a_{41} & a_{42} & a_{43} \\ a_{51} & a_{52} & a_{53} \end{pmatrix} \begin{pmatrix} \Delta I_{\lambda_0} \\ R_{\lambda_0}^s \\ R_{\lambda_0}^\tau \end{pmatrix} \quad (2)$$

$$\begin{pmatrix} R^s_{\lambda_1} \\ R^s_{\lambda_2} \\ \vdots \end{pmatrix} \approx \begin{pmatrix} b_{11} & b_{12} & b_{13} & \cdots \\ b_{21} & b_{22} & b_{23} & \cdots \\ \vdots & \vdots & \vdots & \ddots \end{pmatrix} \begin{pmatrix} R^s_{\lambda_1} \\ R^s_{\lambda_2} \\ \Delta I_{\lambda_1} - \Delta I_{\lambda_0} \\ \Delta I_{\lambda_2} - \Delta I_{\lambda_0} \\ \vdots \end{pmatrix} \quad (3)$$

To parameterize (1), we introduced (2) and (3). Here, $R^s_{\lambda_0}$ and $R^r_{\lambda_0}$ on the right side of (2) are the orthogonal components of $\Delta I^s_{\lambda_0}$ and $\Delta \tau_{\lambda_0}$, respectively. Using (2) and (3), SST can be calculated at each IR band from a pair of $R^s_{\lambda_0}$ and $R^r_{\lambda_0}$. From these calculated SSTs, the most-likely SST and its residual are calculated by the least square method. Calculated residual generally depends on the input pair of the orthogonal components. Therefore, it is reasonable to define the best SST as the most-likely SST which is calculated with the smallest residual. The best SST is derived by iterating the calculation:

$$\mathbf{x}_{n+1} = \mathbf{x}_n + (\mathbf{S}_x^{-1} + \mathbf{K}^T \mathbf{S}_r^{-1} \mathbf{K})^{-1} \mathbf{K}^T \mathbf{r}(\mathbf{x}_n). \quad (4)$$

Here, the \mathbf{x}_n is the orthogonal vector and the $\mathbf{r}(\mathbf{x}_n)$ is the residual vector calculated with the most-likely SST (Rogers 1990 [2], Merchant et al. 2008 [3]).

Clouds are detected with the Bayesian inference method (Merchant et al. 2005 [4]). 10.4, 12.0 and 3.9 micron data and SST analysis are used to calculate cloud probability. SST analysis is generated and provided by JMA. The 3.9 micron data were used as an alternative to visible data. However the use of this is turned off at this point because of a problem around the sun glint area.

3. Validation

We validated Himawari-8 SSTs by comparing with BUOY data. BUOY data were downloaded from iQUAM of NOAA. Himawari-8 SSTs were calculated from 10.4, 11.2 and 8.6 micron data observed in June 2015 to August 2015. We chose SSTs with cloud probability smaller than 0.3 and compared with the BUOY data, which were located and observed within 3 km and 3 hours. Table 1 shows the monthly statistics of the retrieved SST. Statistics are almost constant during this period, i.e., 0.54~0.57 K of RMSD, -0.16~-0.17 K of bias. Calculated negative biases agree with prior research on the skin and bulk SST (Donlon et al. 2002 [5]). Figure 1 shows the dependency on the satellite zenith angle (SZA). While biases are stable at the SZA smaller than 60 degrees in night time, biases in daytime show slight dependency, especially positive tendency against the night time bias at smaller SZA. This tendency can be caused by daytime warming, because the data at smaller angle are located in the equatorial ocean around 140 degrees of east longitude where strong heating is expected in daytime. Large positive tendencies at SZA larger than 60 degrees are shown more clearly in figure 2. Positive biases in the Northern Pacific can be caused by ocean fog. However, this should be examined for carefully.

Month	RMSD	Bias	Stdv	N
June 2015	0.57	-0.17	0.54	395,244
July	0.56	-0.16	0.54	404,079
August	0.54	-0.17	0.51	400,921

Table 1: Monthly statistics of the SST retrieved from 10.4, 11.2 and 8.6 micron data of Himawari-8

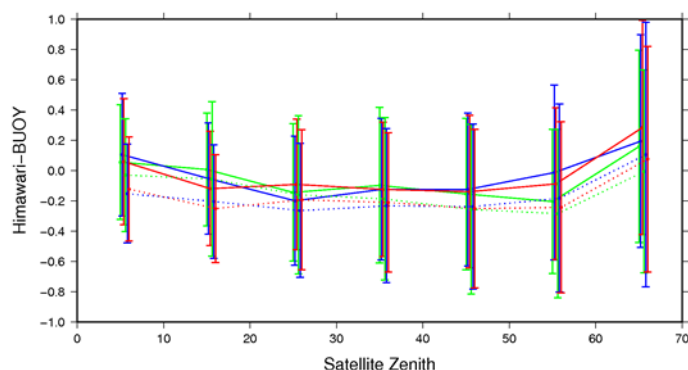


Figure 1: Biases and standard deviations as a function of the satellite zenith angle. The color of green, blue and red denotes the month of June, July and August. The solid line shows the result for daytime and the dotted line shows night time.

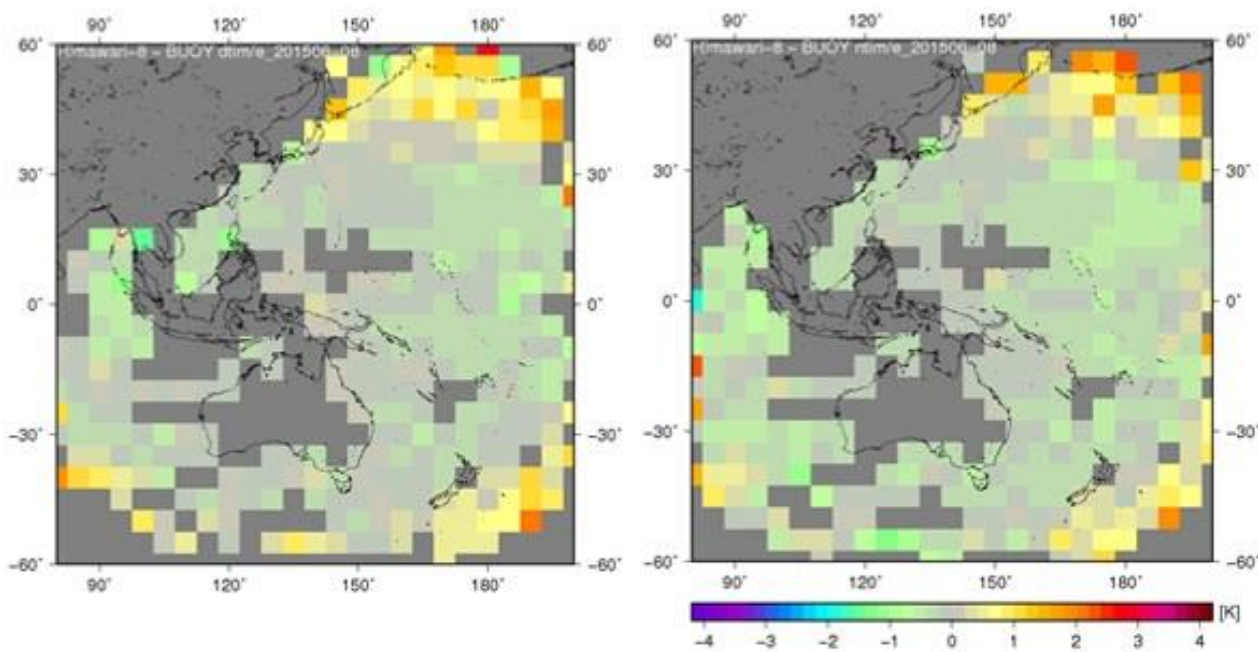


Figure 2: Regional dependency of bias. Biases for daytime (left) and for nighttime (right) are calculated at each 5x5-degree square

4. Conclusion

We developed a new SST algorithm, which calculates skin SST by solving parameterized radiative transfer calculation. We applied this new algorithm to the data from Himawari-8. Validation result shows 0.54~0.57 K of RMSD and -0.16~-0.17 K of bias. These negative biases agree with the mean difference between skin and bulk SSTs by former research. Any remarkable dependency was not found. However, strong positive biases were found in high latitudinal area where the satellite zenith angle is larger than 60 degrees. These biases and seasonal bias will be examined for after annual data become available.

5. References

- [1] JAXA EORC, "JAXA Himawari monitor," JAXA, September 2015. [Online]. Available: <http://www.eorc.jaxa.jp/ptree/index.html>.
- [2] Rodgers, Clive D, "Characterization and error analysis of profiles retrieved from remote sounding measurements," *Journal of Geophysical Research: Atmospheres* (1984--2012), 1990
- [3] Merchant, CJ and Le Borgne, P and Marsouin, A and Roquet, H, "Optimal estimation of sea surface temperature from split-window observations," *Remote Sensing of Environment*, 2008.
- [4] Merchant, CJ and Harris, AR and Maturi, E and MacCallum, S, "Probabilistic physically based cloud screening of satellite infrared imagery for operational sea surface temperature retrieval", *Quarterly Journal of the Royal Meteorological Society*, 2005.
- [5] Donlon, CJ and Minnett, PJ and Gentemann, Chelle and Nightingale, TJ and Barton, IJ and Ward, B and Murray, MJ, "Toward improved validation of satellite sea surface skin temperature measurements for climate research," *Journal of Climate*, 2002

SEA SURFACE TEMPERATURE ESTIMATION IN UPWELLING AREA: ISSUES AND STRATEGIES

Rosa Cristhyna de Oliveira Vieira Paes⁽¹⁾, Rodrigo Carvalho de Sousa⁽¹⁾, Gutemberg Borges França⁽¹⁾

(1) Federal University of Rio de Janeiro, Department of Meteorology, Laboratory of Applied Meteorology, University City Campus, CEP: 21.941-916 Rio de Janeiro, RJ - Brazil.,
Email: rosa,rodrigo,gutemberg@lma.ufrj.br

ABSTRACT

The Sea Surface Temperature (SST) estimation from sensors on board satellites has great importance to assimilation in oceanographic numerical models for many purposes. In order to reach this goal, sub-optimal interpolation scheme has been implemented using NOAA-19, Metop-A, AMSR-2 and Windsat satellites data through REMO (Oceanographic Modeling and Observation Network) to obtain a cloud-free daily SST. In particular, the problem is how to estimate the SST field in upwelling zone alongside of Rio de Janeiro's state coast in Brazil. The area of this upwelling could extend an area of approximately 40.000 km² or even bigger in mentioned region. Due to the upwelling importance for atmospheric-ocean models and others oceanographic issues, a buoy (called IEAPM buoy) was settled on the southern coast of Arraial do Cabo (coordinates 22.994°S and 42.187°W), around 6 km far from the coast, in July 2013. The daily SST buoy has been comparing with SST analysis and the differences between them have shown that SST analysis overestimated the in situ SST in about 4 K during upwelling events. Therefore, our idea is to present alternative ways to estimate appropriately SST analysis - by calibrating regionally the MCSST algorithm - during aforementioned events. Preliminary results will be presented and discussed.

1. Introduction

A simple system for daily cloud free sea surface temperature (SST) composition, named REMO SST, has been updated based on thermal AVHRR data from NOAA 19 and Metop-A, and microwave data from AMSR-2 and Windsat is provided by REMO's group. Barnes' objective analysis (França *et al.*, 2013) is applied as an interpolator to merge these two data sources, which have different spatial and temporal resolutions in a daily SST composition and in a regular grid product (0.05°) in netCDF GDS v2 format. Validation has been carried out with moored and drifting buoys and also against GHRSSST products. The results are quite good in open ocean when compared with in situ data and with GHRSSST products, but near the coast during the upwelling event the differences between SST analysis and SST from the buoy located approximately 6km from the coast are high. The present challenge is to develop a better SST analysis during an upwelling event in Campos and Santos basins as it follows in Figure 1.

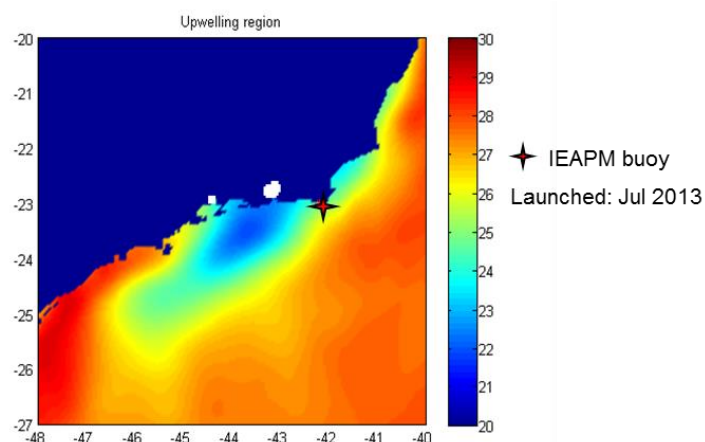


Figure 1: Upwelling region.

2. SST updates at REMO

The previous series available at PODAAC is a daily SST analysis using NOAA18-19 & TRMM data (ftp://podaac.jpl.nasa.gov/OceanTemperature/ghrssst/data/GDS2/L4/SAMERICA/UFRJ/REMO_OI_SST_5km/v1/). NOAA18 and TRMM were discontinued and a new series (spatial resolution of 0.05°) has been produced since March 2015 using NOAA 19, Metop-A, AMSR-2 and Windsat. The results are quite good as illustrated in Figure 2 (a),(b) and Figure 3.

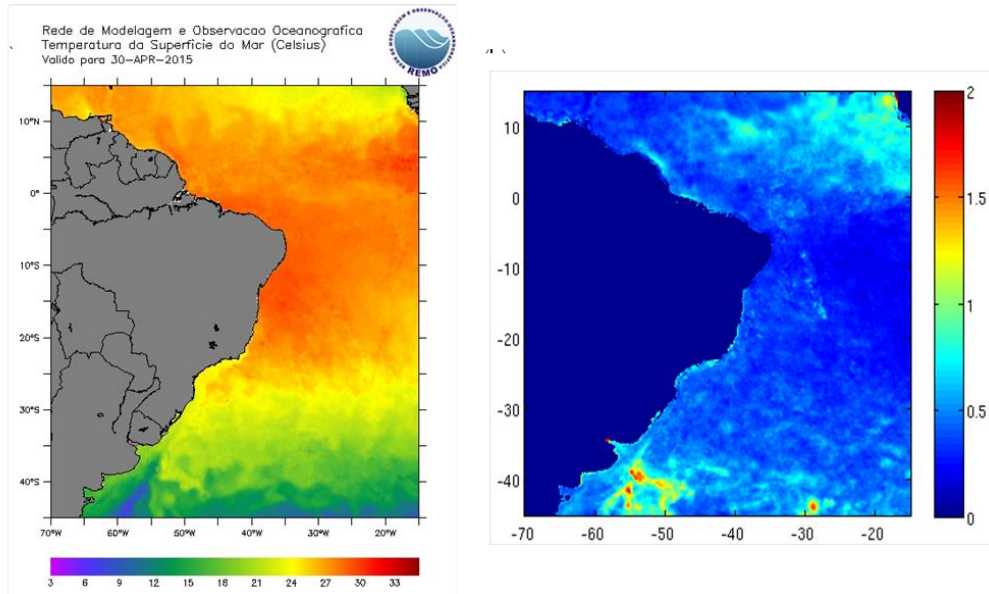


Figure 2: New version of REMO SST (a) and RMSE field generated from REMO SST and OSTIA SST during the period from March 2015 to June 2015 (b).

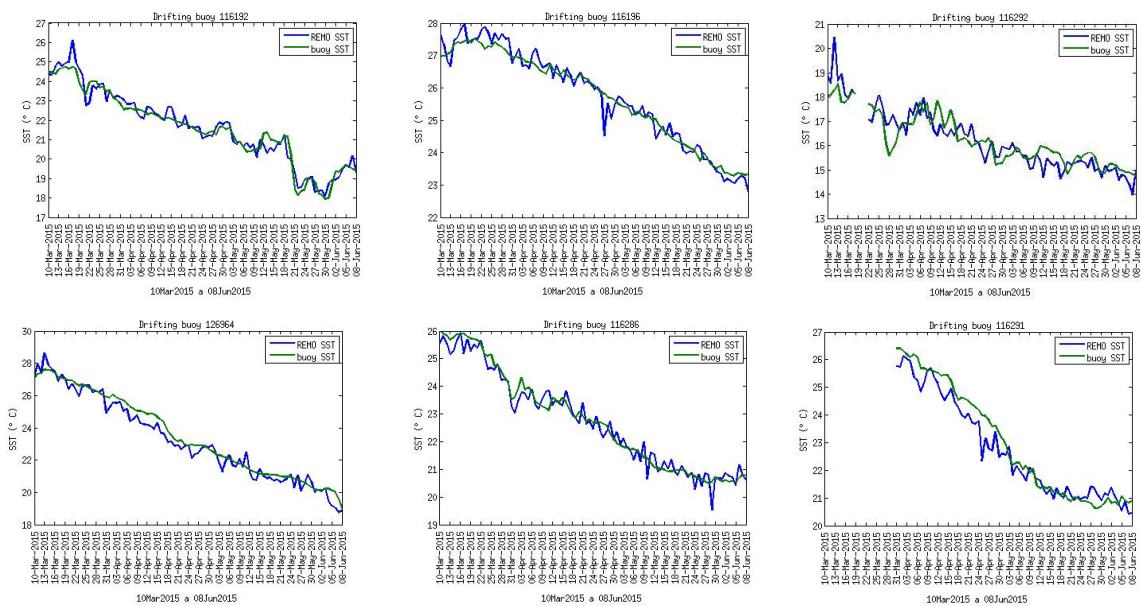


Figure 3: Validation with some drifting buoys (March-June 2015).

3. Applied data and Challenge

A study case related to upwelling event from January 14th to February 14th, 2014 was analyzed. The upwelling study area lies between latitudes 20°S and 27°S and longitudes between 48°W and 40°W where a strong upwelling event was recorded by the buoy (IEAPM buoy) located near the Brazilian coast.

Figure 4 depicts a comparison between buoy and SST products (a) and buoy and SST estimation (b) during the upwelling period. The comparisons between in situ SST from this buoy and all SST products (REMO, OSTIA and MUR) and SST estimations (from NOAA, MSG, GOES and METOP-A) have overestimated SST from the buoy in about 4°C for the period aforementioned (during the summer).

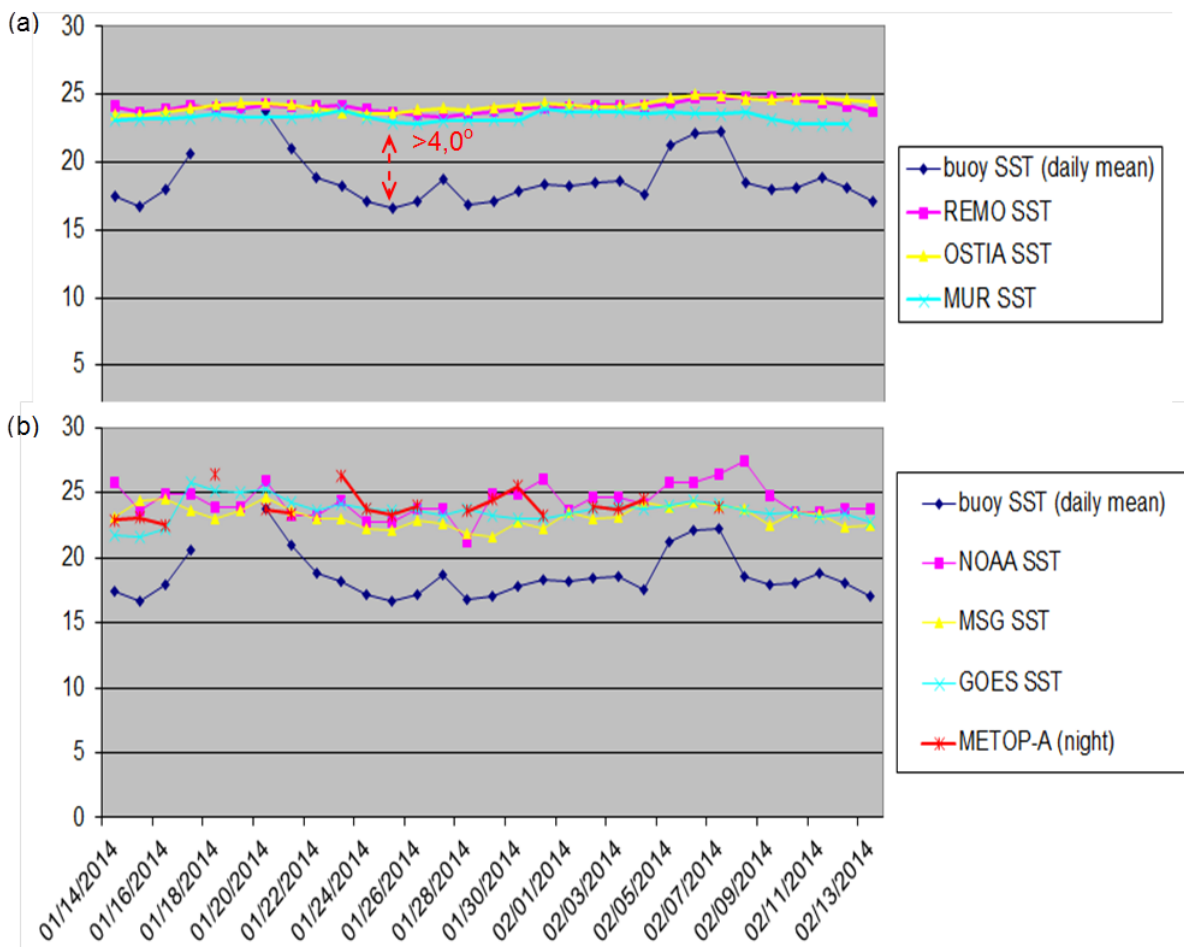


Figure 4: Comparison between buoy and SST products (a) and buoy and SST estimation (b) for upwelling period.

Figure 5 depicts a comparison between in situ SST (buoy), METOP-A SST and METOP-A BT3 and BT4. Unexpectedly, the buoy SST is less than the Brightness Temperature (BT) measured by the satellite. The reason for it is unknown and is being investigated. One hypothesis is a thermal inversion process. Figure 6 depicts the differences between the air temperature and buoy SST, where during the upwelling event are significative.

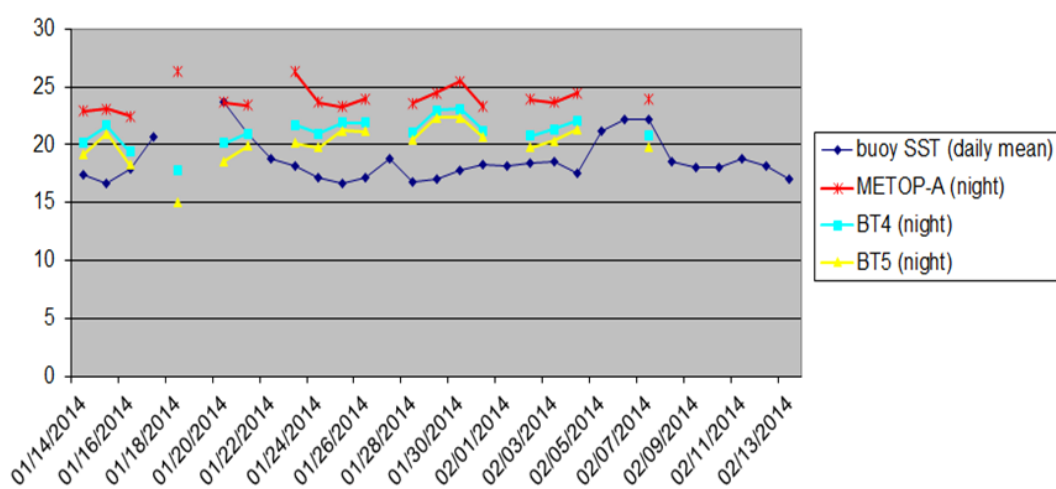


Figure 5: Comparison between in situ SST (buoy), METOP-A SST and METOP-A BT3 and BT4.

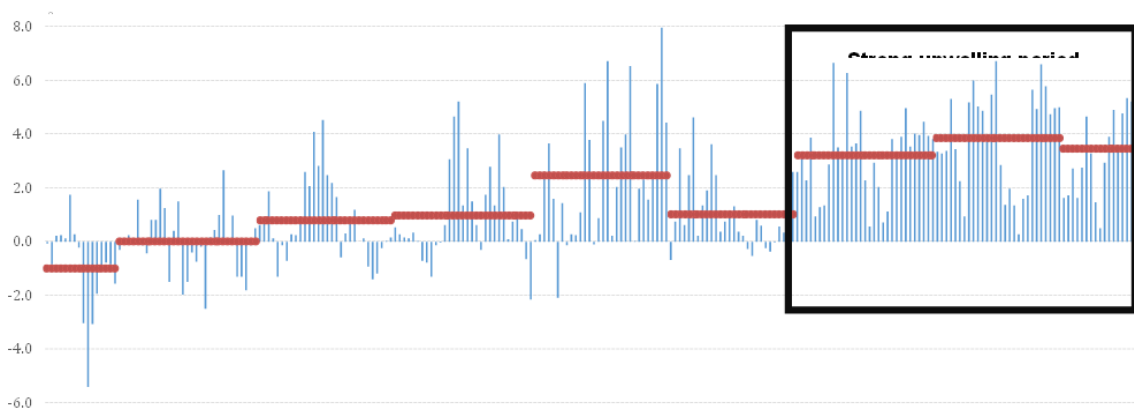


Figure 6: The difference between the air temperature (T_{air}) and buoy SST (SST_b) during the upwelling event. In blue: $T_{air} - SST_b$ (daily difference), in orange: $T_{air} - SST_b$ (monthly mean difference).

4. Considerations and way-forward

It is not clear why, during the upwelling event, the SST estimated by satellites and all products of GHRSSST overestimated the buoy SST. In order to try to solve this problem, some strategies are currently under development for the REMO SST product, as it follows: 1) To estimate local coefficients (*in situ* versus BT's); and 2) To develop local atmosphere correction algorithm.

Regarding estimation of local coefficients, a locally match-up database is building up. For the period of two years (2011 and 2012) the match-up is ready with approximately 60.000 coincident points between METOP-A and buoys database from GTS. Currently, 2013, 2014 and 2015 are under development. The previous results of SST estimated using local coefficients for the first two years show values in upwelling area closer than IEAPM buoy.

5. References

França, G. B.; Paes, R. C. O. V.; Oliveira, A. N. ; Ruivo, B. C. ; Sartori Neto, A. Daily blended microwave and infrared Sea Surface Temperature composition. *Revista Brasileira de Geofísica (Impresso)*, v. **31**, p. 317-328, 2013.

PLENARY SESSION V: DIURNAL VARIABILITY

AN ANALYSIS SYSTEM FOR DIURNAL SEA SURFACE TEMPERATURE

James While⁽¹⁾, Chongyuan Mao⁽¹⁾, Matthew Martin⁽¹⁾, Peter Sykes⁽¹⁾, Jonah Roberts-Jones⁽¹⁾,
Alison McLaren⁽¹⁾

(1) Met Office Fitzroy Road, Exeter, EX2 3PB, UK, Email: james.while@metoffice.gov.uk

ABSTRACT

The Met Office has, through the Copernicus Marine Environment Monitoring Service (CMEMS), recently begun providing a daily gap-free analysis of the global diurnal cycle in SST. This diurnal cycle is combined with the OSTIA foundation SST in-order to produce hourly maps of the ocean skin temperature. SST observations from the SEVIRI, GOES-W, MTSAT2, and NOAA-AVHRR satellite instruments, with geostationary observations being especially valuable, are used to improve the analysis through the use of a variational assimilation technique. In order to assimilate SST observations they must first be converted to observations of diurnal SST; this is done by subtracting a foundation estimate from each observation. Validation using independent near surface Argo measurements has shown the benefit of assimilating these observations.

In this work we describe the analysis system and also demonstrate the impact of assimilating diurnal SST observations. For the observations we describe how nighttime values are used to calculate a biased foundation SST for each data set (i.e. for each satellite). This foundation estimate is then removed from each SST measurement, with the assumed unbiased residuals treated as representing observations of diurnal SST. A 4DVar like scheme is used to assimilate the daytime observations, where the assimilation adjusts the applied wind and heat forcing so that the diurnal model better fits the data.

1. Introduction

The Met Office has since March 2015 been providing a daily analysis product of skin SST to users through the Copernicus Marine Environment Monitoring Service (CMEMS; <http://marine.copernicus.eu/>). This product is the sum of three components - a foundation SST, a warm layer correction, and a cool skin correction – all of which are modeled separately. Furthermore a data assimilation technique is used to improve the representation of the warm layer by assimilating satellite SST data.

A schematic diagram of the diurnal analysis system is shown in Figure 1. The bulk of this document is taken up describing the components shown in this diagram, with details given over the next several sections. The manuscript concludes with a final section presenting validation results against near surface Argo floats.

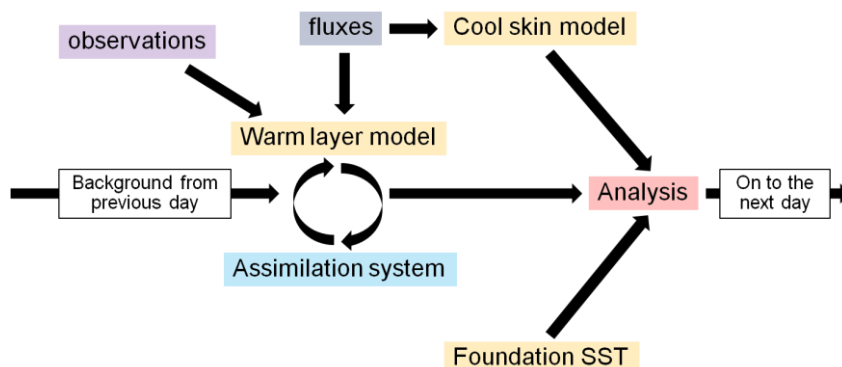


Figure 1: Schematic of the Diurnal analysis system.

2. Foundation SST

Foundation SST within the diurnal analysis system is taken directly from the daily OSTIA SST foundation product (Donlon, 2012). Data from OSTIA is re-gridded from the original $1/20^\circ$ resolution to the $1/4^\circ$ grid used by the rest of the diurnal analysis.

3. Cool skin model

The cool skin represents the cooling effect experienced in the top ~ 1 mm of the water column due to long wave cooling. In our system we use the model of Artale et al (2002) to estimate the magnitude of the cool skin. This is a prognostic model that defines the surface cooling in terms of the instantaneous wind stress and heat flux. A map of the cool skin generated by this model for a range of wind stresses and heat fluxes is shown in Figure 2.

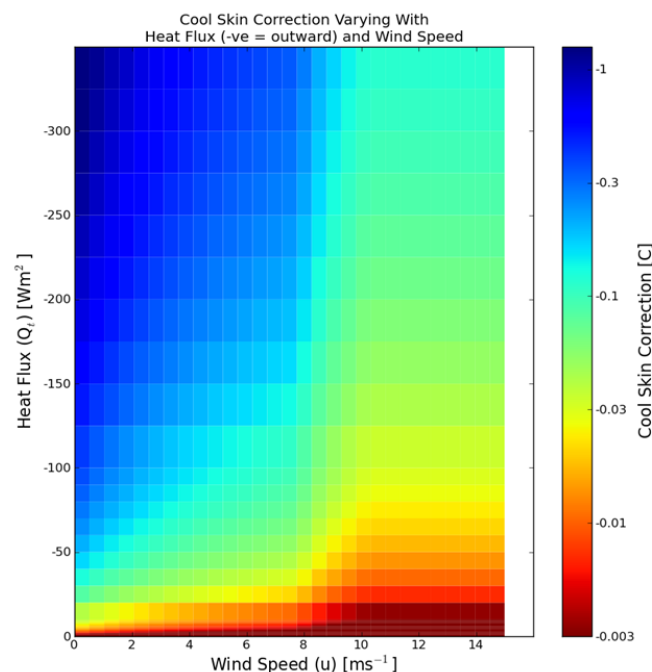


Figure 2: Cool skin value against the applied wind and heat fluxes. Wind stress is given here as a friction velocity. Note that blue represents a more negative value.

4. Warm layer model

The warm layer is the ~ 3 m deep layer in the water column that is warmed due to incident solar radiation. Heat deposited in this layer is either lost back to the atmosphere through long wave cooling, or is mixed to depth by the action of the wind. The balance of heat loss and solar heating leads to a diurnal cycle in this layer. We model the diurnal cycle in the warm layer using the methodology of Takaya (2010), but adapted to use the solar absorption parameterization of Gentemann et al (2008). An example of the output of the Takaya model is shown in Figure 3, which shows the mean diurnal signal for January 2007.

5. Fluxes

The fluxes used to drive the cool skin and warm layer models are taken from the Met Office daily NWP output and are processed using the CORE bulk formulae (Large & Yeager; 2004). Fluxes are updated hourly for

wind speed and every 3 hours for the heat flux; linear interpolation between these fields is used to provide the flux on each model time-step.

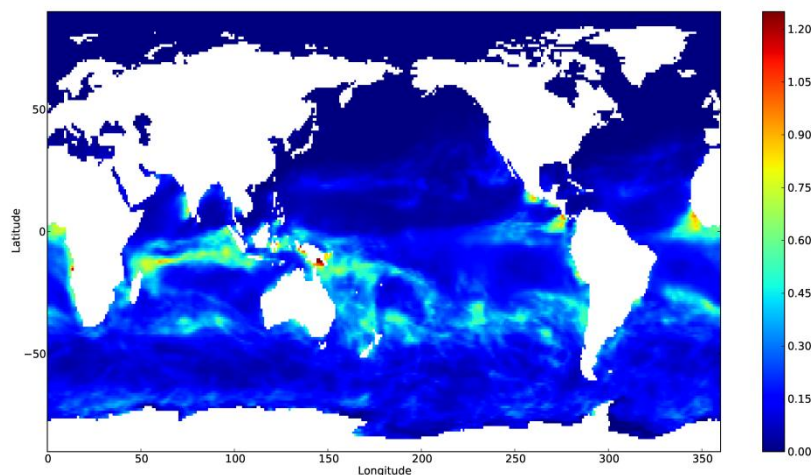


Figure 3. Mean diurnal signal for January 2007 using Met Office NWP Fluxes applied to the Takaya (2010) model.

6. Assimilation system

Within the analysis we constrain the warm layer using a variational data assimilation technique that is similar to 4DVar. The system is implemented using the NEMOVAR framework. (Waters et al; 2014). Observations of the warm layer (see Section 7 for a description of the observations) are assimilated using the methodology of While & Martin (2013). In this technique both the wind stress and heat forcing are adjusted throughout the day so that the warm layer is brought closer to the observations. The assimilation spreads information from observations based upon the correlations in the wind and heat errors. These are taken to be constants at 111 km/4 hours for the heat flux and 178 km/3.4 hours for the wind stress. The magnitude of the assimilation induced changes depends on the ratio between the errors in the fluxes and observations; flux error standard deviations are 55 W/m² for the heat flux and 6×10⁻⁴ m/s for the wind friction velocity. Errors on the observations are taken to have a standard deviation of 0.6 °C.

7. Observations

Observations assimilated into the warm layer come from the polar orbiting NOAA-AVHRR sensors and the geostationary SEVIRI, MTSAT2 and GOES-West instruments. These sources provide data as SST products which need to be converted to observations of the warm layer (referred to here as dSST) before they can be assimilated. As detailed in Figure 4, each satellite instrument is processed individually by calculating a foundation SST from the nighttime observations and then subtracting this foundation temperature from the daytime observations. This procedure yields the dSST values which, because we assume that night and daytime observations are equally biased, should be nearly unbiased. As there can be gaps in nighttime data, and thus the foundation estimate, an additional quality control step is performed on the dSST data to remove observations where the foundation estimate is believed to be poor.

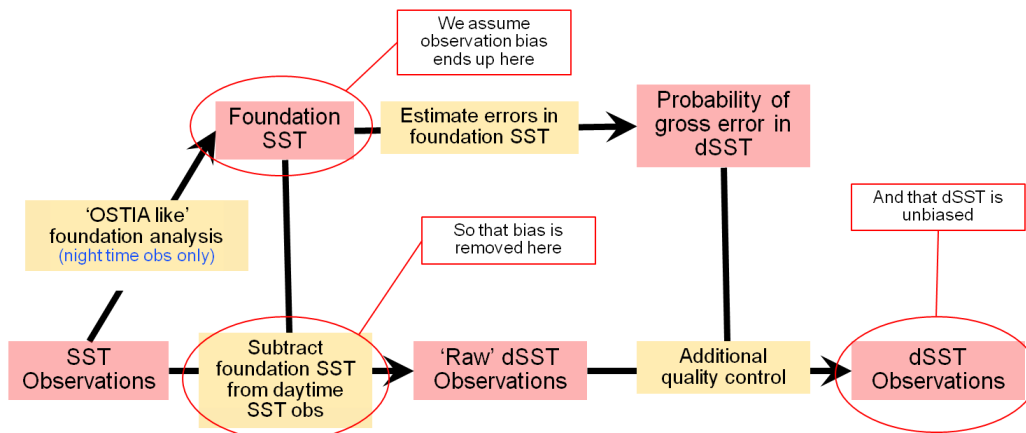


Figure 4. Schematic of the method used to process SST observation to dSST observations.

8. Results

Validation of our skin SST analysis has been done by comparing a 3 month run (September to November 2014) of our system to data from near surface Argo floats in the Atlantic. Results from this comparison, when only considering large diurnal signals ($> 0.4 \text{ }^\circ\text{C}$), are shown in Figure 5. In this figure it can be seen that using the warm layer model does improve the fit to Argo and a further improvement is observed when assimilation is included. However, the reductions are within the standard error, only 32 Argo profiles were available for the validation, and further validation work needs to be done.

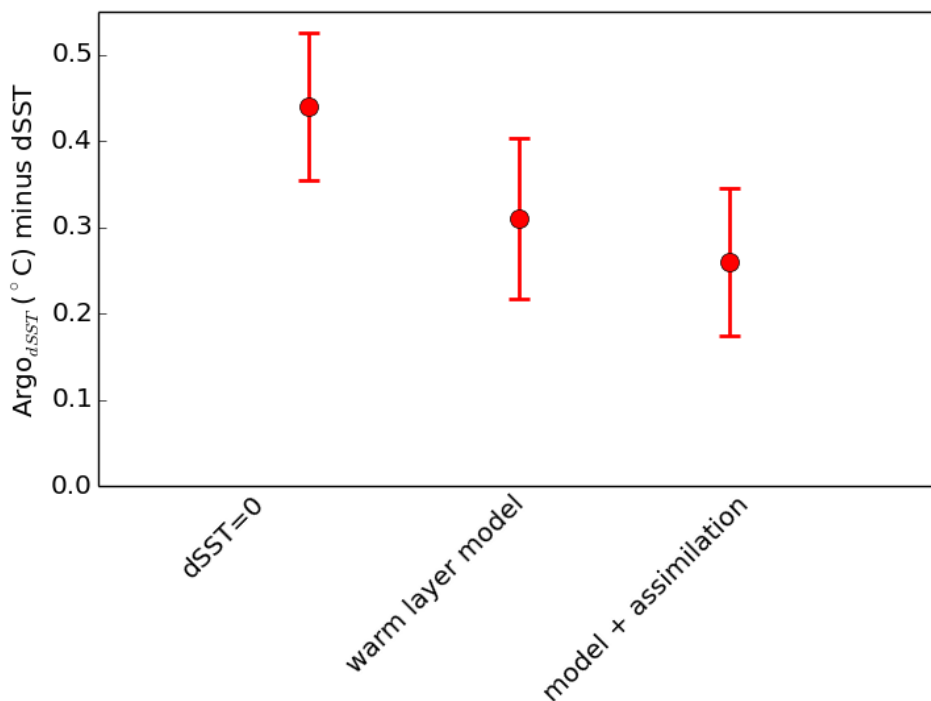


Figure 5. Mean difference between Argo dSST (Argo surface temperature minus Argo 4m temperature) and the models. The dots mark the mean values, while the whiskers are the standard error.

9. References

- Artale, V., Iudicone, D., Santoleri, R., Rupolo, V., Marullo, S., D'Ortenzo, F., Role of surface fluxes in ocean general circulation models using satellite sea surface temperature: validation of and sensitivity to the forcing frequency of the Mediterranean thermohaline circulation, *J. Geophys. Res.*; **107(C8)**; 3120, 2002
- Donlon C.J., Martin M., Stark J., Roberts-Jones J., Fiedler E., Wimmer W. The Operational Sea Surface Temperature and Sea Ice Analysis (OSTIA) system, *Remote Sensing of the Environment*, **116**, 140-158, 2012
- Gentemann C. L., Minnett P. J., Ward B., Profiles of ocean surface heating (POSH): A new model of upper ocean diurnal warming, *JGR*, **114**, C07017
- Large W, Yeager S., Diurnal to decadal global forcing for ocean and sea ice models: the data sets and flux climatologies, *NCAR Technical Note: NCAR/TN-460+STR*, 2004
- Takaya Y., Bidlot, J-R. Beljaars A.C.M. Janssen P.A.E.M. Refinements to a prognostic scheme of sea surface skin temperature, *JGR*; **115**, c060089, 2010
- Waters J., Lea D. J., Martin M. J., Mirouze I., Weaver A., While J.; Implementing a variational data assimilation system in an operational 1/4 degree global ocean model, *QJRM*, **141**, 333–349, 2014
- While J., Martin M.; Development of a variational data assimilation system for the diurnal cycle of sea surface temperature, *JGR: Oceans*; **118**, 2845–2862, 2013

A FACILITY FOR NEAR-REAL TIME ESTIMATION AND EVALUATION OF DIURNAL WARMING

Gary A. Wick⁽¹⁾, Sandra L. Castro⁽²⁾, Andrew Harris⁽³⁾, and Jonathan Mittaz⁽⁴⁾

(1) NOAA Earth System Research Laboratory, Boulder, CO, USA, Email: gary.a.wick@noaa.gov

(2) University of Colorado at Boulder, Boulder, CO, USA, Email: sandrac@colorado.edu

(3) CICS, University of Maryland, USA, Email: andy.harris@noaa.gov

(4) University of Reading, UK, Email: j.mittaz@reading.ac.uk

ABSTRACT

A facility has been implemented at the NOAA Earth System Research Laboratory to provide and evaluate hourly estimates of the amplitude of diurnal warming computed from multiple different models based on forcing data from numerical weather prediction analyses. The facility currently obtains daily heat and momentum flux forcing data from the NOAA Global Forecast System (GFS) model as well as wave parameters from the Wave Watch III model. Data over a two day period are used to force multiple numerical models for the diurnal warming amplitude. Initial models include the Kantha-Clayson model with wave effects and the Coupled Ocean Atmosphere Response Experiment (COARE) warm layer model. Estimates of the amplitude are provided hourly from each model relative to several depths including the skin layer, 20 cm and 1 m. All data are presented via a web-based interface and are available for download. Comparison of the model estimates with available observational measurements will also be provided in the near-future.

1. Introduction

Diurnal changes in the Sea Surface Temperature (SST) complicate the generation and interpretation of daily SST analyses. Observations from different times through the day and different effective measurement depths are all influenced by diurnal warming to differing amounts, and generation of foundation SST analyses requires some approach to treating the effects of diurnal warming. While multiple L4 SST analyses currently exist, only limited information is generally available on the diurnal variations that occur on top of the daily estimates on a global scale. Similarly, little systematic information is available on differences in accuracy of currently available methods for estimating diurnal warming.

To address these factors, a facility has been implemented to provide hourly estimates of the amplitude of diurnal warming at several reference depths based on inputs from numerical weather prediction (NWP) analyses. The diurnal warming estimates will provide a complement to existing foundation products, giving users access to hourly variations in the SST on complete grids consistent with the analyses. The resource will also facilitate the direct and sustained comparison of diurnal warming predictions from multiple models as well as their validation against estimates derived from available satellite measurements.

2. Approach and Facility Description

The basic approach employed is to compute estimates of the diurnal warming amplitude using detailed physical models forced in near-real-time with inputs from NWP models. While the native diurnal warming computations are performed at different temporal and vertical resolutions, the diurnal warming estimates are provided hourly at several standard reference depths. The depths include the subskin, 20 cm (for reference to drifting buoys and existing Climate Change Initiative (CCI) products), 1 m (for reference to moorings and other standard products) and 5 m. In all cases the output is the amplitude of diurnal warming at that depth and time relative to the foundation SST value for that day. Additional depths and temporal resolutions can be easily accommodated based on user feedback.

The focus of this facility is on the output from physically-based 1-D models for the oceanic near-surface layer, though results from simplified parameterizations could potentially be added. The initial demonstration of the facility incorporates the outputs from two models: the Kantha-Clayson (Kantha and Clayson, 1994) turbulence model modified to incorporate wave effects (e.g., Kantha and Clayson, 2004) and the Coupled Ocean

Atmosphere Response Experiment (COARE) warm layer model (Fairall et al., 1996). These models were selected based on their maturity, ongoing use in the community, and our extensive experience in their application. Inclusion of additional models is planned for the near future. A configuration of the Generalized Ocean Turbulence Model (GOTM) has also been implemented and will be incorporated soon.

Forcing for the models is taken from the analysis fields from NWP models. Use of NWP model outputs provides access to all the required inputs on globally complete grids in a timely manner. The primary input fields include the wind stress, radiative and turbulent heat fluxes, and SST. These are currently drawn from the NOAA Global Forecast System (GFS) model which is run every 6 hours at 00, 06, 12, and 18Z. While the resolution of the model was recently increased to near 0.25°, the inputs are presently mapped to 0.5° resolution grids on which the diurnal warming models are run. The analysis fields from each 6-hourly run are temporally interpolated to the time step of the model. Simple linear interpolation is used for all fields except insolation. For insolation, the interpolation is done in the domain of cloud fraction. Near-surface specific humidity and air temperature fields are also extracted and input to the models to allow for modulation of the computed heat flux in the presence of diurnal warming. The GFS model is being utilized for convenience and NOAA priorities. Inclusion of inputs from additional models such as the European Centre for Medium-Range Weather Forecasts (ECMWF) is desired and being pursued.

Additional forcing input on the wave state is taken from the Wave Watch III model. Information on wave state helps account for additional mixing resulting from non-local forcing and has been demonstrated to have a positive impact on simulation of diurnal warming. Extracted parameters include wave period, direction, and significant wave height. Using these, the Stokes drift velocity is estimated assuming the Pierson-Moskowitz spectrum. The wave inputs are obtained from model runs every 6 hours at 0.5° resolution.

The diurnal warming amplitude estimates are generated daily with a 2-day lag. Each of the models is run for a period of 2 days with the output taken from the second day of the simulation. This allows for proper initialization of the diurnal cycle at all longitudes and reduction of any spin-up effects. The domain is global between 60 N and 60 S. Spatial resolution of the output is currently 0.5° but can be increased to 0.25° for the current flux inputs. The models are initialized at each grid point based on the SST fields from the NWP model. The 1-D models are run independently at each grid point meaning that any advective effects are necessarily neglected in the computations.

Access to the facility is via the web at:

http://www.esrl.noaa.gov/psd/psd2/coastal/satres/data/html/diurnal_sst_analysis.php.

An example screen capture of the web site is shown in Figure 1. The page automatically displays the results for warming at the skin for the most recent day in the central portion of the screen. Columns include graphics of the estimated diurnal warming amplitude for each of the models as well as the primary inputs of wind forcing and insolation. Rows contain the results for each hour of the selected day. Clicking on any of the links returns a full-sized graphic of the estimated diurnal warming amplitude (or desired forcing field) at the desired time as shown in Figure 2.

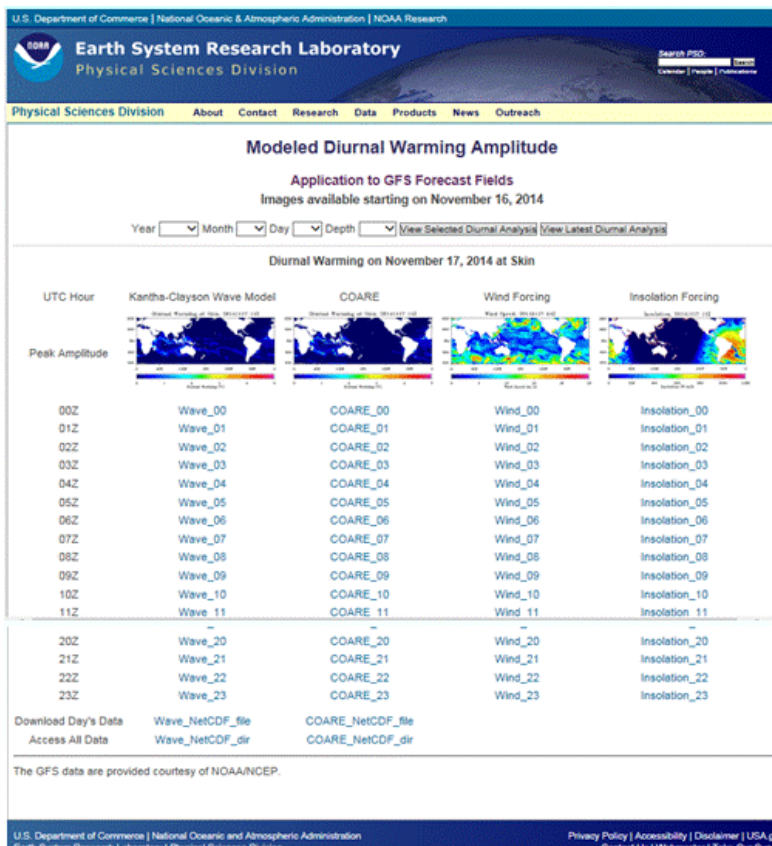


Figure 1: Sample screen capture of the web interface of the diurnal warming facility. See text for description of the webpage contents.

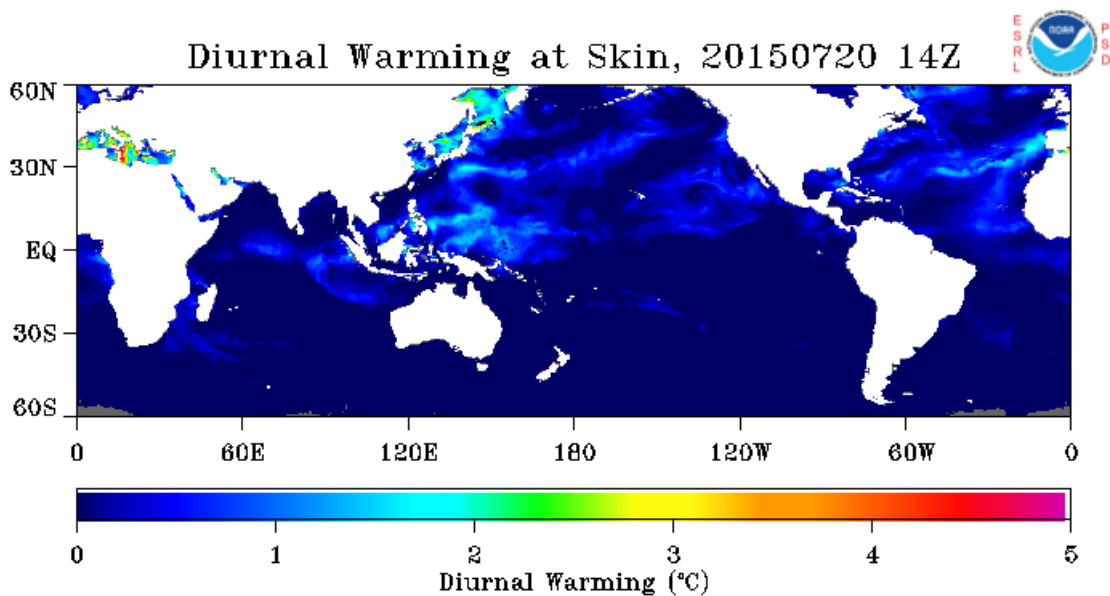


Figure 2: Example graphic of diurnal warming showing the amplitude predicted by the Kantha-Clayson model at the skin layer at 14 Z on 20 July, 2015.

The menu at the top portion of the page allows the user to select the outputs for any desired day and any of the available depth levels. Results are available starting on 1 July 2015 and extend through the present. The results from additional models will be added and backfilled through the starting date as they become available.

Access to the digital data corresponding to the diurnal warming amplitude estimates will be provided through the links at the bottom of the page. The data for the hourly amplitude products at each of the depths will be stored in NetCDF files that can be downloaded from the site. The content and format of these files is currently being finalized and is being designed for maximum consistency with existing GHRSSST format data. Discussions and input from the GHRSSST XVI science team meeting were highly valuable for construction of the data files. The links to the files are included on the existing page but are not yet active.

A complementary web page is currently under development which will compare the simulated warming fields against observations derived from geostationary satellite data. Hourly diurnal warming estimates at the skin layer have been derived using data from the Spinning Enhanced Visible and InfraRed Imager (SEVIRI) on the Meteosat Second Generation (MSG) satellites corresponding to the model predictions. The warming is computed relative to a foundation temperature estimate derived from the data from the previous night. These data have been used in initial product validation (see following section) and will be included on the new web page. Additional satellite products from Himawari-8 and other new satellites will be added as the data become available.

3. Example Model Validation

Initial validation of the model-derived diurnal warming estimates has been conducted using both direct in situ observations and satellite-derived estimates. Previous work using data from research cruises demonstrated the ability of the models to accurately reproduce measurements of diurnal warming at the skin and subsurface depths when forced with direct, high-resolution wind stress and heat flux inputs coincident with the temperature measurements. The uncertainty of the predictions resulting from use of coarser resolution NWP forcing inputs is potentially much larger.

To examine the uncertainty resulting from use of NWP inputs, modeled warming has been compared against hourly estimates derived from SEVIRI as noted at the end of the previous section. Qualitatively, the warming

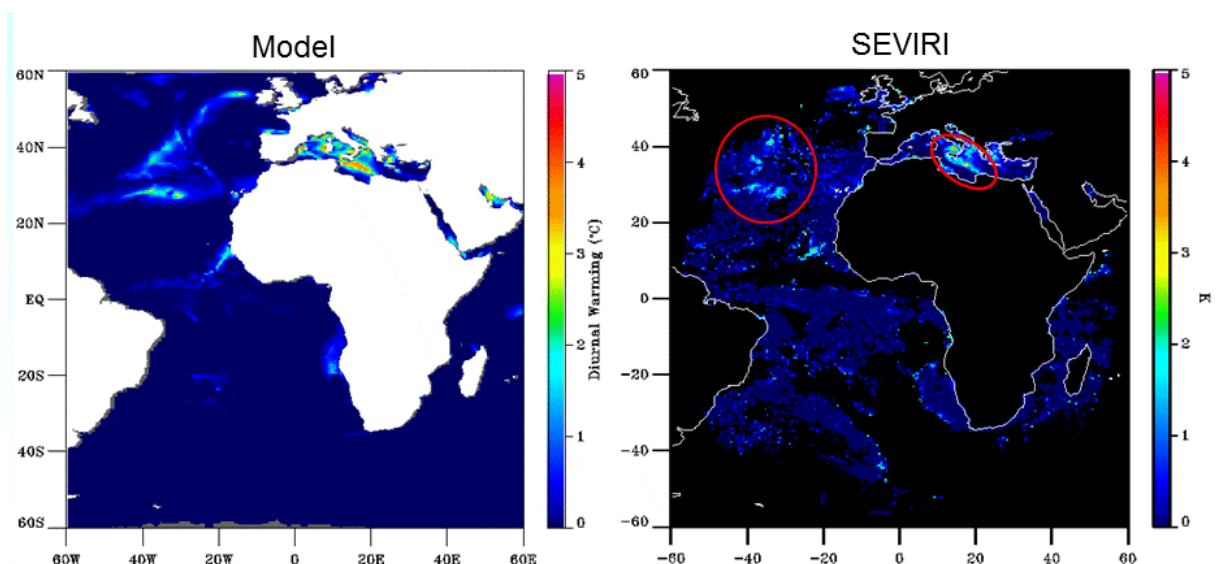


Figure 3: Sample comparison of simulated and observed diurnal warming amplitudes at 14Z on 21 June, 2014. The modelled results on the left are for the Kantha-Clayson model forced with NWP inputs. The results on the right were derived from SEVIRI observations using a foundation estimate from the previous night.

patterns and amplitudes appear quite similar as shown for the example case in Figure 3. To quantify the agreement, comparisons of the distributions of diurnal warming amplitude obtained over multiple weeks were generated. The results obtained using the Kantha-Clayson model with wave effects at several different observation times are shown in Figure 4. While highly favorable overall, the results do suggest a tendency for overestimation of the warming. This tendency was also observed in the predictions from the COARE model. Combined, these results suggest the problem is related to use of the 6-hourly NWP inputs and the lack of higher resolution variability.

Improved results were obtained through introduction of a wind gustiness factor to modify the interpolated wind stress values. The NWP-based representation of integrated solar heating was first investigated by comparison against mooring data available in the eastern Pacific. The results suggested that small scale variations in cloudiness did not appear to have a significant effect on the results. The persistence of low wind speeds over multiple hours, however, was found to have a much larger effect on amplifying diurnal warming. Even small gusts in the local wind speed can inhibit the growth of large diurnal warming amplitudes. Through implementation of a wind gustiness factor (e.g. Zeng et al., 2002) that prevents extended persistence of very low wind speeds, the results were found to agree much more closely in the mean with direct observations.

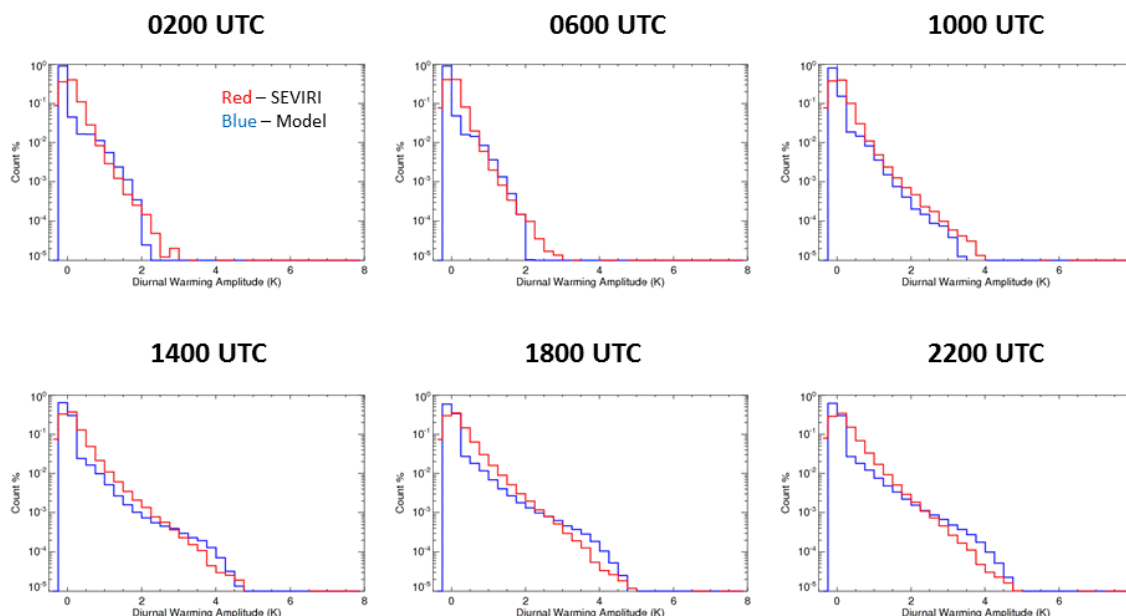


Figure 4: Comparison of modelled and observed distributions of diurnal warming amplitude. The results are shown for the Kantha-Clayson model with wave effects applied on the SEVIRI domain during the period from 21-30 June 2014

4. Conclusion

A new facility has been created to help promote access to and evaluation of global estimates of diurnal warming to complement and extend the application of existing foundation temperature analyses. Hourly diurnal warming estimates at multiple reference depths and a spatial resolution of 0.5 are being generated in near-real-time using physically-based 1-D models forced with NWP analysis inputs. The web-based interface is now live and available for viewing. Digital data for the diurnal warming estimates will soon be available for download from the site in NetCDF format consistent with other GHRSSST products. Enhanced validation capabilities will also be provided through the facility, but initial validation of the modeled estimates are generally very positive. User feedback on the function and content of the facility is highly desired and encouraged.

5. References

- Fairall, C. W., E. F. Bradley, J. S. Godfrey, G. A. Wick, J. B. Edson, and G. S. Young, Cool-skin and warm-layer effects on sea surface temperature. *J. Geophys. Res.*, **101**, 1295-1308, 1996.
- Kantha, L. H., and C. A. Clayson, An improved mixed layer model for geophysical applications, *J. Geophys. Res.*, **99**, 25,235-25,266, 1994.
- Kantha, L. H., and C. A. Clayson, On the effect of of surface gravity waves on mixing in the oceanic mixed layer, *Ocean Modell.*, **6**, 101-124, 2004.
- Zeng, X., Q. Zhang, D. Johnson, and W.-K. Tao, Parameterization of wind gustiness for the computation of ocean surface fluxes at different spatial scales, *Mon. Wea. Rev.*, **130**, 2125-2133, 2002.

PLENARY SESSION VI: UNCERTAINTIES IN L2P PRODUCTS

SESSION REPORT

Chair: Helen Beggs⁽¹⁾, Rapporteur: Werenfrid Wimmer⁽²⁾

(1) Bureau of Meteorology, Melbourne, Australia, Email: h.beggs@bom.gov.au

(2) Werenfrid Wimmer, National Oceanography Centre, Southampton, UK, Email: w.wimmer@soton.ac.uk

ABSTRACT

Three presentations were given during the plenary session on uncertainties in L2P products, followed by general discussion focusing on sensor specific error statistics and quality flags in L2P products.

1. Roles of L2 SSES in a L4 production case – Mike Chin

NASA JPL's MUR SST analysis system uses GHRSSST L2P SST data from MODIS, AMSR-E (prior to Oct 2011), WindSat and AVHRR sensors on NOAA polar-orbiters and METOP-A and METOP-B. The MUR analysis is a multi-scale analysis. MUR assumes a constant correlation coefficient for each grid cell. Sensor Specific Error Statistics (SSES) variance values in the input L2P files are discounted according to pixel density, i.e. the MUR system changes the SSES standard deviation values. Bin averaging of input data does not avoid issues with error correlation. Quality level flags are used for pixel segregation. The SSES provide mean and standard deviation of the difference between the satellite SST observation and an in situ reference (generally drifting buoy SSTs). Can SSES bias be used to get to foundation SST?

The MUR system uses SSES bias to correct for biases in the L2P SST data streams. In addition, Iquam in-situ SSTs are used for bias correction. The use of SSES bias in MUR improves the self-consistency slightly.

Potential issues with SSES:

- Reduction of inter-sensor bias
- What is the reference?
- What is the SSES bias accuracy?
- Definitions / Documentation

Discussion

Andy Harris (AH): SSES_bias do not make much difference on a global basis, but should make a difference on a regional basis.

Mike Chin (MC): I have not looked at a regional basis yet.

AH: Bias of retrieval on a global basis should be close to 0, so difference should make an impact on regional scales.

Chris Merchant (CM): Correlation of pixels, covariance matrix for all pixels not practical. What would you like?

MC: A simple number for all the pixels that fall within a grid box. They are relatively stable, so one value should be enough, however close to 0 some issues. A model that reflects geophysical variation would be better.

Charlie Barron (CB): Errors are too small. Are you doing a pseudo ensemble, or what is the process?

MC: Errors are too optimistic. The standard deviation is high where variability is high, so a spatial figure can scale as can seasonality. GMPE could be an option.

2. SSES in ACSPO version 2.40 – Performance analysis and recommendations for assimilation in L4 SST – Boris Petrenko

The purpose of ACSPO SSES are to provide realistic estimates of SST bias and standard deviation (STD) in the full range of observations conditions at every valid SST pixel. They should minimize the need for bias correction in L4 data. ACSPO SSES are analysed as functions of regressors (terms of SST equations) rather than physical variables. Testing of the ACSPO SSESs has shown that SSES bias correction reduces standard deviation with respect to drifters and CMC L4 SSTs. Correction for ACSPO SSES biases reduces the effects of cloud leakages and angular-dependent biases. During the daytime, it also reduces the effect of diurnal warming. Only quality level 5 SSTs (cloud-free) are used in ACSPO. Stratification of coefficients in the regression space is more efficient for fitting in-situ SST than stratification of physical variables. By subtracting `sses_bias` from the baseline ACSPO SST_{skin}, the de-biased ACSPO SST becomes a better proxy for SST_{depth} (at drifting buoy depths) than the original ACSPO skin SST.

The current ACSPO algorithm has STD with respect to in-situ SST of 0.42 K globally, compared with Pathfinder 0.45 K and LATBAND 0.45 K.

Recommendations for testing ACSPO SSES in L4 systems:

- Assimilate night-time de-biased SST into foundation L4 SST products
 - Compare with assimilation of baseline ACSPO SST
- Assimilate de-biased daytime ACSPO SST.

Discussion

Helen Beggs (HB): What is your method for generating SSES in daytime? How do you correct for diurnal warming?

BP: It is separated and produced that way.

AH: It's complicated. If there is no wind speed but no diurnal warming during the daytime and there is a signal in the BT and that's why the regression works. It makes one think as how it is possible to remove diurnal variation just from the BT?

CM: OSI-SAF global as first cut. Bias is in the OSI-SAF retrieval. Why don't you just correct your SST to the best possible retrieval? After de-biasing you have a better SST (better in respect to drifting buoys). OSI-SAF preserves DV. Yours does not?

BP: After de-biasing the agreement is better with drifters.

Sasha: We are doing piece-wise correction against in-situ SST which is not as sensitive to DV. The piece-wise regression (PWR) is not mature yet, so it won't make a good image/product yet. It should be good for L4 producers, but might not work as a stand-alone product. Regional biases should be reduced by the PWR. Methodology, transition from geophysical space to measurement space with a weight which is realistic. Weighting is not always representative.

BP: Best methods. Last GHRSSST meeting I reported model-based methods. It removes biases in some sense. The PWR does it instantaneously for every single image.

Craig Donlon (CD): Not sure how this connects to the physics. Try to get some harmonization to the terminology. People start to use purely statistical methods – radiative transfer, minimization. The challenge to GHRSSST is to get back to basics. What is the truth? Make sure it is clean (drifters/Argo). Make sure we don't go around in circles. Suggest to get the Science Team to pull this all together and make a short (5 page) report about how it all works.

HB: The report on the SSES discussion from last year's ST-VAL Breakout Session has been sent around.

CD: Sent to all?

HB: To the ST-VAL members and also it is in the GHRSSST-XV Proceedings.

Gary Corlett: They are on the GHRSSST web page.

3. Modeled SST Uncertainties vs Empirical SSES – Claire Bulgin

Limitations of L2 retrieval mean there are uncertainties that vary in time and space. The L2 noise is propagated to L3 gridded products. Missing parameters budget:

- Undetected cloud
- Aerosol variability
- Undetected ice
- Sensor drift
- Skin to depth uncertainty

These uncertainties can be modelled as a function of domain size, clear-sky percentage and SST variability. Where uncertainties are calculated independently of in situ data, these can be used to validate both SST and associated uncertainties.

Discussion

HB: I missed how you folded time and space on one axis.

Claire Bulgin (CB): The 3D has been collapsed and scales are similar.

Chelle Gentemann (CG): How are you calculating the SST variability, e.g. in an upwelling region how would you do that for a year?

CB: SST variability is the remaining component after we overlay the mean mask.

Craig Donlon (CD): It's the mesoscale variability.

CG: Temporal dependence is missing in here.

CB: It's L2 to L3U so it is just gridding.

CD: A mesoscale jet is about 1 hour. Eddy mesoscale is about 1-2 days. Satellite imager is always instantaneous.

Chris Merchant: In an L3 product we sample only part of certain oceanographic features, but this is the spatial uncertainty.

Andy Harris: Retrieval error. How do you model that? Chi squared?

CB/CM: No idea.

4. Open Discussion

HB showed slide of questions to get things rolling:

Uncertainties in L2P Discussion Points:

- 1) How to incorporate "Modelled Uncertainties" per pixel?
 - 2) Do we still need SSES if we have Modelled Uncertainties?
 - 3) Can we expect L2P producers to provide SSES estimates that are consistent across different SST products?
 - 4) If yes, then how would we go about this? Provide recommendations on SSES estimation?
-

Sasha Ignatov (SI): SSES make it easy to compare different datasets – a very practical motivation. Do we still need SSES? We need both. A specific user of the data should determine what we do. What works in L4 should determine what we do. Modeling uncertainties is great, but certain things we just don't know. So we need a practical approach.

HB: In the IMOS Project we model the SSES uncertainties regionally. You can find out more from my presentation during the CDR Breakout Session on Thursday morning.

SI: During last GHRSSST ST Meeting we presented how we produce SSES. We need similar information from the L4 producers on how they use SSES. It would be good to see how people use SSES.

Alexi Kaplan (AK): IC-TAG breakout session on Thursday will discuss how L4 systems use SSESs.

CM: A comment on Sasha's comments. We need both approaches. We don't know all the error sources and how to model them, but if your in-situ is independent we can verify the model, and if you get the dominant uncertainty terms it might be good enough. Back to Basics: SSES tells the user which observation has more or less uncertainty. We can use some similar approaches, but not universal. However, users don't seem to mind too much. How do we validate SSES? It is currently not independent to buoys. How can we tell if SSES is something real? We need modeled uncertainty approach, as SSES can't give random and systematic split. We should quantify spatial scales more rigorously, but can't see how this can be done on a purely empirical approach using buoys.

Rosa Paes (RP): If you wish more use of L2P for L4 then as a user we need information on how confident you are regarding SST on a pixel level. Corrections on bias on an in-situ level will not be sufficient, for multi-sensor bias is time and space dependent. We need to know on a pixel level which are the good ones. We need common definition of SSES for all products. Otherwise it is difficult for users.

CD: Make sure statistics are still connected to the real world.

Mike Chin (MC): For SSES bias is there a reference we have agreed on – skin/subskin/depth?

HB: At the Bureau we reference back to skin using a constant offset of 0.17K (following the convention used for the Pathfinder AVHRR SST v5.2 L3C product). ACSPO sses_bias converts a skin SST to drifting buoy depths.

MC: We need a documented reference. Ed Armstrong could try to survey the users of the quality flags and SSES. It would help organisation on the server side. Survey within two weeks of meeting. Might help answer the questions in HB's slide.

ROLES OF L2 SSES IN A L4 PRODUCTION CASE

T. Mike Chin⁽¹⁾

(1) NASA Jet Propulsion Laboratory, California Institute of Technology, USA, Email: mike.chin@jpl.nasa.gov

ABSTRACT

GHRSSST defines two types of single-sensor error statistics (SSES) for the satellite track (Level 2, or L2P) data: the expected mean (“bias”) and standard deviation (STD) of the measurement error. Both of these play important general roles in production of a multi-sensor gridded (Level 4, or L4) analysis: bias for correction of inter-sensor difference in SST values and STD for data weighting and evaluation of posterior error estimation. The actual roles of L2P SSES values available today are presented for the case of “MUR” L4 analysis production, with discussion of how some of the SSES values are used and not used and why.

1. Introduction

The producers of the L4 data sets represent, along with modelers, some of the potentially heavy users of the GHRSSST L2P SSES parameters. In recent GHRSSST meetings, these SSES parameters have become topics of discussions with respect to their accuracy, accuracy requirements (given certain applications), and actual usefulness of the SSES. This presentation describes how SSES is used in production of the Multi-scale Ultra-high Resolution (MUR) L4 SST analysis.

2. MUR SST

The MUR data set can be considered as a fairly standard daily L4 gridded analysis product, with some specialized characteristics as follows:

- *A high grid-resolution of 0.01x0.01 degrees (approximately 1km resolution), featuring the MODIS L2P data sets combined with AMSR-E, WindSAT, AVHRR, and in-situ (iQuam) data sets. To reconstruct the high-resolution SST features, multiple stages of analysis are performed at several different scales, resulting in a heterogeneous-resolution presentation that “would have high resolution of small-scale features in region of good [MODIS] coverage and lower resolution in regions of poor coverage” (Reynolds et al. 2013). The actual formula for the multi-scale analysis follows the orthonormal wavelet decomposition theory (Mallat 1989).*
- *Use of a wavelet (continuous function) basis function, which leads to a “mesh-less” or “grid-less” interpolation (Chin et al., 2014).*
- *Use of a set of time-weights which are scale dependent, in order to account for presumably faster evolution (thus shorter time-window) of the smaller scale features.*

Despite the above, the core of the interpolation method follows the familiar objective interpolation (OI) formula at each scale stage of analysis (the Multi-Resolution Variational Analysis, MRVA, Chin et al., 1998). Thus, how MUR depends on the SSES parameters maybe similar, more or less, to how other L4 products rely on SSES.

3. Uses of L2P SSES in L4 Analysis

Procedures in L4 data production that can benefit from SSES are:

- a) **Quality control:** choosing and pruning of bad pixels from the input L2P data sets.
- b) **Bias correction:** correcting for (i) the target “SST” for the L4 analysis, i.e., skin or bulk/foundation SST and (ii) inter-sensor bias.
- c) **Data weights:** assigning the observation error variance values.

d) **Posterior error:** estimating the analysis error.

For MUR analysis, quality control is performed mostly by relying on the L2P quality flags, with the SSES STD values playing a minor role in determining pixels to be thrown out of the analysis. The quality flags are more useful than SSES STD here because critical quality determinants such as atmospheric and land effects are perceived (by the MUR producers, hereafter “MUR”) to be more directly addressed by the L2P quality flag(s) than SSES STD.

For bias correction, MUR uses the SSES Bias values for most of its input L2P data sets but finds them to be not fully adequate in reducing inter-sensor bias. MUR hence computes additionally its own sensor bias terms for each data set by co-estimating with its SST analysis, except that such bias is assumed to be zero for the in-situ data set (for the “bulk” temperature). Thus, bias correction in MUR production relies on the quality of the in-situ (iQuam) SST values.

For data weights, MUR uses SSES STD for the diagonal terms of the observation error covariance matrix. However, it is known that the off-diagonal terms, or the pixel-to-pixel correlation, are important (e.g., Kaplan et al. 2003; also a demonstration in Fig.8 of Chin et al. 2014 using AMSR-E and MODIS SST). To this end, MUR assumes a simple correlation model (a constant correlation coefficient for each computational grid box and for each scale stage), which effectively discounts the SSES STD values heavily as described in Chin et al. 2014 depending on the local data density and the analysis scale. Thus, even though the SSES STD values are used, they are heavily altered before being used to control the actual interpolation procedure.

For the analysis error estimation, the formal (Bayesian) posterior variance values tend to become too small, partly due to the effect of using the background (prior) error covariance to control the smoothness of the analysis. MUR scales such formal error variance values back to a higher level by referencing an ensemble variance field series, noting that the root-variance among L4 analysis (i.e., ensemble variance) gives a good indicator of root-mean-squares difference between the analysis and drifter SST (Martin et al., 2012, Fig.5).

In summary, the L2P quality parameters can be ordered according to importance to the MUR production as: (1) quality flag, (2) SSES STD, (3) SSES Bias. The SSES Bias came to be least important because MUR estimates its own bias for each data set. However, SSES Bias has a potential to play a much larger role since it applies directly to the L2P SST values.

4. Conclusion

Gridding is a harsh environment for L2P SSES parameters, particularly because the uses of the prior models (for smoothness etc) and the needs to have external information (error model) for the pixel-to-pixel correlation are combined to effectively alter the SSES STD values beyond recognition. Falling back to an apparently simple and familiar procedure such as the bin-averaging method does not address the fundamental issues such as the critical need for the correlation values. Still, the potential impact of SSES Bias to any L4 analysis seems to be large, due to its roles in both attaining the target “SST” value and correcting for inter-sensor mean differences. To increase the utility of the GHRSSST L2P Bias parameter, documentation and cross-product standardization aspects should be improved.

5. Acknowledgments

The research was carried out at the Jet Propulsion Laboratory, California Institute of Technology, under a contract with the National Aeronautics and Space Administration. Copyright 2015 California Institute of Technology. Government sponsorship acknowledged.

6. References

- Chin TM, Milliff RF, Large WG. 1998. Basin-scale, high-wavenumber sea-surface wind fields from a multiresolution analysis of scatterometer data. *Journal of Atmospheric and Oceanic Technology* **15**: 741-763.
- Chin TM, Vazquez J, Armstrong EM. 2014. On “grid-less” interpolation and subgrid data density. *Journal of Atmospheric and Oceanic Technology* **31**: 1642-1652.
-

Kaplan A, Cane M, Kushnir Y. 2003. Reduced space approach to the optimal analysis of historical marine observations: Accomplishments, difficulties, and prospects. *Advances in the applications of marine climatology: The dynamic part of the WMO guide to the applications of marine climatology, Rev.1 WMO/TD-1081, JCOMM Tch. Rep. 13*, 199-216.

Mallat SG. 1989. A theory of multiresolution signal decomposition: the wavelet representation. *IEEE Transactions on Pattern Analysis and Machine Intelligence 11*: 674-693.

Martin M, Dash P, Ignatov A, Banzon V, Beggs H, Brasnett B, Cayula J, Cummings J, Donlon C, Gentemann C, Grumbine R, Ishizaki S, Maturi E, Reynolds RW, Roberts-Jones J. 2012. Group for High Resolution Sea Surface Temperature (GHRSSST) analysis fields inter-comparisons. Part 1: a GHRSSST multi-product ensemble (GMPE). *Deep-Sea Research II 77-80*: 21-30.

Reynolds RW, Chelton DB, Roberts-Jones J, Martin MJ. 2013. Objective determination of feature resolution in two sea surface temperature analyses. *Journal of Climate 26*: 2514-2533.

REDESIGNED SINGLE SENSOR ERROR STATISTICS IN THE ADVANCED CLEAR-SKY PROCESSOR FOR OCEANS

Boris Petrenko⁽¹⁾, Alexander Ignatov⁽²⁾, Yury Kihai⁽¹⁾, Prasanjit Dash⁽⁴⁾, Maxim Kramar⁽¹⁾

(1) NOAA STAR and GST, Inc., Email: boris.petrenko@noaa.gov

(2) NOAA STAR, Email: alex.ignatov@noaa.gov

(3) NOAA STAR and CSU CIRA, Email: prasanjit.dash@noaa.gov

ABSTRACT

A redesigned algorithm for estimation of Single Sensor Error Statistics (SSES) for the baseline regression SST (BSST) product of the NOAA Advanced Clear-Sky Processor for Oceans (ACSPo) is described. The algorithm employs segmentation of the SST domain in the space of regressors (i.e., terms of the regression equation). For each segment, local regression coefficients and SDs are estimated from the corresponding subsets of matchups with quality controlled *in situ* data. SSES bias is estimated as the difference between the BSST and an auxiliary Piecewise Regression (PWR) SST produced with the local coefficients. Subtracting SSES biases from BSST reduces the effects of residual cloud, angular dependence of biases and, during the daytime, diurnal surface warming. This results in a significant reduction in global SDs of fitting *in situ* SST bringing them close to a level typical for “foundation L4” minus *in situ* SST statistics. While the CMC L4 SST is typically colder than daytime *in situ* SST, the PWR SST is consistent with *in situ* data during both day and night. The PWR SST may thus be viewed as an estimate of the “bulk” SST and can potentially be a better input for assimilation into L4 SST systems, aimed at producing the foundation SST.

1. Introduction

The GHRSSST Data Specification format (GDS 2.0) requires that Single Sensor Error Statistics (SSES), i.e. estimates of bias and standard deviation (SD) of retrieved SST, should be appended to each pixel of an L2/L3 SST product. Currently different processing centers employ different SSES definitions. The GHRSSST-XV meeting has reviewed existing SSES practices and suggested revisiting those (Proceedings of GHRSSST-XV, 2014). In particular, it was noted that no available SSES improves assimilation of L2 or L3 products into the existing L4 analyses. In this context, the initial SSES implementation (Petrenko and Ignatov, 2014b) used in the earlier versions of the NOAA Advanced Clear-Sky Processor for Oceans (ACSPo) SST retrieval system, has been redesigned with the explicit objective to provide a measurable improvement for L4 analyses. Customarily, assimilation of L2 or L3 product into L4 analyses is preceded by a “bias correction” in satellite SSTs with respect to *in situ* SSTs (or with respect to some reference satellite product). Therefore in the new SSES development, the primary objective was to significantly reduce biases in ACSPo SST relative to *in situ* SSTs. Moreover, the SSES SDs should provide a realistic measure of SST uncertainty in pixel, to allow optimization of L2/L3 SST weights during their assimilation into L4. Only the performance of SSES bias correction has been explored so far and it is documented in this paper. The new SSES was implemented in ACSPo v2.40 which became operational at NOAA on 19 May 2015.

2. Methodology

As documented in Petrenko et al. (2014a), the baseline SSTs (BSST, T_s) are produced in ACSPo with the regression equations proposed by Lavanant et al. (2012). Each equation is used with a single set of regression coefficients trained on a global dataset of matchups (MDS). Errors of fitting *in situ* SST with BSST are largely caused by inaccuracy of approximation of a highly variable inverse relationship between BTs and SST with one global regression equation and with a single set of coefficients. As a result, BSST errors essentially depend on observational conditions, i.e. on such variables as view zenith angle (VZA), total precipitable water vapor content in the atmosphere (TPW), etc.

To properly account for the above dependencies, SSES should be separately estimated for different segments of the SST domain relatively uniform in terms of retrieval errors. The previous ACSPo SSES algorithm stratified

the SST domain by VZA and TPW. That approach, however, was found inefficient because the real number of physical variables affecting the retrieval errors is not limited by VZA and TPW. In fact, it is not obvious if it is possible at all to account for all physical factors essentially affecting retrieval errors (including, e.g., underscreened clouds), even with increased number of physical variables.

Instead, the redesigned ACSPO SSES considers the retrieval errors as functions of regressors (i.e. the terms on the right-hand side of the regression equation, excluding the offset), rather than certain geophysical variables. This limits the number of the SSES arguments, no matter how many physical variables the regressors depend on. The criteria for segmentation of the SST domain in the space of regressors (**R**-space) are derived from the statistics of regressors within the training MDS. Once such criteria have been established, the SST pixels and matchups are ascribed to specific segments based on the regressors' values. SSES SDs are estimated for each segment from the corresponding subset of matchups with quality controlled *in situ* data from iQuam (Xu and Ignatov, 2014). Note that we use a combination of drifters and tropical moorings in ACSPO Cal/Val analyses including the SSES. These subsets of matchups are also used to calculate local regression coefficients specific to each segment. The SSES SDs and local regression coefficients for all segments are stored in the lookup table (LUT). During the L2 production, the SSES SDs for every SST pixel are obtained from the LUT and the SSES biases are calculated as differences between the BSST and a Piecewise Regression SST (the PWR SST) calculated with the local regression coefficients.

3. Evaluation of SSES bias correction

As mentioned above, in the redesigned ACSPO SSES, the bias is defined as difference between BSST and PWR SST. Accordingly, applying SSES biases to the BSST transforms it into the PWR SST. Table 1 compares global statistics of fitting *in situ* SSTs in the matchups with BSST and PWR SST over the global MDS collected from 15 May 2013 to 8 August 2014 for VIIRS (onboard S-NPP), MODIS (onboard Aqua and Terra), AVHRR FRAC (on Metop-A and -B) and AVHRR GAC (on NOAA-19). The statistics of fitting *in situ* SSTs in the matchups with the L4 SST by the Canadian Met Center (CMC, Brasnett, 2008) are also shown. Since the data shown in Table 1 used the same MDS for both training and validation, the global biases for both algorithms are 0. PWR SST substantially reduces global SDs compared to BSST. Since CMC is constructed from nighttime satellite retrievals and *in situ* SSTs, it is biased cold with respect to daytime matchups, more so for the afternoon platforms S-NPP, Aqua and NOAA-19. The PWR SSTs do not show daytime biases typical for CMC but bring the global SDs closer to (or even smaller than) the corresponding SDs for CMC minus *in situ* SSTs. Further analyses based on subdividing the MDS into different time intervals and using one of them for training the coefficients, and another one for validation the derived SSTs have demonstrated the temporal stability of the BSST and PWR SST statistics with respect to *in situ* SST.

Table 1. Global biases and SDs of fitting *in situ* SST with BSST, PWR SST and CMC over the full MDS collected from 15 May 2013 – 8 August 2014.

SST	Statistics	S-NPP VIIRS	Aqua MODIS	Terra MODIS	MetOp-A AVHRR	MetOp-B AVHRR	NOAA19 AVHRR
Day							
BSST	Bias	0	0	0	0	0	0
	SD	0.41	0.45	0.46	0.48	0.49	0.50
PWR SST	Bias	0	0	0	0	0	0
	SD	0.31	0.33	0.32	0.33	0.33	0.34
CMC	Bias	-0.19	-0.20	-0.06	-0.02	-0.03	-0.21
	SD	0.34	0.34	0.31	0.31	0.31	0.35
Night							
BSST	Bias	0	0	0	0	0	0
	SD	0.33	0.35	0.35	0.46	0.45	0.46
PWR SST	Bias	0	0	0	0	0	0
	SD	0.25	0.26	0.26	0.30	0.30	0.29
CMC	Bias	0.01	0.02	-0.04	-0.08	-0.07	0.03

SST	Statistics	S-NPP VIIRS	Aqua MODIS	Terra MODIS	MetOp-A AVHRR	MetOp-B AVHRR	NOAA19 AVHRR
	SD	0.27	0.28	0.29	0.31	0.31	0.29

The redesigned SSES methodology was implemented in ACSPO v2.40 (with both L2P and L3U products) and used for processing some test data from six satellite sensors listed above. Fig. 1 demonstrates the effects of daytime and nighttime SSES bias correction by showing the geographical distributions of deviations of BSST and PWR SST from CMC for the S-NPP VIIRS L2P product on 16 February 2015, and corresponding SSES biases. The daytime deviations of BSST from CMC are mainly caused by cloud leakages, daytime warming in the upper surface layer of the ocean and variations in VZA. Nighttime SSES biases are also dependent on VZA and cloud leakages. SSES biases reflect all these effects, to a various degree. This makes correction of SSES biases efficient: the images of PWR SST – CMC are noticeably more uniform than the images of BSST – CMC. Note that comparison with CMC L4 in Fig.1 independently verifies the LUT derived from *in situ* data shown in Table 1 (from 15 May 2013 – 8 August 2014), in a global domain, and for the data outside the training time interval.

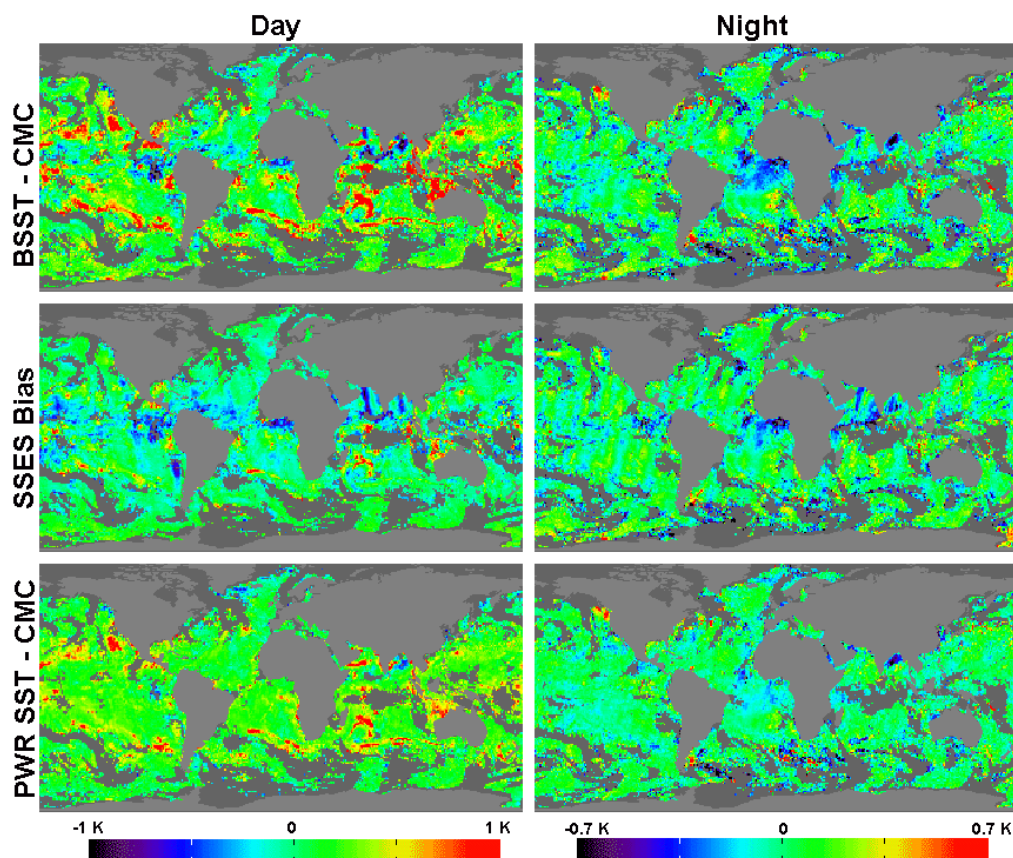


Fig.1. (Left panels) daytime and (right panels) geographical distributions of (top) BSST – CMC SST, (middle) SSES bias, (bottom) PWR SST - CMC SST from S-NPP VIIRS observations on 16 February 2015.

Fig.2 shows time series of daytime biases and SDs of BSST, PWR SST and CMC with respect to *in situ* SST, for six satellite sensors from 24 November 2014 to 10 March 2015. (Note that this is an independent verification of the LUT derived from the 15 May 2013 – 8 August 2014 data set and used for training of the PWR SST coefficients.) The statistics for all three SSTs were estimated from daily matchups and smoothed with a 7-day time window. Comparison of the BSST and PWR SST shows that the SSES bias correction makes the statistics

more stable and consistent between the sensors. It also reduces the peak-to-peak range of variations in the global SDs from $\sim 0.35\text{-}0.52$ K for BSST to $\sim 0.27\text{-}0.38$ K for PWR SST. Fig. 2 also shows the difference in daytime CMC biases for different sensors caused by the diurnal surface warming. The CMC biases are close to zero for the MetOp-A and -B whose equator crossing time (ECT) is 9:30 am, several hundredths of K colder for Terra, whose ECT is 10:30am, and close to -0.2 K for the S-NPP, Aqua and NOAA-19, which cross the equator around 1:30 pm. The PWR SST brings global daytime SDs closer to the level typical for CMC but produces much more consistent biases, for all platforms. This may suggest the benefit of assimilating the daytime PWR SST into L4 analyses (recall that daytime SSTs, especially with low winds, are often excluded from L4 analyses), or even creating a “daytime” L4 SST product (whose performance based on our analyses is expected to be comparable with the L4 SSTs produced from nighttime SST retrievals).

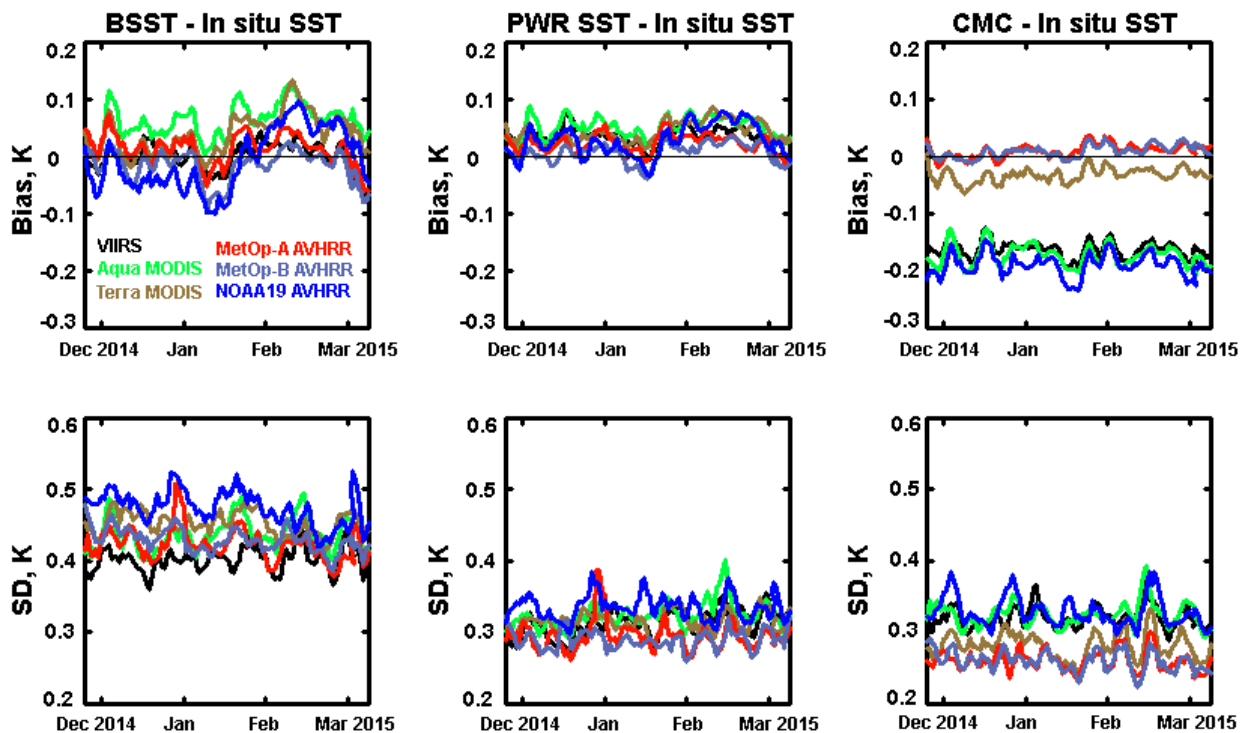


Fig. 2. Daytime time series of daily global biases and SDs of fitting *in situ* SST with BSST, PWR SST and CMC, for six satellite sensors, from 24 November 2014 to 10 March 2015.

4. Summary and conclusions

The redesigned ACSPO SSES algorithm performs segmentation of the SST retrieval domain in the space of regressors deriving the segmentation parameters from the statistical structure of regressors within the training MDS. SSES biases are calculated as differences between the BSST and the PWR SST estimated with coefficients specific to each segment. Applying SSES biases defined this way results in significant reduction in the global SDs of fitting the *in situ* SST with PWR SST, compared to the BSST.

Thus, ACSPO v2.40 provides the PWR SST, in addition to the BSST. The PWR SST is not represented in the output ACSPO files as a separate layer but can be obtained by subtracting the SSES bias from the BSST. The two products have different features. The BSST provides a reasonable combination of precision with respect to *in situ* SST and sensitivity to “skin” SST (Petrenko et al., 2014b). As such, it is considered the “skin” SST product (although trained against “bulk” *in situ* SST). The PWR SST, on the other hand, fits *in situ* SST much

more precisely than the BSST. Therefore, it may be considered an estimate of the “bulk” SST. Currently the PWR SST undergoes a comprehensive testing and, depending on results and users’ feedback, it may be designated as a standalone “bulk” product in the subsequent versions of ACSPO.

A full range of potential applications of PWR SST is yet to be determined. In particular, it is expected to benefit producers of the “foundation” L4 SST, by reducing (or even eliminating) the need in the L4-specific “bias correction”. The fact that the daytime PWR SST has global precision comparable with that of L4 SST, but is not biased cold with respect to *in situ* SST, may suggest the possibility of assimilating daytime ACSPO SSTs into the current L4 analyses, or even creating a new “daytime” L4 SST.

The SSES SDs in ACSPO v.2.40 are calculated for each segment as SDs of BSST minus *in situ* SST. The performance of the new SSES SD has not been evaluated yet. This could be done by using the SSES SDs for weighting BSST differently than the *in situ* SST, during their assimilation into the L4 analyses. Note that the SDs for the PWR SST are not currently reported because the GDS 2.0 format does not allow for two SSES statistics. However, it may be easily added to the ACSPO output per users’ request.

Note that no special effort was made in ACSPO 2.40 to provide a seamless connection between the values of PWR SST at the boundaries of different segments. As a result, the PWR SST images may include some discontinuities. Our analyses show, however, that such artifacts are typically small enough, rarely reaching several tenths of a degree Kelvin, and should not affect the L4 analyses which assimilate the L2/L3 data and perform additional smoothing in space and/or time. This problem will be addressed in the future versions of ACSPO. In the meantime, caution is advised in analyzing the SSES corrected SST imagery using data of ACSPO 2.40.

5. Acknowledgments

This work was conducted under the JPSS and Geostationary Operational Environmental Satellite-R Series (GOES-R) SST Projects funded by the respective Program Offices, and by the Himawari-8 SST Project and the NOAA Ocean Remote Sensing Program. We thank JPSS Program Scientist Mitch Goldberg, GOES-R STAR Manager Jaime Daniels, NOAA PSDI Manager Tom Schott, and ORS Manager Paul DiGiacomo. Thanks also go to our NOAA colleagues John Sapper, John Stroup, Xingming Liang and Xinjia Zhou for assistance, discussions, and feedback. The views, opinions, and findings contained in this paper are those of the authors and should not be construed as an official NOAA or US Government position, policy, or decision.

6. References

- Brasnett, B. (2008), The impact of satellite retrievals in a global sea-surface-temperature analysis, *Q. J. R. Meteorol. Soc.*, **134**, 1745-1760, doi: 10.1002/qj.319.
- Lavanant, L., P. Le Borgne, G. Legendre, A. Marsouin, S. Pere, and H. Roquet (2012), VIIRS SST at OSI-SAF, *GHRSSST XIII Science Team Meeting*, Tokyo, Japan.
- Petrenko, B., A. Ignatov, Y. Kihai, J. Stroup, and P. Dash (2014a), Evaluation and selection of SST regression algorithms for JPSS VIIRS, *J. Geophys. Res. - Atmos.*, **119**, 4580–4599, doi: 10.1002/2013JD020637.
- Petrenko, B. and A. Ignatov, 2014b, SSES in ACSPO, Proceedings of the GHRSSST XV Science Team Meeting, Cape Town, South Africa, 2-6 June 2014, pp.219-220, <https://www.ghrsst.org/documents/q/category/ghrsst-science-team-meetings/ghrsst-xv-cape-town-south-africa/>
- Proceedings of the GHRSSST XV Science Team Meeting, Cape Town, South Africa, 2-6 June 2014, pp. 197-199, <https://www.ghrsst.org/documents/q/category/ghrsst-science-team-meetings/ghrsst-xv-cape-town-south-africa/>.
- The recommended GHRSSST Data Specification (GDS) Revision 2.0 (2005), <https://www.ghrsst.org/documents/q/category/ghrsst-science-team-meetings/ghrsst-ix-perros-guirec-france/presentations/breakout-sessions/gds-2-0/>
-

Xu, F., and A. Ignatov (2014), In situ SST Quality Monitor (*iQuam*), *JTech*, **31**, 164-180, doi:10.1175/JTECH-D-13-00121.1.

MODELLED SST UNCERTAINTIES VS EMPIRICAL SSES

Claire Bulgin⁽¹⁾, Chris Merchant⁽²⁾, Owen Embury⁽³⁾, Gary Corlett⁽⁴⁾

(1) *Department of Meteorology, University of Reading, UK, Email: c.e.bulgin@reading.ac.uk*

(2) *Department of Meteorology, University of Reading, UK, Email: c.j.merchant@reading.ac.uk*

(3) *Department of Meteorology, University of Reading, UK, Email: o.embury@reading.ac.uk*

(4) *University of Leicester, Department of Physics and Astronomy, UK, Email: gkc1@leicester.ac.uk*

ABSTRACT

Empirical Single Sensor Error Statistics (SSES) are provided as standard in all GHRSSST format products. These are comprised of the mean difference and standard deviation of remotely sensed SST matched to a reference dataset. These SSES are typically calculated during validation activities and are often globally invariant. We demonstrate here, that for a well-calibrated instrument and well-characterised retrieval algorithm we can estimate uncertainties as part of the retrieval process itself. These uncertainties arise from both random and locally systematic effects and can be quantified on a per-pixel basis in L2 products. These uncertainties can also be propagated into higher-level products and validated alongside the SST using in-situ datasets. We demonstrate how these uncertainties more closely represent the true uncertainty distribution than SSES.

1. Introduction

Uncertainties are inherent in all geophysical measurements and need to be quantified for their scientific application. The terms 'error' and 'uncertainty' are often used interchangeably in scientific communities but have standard and distinct definitions. Error is the difference between the measured value and the true value of the measurand whilst uncertainty is a parameter describing the dispersion of values that could reasonably be attributed to the measured value (JCGM, 2008). In practice, for any given SST retrieval, we do not know the error in the measurement, or we would correct for this. However, we can often estimate the distribution of errors and from this quantify the uncertainty.

Within the SST Climate Change Initiative (CCI) project we have an objective to make an estimate of the standard uncertainty available to users for every SST value we provide. This includes all data levels (L2-L4), all spatial resolution and all types of SST product (skin SST and 20cm depth SST). We want the uncertainties provided to be realistic for the context in which SST is derived and that have been validated to give users confidence that they are realistic.

The GHRSSST standard for SST measurements is to provide SSES bias and standard deviation estimates with all SST products. These are often derived with reference to buoy data, taken as 'truth', but which in itself has an inherent uncertainty. We propose a new approach to the provision of uncertainty information using physics-based models within the retrieval process to estimate and propagate uncertainties from different sources. In this extended abstract we exemplify this approach using data from the Advanced Along Track Scanning Radiometer (AATSR) and a coefficient based SST retrieval (Embury and Merchant, 2012).

2. Uncertainties in Level 2 Products

When considering uncertainties in Level 2 products (and their propagation into higher level products) there are three main sources of uncertainty. The first arises from error due to random effects, for example radiometric noise in the satellite observations. The second is error due to locally systematic effects, for example retrieval errors or intermittently determined calibration parameters correlated over synoptic scales. The third is error due to larger scale systematic effects for example errors in the spectral response function or emissivity parameterisation. Here we consider estimation of the first two types of uncertainty.

Figure 1 provides an example of the noise propagation into Level 2 products. In the upper panels we have simulated the error in the 11 and 12 micron channels by randomly sampling a Gaussian distribution with 0.0 K mean temperature and 0.05 K standard deviation consistent with noise equivalent delta temperature (NEdT) estimates for these channels. In the lower panels we see how these errors propagate into SST retrievals using two different retrieval algorithms. The N2 retrieval uses the 11 and 12 micron channel in the nadir view only whilst the D2 retrieval uses both channels in both the nadir and forward views. Error propagation is as the sum of the errors in each channel multiplied by the retrieval coefficient for the channel, so where we have more channels the errors are higher ie. in the D2 retrieval. Notice that errors here are both positive and negative whereas uncertainty estimates are always positive.

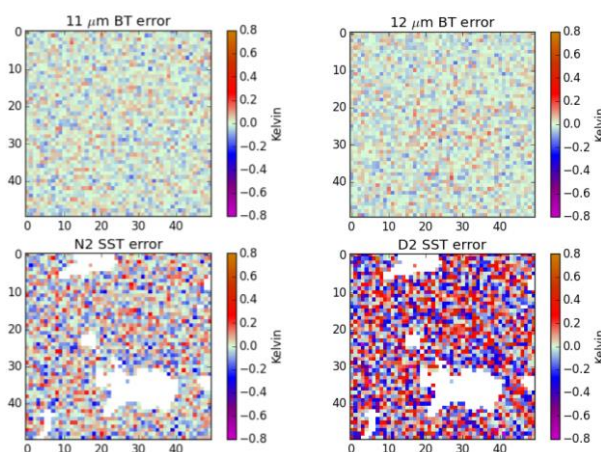


Figure 1: Simulated errors for AATSR 11 and 12 micron channels (upper panels) and propagation of these errors into N2 and D2 retrievals (lower panels). Cloud fields are overlaid in white.

The second source of error that we consider for L2 retrievals is that arising from locally systematic effects. SST retrievals are made through the atmosphere and ambiguities in/limitations to this process will result in errors correlated over synoptic scales. We can evaluate the magnitude of these on the basis of simulation studies. In this case we take an NWP SST field as the 'truth' and simulate the brightness temperatures associated with this field. We then use these brightness temperatures as input to our retrieval and derive the retrieval uncertainty as the difference between the retrieved and 'true' SST.

3. Uncertainties in Level 3 Products

When considering higher-level products, uncertainties existing in the products from which they are derived must be correctly propagated through into the new products. In some cases, the development of the higher-level product will also result in the introduction of a new source of uncertainty. Level three data are gridded products, often at 0.05 or 0.1 degree resolution for SST.

Considering first the errors in the per-pixel data due to noise we can look at the gridded average error (Figure 2, middle panels). The values here have a smaller range than the per-pixel errors but can be either positive or negative. Gridded uncertainties for the same data are shown in the bottom panel. These can only be positive and are scaled as a function of $1/\sqrt{n}$. Therefore when all the pixels are available in a given grid box the uncertainty is consistent (for a given brightness temperature and set of coefficients). Where cloud cover or data loss limits the number of observations in a grid cell for example around cloud edges, the uncertainty in that grid cell is higher.

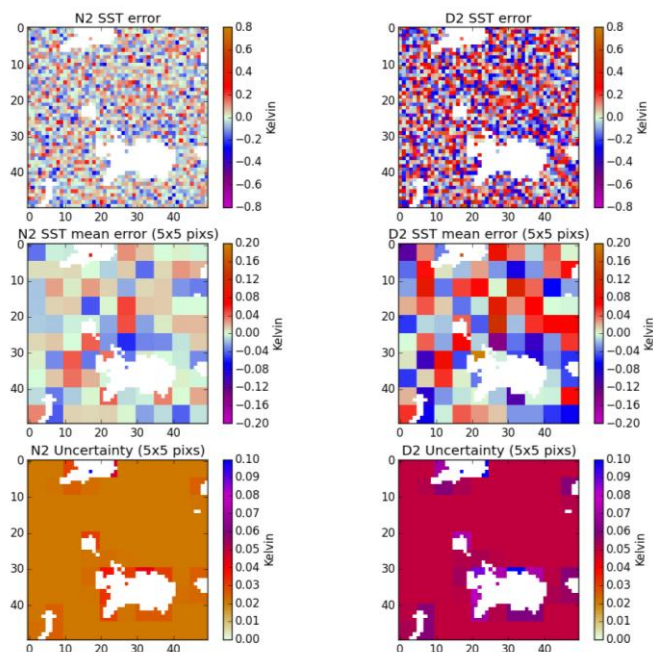


Figure 2: Propagation of errors from uncorrelated effects into L3 data. Top two panels show simulated L2 per-pixel errors for N2 and D2 retrievals. The middle panels show the average errors over a 5x5 pixel domain, and the lower panels the uncertainties over the same gridded domain.

In L3 data, a further source of uncertainty is introduced where data are gridded. For geophysical retrievals using infrared channels, observations cannot be made under clouds. In some cases cloud may cover an entire grid cell, whilst in others only a fraction of the pixels within the grid cell. In the former case, no SST retrieval can be made in that grid cell. In the later case, an average SST would be calculated from the available pixels, which are only a subsample of the full number of pixels. This average SST will differ from the average across the grid cell were all data available, thus introducing a sampling uncertainty.

SSTs are correlated between pixels on the scales on which L3 products are provided, typically 0.05-0.1 degrees. Sampling uncertainties can be calculated as a function of the percentage of clear-sky and the underlying SST variability in the subsample. The smaller the number of clear-sky pixels available, the larger the sampling uncertainty will be. For SSTs in frontal regions with strong gradients, sampling uncertainties will be larger than in homogenous regions.

4. Validating uncertainty estimates

The advantage of estimating the uncertainties in SST within the retrieval process itself is that these can be validated along with the retrieved SST, using in-situ data. We can do this by comparing the standard deviation of the retrieved minus in-situ SST difference with the total uncertainty estimate (calculated by adding the different components in quadrature). We validate per-pixel SSTs using a multi-sensor matchup database to collocate satellite and in-situ observations in space and time. Figure 3 shows four years of validation data (2006-2010) for AATSR for both the N2 and D2 retrievals. The dashed lines on the plot show the uncertainty model we expect, and do not reach zero on the y-axis as there is also an uncertainty in the buoy measurement and geophysical uncertainties from the match-up process. We find that for our N2 retrieval we tend to overestimate per-pixel uncertainties, but that for the D2 retrieval our uncertainty estimates validate well.

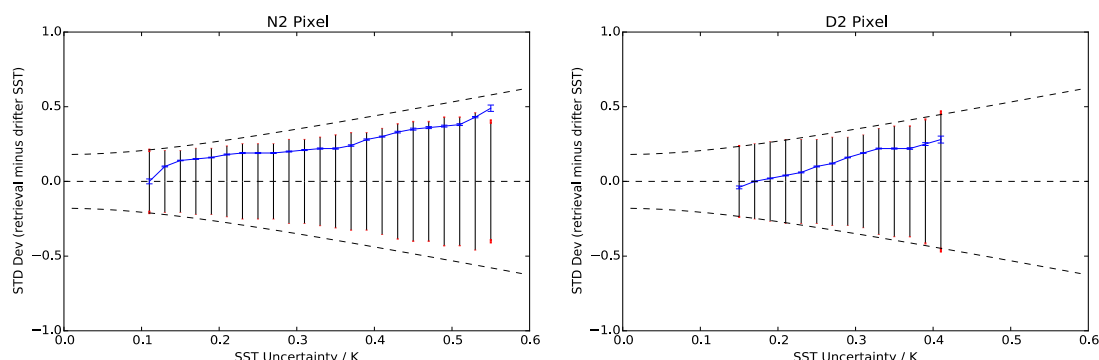


Figure 3: Validation of per-pixel uncertainties for N2 and D2 SST retrievals against in-situ drifting buoy observations.

Not all sources of uncertainty are considered at present within our uncertainty budget. Undetected cloud or ice, aerosol variability and sensor drift will also contribute further sources of uncertainty, and further work is needed to quantify these sources of error within the retrieval process. The magnitude of the uncertainties due to undetected cloud is potentially a significant contributing factor but depends on the skill of the cloud detection algorithm used. For instantaneous measurements, not averaged in either space or time, the dominant sources of error are the uncorrelated and locally systematic effects. Large-scale systematic effects account for a larger proportion of the total uncertainty over longer time scales and spatial averages. We estimate the dominant sources of uncertainty for the types of observations considered here and they validate well despite the further work required to fully quantify the uncertainty budget.

5. Conclusions

We discuss here a methodology for estimating uncertainties in SST retrievals with the retrieval process itself, which can then be validated independently using in-situ data. We calculate uncertainties due to uncorrelated and locally systematic effects in L2 data and consider how these propagate into L3 data. We validate per-pixel SST retrievals using matches to drifting buoys and find that for N2 retrievals we slightly overestimate the uncertainty, but for D2 retrievals our uncertainties validate well.

6. References

Embury, O. Merchant, C. J. (2012). A reprocessing for climate of sea surface temperature from the along-track scanning radiometers: A new retrieval scheme. *Remote Sensing of Environment*, **116**, 47-61.

Joint Committee for Guides in Metrology (2008). Evaluation of measurement data – Guide to the expression of uncertainty in measurement. Bureau International des Poids et Mesures, available from www.bipm.org/en/publications/guides/, pp.130.

PLENARY SESSION VII: APPLICATIONS

SOLAR WARMING OF SOUTH CENTRAL AND NORTH WEST PACIFIC

W. Timothy Liu¹, Wenqing Tang¹, Xiaosu Xie¹ and Rachel T. Pinker²

(1) Jet Propulsion Laboratory, California Institute of Technology, Pasadena, California, USA,
Email:w.t.liu@jpl.nasa.gov

(2) Department of Atmospheric and Oceanic Science, University of Maryland, College Park, Maryland, USA

1. South Pacific Warming

A record-warming event occurred in south-central Pacific (SCP) and peaked in December of 2009 (Lee et al. 2010). Surface short wave radiation (SSWR) is found to contribute significantly and positively to the warming (Liu et al. 2014). The SCP region is within a positive teleconnection pattern between sea surface temperature (SST) anomalies in the equatorial Pacific and the basin-wide SSWR, as revealed by the 24 years of data. The pattern extends southeast from the western equatorial Pacific toward the SCP region, as seen in Fig. 1. Positive Nino 3 and Nino 4 SST anomalies (El Nino indices) correspond to positive SSWR into the ocean at SCP. Fig 2 shows that, for the 24 years period examined, large El Nino/La Nina episodes, indicated by Nino3 and Nino4 indices, are associated with warming and cooling in the SCP region.

2. Northwest Pacific Warming

A strong warming event was also observed in the Northeast Pacific during the winter of 2013-2014 (Bond et al. 2015). Its relation with climate indices of El Nino and Pacific Decadal Oscillation has been suggested. Fig. 3 demonstrates the significant correlation between SST and SSWR for the 32-year period, with Pacific decadal oscillation index superimposed. The negative correlation between SSWR and surface wind speed can also be discerned (Fig. 4).

3. Data

The 24 years of SSWR used in Fig. 1 and 2 were obtained from the International Satellite Cloud Climatology Project (ISCCP) (Rossow and Schiffer 1999). The 32 years of SSWR used in Fig. 3 and 4 were provided by Rachael Pinker (Wang and Pinker 2009). SST data are from the Advanced Very High Resolution Radiometer (AVHRR) (Reynolds et al. 2007), produced by the Group for High Resolution SST (GHRSSST).

4. Discussion

High SST anomalies are usually found under persistent high pressure systems, with low wind speed and reduced evaporative cooling. Clear weather also means strong warming from increased solar heating, which should not be ignored.

5. Acknowledgment

This research was carried out at the Jet Propulsion Laboratory, California Institute of Technology, under a contract with the National Aeronautics and Space Administration (NASA).

It was jointly supported by Precipitation Measuring Mission, Energy and Water Cycle Studies, and Physical Oceanography Program of NASA

© 2015 California Institute of Technology. Government sponsorship acknowledged.

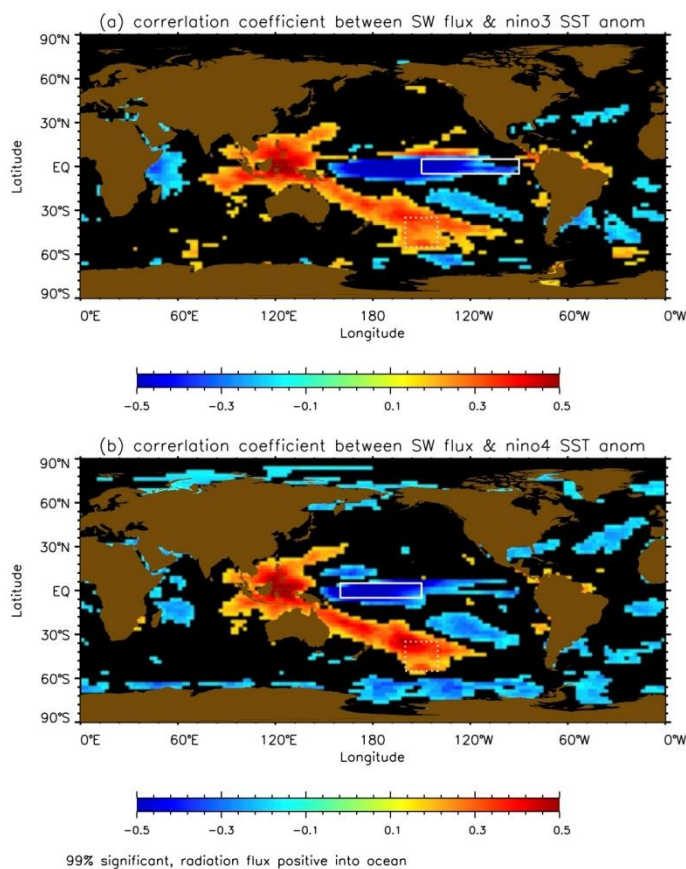


Fig. 1 Remote contemporary correlation coefficient between (a) Nino3 and (b) Nino4 SST anomalies and SSWR anomalies.

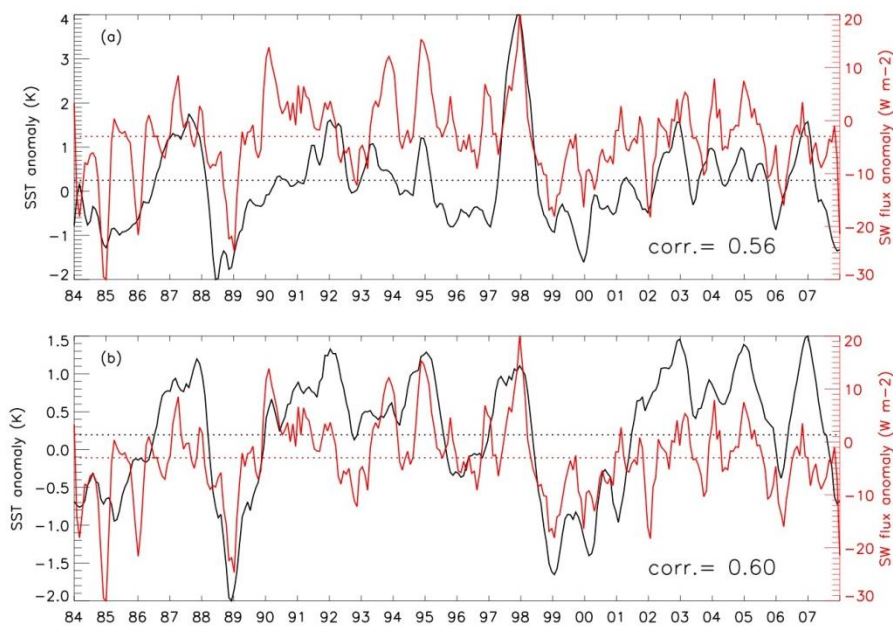


Fig. 2 Time series of (a) Nino3 and (b) Nino4 SST anomalies (black) and SSWR anomalies (red) averaged in SCP area. Data are smoothed with 3-months moving average.

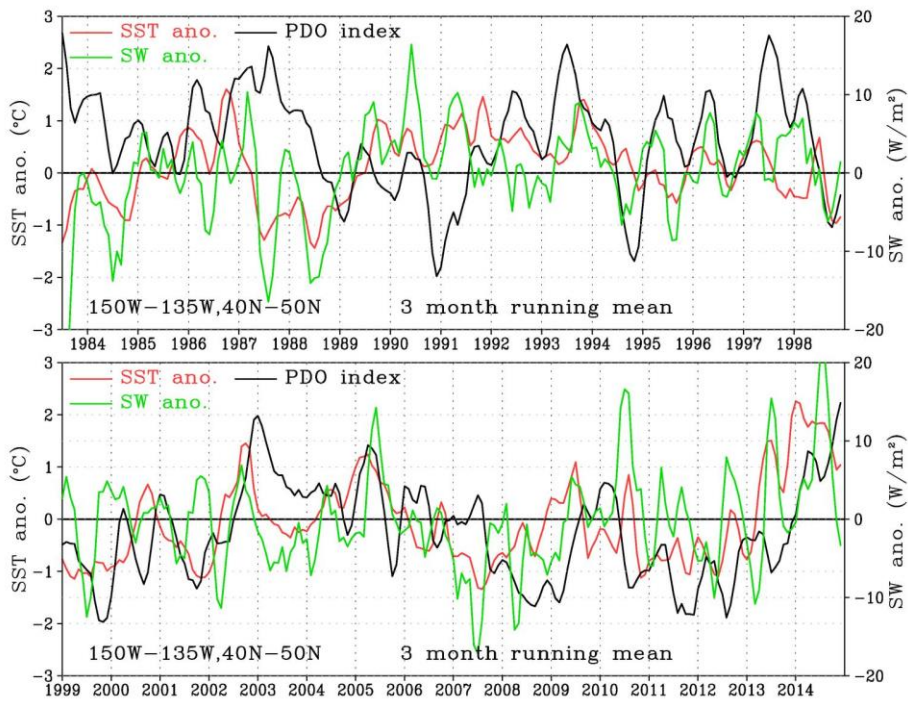


Fig. 3 Time series of SST (red), SSWR (green) anomalies, and PDO index (black). The SST and SSWR anomalies are averaged between 150°W-135°W and 40°N-50°N, with annual cycle removed. 3-month running mean was applied.

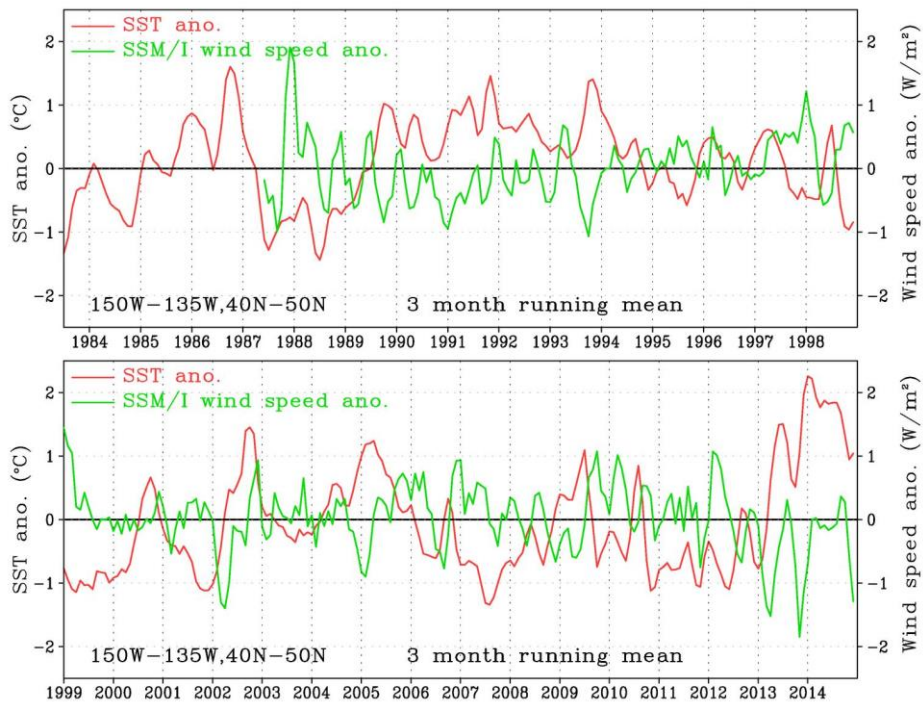


Fig. 4 Same as Fig. 3, except for wind speed anomalies from the Special Sensor Microwave Imager (SSM/I).

6. References

- Bond, N. A., M. F. Cronin, H. Freeland, and N. Mantua, 2015: Causes and impacts of the 2014 warm anomaly in the NE Pacific. *Geophys. Res. Lett.*, **42**, 3414–3420. DOI: 10.1002/2015GL063306
- Lee, T., W.R. Hobbs, J.K. Willis, D. Halkides, I. Fukumori, E.M. Armstrong, A.K. Hayashi, W.T. Liu, W. Patzert, O. Wang, 2010: Record warming in the South Pacific and western Antarctica associated with the strong central Pacific El Niño in 2009-10. *Geophys. Res. Lett.*, **35**, L13808, doi:10.1029/2008GL034172.
- Liu, W.T., W. Tang, R. Pinker, X. Niu, and T. Lee, 2014: Solar warming of south central Pacific. *Int. J. Remote Sensing*, DOI: 10.1080/01431161.2014.926426.
- Reynolds, R. W., T. M. Smith, C. Liu, D. B. Chelton, K. S. Casey, and M. G. Schlax, 2007: Daily High-Resolution-Blended Analyses for Sea Surface Temperature. *J. Climate*, **20**, 5473–5496. DOI: <http://dx.doi.org/10.1175/2007JCLI1824.1>
- Rossow, W.B., and Y.-C. Zhang, 1999: Advances in understanding clouds from ISCCP. *Bull. Amer. Meteorol. Soc.*, **80**, 226-2278.
- Wang, H. and R.T. Pinker, 2009: Shortwave radiative fluxes from MODFIS: model development and implementation. *J. Geophys. Res.*, **114**, D201201, DOI:10.1029/2008JD010442.

PLENARY SESSION VIII: L4 ANALYSIS

THE NEW HIGH-RESOLUTION, OPTIMALLY INTERPOLATED SST DATASET (1982-2012) FOR THE MEDITERRANEAN SEA

Andrea Pisano⁽¹⁾, Bruno Buongiorno Nardelli^(1,2), Cristina Tronconi⁽¹⁾ and Rosalia Santoleri⁽¹⁾

(1) CNR-ISAC UOS Roma, Via Fosso del Cavaliere 100, 00133 Roma, Italy,

Email: andrea.pisano@artov.isac.cnr.it, (cristina.tronconi@artov.isac.cnr.it, r.santoleri@isac.cnr.it)

(2) CNR – Istituto per l'Ambiente Marino Costiero – Napoli, Italy, Email: bruno.buongiornoardelli@cnr.it

ABSTRACT

The latest AVHRR Pathfinder reprocessed dataset, version 5.2 (PFV52), has been used to build daily (night-time) gap-free sea surface temperature (SST) maps (L4) over the Mediterranean Sea) from 1982 to 2012. The interpolation has been carried out by adapting to PFV52 data the CNR-ISAC-GOS SST processing chain (Buongiorno Nardelli et al., 2013) developed in the framework of the MyOcean projects. This new historical dataset thus extends and improves previous L4 Mediterranean SST dataset (based on Pathfinder V5.0, see Marullo et al., 2007). In order to quantify the accuracy of the time series analysis and to exclude spurious trends, a validation of both PFV52 and L4 data is provided, using an independent dataset of drifter measurements for the 2004-2012 period.

1. Introduction

Accurate, high-resolution multi-year SST time series are essential for climate studies, seasonal forecasting and reanalysis activities.

Today, there is a wide range of satellite SST products, from upstream observation to elaborated data, provided in near real time by several international institutions and programs. Among these, the AVHRR Pathfinder program, established in 1990 as a NOAA-NASA joint project, is one of the main activities devoted to the creation of long-term historical SST (non-interpolated) datasets based on all AVHRR sensors on board the NOAA satellite series. Over its twenty-year history, Pathfinder has produced five versions of AVHRR reprocessed data and is now preparing the sixth. The AVHRR Pathfinder V5.2 (PFV52) (Casey et al., 2010) is the latest release of the Pathfinder program and improves previous releases. In particular, including the year 2012, it represents the longest and most consistent SST data record built from the same class of sensors.

Based on previous Pathfinder versions, we can remind the works of Marullo et al. (2007) and Roberts-Jones et al. (2012). The former has produced 21 years of interpolated SST maps for the Mediterranean Sea (1985-2005), with a resolution of 4 km and an accuracy of about 0.5 K. The latter has built a global, 5 km SST and sea ice concentration reanalysis, from 1985 to 2007, based on the Operational SST and Sea Ice Analysis (OSTIA) system. The OSTIA product accuracy is of 0.55 K with a cold bias of 0.1 K on a global scale.

We present here the long-term time series (January 1982 - December 2012) of daily (nighttime), 4 km resolution, gap-free SST analysis (L4) over the Mediterranean Sea built from the PFV52 dataset and produced within MyOcean.

2. Methods

PFV52 data are available as daytime and nighttime files, at 4 km spatial resolution gridded on a uniform latitude-longitude grid. Also, they are provided in netCDF-4 format, nearly compliant to the Group for High Resolution SST (GHRSSST) Data Specification Version 2.0 (GDS v.2), and available through the US National Oceanographic Data Center (NODC) access system (<http://www.nodc.noaa.gov>). Table 1 shows the timeline of the NOAA satellites used in the PFV52 reprocessing.

Satellite	Start Time (Year - Day)	End Time (Year - Day)
NOAA-7	1981-305	1985-004
NOAA-9	1985-005	1988-313
NOAA-11	1988-314	1994-257
NOAA-9	1994-257	1995-018
NOAA-14	1995-019	2000-285
NOAA-16	2000-286	2002-190
NOAA-17	2002-191	2005-156
NOAA-18	2005-157	2010-365
NOAA-19	2011-001	2012-366

Table 1: Satellite platforms available during the Pathfinder AVHRR 1982-2012 reprocessing period.

First, since we were interested only in the reconstruction of the foundation temperature, i.e. the temperature free of diurnal warming, over the Mediterranean domain, we selected only the nighttime PFV52 files to produce our L4 data, extracting the area of interest. Then, the interpolation of PFV52 data was obtained by adapting the CNR-ISAC-GOS near-real-time (NRT) SST processing chain (Buongiorno Nardelli et al., 2013) to the PFV52 input dataset.

The NRT processing chain, set up within the MyOcean projects, is devoted to the operational production of Mediterranean and Black Sea SST L4 data by using different input satellite data and is fully detailed in Buongiorno Nardelli et al. (2013). The main difference with respect to the NRT chain is a simplification in that the PFV52 data are already available as collated (merged) daily images, namely as GHRSSST L3C, and (super)collation of data is thus not needed. Furthermore, a new covariance model was applied in order to improve the quality of the optimal interpolation algorithm used here to produce the L4 data (Buongiorno et al., 2014, under revision). Finally, associated with each SST L4 product, the corresponding error map in Kelvin is available. These data are available on the MyOcean web portal (<http://www.myocean.eu/>).

The accuracy of both PFV52 and L4 SST products has been assessed by comparison to independent drifter data. For this purpose, we collected all the available drifter measurements from the MyOcean In Situ Thematic Assembly Centre (In Situ-TAC) and built a matchup database of collocated observations between satellite and in situ observations.

3. Results

The baseline for the validation of PFV52 and L4 SST products is to use drifting buoy measurements only, as recommended by the GHRSSST on satellite SST validation (STVAL).

More in detail, the validation was carried out by building a matchup database between satellite SST products and surface drifting buoy measurements provided by the MyOcean In Situ – TAC, covering the period 2004 – 2012.

Before computing the statistics of the differences between satellite and in situ SST estimates, specific quality control (QC) procedures and matchup protocols were applied. In particular, drifter data were quality controlled by the assignment of an index flag and we collected only the data with the highest quality index, i.e. 1. Regarding the validation of L4 data, additional tests were applied. They include a comparison with the daily climatological SST field that is used to compute the SST L4 anomalies (rejecting all values exceeding a difference of 5°C), and a comparison with the previous day L4 product (rejecting all values exceeding a difference of 1.5°C).

The matchup has been restricted to night-time data, i.e. between 9 p.m. and 6 a.m. local time. For each interpolated day, the series of drifter measurements available are ordered as a function of time and only the closest measurement to the interpolation nominal time is taken for each grid point.

Figure 1a and b respectively show the spatial distribution of the matchup points between satellite and in situ observations for the PFV52 L3C and interpolated L4 data. Also, the color associated to each point represents

the temperature difference between satellite data and collocated drifter measurement. The mean bias error (MBE) and root mean squared error (RMSE) with respect to in situ data have been computed using the entire matchup database (2004 – 2012), with 15675 and 102164 matchups for PFV52 and L4 data, respectively (Table 2). RMSE for the Pathfinder product is 0.73 K and the mean bias is -0.22 K. RMSE for the L4 product is 0.52 K and the mean bias is -0.23 K. Then, while MBE is quite similar for the two products, RMSE is quite different and this is probably due to noise in Pathfinder data that is filtered through the optimal interpolation.

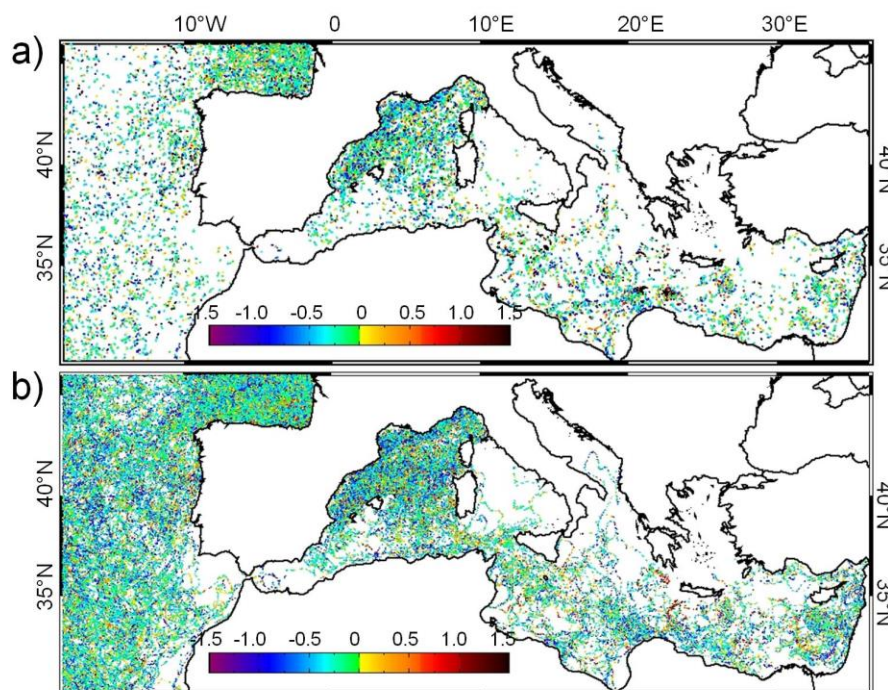


Figure 1: Spatial distribution of the satellite/in situ matchups and associated SST difference for the (a) PFV52 L3C data and (b) L4 SST data, for the period 2004 – 2012.

Data Product	Start Time (day/month/year)	End Time (day/month/year)	MBE	RMSE	Samples
PFV52 SST Dataset	23/10/2004	30/12/2012	-0.22	0.73	15675
OI L4 SST Dataset	21/10/2004	31/12/2012	-0.23	0.52	102164

Table 2: Mean bias (K), root mean square error (K), and number of matchups for the differences between PFV52 L3C /L4 data and in situ drifter measurements. The statistics were computed over the Mediterranean Sea from 2004 to 2012.

Yearly statistics (MBE and RMSE) of the differences between L4 and drifter matchups are shown in Figure 2. The uniform behavior of the mean bias during the 2004 – 2012 period excludes the possibility of spurious trends due to the use of different sensors. This result demonstrates the consistency of the interpolated time series and thus the appropriateness of its usage for climate studies. However, validation must be extended over the entire reprocessing period, i.e. 1982 – 2012.

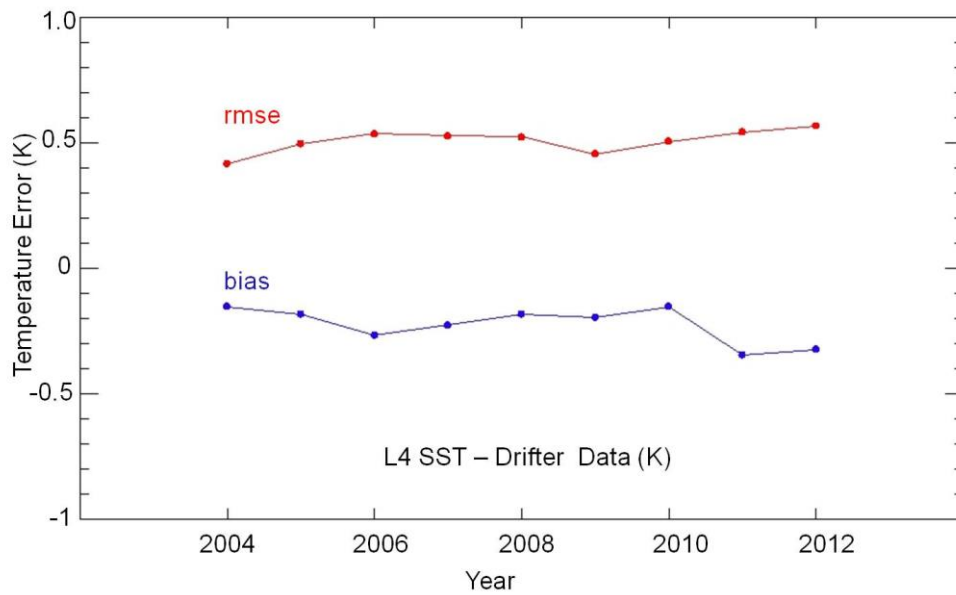


Figure 2: Yearly statistics (MBE and RMSE) of the differences between L4 and drifter matchups.

Finally, Figure 3 shows the L4 statistics (MBE and RMSE) as a function of the interpolation error, expressed in degrees Kelvin. Basically, this plot tells us that: 1) when the interpolation error is equal 0 K (all observations, no data voids) the corresponding RMSE is about 0.4 K, which corresponds to the minimum RMSE in the curve; 2) the RMSE remains practically constant, i.e. around 0.5 K, if we exclude the last three values. Then, we can say that our optimal interpolation algorithm error (OI error, in Figure 3) overestimates the RMSE.

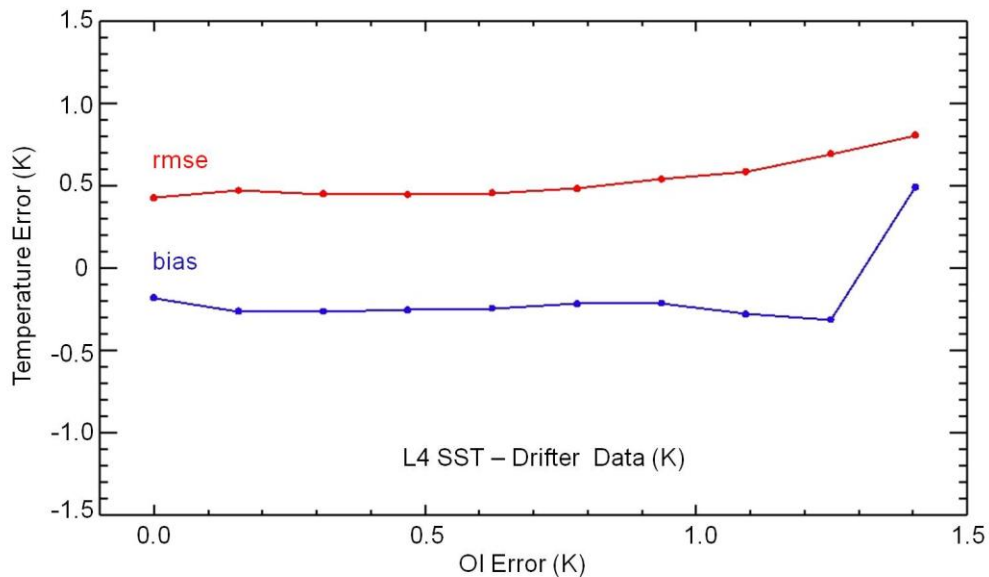


Figure 3: MBE and RMSE of the differences between L4 and drifter matchups as a function of the interpolation error expressed in K.

4. Conclusion

We produced 31 years of daily (nighttime), gap-free, 4 km resolution SST maps (L4) over the Mediterranean Sea by using the latest version of the AVHRR Pathfinder dataset (PFV52), from 1982 – 2012. Validation of both PFV52 and L4 SST time series has been carried out by using collocated in situ drifter observations (from In Situ – TAC, for 2004 – 2012). The RMSE of the differences between satellite and drifter data ranges from 0.73 for PFV52 data to 0.52 for L4 data. The uniform behavior of the L4 data RMSE demonstrates the consistency of the time series, excluding sensor drifts.

A more complete validation must be provided, extending this check to the entire AVHRR Pathfinder reprocessing period, i.e. 1982 – 2012. This can be done by collecting all the available in situ data from the MyOcean In Situ – TAC, such as those provided by CTDs, Argo floats and XBTs.

5. References

Buongiorno Nardelli, B., C. Tronconi, A. Pisano and R. Santoleri, High and Ultra High resolution processing of satellite Sea Surface Temperature data over the Southern European Seas in the framework of MyOcean project. *Remote Sensing of Environment*, **129**, 1-16, 2013.

Buongiorno Nardelli, B., A. Pisano, C. Tronconi and R. Santoleri, Evaluation of different covariance models for the operational interpolation of high resolution satellite Sea Surface Temperature data over the Mediterranean Sea. *Remote Sensing of Environment*, under revision.

Casey, K. S., T. B. Brandon, P. Cornillon and R. Evans, The Past, Present and Future of the AVHRR Pathfinder SST Program. In *Oceanography from Space: Revisited*, eds. V. Barale, J.F.R. Gower, and L. Alberotanza, Springer, 2010. doi: 10.1007/978-90-481-8681-5_16.

Roberts-Jones, J., E. K. Fiedler, and M. J. Martin, Daily, Global, High-Resolution SST and Sea Ice Reanalysis for 1985–2007 Using the OSTIA System. *J. Climate*, **25**, 6215–6232, 2012. doi: <http://dx.doi.org/10.1175/JCLI-D-11-00648.1>

Marullo S., B. Buongiorno Nardelli, M. Guarracino, and R. Santoleri, Observing The Mediterranean Sea from Space: 21 years of Pathfinder-AVHRR Sea Surface Temperatures (1985 to 2005). Re-analysis and validation. *Ocean Sci.*, **3**, 299-310, 2007.

ASSIMILATING RETRIEVALS OF SEA SURFACE TEMPERATURE FROM VIIRS AND AMSR2 IN THE EXPERIMENTAL HIGH RESOLUTION CMC SST ANALYSIS

Bruce Brasnett and Dorina Surcel Colan

Numerical Environmental Prediction Section, National Prediction Development Division, Meteorological Service of Canada, Environment Canada, Email: bruce.brasnett@gmail.com, and dorina.surcel-colan@ec.gc.ca

ABSTRACT

Experiments are carried out to assess the potential contributions from two new satellite datasets in an experimental version of the Canadian Meteorological Centre (CMC) sea surface temperature (SST) analysis. The most important changes to the analysis methodology include a reduction of the spacing of the satellite and ice observations assimilated, an improvement in the analysis grid resolution from 0.2° to 0.1° and a reduction in the background error correlation length scale in middle and high latitudes. It is shown that the contribution from prior observations is a vital component of the analysis methodology. The experimental version of the analysis assimilating data from the Visible Infrared Imaging Radiometer Suite (VIIRS), the Advanced Microwave Scanning Radiometer 2 (AMSR2) and several Advanced Very High Resolution Radiometer (AVHRR) instruments is verified against independent data. This verification shows that the experimental analysis performed very well, with global average standard deviation consistently better than that of the GHRSSST Multi-Product Ensemble (GMPE) real-time system. The experimental analysis is shown to outperform the currently operational CMC SST analysis, with most of the improvement being due to its assimilation of the VIIRS and AMSR2 retrievals and a further small gain being due to changes to the analysis methodology (including higher resolution).

1. Introduction

The release in 2014 of SST datasets from two new instruments, VIIRS onboard the Suomi National Polar-Orbiting Partnerships (S-NPP) satellite and AMSR2 onboard the Global Change Observing Mission-Water (GCOM-W) satellite, raised the question of the potential contribution of these two datasets to SST analyses. In this study, we present findings from the inclusion of VIIRS data produced by the National Oceanographic and Atmospheric Administration (NOAA) using the Advanced Clear-Sky Processor for Oceans (ACSPO) and the AMSR2 product from Remote Sensing Systems (RSS) into an experimental 0.1° version of the CMC analysis.

Section 2 presents the changes to the assimilation methodology employed in the experimental analysis. Section 3 begins with a discussion of the contribution made by prior observations to each analysis, particularly the capacity of the system to resolve small-scale features. Results of verification against independent data are also presented in section 3, followed by conclusions.

2. Assimilation methodology

The essential components of the method are as described in Brasnett (2008). Briefly, the method of statistical interpolation is applied to the analysis problem, the satellite bias estimation and the observation quality control. The SST assimilation methodology uses anomaly from climatology as the analysis variable. The background is based on simple persistence. In practice, this means taking the most recent (24 hour-old) analysis and modifying it by a return to climatology for use in the analysis procedure. The return to climatology consists of scaling the anomalies by 0.983, equivalent to an exponential decay with an e-folding time of 58 days. With this field as the background, current observations are assimilated, including retrievals from the two new instruments, AMSR2 on board GCOM-W and VIIRS on board S-NPP. The AMSR2 and daytime VIIRS retrievals are ascribed an observation error of 0.9 K and nighttime VIIRS retrievals are assimilated with an error of 0.7 K.

a. Background error spatial scales and retrieval spacing

Along with increasing the resolution of the analysis grid to 0.1° , additional changes were needed to fully benefit from the improved resolution. In order to resolve smaller spatial scales, the length scales (e -folding distances) of the background error correlations were modified as shown in figure 1. The length scales are isotropic and symmetric about the equator and there is no difference between the low resolution and high-resolution analyses from the equator to $\pm 37.5^\circ$. Different experiments were performed varying these length scales and the values chosen minimized the estimated analysis error. In this way, it was determined that the analysis cannot be improved at low latitudes by reducing the length scale but modest improvement at high latitudes is possible. Accordingly, at high latitudes where the smallest length scale is used, the value of this length scale is 24 km in the 0.1° analysis compared to 43 km in the 0.2° analysis.

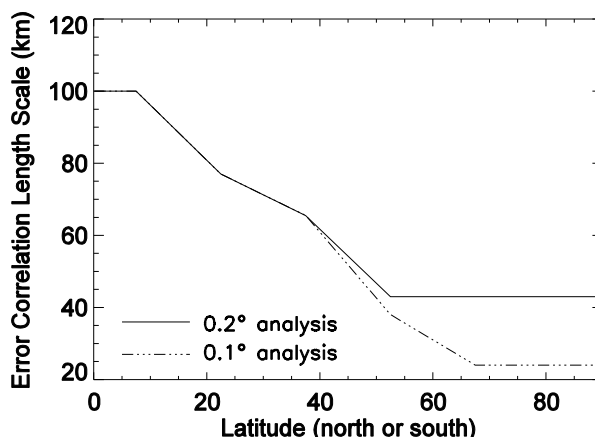


Figure 1. Length scales (e -folding distances) of the background error correlations for the 0.2° analysis (solid line) and the 0.1° analysis (dot-dashed line).

The density of the satellite data assimilated is critically important. Liu and Rabier (2002) studied the connection between the observations density, the observations resolution and the resolution of the model grid. They showed that the analysis quality decreases if the density of the observational dataset is too large and the error correlations are neglected. Satellite retrievals are fundamentally different from conventional observations. All retrievals in a satellite swath originate from the same instrument, whereas many instruments are needed to obtain similar coverage from buoys. Even with a satellite bias correction scheme, it cannot be assumed that retrievals from a single sensor are unbiased. Moreover, the statistical interpolation methodology employed here does not take account of correlated observations errors. As a consequence of these facts, satellite retrievals must be thinned prior to assimilation so that they do not receive undue weight in the analysis. It was found by experimentation that an appropriate spacing for infrared retrievals from a single satellite instrument is 33 km north of 40N and south of 40S, increasing to 80 km at the equator. The smallest spacing of satellite data used in the operational 0.2° analysis is 44 km. For the AMSR2 instrument, the gridded retrievals have a spacing of 0.25° , but for assimilation, a 55 km spacing is used everywhere except north of 60N and south of 60S where the spacing is 89 km.

b. Insertion of ice information

The 0.1° SST analysis adds ice information by inserting proxy SST data at locations where ice is present. As part of its Numerical Weather Prediction (NWP) activities, CMC produces a 10 km global ice analysis four times per day. For application to SST, the ice analysis valid at 1800 UTC is sampled. Each day, proxy observations are generated at every third grid point along the orthogonal lines of grid points yielding a spacing of 30 km. The proxy observations are produced where the ice concentration is 0.6 or larger. The sampling starts from a reference grid point of the ice analysis grid, which is displaced daily so that a complete sampling of the 10 km grid occurs over a 9-day period. In most cases, the ice proxy value is -1.8°C , the freezing point of seawater with a salinity of 33 psu. However, when melt water is present, the three phases of H_2O

coexist at the air-water-ice interface. Thus, by definition of the triple-point temperature of H₂O, a proxy value of 0°C is used in this situation (Halliday and Resnick, 1974). To identify those grid points where the ice is likely to be melting, a time average of the surface air temperature is used. This time average is produced from analyses of air temperature valid at 6-hour intervals using a 6-hour forecast from the CMC global atmospheric model (Charron et al., 2012) as background, and incorporates all available air temperature reports from drifters, ships and land stations. These temperature analyses are exponentially weighted by combining the current temperature analysis with the mean from 6 hours earlier, using weights of 0.2 and 0.8, respectively. At locations where this updated running mean is greater than 0°C and the ice concentration is between 0.6 and 0.9, a proxy SST of 0°C is used. Where the ice concentration exceeds 0.9, a proxy value of -1.8°C is used regardless of the average temperature. The proxy SSTs are then assimilated with an ascribed observation error of 1.0°C. This error is greater than the error ascribed to any other observation type.

Several changes to the analysis methodology result in better definition of the SST gradient near the ice edge. This is illustrated in fig. 2, which shows the region of the Beaufort Sea, Banks Island and western Victoria Island on 1 August 2014. Ice cover on this day was extensive over the northwest quadrant of the region, as indicated by the locations of ice proxy observations assimilated by each analysis (white dots). Besides the area of open water between 70N and 72N, there was also an area of open water bounded approximately by 72N and 74N and 125W and 130W. Each analysis has large gradients to the west and north of this latter region but the gradients in the experimental analysis (left panel) are 5 K/100 km larger at several locations. The larger gradients are likely due to a combination of factors including the smaller correlation length scales at these latitudes (fig. 1), the denser spacing of observations, the inclusion of VIIRS retrievals and the finer resolution of the analysis grid. One prominent difference between the two panels of fig. 2 is the area of large gradient in the experimental analysis near 69.5N and 135W. The experimental analysis captured a plume of warm water from the Mackenzie River, which flows into the Beaufort Sea here, a feature missed by the operational analysis (right panel).

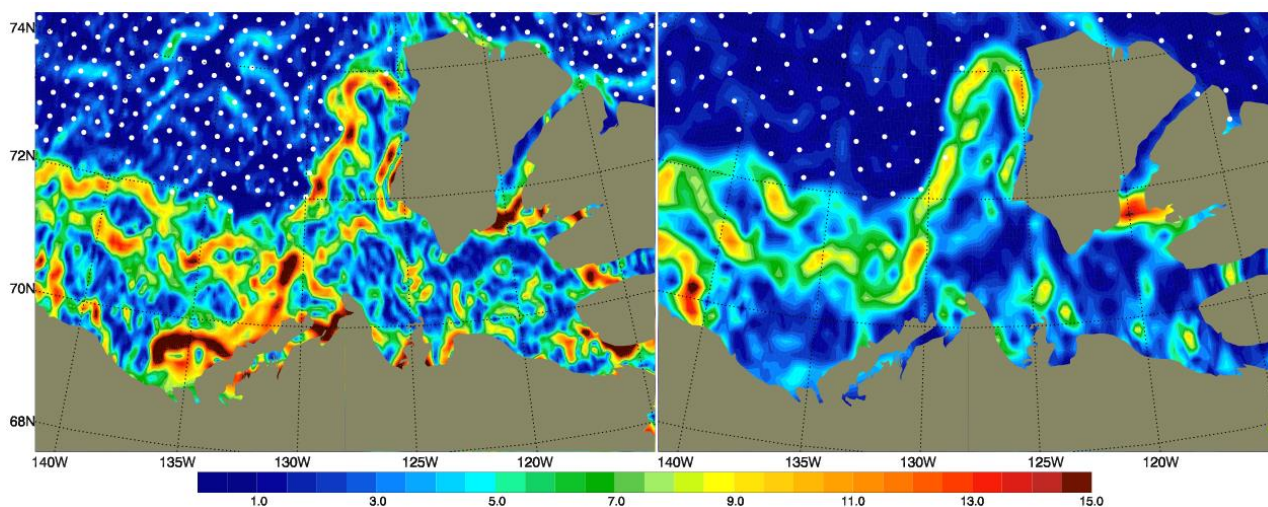


Figure 2. Magnitude of SST gradient (K/100 km) computed from 1 August 2014 analyses. The left panel shows the experimental 0.1° analysis gradient and the right panel shows the operational 0.2° analysis gradient. White dots indicate the locations of ice proxy data assimilated by each analysis.

3. Assessment of contributions from AMSR2 and VIIRS

As stated in section 2a, the thinning of high-resolution retrievals from satellite sensors makes it possible to neglect the correlations in the observation errors of these retrievals. Here we show that the analysis may still adequately represent small-scale features due to the contribution to each analysis from prior observations. Figure 3 shows the results of several experiments carried out to assess the ability of the experimental analysis to preserve SST information on the analysis grid when observations are not available. Here, the analysis errors from each experiment were estimated using independent, quality controlled observations from Argo floats. The

figure shows the global average of the analysis standard deviation for the normal analysis which has used the full complement of data every day during the period (green dot-dashed line), the climatology (solid black line), an experiment where all data were denied on the current day (black dot-dashed line), an experiment where data was denied for seven days (red line) and finally, an experiment where data was denied for 30 days (blue line). The climatology is an important reference because the analysis is designed to gradually return to climatology if there are no new observations, as explained in section 2 above. Hence, if data is denied for long enough, the analysis error will approach the error of climatology asymptotically, making the latter the upper bound on the analysis error. It should be noted that the analysis that is denied data on the current day is identical to the background for the normal analysis. It is clear from the figure that the reduction in error achieved from assimilating the current day's observations (difference between the two dot-dashed lines) is small compared to the reduction in error achieved from using the most recent analysis as the background instead of climatology (difference between the two black lines). This is an intrinsic property of the analysis described here. The figure illustrates the excellent quality of the background in the normal analysis. This background represents the information retained from all prior observations. Note also that the analysis denied data for 30 days (blue curve) continues to have significant skill over climatology, indicating that even 30-day old observations contain some information on the current SST and also showing that the analysis has preserved this information over this period. Moreover, the only constraint on the spatial scales of the information stored on the analysis grid is the grid length and therefore, one should expect all spatial scales that can be resolved on the grid to be present. These results suggest that if information with spatial scales smaller than those of the thinned observations accumulates in the analysis through random sampling then the system will preserve this information on the grid for weeks.

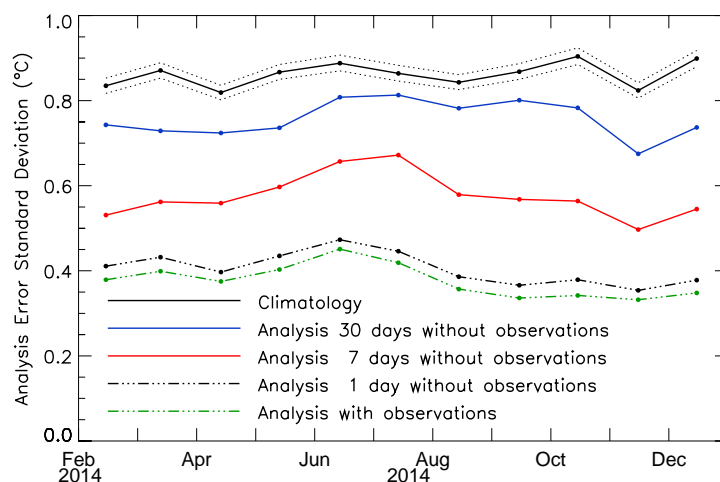


Figure 3. Time series of global analysis error standard deviation (°C) estimated using quality controlled Argo floats for the experimental analysis (green), climatology (solid black) and three data denial experiments: data denied for the current day (black, dot-dashed), data denied for seven days (red) and data denied for 30 days (blue). The dotted lines indicate the 95% confidence interval for the error of climatology.

In fig. 4, a 12-month time series of analysis standard deviations and biases is shown for the 0.1° analysis, the CMC operational analysis and the GHRSSST multi-product ensemble (GMPE). The 0.1° analysis used NAVO AVHRR data from NOAA-18 & 19 and METOP-A as well as data from RSS AMSR2, ACSPO VIIRS, the new 10 km CMC ice analysis, ships and buoys. The operational analysis during the same period used data from in situ sources, the operational CMC ice analysis (resolution 37 km) and NAVO AVHRR data from NOAA-18&19 and METOP-A. The GMPE product, described in Martin et al. (2012), is the median of several (typically ten or eleven) real-time analyses and was found to be more accurate than any of the contributing analyses. The 0.1° product is consistently more accurate than the operational CMC analysis and the GMPE product.

Only in April, a month for which no ACSPO VIIRS data was available, the error difference between the experimental analysis and GMPE was not statistically significant.

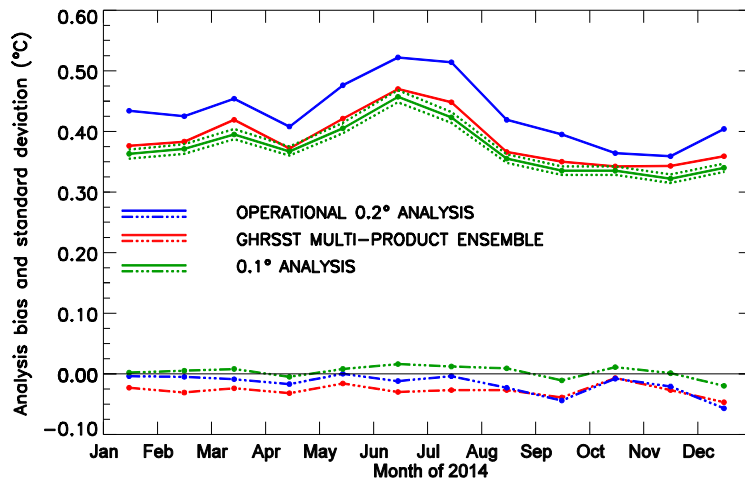


Figure 4. Monthly verification statistics for 2014 using independent data from Argo floats as truth. Standard deviation (°C, solid lines) and bias (dot-dashed lines) for the operational analysis are in blue while the GMPE median is in red and the 0.1° analysis including RSS AMSR2 and ACSPO VIIRS is in green. The dotted lines show the 95% confidence interval for the 0.1° analysis error standard deviation.

Figure 5 shows average analysis errors for the global ocean and several regions. As in fig. 4, the results are for the period 1 January 2014 to 31 December 2014 and show the same three analyses. The global statistics confirm what was seen in fig. 4 with the 0.1° product showing the smallest standard deviation and bias. Only for the Indian Ocean the error difference between the experimental analysis and GMPE was not statistically significant.

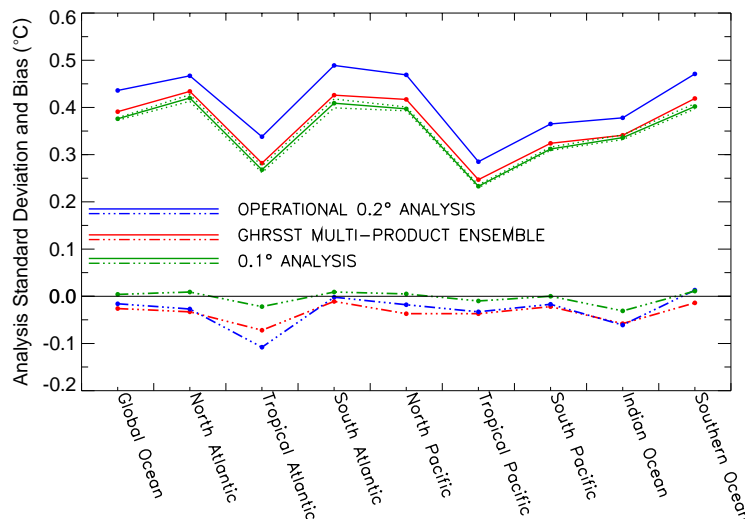


Figure 5. Analysis bias (°C, dot-dashed lines) and standard deviation (solid lines) for several regions for 2014. The results for the operational analysis are shown in blue, statistics for the GMPE product are in red and those for the 0.1° analysis are in green. The dotted lines show the 95% confidence interval for the 0.1° analysis error standard deviation.

The results of figures 4 and 5 raise the question of whether the gain in skill of the experimental analysis is due primarily to improvements in the analysis methodology (including analysis resolution) or to the addition of the

RSS AMSR2 and ACSPO VIIRS datasets. This question is addressed by the results of fig. 6, which shows the monthly average standard deviations and biases for three analyses. The first (blue curves) is the operational 0.2° analysis as described above. The second (red curves) is the same 0.2° analysis but with RSS AMSR2 and ACSPO VIIRS data assimilated, in addition to the NAVO AVHRR, in situ and ice data assimilated in the operational analysis. The same data are assimilated in the third analysis (green curves), which is the 0.1° experimental analysis and includes the modifications to the analysis methodology described in section 2. The results clearly show that most of the reduction in analysis standard deviation results from the addition of AMSR2 and VIIRS data. However, the changes to the analysis methodology do consistently provide a small gain over the 0.2° analysis using the same data, although this improvement is only statistically significant for February, April and July.

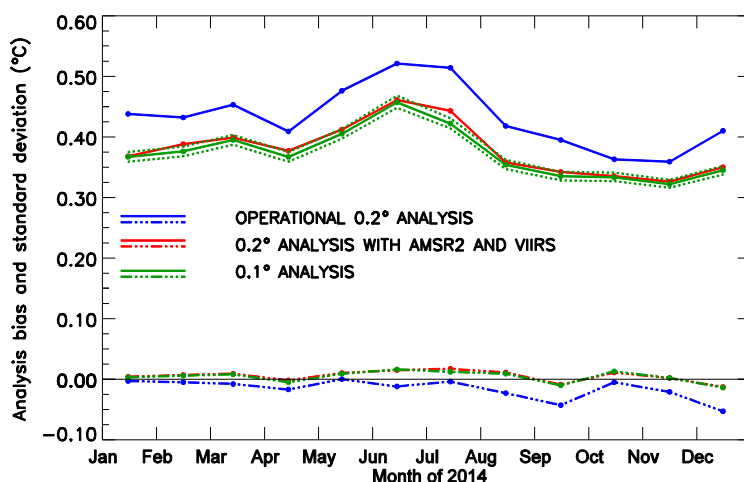


Figure 6. Monthly analysis biases (°C, dot-dashed lines) and standard deviations (solid lines) for 2014 using Argo float temperatures as truth. The 0.2° (operational) analysis is shown in blue, the same analysis but with RSS AMSR2 and ACSPO VIIRS data added is shown in red and the experimental 0.1° analysis is shown in green. The dotted lines show the 95% confidence interval for the 0.1° analysis error standard deviation.

4. Conclusion

SST retrievals from two new satellite instruments, the S-NPP VIIRS and the GCOM-W1 AMSR2, were assimilated by an updated, 0.1° resolution, CMC analysis system. The results were encouraging with the experimental product showing more skill than the existing CMC analysis and indeed more skill than the GMPE product. It was also demonstrated (fig. 6) that most of the improvement of the new analysis relative to the operational analysis was due to the addition of the RSS AMSR2 and ACSPO VIIRS datasets. It should be pointed out, therefore, that due to the recent release of the new datasets, it is unlikely that very many of the member analyses of the GHRSSST multi-product ensemble were assimilating the two new datasets during the period considered. Thus, perhaps it is not surprising that the experimental analysis showed more skill than the GMPE product. A more meaningful comparison will be possible when a majority of the members of the ensemble are assimilating the new datasets. Nevertheless, since the GMPE product is recognized as the most accurate global SST product available in real-time, it remains an important benchmark for assessing analysis accuracy.

5. References

Brasnett, B., The impact of satellite retrievals in a global sea-surface-temperature analysis. *Quart. J. Roy. Met. Soc.*, **134**, 1745-1760, 2008.

Charron, M., and Coauthors, The stratospheric extension of the Canadian global deterministic medium-range weather forecasting system and its impact on tropospheric forecasts, *Mon. Wea. Rev.*, **140**, 1924-1944, 2012.

Halliday, D. and R. Resnick, *Fundamentals of Physics*, Wiley, 827pp, 1974.

Liu, Z.-Q. and F. Rabier, The interaction between model resolution, observation resolution and observation density in data assimilation: A one-dimensional study, *Quart. J. Roy. Met. Soc.*, **128**, 1367-1386, 2002.

SECTION 3: BREAKOUT SESSION REPORTS

BREAKOUT SESSION REPORTS

THE APPLICATIONS AND USER SUPPORT TECHNICAL ADVISORY GROUP (AUS-TAG) BREAKOUT MEETING REPORT

Jorge Vazquez⁽¹⁾ and Prasanjit Dash⁽²⁾

(1) Jet Propulsion Laboratory, California Institute of Technology, Pasadena, CA, USA,
Email: jorge.vazquez@jpl.nasa.gov

(2) NOAA STAR and CSU CIRA, USA, Email: Prasanjit.Dash@noaa.gov

1. Agenda

1.1. Terms of reference (overall direction of AUS TAG):

- Jorge Vazquez opened the discussion and facilitated further

Responsibilities:

1) Manage all aspects of the GHRSSST User Manual

This includes overseeing all new versions, providing periodic reviews, as deemed necessary by the Science Team, and making the latest version available to the user community.

2) Maintain and develop methods for data discovery within the GHRSSST R/GTS.

This includes making recommendations to the science team on new technologies that could improve data access and usability. AUS-TAG will also work closely with the Data and Assembly System (DAS-TAG) in the implementation of these new technologies.

1.2. Presentation of the newer GHRSSST web site and discussions:

- *Gary Corlett and all participating in discussion*

1.3. Discussions on a User survey discussion; quick start guide

- *Gary Corlett and all participating in discussion*

1.4. Gap analysis for GHRSSST services

- *Prasanjit Dash and all participating in discussion*

Discussion on identifying any gaps

- *knowledge gap, e.g., not knowing what is desired (user comes in with no knowledge of SST. How well do we know what products users want? Current search capabilities don't really account for such a user;*
- *communication gap, e.g., not providing clear instructions on which products to choose, delivery gap, e.g., data interruptions)*

1.5. User support (roles of GDAC and LTSRF):

- *Jorge Vazquez/Ken Casey*
-

1.6. Review of trends of user statistics

- *Jorge Vazquez*

1.7. Future of AUS TAG membership

- *Jorge Vazquez/Prasanjit Dash*

2. Minutes

2.1. General opinion (Ken C., Ed A., Gary C.):

A few members of AUS TAG do some substantial work in the background during the year, but AUS TAG as such does not have a strong participation on the fore-front. May be we should think of 'joining forces' with DAS TAG and other web-activities and come-up with a sub-team, rather than a dedicated TAG. Another way would be to create a few position/s as point of contact (POC) for the users.

Regarding update of GHRSSST document, Ken suggested that many people do not read documents; we should have a quick read guide rather than a lengthy document.

Alexey K: when I came to GHRSSST, this document was very helpful for me to understand the activities rather than skimming through pages and printing out suitable material

(Substantial debate took place in for and against of a 50-60 page document)

2.2. Web revamping, Gary C.

Explained rationale of why we need a revamped webpage and only thing we can do is 'Start Again' rather than modifying the older page that is less economic.

Showed a screenshot which did not give a full flavor. Eileen/Alexey and others did not like the look (as was seen from a screenshot). This perception may (and likely will) change, once a Live link is sent for review.

Discussions on the design of logo.

Conclusion: Need to show a Live version before this can be discussed.

2.3. 3. Gaps in GHRSSST service to the users, Prasanjit D:

Showed examples of various gaps (knowledge, standard, delivery and communication). Examples of how 'corrupt data' are being served at the PO.DAAC facility and LTSRF that regular users have no knowledge of. Raised questions on how GHRSSST Data Serving facility can identify and flag those datasets that have no physical meaning.

Ken C. mentioned there is some check for a given set of products, at LTSRF, but not for all products and SST.

2.4. Trends of user statistics, Jorge V.:

Explained how user statistics for individual products are collected at PO.DAAC and shows relative demand of various products.

Ken,Ed: provide those user stats in some interface to the RDAC so that the data producers are aware of the relative demand for their products. It will be really useful.

3. Action items:

- 3.1. While the activities pursued by AUS TAG in the background are important, its independent existence as a TAG was questioned and suggestions were made to join forces with DAS TAG. Seek opinion and explore if a restructuring and renaming will be beneficial.
- 3.2. Provided that the TAG continues to exist, update the GHRSSST document
- 3.3. Based on the analysis from 'user survey', formulate a quick start guide
- 3.4. Find a way to share 'trend of user statistics' with the RDACs, along with relative ranking of other products so that the producers are aware about the use of their data.

Jorge will follow-up on this from the PO.DAAC perspective. The plan would be to setup a password protected site where the RDACs can go to get their stats, including trends on users and volumes. However to do this we need to go back to an ongoing issue. Get official representatives from each RDAC to act as members of the AUS-TAG, as is possible and appropriate.

This has been difficult to do in the past. It needs to be addressed again.

- 3.5. Alert the RDACs and GDACs to communicate and see what can be done when the data are corrupt (physically not meaningful due to random technical incidents); i.e., who should alert whom and how to flag or at least issue a Visible warning to the potential users.

(This is where we need to use webinar, etc. technology better to communicate. As GHRSSST evolves, this will be more critical. This could be addressed in the user survey for feedback on how to setup.)

THE CLIMATE DATA RECORDS TECHNICAL ADVISORY GROUP (CDR-TAG) BREAKOUT MEETING REPORT

Chair: Jonathan Mittaz^(1,2); Rapporteur: C.E.Bulgin⁽³⁾

(1) University of Reading, Reading, UK, Email: j.mittaz@reading.ac.uk

(2) National Physical Laboratory, Teddington, UK, Email: jonathan.mittaz@npl.co.uk

(3) University of Reading, Reading, UK, Email: c.e.bulgin@reading.ac.uk

ABSTRACT

A report on the discussions and recommendations made during the climate data records technical advisory group breakout session. A discussion was had regarding the usability of the CDAF (climate data assessment framework) and a longer discussion on uncertainties in climate data records.

1. Introduction

The CDR-TAG met to discuss a number of different issues. The first issue was the lack of a Vice-Chair for the CDR-TAG. There was one nomination, Viva Banzon from NCEI Asheville who was duly voted in as Vice-Chair. Unfortunately as Viva could not make this GHRSSST meeting she was not present to start immediately and Claire Bulgin was cajoled to be the rapporteur for the current breakout session. The International Project STATUS of CDRs was then gone through which showed that there are a number of different on-going reprocessing projects of relatively long-time period data. The breakout then concentrated on two main topics – the use of the CDAF and uncertainties in CDRs. Finally there was a discussion on the future of the CDR-TAG.

Discussion

The slide about the MUR global SST at L4 provoked some discussion about whether any reprocessing was scheduled. At present this is not planned but it was felt that GHRSSST should support such reprocessing. Therefore letters of support from GHRSSST (and from other organisations interested in using the data) will be written in order to encourage reprocessing. An action was created for drafting a template for this letter (which will be drafted by Jorge Vazquez) and circulating it to relevant parties before sent onto NASA.

Talks

Helen Beggs gave a talk on the IMOS HRPT AVHRR SST project. At present this dataset runs for 23 years back to 1992 covering the area around Australia and data are available at L2 and L3. The dataset uses a running one-year calibration window adjusted monthly. SSES also change with time, again using a one-year window but adjusted every five days. These are calculated per pixel and vary continuously across the field of view (smoothly rather than step-wise). SSES statistics are given for all quality levels of the data.

Eileen Maturi gave a presentation on NOAA/NESDIS Star reprocessing. This will involve reprocessing of 5km SST analyses. This involves reprocessing geostationary and polar data back as far as GOES-8 (1994). This reprocessing is of particular interest in coral reef bleaching studies. There are checks to ensure that the reprocessing is performing in a similar way to the operational processing. SSES will be calculated from the match-up database and put into the L2P data retrospectively.

2. Use of the CDAF

The next item for discussion was the status of the CDAF. While the CDAF is now in place as a document there has been very little pickup from CDR (or long timeseries) data producers to date. One of the problems is the lack of a set of tools to help derive the numbers needed to complete the CDAF. Some sort of tool has been suggested to help with this process.

Discussion

Ken Casey thought that an independent group to provide tools to facilitate the use of CDAF would be really useful. Tools are probably required to help data producers create the metrics needed to fill out the CDAF. Discussions as to how this should be done decided that a group of relevant people would convene to determine ways of providing the information. To begin Sasha and Prasanjit will read the CDAF and assess the capability of SQUAM to help with some of the metrics. Felyx will also be investigated as a possible solution and some combination of the two may be usable. Depending on an as yet to be found source of funds tools may then be created to help with the CDAF. It was pointed out that not all of the CDAF metrics are required and that some of the metrics can be left blank if the information is difficult to obtain. Depending on the findings of the reviewing group (tentatively Jon Mittaz, Chris Merchant, Gary Corlett, J-F Piolle, Sasha Ignatov and Prasanjit Dash) a recommendation as to the way forward will be made. An action was also taken to send a link to the latest version of the CDAF to the CDRTAG.

3. Uncertainties in CDRs

The next topic and somewhat of a common theme across a number of breakouts is that of SSES (single sensor error statistics) or uncertainties in CDRs. Examples from different current CDR generation producers were shown which included the ESA CCI SST project as well as the FIDUCEO project.

From the CCI project a proposed list of possible uncertainty components was shown which included random and locally (spatial) systematic components. It also included suggestions for the ability to convert from single skin retrieval to a range of different SSTs including at depth as well as SSTs at times away from the satellite observation times. A proposal for a 'lite' GHRSSST product and a full metrological product was presented from the ESA CCI SST project.

Then work being started under the FIDUCEO project was presented. FIDUCEO is attempting to apply metrology (the science of measurement) to Earth observation and works from the physics of the instrument, through the retrieval process to provide random and systematic uncertainties for (in this case) SST. An example of a Monte-Carlo simulation system of the AVHRR instrument that includes known noise sources as well as errors introduced by the calibration was shown. A simulation of the Earth giving brightness temperatures from input SST including variations due to the atmosphere was also run in both an 'observed' mode where the top-of-atmosphere BTs are considered correct (observed) plus a 'modeled' version using a different prior SST/atmospheric profile/RTM. This can then be used to determine traceable errors and therefore determine the underlying probability density function of SST retrieval errors. This can be done for individual retrievals that were shown to be clearly non-Gaussian. Looking at the statistics of a range of retrievals it was also shown that in the case of the simulated 'World' and Optimal Estimation the dominant source of error is the retrieval error rather than from instrumental noise. So one possible direction for uncertainties in CDRs is via similar processes of tracing through the retrieval process to L2P with modeling to higher levels. In theory this gives an independent estimate of SST uncertainty to that provided by the in-situ network and use in-situ for validation. This is a departure from many SSES algorithms and is a different approach.

Discussion

Simon Good mentioned that the issue of uncertainties was important for NRT activities and validation of these was important. Uncertainty components can now feed into NRT data (via the CCI project). Peter Cornillon suggested looking at temporal variability in geophysically 'quiet' areas to bound the calibration uncertainty (although this does not separate locally systematic and random effects). Jaxa are looking at microwave reprocessing (AMSR-E and AMSR-2) and considering inter-calibrations between the two instruments. Peter Minnett was surprised by the non-Gaussian distributions seen in Jon's presentations on the digitization uncertainty.

4. Instrument Calibration impacts

It was pointed out that instrument calibration is a critical aspect of CDR generation. Currently GHRSSST does not have a dedicated team to monitor and assess calibration issues for used sensors but some members of the TAG thought it would be extremely useful. The question is then if such a group should exist, and if so which under which WG/TAG should it be placed. Given the possible re-organisation of GHRSSST WG/TAGs the question of which group could contain such a group has been put on hold while things are resolved

Discussion

Tim Nightingale supported the notion that calibration from L0 to L1 should be represented somewhere within GHRSSST.

5. Future of the CDR-TAG

With the request for a discussion on the structure of GHRSSST a discussion was held on if the CDR-TAG needs to exist in its current form. In favour are issues such as the maintenance of the CDAF (and associated support), the question of pushing for uncertainties relevant to CDRs (SSEs or multiple component uncertainties and/or ensembles etc.) and instrument calibration. Or should these be placed into a new structure?

Discussion

Jon Mittaz suggested that there are some issues relevant to climate that should be still be addressed within a CDRTAG. Maintaining the CDAF and pushing for SST uncertainties which are suitable for climate data records was also mentioned. This issue of a place for a calibration group was also raised and if the CDR-TAG is a sensible location for such a group. These issues will be raised to the main GHRSSST group.

6. Recommendations for the next year

- An official letter from GHRSSST supporting reprocessing of MUR was proposed and a template will be put together by Jorge Vazquez. Additional letters from other organisations were also recommended.
- Send a link to the CDAF to all members of the CDRTAG (Jon Mittaz).
- Make an analysis of the capabilities of SQUAM against the CDAF (Sascha/Prasanjit).
- Analyse Felyx and SQUAM with respect to the CDAF metrics to check ability to create some of the CDAF metrics (Jon Mittaz/Gary Corlett/Chris Merchant/J-F Piolle/Sasha Ignatov/Prasanjit Dash).
- Report on possible CDAF tools at next GHRSSST meeting
- Do something regarding instrument calibration and decide where such a group would exist (which is potentially a wider GHRSSST issue).

RESCUE & REPROCESSING OF HISTORICAL AVHRR ARCHIVES WORKING GROUP (R2HA2-WG) BREAKOUT MEETING REPORT

Chairs: Hervé Roquet⁽¹⁾, Peter Cornillon⁽²⁾

(1) Météo-France (France), Email : Herve.Roquet@meteo.fr

(2) University of Rhode Island (United States), Email : pcornillon@me.com

During GHRSSST-XVI, a breakout session of the R2HA2 Working Group took place on Thursday 23rd of July 2015 from 17:00 to 19:00, with a total of 8 participants. In the introduction, P. Cornillon, as current Chair of the Working Group, recalled the working group objectives:

- *Rescue historical data from worldwide HRPT Direct Readout stations, with a focus on pre-MODIS era, these data being the only source of full resolution AVHRR data (1km),*
- *Define a common netCDF format for HRPT L1b AVHRR data,*
- *Make data available in this common format with consistent calibration and geolocation information, provided an appropriate source of funding has been found.*

First objective:

P. Cornillon summarized the various HRPT data sets which he was able to collect since the start of the R2HA2 Working Group activities, and to store on his own disks (\approx 20 TB of data):

- *University of Tokyo : 1985- 2000 (about 15 000 passes)*
- *West coast of the US : 1992 – 2002 (about 10 000 passes)*
- *Wallops Island : 1981 – 2014 (121 800 passes)*
- *Berlin : 1989 – 2007 (71 700 passes)*
- *Cape Town : TBD*
- *Lima (IMARPE) : 1998 – 2007 (5 400 passes)*
- *Lannion (Météo-France/CMS) : 1996 – 2003 (43 600 passes)*

He mentioned that he has also other data on tapes or optical disks, which he has not been able to read up to now. He is also in touch with P. Flament (University of Hawaiï), who is ready to provide his historical data set.

Second objective:

H. Roquet recalled that in 2012, he defined and proposed to the other members of the group a netCDF template for NOAA/AVHRR I1b direct readout data, which was mirroring very closely the content of the official NOAA/AVHRR I1b format.

Third objective:

Some initiatives took place in the last years to get this reprocessing activity (even partially) funded, but none of them has been successful. The last initiative on the European side, reported by H. Roquet, was in the framework of the EUMETSAT Satellite Application Facility on Numerical Weather Prediction (NWP SAF), which is led by the UK Met Office, with a contribution of Météo-France/CMS. The NWP SAF is responsible for the development, maintenance and distribution of a software package for direct readout data pre-processing, called AAPP, which has a large number of users around the world, and which can also include an automatic image navigation step using landmarks. The NWP SAF is preparing its proposal for the next 5-year contract with EUMETSAT (2017-2022), and as part of it, CMS proposed to re-process historical HRPT data sets

collected by P. Cornillon up to level 1c with AAPP. To support this proposal, CMS received a letter from the GHRSSST Science Team Chair. However, in the course of the negotiations between UK Met Office and EUMETSAT, this activity was finally discarded.

J. Mittaz (University of Reading) mentioned a meeting co-organized by ESA (B. Bojkov) and DLR (T. Christensen) on 20-21 April 2015, with twenty-two participants including experts on AVHRR LAC data as well as representatives of various interested user communities in Europe. This meeting produced a list of recommendations, some of them being very consistent with the objectives and the approach of the GHRSSST R2HA2 Working Group. As part of the concluding remarks of the meeting, B. Bojkov explained that there may be a possibility for an ESA ITT by late Summer to address some of the issues raised during the meeting.

H. Roquet mentioned also the Copernicus Climate Services, funded by the European Union, which could in the future provide some opportunities for funding HRPT NOAA/AVHRR reprocessing activities.

At the end of the breakout session, P. Cornillon proposed that H. Roquet takes over as R2HA2 Working Group Chair, which was agreed by the participants.

THE ESTIMATION AND RETRIEVALS WORKING GROUP (EARWiG) BREAKOUT MEETING REPORT

Chair: Andy Harris⁽¹⁾, Rapporteur: Owen Embury⁽²⁾

(1) NOAA-CICS, University of Maryland, College Park, MD, USA, Email: andy.harris@noaa.gov

(2) Dept. Meteorology, Univ. Reading, Reading, UK, Email: o.embury@reading.ac.uk

1. Introduction

EARWiG is the primary GHRSSST forum for discussion of SST retrieval methodology, including cloud detection, and the estimation of uncertainties associated with retrievals. It has overlap with a number of other GHRSSST TAGs and WGs, including ST-VAL, HL-TAG, IWWG and IC-TAG. This year's EARWiG session included discussion on the future direction of the activity and the definition and use of SSES uncertainty estimates. There were also two science talks

2. Sensor Specific Error Statistics

The discussion on SSES was very wide-ranging. The SSES fields are perhaps the primary "value-added" information in the GHRSSST L2P format beyond the basic product information (SST, location, time, QC). The particular issues discussed were:

- Which TAG/WG should be responsible for SSES?
 - i. SSES discussions have occurred throughout many TAG/WGs during the meeting
 - ii. Proposal: EARWiG defines SSES/uncertainty, since they are closest to the L2 producers; while ST-VAL validates them. High-quality drifting buoy data may be useful in this regard, but ST-VAL has a number of tools/techniques
 - Definition of SSES is potentially ambiguous
 - i. How should they be interpreted? Should `sses_bias` be added or subtracted to SST value (or not used at all). If one assumes that SSES values are "satellite – reference", then they should be subtracted
 - ii. Are *in situ* buoys an appropriate reference? In the absence of other suitable reference data (~unbiased", sufficient coverage), it would seem so.
 - iii. Some L4 producers appear to be treating `sses_standard_deviation` as an uncertainty due to random effects. It is important to bear in mind that, while this may be true, averaging will only remove some of the uncertainty
 - Does anyone actually use them?
 - i. Some L2/L3 producers felt they were a lot of effort, as their users don't use them. There is a clear need to assess the usefulness of the SSES
 - ii. BoM ignores SSES provided with L2 as it is easier to generate their own to ensure consistency as each data provider does something different
 - iii. Most L4 producers include a bias adjustment step in their OI scheme so `sses_bias` is not so important. It would at least be useful to see if the residual biases are reduced. Since SSES are produced by the data provider, who may have access to additional information at production time, they can be physics-based, whereas most bias correction schemes are stochastic
 - iv. UKMO does make use of SSES, especially from SST-CCI products
-

- NOTE – “SSES” variable included in CCI products are actually uncertainties. There are efforts to apportion uncertainties into different categories (random, correlated, systematic)
- v. SLSTR products will provide uncertainties rather than SSES
- Validation of SSES
 - i. Some L2 producers want users (L4 producers) to validate SSES by running with / without use of SSES. Since it was already proposed that ST-VAL validates SSES, a combined approach seems reasonable
 - ii. L4 producers want uncertainties to be validated before they use them. However, even if SSES are validated, they may not have high impact because of the bias correction schemes.
- Uncertainties
 - i. Some data providers are moving towards use of uncertainty estimates (SST-CCI, SLSTR, IASI)
 - ii. Some differences in terminology (modelled vs. theoretical uncertainties), but common approach of estimating uncertainties is desirable
 - Possibly decomposed into random, correlated, and systematic
 - iii. Uncertainties can be calculated for regression or physical based retrievals
 - iv. Uncertainties can be validated using *in situ* data (same as retrievals), including using 3-way error analysis comparisons with subsets of high-accuracy drifting buoy data
 - v. There are plans to simulate end-to-end error sources (calibration, atmospheric & surface effects, *etc.*) via the FIDUCEO project, which may help answer a number of questions and help partition effects which are currently being combined into the SSES values

In summary, the topic of SSES primarily falls within the remit of EARWiG. The WG should be responsible for definition and recommendations for best practice. Validation should be done in conjunction with ST-VAL, and usefulness should be assessed in close collaboration with IC-TAG, with a feedback loop to assist in further development and implementation. While there was some suggestion that SSES were obsolete, it was recognized that end users had only recently started to make use of them, thus it was appropriate to continue with their assessment, development and provision for the time being until the next phase (decomposition into different types of uncertainty) is a) more mature, b) can be utilized by end-users.

3. PURPOSE AND FUTURE OF EARWiG

As alluded to above, EARWiG is the primary forum for improving L2 product quality. L2 data providers are a core component of GHRSSST and this is where they get to exchange ideas, refine methodologies and make recommendations for standard practice. In order to allow EARWiG to flourish, the following inter-sessional activities were discussed:

- Inter-sessional telecons
 - i. Task-specific, to ensure interest, with each task assigned a lead who is responsible for polling ST members and conducting the telecons
 - ii. Make use of WebEx where appropriate for the sharing of materials
 - iii. Topics for the following year identified at ST meetings
 - Inter-sessional workshops
 - i. Some of these have been more successful than others
 - ii. The above-mentioned telecons should ensure that adequate preparation is done
-

- iii. Workshops with other WGs/TAGs has been successful in the past, and members from those groups have expressed interest in various focus topics

In summary, it is recognized that one 2-hour breakout session per year is inadequate to conduct meaningful collaborative work. There are benefits to face-to-face, WebEx and telecons, so EARWiG will take advantage of all vehicles as appropriate to advance specified topics during the year. The three topics identified at the breakout are:

- SSES and L4 intercomparison
 - i. SSES and L4 intercomparison. Lead – A Harris
 - ii. Post-processing to unmask fronts. Lead – A Ignatov
 - iii. Use of new high-resolution geostationary HIMAWARI-8. Lead – H Beggs

Topic leads are responsible for hosting telecons, *etc.*, and the GHRSSST Project Office will provide assistance as needed, *e.g.* conducting user polls, and providing other technical support/facilities as needed.

4. SCIENCE PRESENTATIONS

There were two science presentations. The first, given by Prabhat Koner, concerned how best to advantage of the extra channels in modern IR imager instruments. The methodology employed was the recently published deterministic MTLT technique, which calculates a regularization strength for the gain matrix based on the goodness-of-fit of the input data (NWP and satellite) and condition number of the jacobian. The advantage of this data-driven regularization is not needing to know the correct covariance of the input data. It was found that, for MODIS data, adding aerosol to the retrieval vector improved retrieval accuracy but also substantially increased the sensitivity of the retrieval to SST, even when the initial guess is close to truth. The implication is that, when there are sufficient channels, adding aerosol improves partitioning of the signal between various geophysical signals. MODIS has a number of extra channels that could permit some water vapour structure information to be included in the retrieval vector. As an aside, it should be noted that the retrieval accuracy is now very close to the intrinsic error in the *in situ*.

The second presentation concerned the unflagging of good data masked by false alarm in ACSPO-screened VIIRS SST imagery. The overlapping “bow-tie” effects in VIIRS make pattern recognition very difficult, so resampling is used to improve the basic cloud mask. Then, pattern recognition techniques are used to identify oceanic fronts that have been erroneously masked due to their inherent variability. As a byproduct, the ocean fronts themselves are obtained. The SST field is referenced to the CMC analysis. Obviously there is a risk of feedback if such data were then used to create the next analysis. This underscores the need to have a common validation framework, such as Felyx or iQUAM/SQUAM. *N.B.* Felyx is anticipated to be complete by end-Summer 2015, and will then undergo a 6 month testing period. As noted above, A Ignatov will be leading an EARWiG topic on the frontal detection and unmasking of falsely flagged active regions of the ocean.

THE SATELLITE SEA SURFACE TEMPERATURE VALIDATION GROUP (ST-VAL) BREAKOUT MEETING REPORT

Helen Beggs⁽¹⁾, Werenfrid Wimmer⁽²⁾

(1) Bureau of Meteorology, Melbourne, Australia, Email: h.beggs@bom.gov.au

(2) National Oceanography Centre, Southampton, UK, Email: w.wimmer@soton.ac.uk

ABSTRACT

The Satellite SST Validation Technical Advisory Group met for two hours during the 16th GHRSSST Science Team Meeting in ESTEC on the 23rd July 2015. Themes of presentations and discussions were:

- Ship-borne radiometer L2r data and L2i/L2r format
- Satellite SST validation
- SSES and Quality Level methodologies
- Terms of Reference of ST-VAL Technical Advisory Group

1. Introduction

The meeting was chaired by ST-VAL Chair, Dr Helen Beggs. The session was rapporteured by Dr Werenfrid Wimmer. The agenda followed during the meeting was:

Overview of ST-VAL activities since GHRSSST-XV (Helen Beggs)

Actions arising from 2015 ST-VAL Meeting: Hosting the ship-borne radiometer L2r data and feedback on L2i/L2r format

- Presentation from Tim Nightingale on Shipborne SST Radiometer Network format (L2r) and web site
- Presentation from John Stroup/Sasha Ignatov/Xinjia Zhou (NOAA/NESDIS) on feedback to L2i/L2r format.

Discussion of issues relating to satellite SST validation: (slides from Prasanjit Dash)

- Sensitivity of validation statistics to collocation criteria (space-time)
- Random error from a carefully implemented triple-collocation method, time-series implementation SSES Methods

Sensor Specific Error Statistics (SSES) and Quality Level (QL) methodologies:

- Including 1 to 2 slides from L2P/L3 producers on Quality Level methodologies and issues

Open Questions:

- i) How should Quality Level be defined?
 - ii) How to create consistency in QL across different sensors?
 - iii) How to create continuous uncertainties across QL?
 - iv) Should we aim for consistent SSESs against common reference? How?
 - v) How to incorporate "Modelled Uncertainties" per pixel?
 - vi) Do we still need SSES if we have Modelled Uncertainties?
 - vii) Next steps.
-

Terms of Reference of ST-VAL Technical Advisory Group

- Including discussion of do we need an ST-VAL TAG, what we should cover, future meetings/telecons.

Presentations are available for download from <https://www.ghrsst.org/documents/q/category/ghrsst-science-team-meetings/ghrsst-xvi-esa-estec-the-netherlands/g-xvi-presentations/thursday-23rd-july-2015/stval-breakout-session/>

2. Overview of ST-VAL activities since GHRSSST-XV (Helen Beggs with contributions from ST-VAL TAG)

- ISAR installed on the RV Investigator along with SBE38. First science cruise 21st to 29th March 2015. ISAR experienced some technical issues with rain shutter not closing.
- IQUAM2 updates: Data added from Argo, HR drifting buoys, NOAA Coral ReefWatch Moorings and IMOS Ships.
- SQUAM updates: Added ACSP0 products - VIIRS L2P, Himawari-8 L2P and MTSAT-2 L2P.
- BoM: New webpage for validation of real-time and reprocessed IMOS HRPT AVHRR L2P SSTs.
- EUMETSAT: Metop and IASI new retrieval with smaller cool bias. New SSES scheme based on water vapour for IASI.
- OSI-SAF METOP-A AVHRR buoy SST.

3. Actions arising from 2015 ST-VAL Meeting: Hosting the ship-borne radiometer L2r data and feedback on L2i/L2r format

a. Tim Nightingale (TN) presented “Cooperative *in situ* radiometer activities”.

- TN has developed a provisional *in situ* radiometer format, “L2r”
 - Follows GHRSSST GDS style format and variable naming choices where possible
 - Draft available (contact tim.nightingale@stfc.ac.uk)
 - Already implemented in ISAR and SISTeR processors
- Logical extension is a cooperative radiometer network centred around an archive of *in situ* radiometer data
- Website set up to share radiometer documents, data, tools: <http://isrn.rl.ac.uk/home.shtml>
 - Website is “bare bones” at the moment – will need a bit of support from elsewhere to take it significantly further
 - Priorities include:
 - Basic QA for uploaded data, including format checking
 - Felyx tool to generate automated validation reports – starting a discussion with CEDA about the practicalities of hosting a Felyx instance

Questions/Comments:

Sasha Ignatov (SI): What data will the website host?

TN: All shipborne SST radiometer data, started with SISTeR.

SI: Near real-time or delayed mode?

TN: Delayed mode.

Helen Beggs (HB): IMSO will be NRT but needs post-cal for proper QA.

Jean-Francois Piolle (JFP): What is the granularity of the data?

TN: It's daily files at the moment.

JFP: Some standard would be good.

b. Sasha Ignatov presented "NOAA STAR iQuam2: Feedback to "The Recommended GHRSSST L2i Data Specification" ("GDS L2i"), V1.0, Rev 2, Tim Nightingale, 29 May 2014"

- IQUAM v2 QC'd monthly in situ SST data are available for preview, in netCDF "L2i" format based on TN's L2r format, from <http://www.star.nesdis.noaa.gov/sod/sst/iquam/v2/data.html>
- Proposal to host iquam2 L2i in situ data with GHRSSST data at the GDAC
- L2r format assumes only one platform per file, whereas iQuam has 8-111 data sources for any one monthly file
- Time variable is long and should be int64 - like GDS2 time and sst_dtime?
- Should we define an sst_dtime variable?
- The data type of "sst" is double precision (all other floating-point variables are single precision). Is this level of precision really needed?
- "sst_total_uncertainty" is absent in the current iQuam2, but may be included in the future iQuam upgrades
- CF type "point" missing in L2r format but needed in L2i format
- In iQuam2, the mandatory "sea_surface_temperature" layer was renamed "sst", for brevity
- Global attributes not used in iQuam2 L2i format are Sensor and Spatial Resolution
- All iQuam2 platforms measure temperature at depth, but do not report their depth (except for ARGO floats). Thus, "depth" is not included as a coordinate of the "sst" variable (but it is reported for all ARGO floats for which it is available).
- iQuam2 L2i filenames not quite same as L2r filenames: E.g. 201506-STAR-L2i_GHRSSST-SST-iQuam-V2.00-v01.0-fv01.0.nc for monthly iQuam2 SST data from June 2015.
- iQuam2 will be operational in October 2015. Feedback on L2i format sought by end of August 2015.

Action STVAL/16/1: ST-VAL to comment on iQuam2 "L2i" format by 31 Aug 2015.

Questions/Comments:

TN: Detailed response directly to Sasha. Iquam2 L2i is more like an L3 data set.

HB: Radiometer data has good metadata, but data from the GTS does not have metadata. Also, in situ SSTs are not gridded data so more like L2.

SI: Argo has depth but no other variables.

Peter Minnett (PM): No problem, depth is needed.

Chelle Gentemann (CG): Please be as CF compliant as possible.

PM: Radiometer data should be supplied separately to L2i data as they are not in-situ – it's remotely sensed data!

SI: Iquam wants to use data. Advice welcome.

Andy Harris (AH): Buoys measure current from a thermistor. Searching for L2r is much quicker for radiometer.

BH: "L2r" for radiometer data and "L2i" for iQuam2 data?

TN: Call Iquam2 dataset "L2i" and radiometer dataset "L2r".

General agreement from ST-VAL TAG.

4. SST Validation Discussion

Prasanjit Dash (presented by Sasha Ignatov): "Effect of Space-Time Collocation on validation statistics".

Showed triple collocation of on a year's worth of matchups for various satellite SST products (VIIRS, METOP-A, METOP-B, etc) produced by various agencies.

Conclusions: Random error for a given product, calculated using different triplets, are consistent with each other. 3-way error analysis, when implemented carefully (to avoid the effect of correlated error) is an effective way to characterize the true error in a product.

e.g., Day OSI SAF Metop-A from:

OSI SAF MetopA, ACSPO Terra, Drifter: 0.33K (N=102,875)

OSI SAF MetopA, ACSPO MetopB, ACSPO Terra: 0.33K (N=69,699)

Questions/Comments:

Peter Minnett (PM): Very good. Two questions. What do you use for your night-time product?

SI: Not 3.9 micron.

PM: Do you get an estimate of the quality of the drifters?

SI: Yes, it will give you that. The random error of the different triplets is consistent – but watch the correlation issues.

5. SSES and Quality Level

Some outcomes from the G15 STVAL session were:

- SSES and QL need to be de-coupled
- QL should be more continuous rather than a step function

HB showed slides summarising Quality Level and SSES in products from four GHRSSST L2P producers:

Quality Level

ABoM: $f(\text{proximity to cloud})$

- Quality level is determined from proximity to cloud using the CLAVR cloud determination system
-

- Some issues with over-detection of cloud
- QL = 0, 1, 2, ..., 5 based on km to nearest cloud
- L2P files have SSTs for QL ≥ 1
- L3 files only have SSTs for QL ≥ 2

ACSPO: f(clear sky values)

- The recommendation to ACSPO users: only use data with QL=5 and associated SSES statistics

IASI: f(binned TPWV from IASI L2 sounding data – 0 to 5). Useable quality starts from QL = 2.

- New version of IASI L2P different to what was reported at GHRSSST-XV.
- quality_level:flag_meanings = "no_data bad_data worst_quality low_quality acceptable_quality best_quality" ;

JAXA: Definition of Proximity Confidence (for microwave SST products)

proximity_confidence=11: near the coast (< 50km)

proximity_confidence=12: far from the coast (=> 50km) & sea surface wind speed is strong (6 <= SSW < 20 m/s)

proximity_confidence=13: far from the coast (=> 50km) & sea surface wind speed is weak (0 <= SSW < 6 m/s)

proximity_confidence=14: far from the coast (=> 50km) & sea surface wind speed is weak or strong (SSW < 0 m/s, or, 20 <= SSW)

proximity_confidence=-128 (missing): far from the coast (=> 50km) & sea surface wind speed is missing.

SSES

- **ABoM**: Adaptive error statistics. Smoothly varying bias and STD inc at edges of swaths. SSES model = $f(\text{SZA, lat, lon, time, QL})$
- **ACSPO**: Segmentation Method (GXVI Wed am talk)
- **IASI**: Derived from 1D-VAR
- **OSI-SAF**: Two axes related to cloudiness and algorithm. Two risk factors and QC are mapped into the 2 axes to get numerical value for SSES.
- **JAXA**: Initially categorise each pixel to five groups according to *proximity_confidence* that is defined by distance from the coast and wind speed. Then calculate *sses_bias* and *sses_standard_deviation* of each group using buoy match-up data during previous 30-days. Pixels that are categorised to the same group will have same SSES information.

Discussion:

CM: At GHRSSST-XV it was not agreed that SSES and QL need to be decoupled – it was only discussed. Did we decide on a continuous QL last year? No recollection of this. It was more a discussion item. Something like a chi-squared test will give you a number to map on, but needs discussion.

Anne O'Carroll (AOC): From this week's discussion, not many people are using *sses_std*, which was originally derived as a reference to drifters. Should we use modeled SSES standard deviation and calculate SSES bias against drifters? EUMETSAT would like to do that but it needs agreement from within GHRSSST.

SI: It would be good to have L4 input (1 slide summary) on how L4 producers use L2P products in respect to SSES and QL. Bias and std should be decoupled. L4 systems are set up to use both. We need a recommendation as a group. Some L4 systems use no pixel specific std – e.g. all AVHRR is used with 0.4 K. I recommend that pixel level std be used in L4 production. For example, debias first and then weight on pixel level std squared.

CM: An issue with SSES is that it is not clear what is random and what is systematic error. To answer AOC it might not be the right way to use the SSES field for the modeled uncertainty and keep SSES as defined.

It should be a 5 year ambition of GHRSSST to develop a more systematic approach to model uncertainties and in the interim preserve SSES, with the modeled single pixel uncertainties as an experimental field in L2P files. Once the modeled uncertainties are reliable, update the GDS and drop SSES.

TN: I agree. The bias is often used for skin to bulk conversion and only one uncertainty field (sses_standard_deviation) is then available in the L2P file.

HB: SSES bias should not be used for skin/bulk correction.

CM: SSES was meant to be a difference to a reference SST.

PM: SSES are meant to reflect uncertainty in the SST.

HB: What is the GDS definition for SSES? Should sses_bias be an estimate of bias in SST retrieval to a reference at the satellite sensor depth or should it be the bias from SSTskin to SSTdepth?

Simon Good (SG): We use both SSES bias and SSES std in OSTIA. As a user it is important to know what SSES means and it should be consistent in all cases.

HB: I agree SSES need to be consistent, and the same for QL.

SI: We need to agree on a metric on how SSES affects the L4. We need a test for improvement on the analysis by using SSES. Years ago we said Argo should be used for that and not assimilated to have independent data. We need L4 producers to test for separate use of sses_bias and sses_standard_deviation in L4.

Peter Cornillon (PC): I don't use SSES and only QL. But I find a lack of consistency in QL. There is no distinction between cloudy and high gradient areas.

HB: Agree. I talked to Keith Willis about NAVO GAC AVHRR SST being flagged as cloudy along SST fronts.

PC: This is an issue in all HR products.

Chelle Gentemann (CG): I calculate my MW QL based on what L2P flag is set. GDS2 is very specific re QL. All QL3 should be useable data. For quality level in MW products, the information is recoverable from the l2p_flags, so for your own screening you could use the l2p_flags.

PC: Pathfinder use to be like that.

SI: ACSPO reports all individual flags. The product should only have one QL and it should retain all features.

ACSPO QL different to most other L2P products (see Appendix A.1).

SI: ACSPO will give you more pixels in QL5 than other products in QL3, 4 and 5.

HB: ACSPO products could have QL4 going to QL2 and QL3 going to QL1. Then ACSPO will not use QL3 or QL4.

TN: I just checked the GDS2.0. SSES bias definition is vague. The difference to reference needs rewording. (See Appendix A.2).

Action ST-VAL/16/2: Reword SSES bias in GDS for consistency (ST-VAL Chair with input from ST-VAL TAG).

TN: The GDS2.05 is very specific about quality level. "The value 0 shall be used to indicate missing data and the value 1 shall be used to indicate invalid data. The remaining values from 2-5 are set at the discretion of the L2P provider with the proviso that the value 2 shall be used to indicate the worst quality of usable data and the value 5 shall be used to indicate the best quality usable data."

CM: I agree with PC. QL needs to be consistent over all L2P products.

There was general agreement that the definition for quality level in the GDS2.05 is fine. Producers should provide a short note on how they produce quality level.

Action STVAL/16/3: All L2P producers provide HB with how QL are derived.

PM: For MODIS to distinguish between QL 4 and 5 satellite zenith angle is used. SSES are only produced for QL 4 and 5 in MODIS L2P files.

CM: I propose that we keep SSES and add modelled uncertainty as an optional experimental field in L2P files, but at the next GDS update retire SSES and use modelled uncertainty.

CG: Good way for the future. Most L4 producers don't use SSES as they are too different between sensors and there is discontinuity within sensors. There are lots of possible ways forward, e.g. Uni of Miami Hypercube as this results in a smoothness of errors. I'd like to see a LUT that is physically based.

CM: I don't quite get that, because there is an understanding of your measurements and you can model your confidence, which can be a physics-based framework. An empirical-based approach won't allow you to separate systematic and random components.

6. ST-VAL Terms of Reference

HB: Time is very short in the ST-VAL Breakout sessions for all discussions. We need to be more selective with what we cover.

PM: I am not in conflict with the terms of reference, but it would be better to have more frequent meetings.

CG: Once a year is too limiting. Should we use video conference tools more?

HB: Inter-session meetings are important, but I am short on time. Has someone more time inter-sessionally to organize face-to-face meetings? Should we have teleconferences on specific topics? My preference is for Webex.

PM: Teleconferences are efficient, if there is a regular time slot. The meeting can be short if there is nothing to discuss.

CM: I think we should have a teleconference to solve one problem.

PC: For example, data providers could get together to sort out a consistent QL.

HB: Do we need an ST-VAL Technical Advisory Group? Are we making progress?

Action STVAL/16/4: HB with help from GHRSSST P.O. to schedule a Webex teleconference on QL definitions for October 2015. L2P producers to supply their QL definition and method beforehand if not already available.

7. Actions Arising from Meeting

Action STVAL/16/1: ST-VAL to comment on iQuam2 "L2i" format by 31 Aug 2015.

Action ST-VAL/16/2: Reword SSES bias in GDS for consistency (ST-VAL Chair with input from ST-VAL TAG).

Action STVAL/16/3: All L2P producers provide HB with how QL are derived.

Action STVAL/16/4: HB with help from GHRSSST P.O. to schedule a Webex teleconference on QL definitions for October 2015. L2P producers to supply their QL definition and method beforehand if not already available.

Appendix A

GHRSSST Specification of Sensor Specific Error Statistics and Quality Level

A.1 Quality Level

The GHRSSST Data Processing Specification version 2.07 (GDS2.0) (<https://www.ghrsst.org/documents/q/category/ghrsst-data-processing-specification-gds/operational/>) states:

Section 9.18:

"The L2P variable '**quality_level**' provides an indicator of the overall quality of an SST measurement in an L2P file. The GDS requires the following:

The L2P variable '**quality_level**' shall use an incremental scale from 0 to 5 to provide the user with an indication of the quality of the L2P SST data. The value 0 shall be used to indicate missing data and the value 1 shall be used to indicate invalid data (e.g. cloud, rain, too close to land - under no conditions use this data). The remaining values from 2-5 are set at the discretion of the L2P provider with the proviso that the value 2 shall be used to indicate the worst quality of usable data and the value 5 shall be used to indicate the best quality usable data. The L2P provider is required to provide a description of the quality levels provided as part of the product documentation. The L2P variable **quality_level** reflects the quality of SST data from a single sensor and does not provide an indication of the relative quality between sensors.

Table 9.21:

quality_level:flag_meanings = "no_data bad_data worst_quality low_quality acceptable_quality best_quality"

Issue for future ST-VAL discussions:

Not all producers of GDS2 L2P products follow the GSD2 flag_meaning for quality_level as specified in the GDS 2.0 table 9.21. Should the flag meanings be consistent?

ACSP0 VIIRS L2P: invalid not_used not_used **cloudy probably_clear clear**

OSI-SAF METOP-A IASI L2P: no_data bad_data worst_quality low_quality acceptable_quality best_quality

NAVO METOP-B AVHRR L2P: no_data bad_data worst_quality low_quality acceptable_quality best_quality

NAVO VIIRS L2P: not used, not used, not used, cloudy, probably cloudy, clear

ACSP0 MTSAT-2 L2P: no_data bad_data worst_quality low_quality acceptable_quality best_quality

JAXA Himawari-8 L2P: no_data bad_data worst_quality low_quality acceptable_quality best_quality

BoM Himawari-8 L2P: no_data bad_data worst_quality low_quality acceptable_quality best_quality

A.2 Sensor Specific Error Statistics

The GHRSSST Data Processing Specification version 2.05 (GDS2.0) (<https://www.ghrsst.org/documents/q/category/ghrsst-data-processing-specification-gds/operational/>) states:

Section 9.5:

"The uncertainties associated with each observation in a data stream are provided as Sensor Specific Error Statistic (SSES) <http://www.ghrsst.org/SSES-Single-Sensor-Error-Statistics.html> . The SSES are based on understanding the errors associated with the in-flight performance of an individual satellite instrument for the retrieval of SST from the measured radiances. The SSES are provided as a mean bias error and its associated standard deviation. There are a variety of methods for determining SSES as they depend on the specific characteristics of each satellite instrument. Consequently, the L2P provider can define their own scheme for producing SSES that is tailored to their specific dataset. However, the SSES scheme must conform to a set of agreed SSES common principles. The SSES common principles are maintained on the GHRSSST website at <http://www.ghrsst.org/SSES-Common-Principles.html>, and have been approved by the GHRSSST Science Team. The L2P provider must provide documentation that summarizes the theoretical basis of their SSES scheme, its implementation, any recommendations for users, and its conformance to the agreed SSES common principles. The SSES documentation will be maintained through the GHRSSST website at <http://www.ghrsst.org/SSES-Description-of-schemes.html>."

<https://www.ghrsst.org/ghrsst/tags-and-wgs/stval-wg/sses-single-sensor-error-statistics/> states:

"SSES are based on understanding errors associated with a specific satellite instrument and errors associated with the geophysical retrieval of SST for each individual satellite scene. The simplest L2P SST uncertainty estimation is based on matching satellite SST with in situ observations co-located in space and time to within 25 km and 6 hours. A large match-up database of data is required for each satellite instrument which is then periodically analyzed to derive a mean bias and standard deviation for each satellite system."

<https://www.ghrsst.org/ghrsst/tags-and-wgs/stval-wg/sses-common-principles/> states:

"SSES (Single Sensor Error Statistics)

- Compliant with QA4EO. Derivation of quality indicator (i.e.SSES) to be traceable, i.e. documented and available. But... need common reference. includes QC of reference data
 - SSES are to provide users with a common uncertainty estimate in comparison to the agreed reference source
 - SSTs should be the best estimate prior to SSES production. Responsibility of the SST producer
 - SSES are for users NOT for producers
 - At present the reference is drifting buoys. By convention (only really global source)
 - Content: A bias (not a correction term) and a standard deviation reflecting the local accuracy (at pixel) of the SST estimate. Application of SSES is consistent with the product definition (skin; sub-skin)
 - Hierarchical SSES references can be used. Global stats to DRIFTING BUOYS, regional stats using other reference sources such as radiometers, the GTMBA (Tropical moored buoys) or L4 analyses
 - Use of common match-up thresholds for SSES: Centre pixel clear; +/- 2 hrs (ideally 30 mins) for all sensors.
-

- Continuous fields preferred, i.e. no discontinuities between Quality Levels although discontinuities may be inevitable
- SSES must be free from diurnal variability and ideally estimated from night time match-ups
- A common skin to sub-skin adjustment of 0.17 K should be used"

<https://www.ghrsst.org/ghrsst/tags-and-wgs/stval-wg/sses-description-of-schemes/> currently has no useful information (apart from stating "Please contact the Chair of the STVAL for more details") and needs to be populated by the ST-VAL Chair using information from L2P producers.

SECTION 4: POSTERS AND POSTER ABSTRACTS

POSTERS

POSTER 1: IMPROVING APPLICATION OF DATA QUALITY INFORMATION IN ACCESSING AND USING SATELLITE DATA

National Aeronautics and Space Administration

ACCESS: Improving application of data quality information in accessing and using satellite data

Edward M. Armstrong¹, Thomas Huang¹, Sri Iodha Khalsa¹, Zhangfeng Xing¹, Toshio M. Chin¹, Chantal Fyfi¹, and Christian Alarcón¹

¹NASA Jet Propulsion Laboratory/California Institute of Technology, Pasadena, California, USA²

³NASA National Snow and Ice Data Center, Boulder, Colorado, USA²

Introduction

When working with satellite-based earth science data records users often need to access, understand and apply data quality information, such as that contained in flags. In addition, most visualization packages do not understand how to apply quality information. The Virtual Quality Screening Service (VQSS), a 2013 NASA ACCESS project, aims to address these issues and concerns. The project is developing an infrastructure to expose, apply, and extract quality screening information through implementations of Map Reduce workflows, data discovery, ontologies and exposure of granule-based quality information. This infrastructure is being deployed on data from the NASA Soil Moisture Active Passive (SMAP) Mission and the Group for High Resolution Sea Surface Temperature (GHRSSST).

Goal: Implement web services and related infrastructure for quality screening of GHRSSST and SMAP L2/L3/L4 data. Allow users to explore meaning and effect of quality variables. Share and store URLs to explicitly extract and screen geophysical data from granules.

How?

- Expose data granules from SMAP/GHRSSST mission through Webification (see panel on right)
- Extend a component of the PO.DAAC web services, also known as the Extensible Data Gateway Environment (EDGE) as an external data service for granule searching
- Provide a portal for the public exposure of VirtualQSS that will allow users to:
 - Search for SMAP/GHRSSST granules using spatial-temporal constraints
 - Review quality, error estimates and others ancillary variables and information specific to a unique data type exposed through a semantic layer or lexicon
 - Apply quality flag filtering based on exact user specifications to granules
 - Subset and return filtered results as single granules and/or aggregates in preferred formats such as netCDF, HDF, JSON, and CSV
 - Store filtering queries and share them with other scientists and the community

Webification (w10n)

Webification is a specification (<http://podaac-w10n.jpl.nasa.gov/>) that can be applied to any structured data store/container/data model. Already supported under the PO.DAAC's w10n instance.

Make inner components of an arbitrary data store, such as attributes, labels, image bands, and data arrays, are directly addressable and accessible by well-defined and meaningful URLs

- Allows contents of remote HDF and NetCDF files to be extracted via RESTful URLs
- Results of W10n calls return specified measurement arrays or metadata elements via subset by array
- Data formats (NetCDF, HDF, GRIB, FITS, TEXT)
- Remote service (OPENDAP): possible to use w10n to proxy to any local and remote OPENDAP service
- Share and visualize results

NEXUS: DATA ANALYSIS PLATFORM

- Data analysis platform on the Cloud
- Data management and transformation
- Multi-oscipy data coordination
- On-the-fly analysis services
 - Time series
 - Correlation
 - Data resampling
 - Data visualization service
- RESTful access to geospatial array data

Leveraging NEXUS, NEXUS, a data analysis and visualization project adapted for SMAP data using cloud-based technologies, will allow for on the fly analysis of time-series data. An analysis tool about time series of rain/precipitation and other histogram measurement information for a SMAP L3 active/passive product in west Africa

VQSS will leverage NEXUS technology for ingest/metadata harvesting of SMAP data and possibly plotting capabilities

Prototype Interface. Results from a MOOS Apsis S1 granule search request.

Sample SMAP use case scenario for quality information screening

- User wants a time series of soil moisture over a particular watershed as part of a hydrological model predicting runoff from future precipitation events. User selects the SMAP L2 Radar/Radiometer Soil Moisture product and specifies a spatial and temporal domain of interest.
- User first wants to know whether or not the 5km soil moisture data in this area is usable, e.g. a constant RF1 source may be close by and mitigation wasn't successful. User asks "are more than 50% of the pixels in my region of interest not useful according to the retrieval_qual_flag" (first bit of flag on)
- User now wants to extract all the data meeting his/her quality criteria, and so wants to inspect all the bits of retrieval_qual_flag. She/he is not sure of the meaning of each so is presented with the list and associated definitions.
- User knows that in the complex terrain of his/her watershed that the downscaling of the 50km brightness temperature may cause problems, and that the small lakes in the watershed could also introduce errors, but that thick vegetation is not an issue and it's summer so neither is frozen ground. So, she/he specifies that she/he wants only pixels that have bits 1, 3, 4 and 6 off. The other pixels in the soil moisture array should be set to missing in the output. The flags being tested are:
 - Retrieval success flag
 - Radar water body detection success flag
 - Disaggregated brightness temperature quality
 - Other

Since there are also some built-up areas in the study region, user wishes to also screen on the basis of the urban area flag, as well as the static water body flag and mountainous terrain. Thus, screening is also performed based on **surface_flag** being off for bits 1, 3 and 8.

Architecture of VQSS system. Webification for high performance array extraction is linked directly to the JPL PO.DAAC to serve its granules. Other data sources are served via "proxy". VQSS will leverage and extend a granule and metadata discovery service at the PO.DAAC called EDGE to expose granules and their attributes and metadata for SMAP. A user interface will be developed to expose all these services to the science community. The VQSS architecture will be leveraged to apply quality information to create quality screened products

NSIDC

po-daac

GHRSSST

SMAP

These activities were carried out at the Jet Propulsion Laboratory, California Institute of Technology, under a contract with the National Aeronautics and Space Administration. © 2015 California Institute of Technology. Government sponsorship acknowledged.

Page 170 of 225

POSTER 3: IMOS AVHRR SST PRODUCTS SUITABLE FOR NEAR-COASTAL APPLICATIONS

23 year sea surface temperature products from IMOS

Helen Beggs¹, Leon Majewski¹, Christopher Griffin¹, Edward King² and Janice Sisson¹

¹Bureau of Meteorology, Melbourne, Victoria, Australia
²CSIRO Oceans and Atmosphere Flagship, Hobart, Tasmania, Australia



Bureau of Meteorology



Introduction

Satellite imagery for sea surface temperatures (SST) has been acquired around Australia on a daily basis since the early 1980s. Building on the archives and processing expertise of CSIRO and the Bureau of Meteorology, IMOS has made a commitment to provide a long-term, high quality, and consistent SST data set for the Australian and Antarctic region. The collection consists of all overpasses recorded in the Australian and Antarctic region (Fig. 1) from Advanced Very High Resolution Radiometer (AVHRR) Polar Orbiting Environmental series from April 1992 to the present, and stored with full resolution (1 km at nadir). The SST observations from drifting buoys in the region. The system anomaly and automatically corrects for changes in each AVHRR sensor's bias using a warming correction algorithm. The data are then adjusted for atmospheric attenuation according to the corrected standards of the International Group for High Resolution SST (GHRSST) collaboration (www.ghrsst.org). The data records contain time varying error estimates and quality level flags for each SST value, respectively. These records form a unique 23-year data set that supplies quality-assured SST values to within 2 km of coasts.

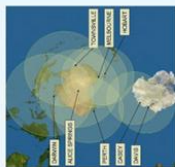


Fig. 1. Location and approximate range of Australian ground-station coverage from NOAA polar-orbiting satellites.

Range of Products

The foundational data product, from a level 2 Pre-processed (L2P), is an ungridded swath of data location and calibrated data. These data are then gridded to a 1 km resolution and are related and compared with other observations (and model outputs), and also products without gaps due to cloud. To meet these needs, a hierarchy of mapped (0.02° x 0.02°) and time-averaged data sets are derived from the L2P data. These data are known as the Level 3 (L3) products. The L3 products are available daily, averaged over 1, 3, 6 and 14-day intervals, and are also available averaged monthly. The IMOS L2P and L3 products are generated routinely in near real-time by the Bureau of Meteorology. The L2P and L3 products are available to the public through the IMOS data portal (www.imos.gov.au) and from OPeNDAP and WMS servers or as individual L2P files. See <http://imos.gov.au/australiaproducts.html> for data access and further information.

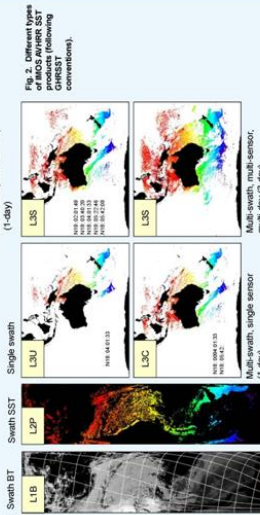


Fig. 2. Different types of SST products following GHRSST conventions.

Applications

The IMOS L2P and L3 products are currently available in the operational level 4 (L4) SST analyses (www.bom.gov.au/australiaproducts.html). The 2 km resolution of the IMOS AVHRR L3 products makes them particularly useful in coastal applications where the coarser (4 km) globally available L3, and 1 km resolution L2P products are not available. The IMOS L2P and L3 products are also used to measure diurnal or night-only IMOS SST products such as those shown in Fig. 3 can be used to measure diurnal warming in coastal regions and SST changes over 2 km spatial scales to within 2 km of coasts.

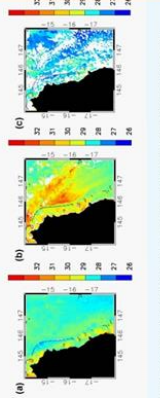


Fig. 3. Sea surface temperatures from (a) MESA's OceanView Global daily 1 km resolution LST "L4" products, (b) night-only L2P products, and (c) night-time composite L3P products for the same date.

IMOS night-only and day-only level 3 products are being used in PhD projects by Xiaodong Zhu (University of Queensland), and in a project by the Tropical Marine Food, respectively. Some applications that currently use IMOS GHRSST level 3 products are regional seasonal climatologies, real-time maps for recreational fishers (www.fishtrack.com.au), and monitoring of coral bleaching events IMOS Dashboard. www.imos.gov.au/australiaproducts.html and ReefTemp NanoGen. http://www.bom.gov.au/australiaproducts/australiaproducts.html#reeftemp_nano (Fig. 4).

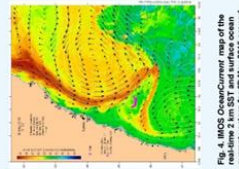


Fig. 4. IMOS OceanCurrent map of the real-time 2 km SST and surface ocean current from the IMOS L3 SST products for 1st January 2014.

Validation

Time series validation plots for the IMOS L2P SST are available on-line for each NOAA satellite, with the NOAA SST calibration therefore appears stable across satellites. More recent satellites (NOAA-18 and NOAA-19) are available on-line for validation web pages. See <http://imos.gov.au/australiaproducts.html> for links to validation web pages.

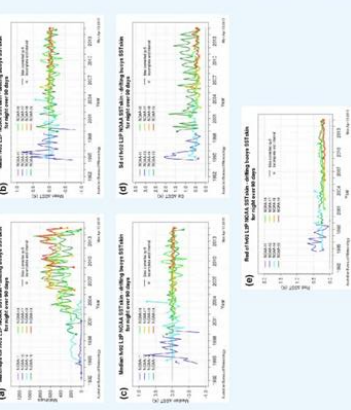


Fig. 6. Validation plots showing time series of (a) number of matchups and (b) mean, (c) standard deviation, (d) maximum, and (e) minimum of the differences between the IMOS L2P SST and NOAA SST data for each satellite and sensor. Measurements are considered co-located if the satellite observation is within 3 km and 60 minutes of the NOAA SST observation. Only matchups where the satellite observation is within 5 km horizontally from the nearest detected cloud, are included here. Known biases with respect to the drifting buoy SST data have also been removed.

Future Plans

NOAA-18 launched in 2009. In the last 5 years of NOAA Data, Chubing Environmental Satellites (NPDES). In order to continue the IMOS 2 km L3 SST data record, during 2016 to 2017 we aim to include direct broadcast, high resolution SST observations from the European Space Agency's Sentinel-3 polar-orbiting satellite and NOAA's Suomi National Polar-orbiting Partnership (SNPP) satellite.



IMOS Integrated Marine Observing System



NCRIS National Collaborative Research Infrastructure supported by Australian Government



UNIVERSITY OF TASMANIA

FOR FURTHER INFORMATION
www.imos.org.au
h.beggs@bom.gov.au
Edward.King@csiro.au
<http://imos.gov.au/australiaproducts.html>

ACKNOWLEDGEMENTS

We acknowledge the provision of raw AVHRR data from ground stations operated by the Bureau of Meteorology, Australian Institute of Marine Science, Western Australian Marine Sciences Institute, and Commonwealth Scientific and Industrial Research Organisation (CSIRO).

POSTER 4: CLOUD DETECTION FOR SEA SURFACE TEMPERATURE FROM GLOBAL AREA COVERAGE PRODUCTS



ESA Climate Change Initiative Phase-II Sea Surface Temperature
www.esa-sst-cci.org

Cloud Detection for Sea Surface Temperature Products from Global Area Coverage Products

Claire Bulgin, Chris Merchant, Owen Embury, Gary Corlett

Cloud clearing is a fundamental pre-processing step in sea surface temperature (SST) retrieval from satellite data. Challenges remain in cloud detection, particularly in classifying features such as cloud edges, pixel or sub-pixel cloud and fog. The Global Area Coverage (GAC) products from the Advanced Very High Resolution Radiometer (AVHRR) instruments are provided at a reduced resolution to the native observations providing an additional challenge to cloud detection. The nominal resolution of the GAC products in the nadir is 4 km (with full resolution observations at 1.1 km). Each GAC observation covers 3x5 native resolution pixels and is provided as an average across four pixels. We demonstrate here an adaptation of a Bayesian cloud detection scheme for full resolution AVHRR and GAC AVHRR data.

1. Generating AVHRR PDFs

Bayesian cloud detection within the SST CCI project uses RTTOV 11.2 to simulate clear-sky conditions. Cloudy observations are represented by empirical PDFs. We calculate these from the EUMETSAT METOP-A full resolution area coverage (FRAC) archive between 2007-2014. We construct single channel (1.6 μm), two-channel (0.6 and 1.6 μm) and three-channel (0.6, 0.8 and 1.6 μm) spectral PDFs in the visible. In the infrared we construct two (11 and 12 μm) and three channel (3.7, 11 and 12 μm) PDFs.

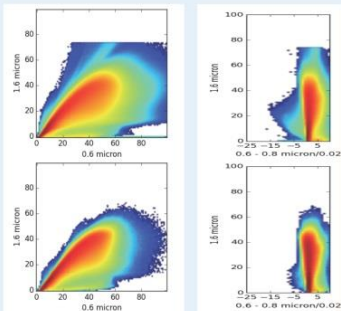


Figure 1.1: Two dimensional visible PDFs (left) for different atmospheric path lengths (1-1.35 for the top plot, and 1.7-2.05 for the bottom plot). Three dimensional visible PDFs (right) for the same atmospheric path bins as on the left. Data are plotted for a solar zenith angles between 37.5-40 degrees.

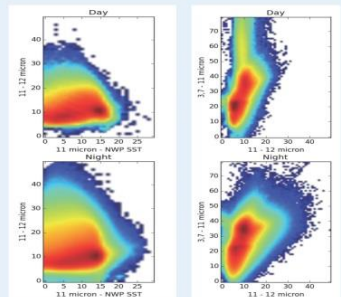


Figure 1.2: Three dimensional infrared PDFs for day and night using the 3.7, 11 and 12 micron channels. State variables chosen here are an NWP SST of 285-287.5 and atmospheric path length of 1-1.35.

2. Bayesian Cloud Detection for AVHRR FRAC data

Bayesian cloud detection for AVHRR FRAC was prototyped using ATSR cloudy PDFs. A spectral shift was applied to the AVHRR data to emulate ATSR data just prior to the PDF look-up. We will employ a similar method in applying PDFs generated from Metop-A FRAC to other AVHRR instruments.

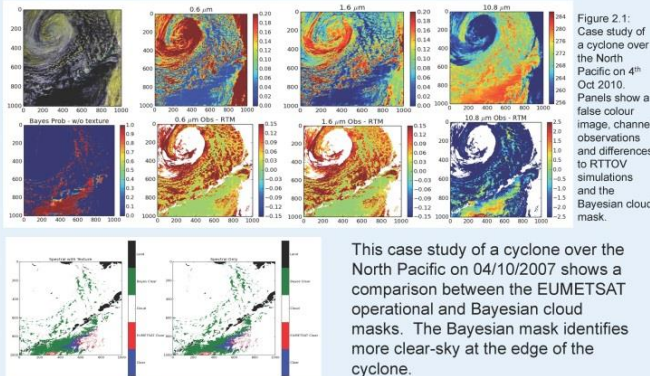


Figure 2.1: Case study of a cyclone over the North Pacific on 4th Oct 2010. Panels show a false colour image, channel observations and differences to RTTOV simulations and the Bayesian cloud mask.

Figure 2.2: Comparison plot of cloud/clear classifications between EUMETSAT and Bayesian mask. White/blue colours are agreement in cloud/clear respectively. Green denotes Bayesian clear whilst EUMETSAT cloud and red the reverse.

This case study of a cyclone over the North Pacific on 04/10/2007 shows a comparison between the EUMETSAT operational and Bayesian cloud masks. The Bayesian mask identifies more clear-sky at the edge of the cyclone.

3. GAC Sampling

GAC data is a subsample of full resolution AVHRR data achieved by observing four in every five pixels across track, and skipping two along track scan lines between observations. The data resolution are nominally given as 4 km, representing a ground area of 3x5 pixels. Observations in each channel are averaged across the four pixels that are sampled. We can generate GAC data from AVHRR FRAC case studies and assess performance with respect to the cloudmask for the full resolution data.

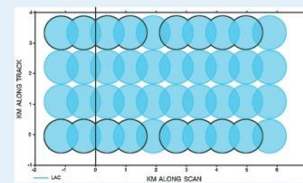


Figure 3.1: Simulated earth-surface footprints for AVHRR/3 showing relation between full resolution data (Local Area Coverage, LAC, in blue) and reduced resolution Global Area Coverage (GAC, black outlines). <http://siswww.eumetsat.org/WEBOPS/eps-pg/AVHRR/AVHRR-PG-4ProdOverview.htm>

4. Textural PDFs

When using Bayesian cloud screening techniques with full resolution data we use textural as well as spectral PDFs to discriminate between cloudy and clear observations. We will investigate whether these are useful when considering GAC data.

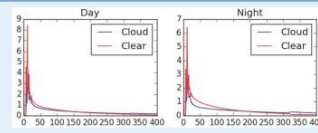




Figure 4.1: AVHRR FRAC 11 micron textural PDFs generated using the EUMETSAT cloud mask.

POSTER 5: VALIDATION OF SATELLITE-DERIVED LAKE SURFACE TEMPERATURE



Validation of Satellite-derived Lake Surface Temperature

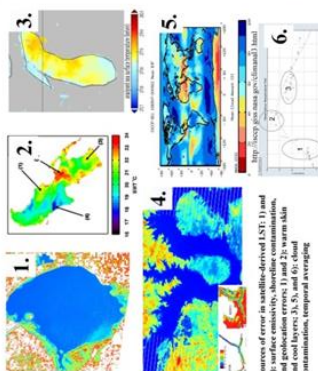
Erik Grosman, John Horel, Nate Larsen, Will Howard
Department of Atmospheric Sciences, University of Utah



Background

- Lake surface temperature (LST) is a critical parameter for lake ecosystems, climate change, and numerical weather prediction
- In situ data limited (Sharma et al. 2014), and obtaining sufficiently accurate and timely satellite-derived LST is a challenge
- LST errors associated with clouds, sub-pixel and shoreline contamination, geolocation, temporal averaging, warm skin and cool layers, surface emissivity, and atmospheric correction algorithms
- Goals:
 - Document issues associated with satellite-derived LST and compare algorithms presented in literature
 - Validate multiple satellite LST products to further understanding of error sources
 - Provide recommendations

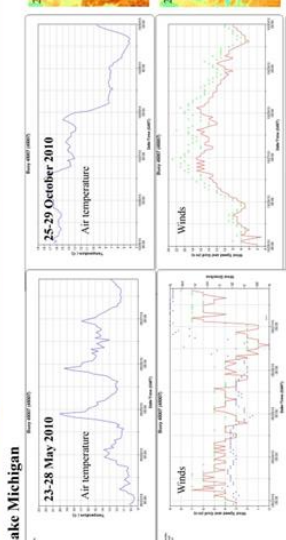
Sources of Error



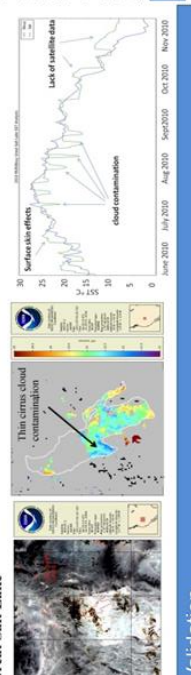
Sources of error in satellite-derived LST: 1) and 2) are associated with atmospheric correction, and cool layers, 3, 5, and 6) cloud contamination, temporal averaging

Case Studies

Lake Michigan

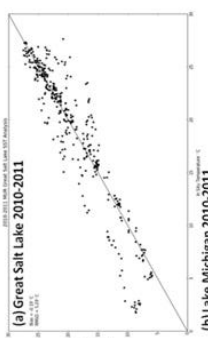


Great Salt Lake

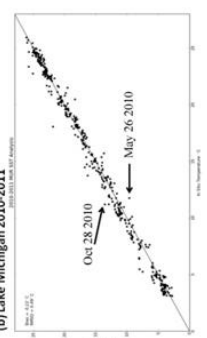


Validation

(a) Great Salt Lake 2010-2011



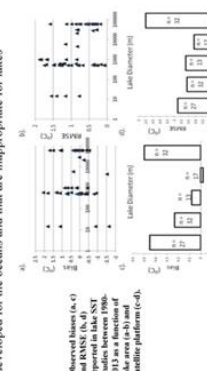
(b) Lake Michigan 2010-2011



Literature Review 1980-2014

Source: <http://large lakes.jpl.nasa.gov/>

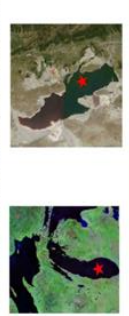
- Over 50 studies of satellite-derived LST reviewed
- The bias and RMSE decrease for larger lakes
- Mean biases (-0.45) and RMSE (-1.7) associated with the AVHRR instrument are higher than MODIS (bias - 0.1; RMSE - 0.7) or the AATSR (bias -0.05; RMSE -0.5)
- Night biases and RMSE are reported to be significantly lower than during daytime, supporting other findings that suggest using only nighttime satellite retrievals over lakes
- A lack of in situ data (lake buoy temperature and atmospheric profile) over many lakes results in using split-window coefficients developed for the oceans and that are inappropriate for lakes



Observed biases (a) and RMSE (b) for AVHRR, MODIS, and AATSR LST studies between 1980-2014 as a function of lake size (in km²) and satellite platform (c).

Satellite LST and In Situ Data

- Satellite LST and buoy data 2010-2011
- NASA Multi-scale Ultra-high Resolution (MUR) Sea Surface Temperature (SST) <http://muur.jpl.nasa.gov/index.php>
- NASA LST <http://modis.gsfc.nasa.gov/data/dataprod/modis/MOD11.php>
- NOAA AVHRR COASTWATCH <http://coastwatch.glerl.noaa.gov/>
- USGS Great Salt Lake Buoy and Lake Michigan NOAA buoy - 45007



Summary

Product	Great Salt Lake, Utah			Lake Michigan		
	RMSE	Bias	RMSE Bias	RMSE	Bias	RMSE Bias
NASA	8.50	2.0	-0.44	0.06	0.30	-0.60
MUR SST	0.60	1.20	-0.30	-0.20	0.10	-0.30
NOAA	0.60	1.20	-0.30	-0.20	0.10	-0.30
Coast Watch						

Table 1. Summary of validation RMSE and Bias statistics

Recommendations and Future Work

- Great Salt Lake LST retrievals are of lower quality than over Lake Michigan
- Both Great Salt Lake and Lake Michigan suffer from cloud contamination issues
- Temporal representativeness issues (long cloudy periods)
- Rapid surface warming during light winds
- Rapid surface cooling during cloudy conditions
- Interannual variations in bias and RMSE a concern for climate trend studies

Acknowledgements and References

We gratefully acknowledge discussion with all members of the GHRSSST Near Shore Water Working Group (NSWWG), and helpful discussions with Jorge Vazquez, Ed Armstrong, Mike Chin, Simon Hook, and John D. Lenters and discussions with the Global Lake Temperature Collaboration (<http://www.laketeperature.org/>). Funding for this work is through NASA grant NNN11SC1096, entitled "Multi-sensor Improved Sea Surface Temperature Retrieval for the Great Lakes" and the NASA Earth Observing System and Remote Sensing Systems for the opportunity to collaborate with this work.

Croaman, E., and J. Horel, 2009: MODIS-derived surface temperature of the Great Salt Lake. *Remote Sensing of Environment*, 113, 73-81

Grosman, E., J. Horel, and E. Croaman, 2013: Techniques for Using MODIS Data to Retrieve Great Lakes Water Surface Temperatures. *J. Atmos. Oceanic Technol.*, 30, 2434-2451

Horel, G.C., S.J. Hook & P. Schneider, 2011. Optimized split-window coefficients for deriving surface temperatures from inland water bodies. *Remote Sensing of Environment*, 115, 3783-3799

MacCallum and Merchant, 2012. Surface Water Temperature Observations of Large Lakes by Optimal Estimation. *MacCallum, Can J Remote Sensing*, 38(1), 25-45

Sharma, S., and coauthors, 2014. Globally distributed lake surface water temperatures collected in situ and by satellites: 1982-2009. Long-Term Ecological Research Network

POSTER 6: VALIDATION OF SST AGAINST *IN SITU* DATA: EFFECT OF SPACE-TIME COLLOCATION CRITERIA



1. Background

- SQUAM is a web-based near real-time tool that monitors several global L2 and L3 SST products produced by NOAA and other agencies. Routine validation of these products is performed against quality controlled *in situ* SSTs from QJAM.
- In the current match-ups, only one clear-sky satellite SST for each *in situ* data closest in space is stored, within a space-time window of 20km and 4hrs. For validation, space-time windows of 2kmx4hr for polar and 5kmx4hr for Geo are used.
- Validation statistics depend on several criteria including collocation choice (space-time), however, relative performances are assessed using a consistent approach.
- The objective of this study is to further understand the current match-up scheme and the effect of space and time separation on the validation statistics, for which special extended match-ups (in space and time) were generated.
- Towards the above-stated objective, three sets of match-ups for the two newest instruments processed at NOAA with ACSP0 are analyzed: two from the S-NPP VIIRS (L2P, L3U), and one from Himawari-8 AHI (L2P).

SQUAM: SST Quality Monitor www.star.nesdis.noaa.gov/sst/sst/squam
 ACSP0: NOAA Advanced Clear-Sky Processor for Oceans
 VIIRS: Visible Infrared Imager Radiometer Suite sensor onboard S-NPP
 AHI: Advanced Himawari Imager onboard Himawari-8 geostationary satellite

2. VIIRS and AHI SSTs for sensitivity study

- ACSP0 S-NPP VIIRS (launched October 2011)
 - GDS2 L2P VIIRS SST produced since May 2014 and archived with GHRSSST
 - GDS2 0.02° L3U VIIRS SST launched in May 2015 (also archived with GHRSSST)
 - Both products are monitored in SQUAM (L3U monitoring added after 2014 GHRSSST meeting www.star.nesdis.noaa.gov/sst/sst/squam/L3U)
- ACSP0 Himawari-8 AHI (launched October 2014)
 - An experimental GDS2 L2P 10min full-disk product is generated since June 2015 at NOAA ftp.star.nesdis.noaa.gov/sst/sst/ahis2p_01652015/
 - Monitoring in SQUAM was established which includes full-disk maps, histograms, and time series www.star.nesdis.noaa.gov/sst/sst/squam/GED/
 - The results presented here are our first take on the end-to-end production and diagnostics, and are expected to dynamically evolve in the near future
 - Work is underway at NOAA to generate a GDS2 L3 H8 ACSP0 product and explore archiving with GHRSSST
 - In March 2016, GOES-R will be launched which will carry Advanced Baseline Imager (ABI), similar to AHI. Experience with analyses of H8-AHI SST will also contribute towards monitoring of GOES-R ABI SST

3. Methodology (current SQUAM and beyond)

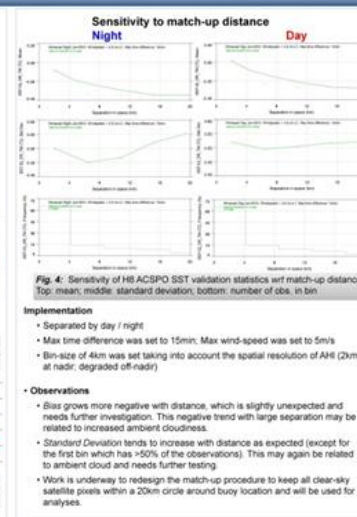
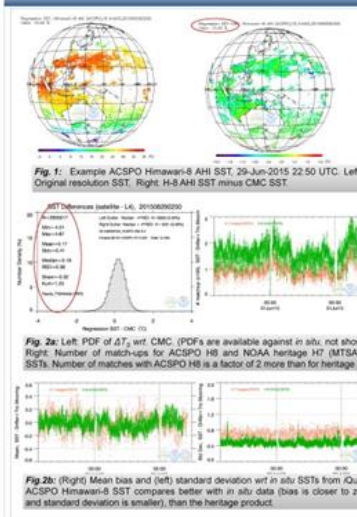
Current SQUAM implementation

- Analyzed in SQUAM are SST residuals: $\Delta T_s = T_{sat} - T_{ref}$
- T_{ref} is either L4 (CMC, OSTIA, Reynolds) or QCed *in situ* SST from QJAM. L4 is used for monitoring and *in situ* for validation.
- ΔT_s are analyzed by: Maps, Histograms, Time series and dependences
- PDFs of ΔT_s are near-Gaussian

Analyzing effects of space-time collocation using *in situ* data: beyond SQUAM

- A month worth of data is chosen with extended match-ups
- These 'super match-ups' have multiple time and distance (if data absent within the first circle) attached to each *in situ* location
- For testing sensitivity of validation statistics to time difference: Matches within a given distance (Polar: 20m, Geo: 4km) are sub-selected and dependences of statistics on binned time differences are shown for -4 to +4 hours
- For testing sensitivity of validation statistics to separation distance: Matches within a given time difference (Polar: 3hr, Geo: 15min) are sub-selected and dependences of statistics on binned distances are shown for 0 to 20 kms
- Wind-speed is also constrained to avoid effects of mechanical mixing

4. ACSP0 Himawari-8 AHI L2P SST



Implementation

- Separated by day / night
- Max time difference was set to 15min; Max wind-speed was set to 5m/s
- Bin-size of 4km was set taking into account the spatial resolution of AHI (2km at nadir, degraded off-nadir)

Observations

- Bias grows more negative with distance, which is slightly unexpected and needs further investigation. This negative trend with large separation may be related to increased ambient cloudiness.
- Standard Deviation tends to increase with distance as expected (except for the first bin which has ~50% of the observations). This may again be related to ambient cloud and needs further testing.
- Work is underway to redesign the match-up procedure to keep all clear-sky satellite pixels within a 20km circle around buoy location and will be used for analyses.

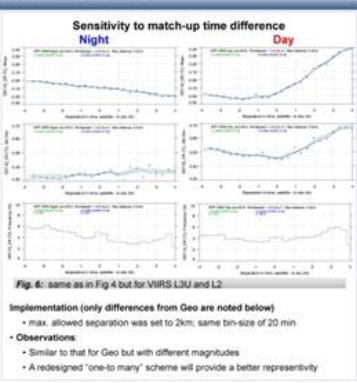
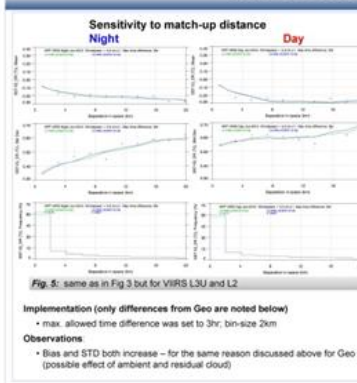
Implementation

- Analyses are separated by day / night, due to different rate of diurnal warming
- Match-up distance is 4km; Wind speed 5m/s
- Bin size of 20min was used (AHI takes full-disk every 10min)
- A negative time difference means an earlier satellite observation

Observations

- Unlike collocation in space, the bins are distributed more uniformly because there is no 'closest in time' selection criteria
- At night, a cooling trend is observed in bias, due to gradual diminishing of diurnal thermocline. During the daytime, a warming trend is observed, due to forming the diurnal thermocline.
- Standard Deviation increases with time-difference on both sides, as expected. The U-shape is more pronounced during the daytime. The nighttime asymmetry needs further investigation

5. ACSP0 S-NPP VIIRS L2P/L3U SSTs



Summary and Outlook

- Validation statistics show variations with space and time separation
- Bias grow cold with separation in space, likely due to the current 'closest in space' design of the NOAA match-up scheme.
- Redesign towards 'one-to-many' is expected to provide a better match-up representation for this sensitivity analyses
- The 'sign' of the time-difference should be taken into account
- The standard deviation tends to increase with separation. This trend can be complicated by locations (e.g., the TWP in H8 domain).


Future extensions

- Perform analyses on longer time-series as data become available and with one-to-many match-up scheme
- Contribute towards consensus collocation criteria, discuss in ST-VAL
- In addition to characterizing standard statistics, which contains error from both products and references, stratify product-specific internal noise using triple-collocation method

Acknowledgements & Disclaimer

This work was supported by JPSS and GOES-R Program Offices, and NOAA PMD, NCE and ORS Programs. We thank our NOAA, GSFC, U. Miami, and MAVO SST colleagues and wider GHRSSST community for making products available, and helpful discussions. The views and findings are those of the authors and should not be construed as an official NOAA or US Government position, policy, or decision.

POSTER 7: SST CCI STATUS AND PROGRESS




ESA Climate Change Initiative Phase-II Sea Surface Temperature

www.esa-sst-cci.org

SST CCI Status and Progress

Owen Embury | Chris Merchant | Craig Donlon

The ESA Climate Change Initiative



The study of climate change demands long-term, stable observational records of climate variables. ESA's Climate Change Initiative was set up to unlock the potential of satellite data records for this purpose. As part of this initiative, 13 projects were established to handle the data records for different essential climate variables, see: <http://www.esa-cci.org>

Requirement	GCCS (2011)	SST CCI URD L3/L4 breakthrough	SST CCI Phase 1 result	SST CCI Ph2 target
Accuracy / scale demonstrated	0.1 K / 100 km	0.02 K / 100 km	Generally ~0.2 K / regionally	0.1 K / 1000 km ATSR era 0.2 K / 1000 km in 1980s.
Precision	None	0.05 K / 100 km	Varies, quantify it	Varies, quantify it
Stability ¹	0.03 K / decade	0.02 K / decade 0.05 K seasonally, diurnally	Mostly <0.05 K / decade after 1996 Seasonal stability generally ~0.2 K, locally greater	<0.05 K / decade after 1991 ~0.1 K / decade overall
Spatial resolution	1 km	0.1 deg	0.05 deg	0.05 deg
Temporal resolution	Daily	Day/night (UTC)	Day/night on standardized local time (L2, L3); daily (L4)	Day/night on standardized local time; UTC daily mean
Uncertainty information	None	Total uncertainty	Total and components	Total and components, corr. length scales
Type of SST	Blended	Skin & buoy-depth	Skin and buoy-depth	Skin and buoy-depth (IR&O on sub-skin)
Period	~1980 - now	1991 - 2010	1981 - 2016	

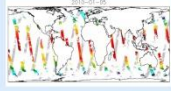
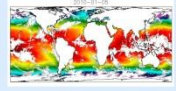
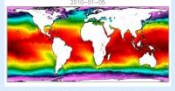
1 - Currently only assessable retrospectively against tropical moorings.

SST CCI Overview

Aim: Satellite-derived global sea surface temperature datasets for climate.

Why: Quantify multi-decadal marine change independently. Ocean ecosystems, dynamics, air-sea interaction etc. Climate model evaluation and development.

How: Accuracy and stability from dual-view Along Track Scanning Radiometers. Coverage and repeat observations from meteorological sensors (AVHRRs). High resolution blend (analysis) with ATSRs as SST reference

ATSRs are dual view sensors, stable and accurate for SST. Use as SST calibration reference.

AVHRRs are single view, and not designed for climate, but give good coverage and a longer history.

Level 2/3 SSTs from ATSRs and AVHRRs are blended using an improved version of "OSTIA".

Phase-I dataset released covering 1991 to 2010

- No in situ, satellite only based on ATSR and AVHRR GAC
- Skin SST retrieved
- Estimate SST 20cm at 10:30 local time using diurnal variability model
- Uncertainty estimates (random, locally systematic, adjustment)

Phase-II will extend dataset to cover 1981 to 2016

- Add AVHRR FRAC from Metop satellites
- Add UTC daily mean estimate
- Improved SST retrievals
- Improved uncertainty estimates
- Research SST retrieval from microwave sensors (AMSR2)

For details on uncertainties see poster 25 by Rayner et al. and talk by Bulgin in session III

AVHRR GAC L1

We have assembled a European archive of NOAA AVHRR Global Area Coverage (GAC) L1b data which can now be accessed via the UK Centre for Environmental Data Archive (www.ceda.ac.uk). The L1b data are currently available in the original NOAA format. Prior to use in the SST retrieval algorithm the GAC data are pre-processed to "L1c" in NetCDF-4 format adding:

- CLAVR-x updates to geolocation
- CLAVR-x cloud mask
- SST-CCI corrections to AVHRR calibration as they become available

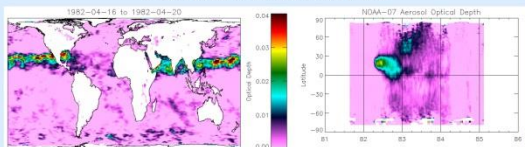
Work is currently under-way to add the Bayesian cloud mask (see poster 4 by Bulgin et al.) to the L1c files and in the future we will make use of the output of the FIDUCEO project (see poster 23 by Mittaz et al.)

Stratospheric Aerosol

The eruptions of El Chichón in 1982 and Mt Pinatubo in 1991 both injected sulphur dioxide into the stratosphere where formed a sulphuric acid aerosol causing a significant cold bias in most SST retrievals. Aerosol robust retrievals from ATSR data are possible due to its dual view geometry; however an alternative approach is required for other instruments.

- Use HIRS sounder to generate an independent estimate of volcanic sulphate aerosol optical depth at infra red wavelengths
- Include volcanic aerosol in SST retrieval scheme

Initial AOD estimate from HIRS



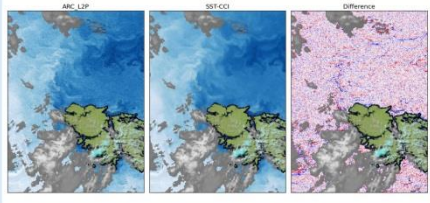
Atmospheric Correction Smoothing

In order to reduce the impact of radiometric noise in full resolution L2P products (ATSR and AVHRR FRAC) we have implemented two forms of atmospheric correction smoothing. For ATSR we use a generalised atmospheric correction:

$$\bar{x} = (x) + b^T (y - \langle y \rangle)$$

Where (x) is the average SST in an $N \times N$ box, y is the BT vector, and b is a weighting vector allowing multiple channels to be used.

Impact of atmospheric correction smoothing



For AVHRR we use the smoothed optimal estimation method. (Merchant et al. 2013; also see poster 27 by Saux Picart et al.)

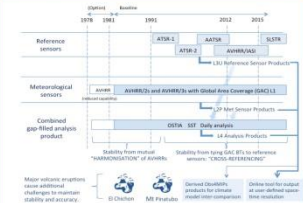
Data










Phase-I data available from NEODC: browse.ceda.ac.uk/browse/neodc/esacci_sst

For documentation see: <http://www.esa-sst-cci.org/PUG/documents>

Journal article: Merchant et al. 2014
doi: 10.1002/gdj3.20

For more information contact:
science_leader@esa-sst-cci.org
c.j.merchant@reading.ac.uk



Page 176 of 225

POSTER 8: UNCERTAINTIES IN VALIDATION OF SST ANALYSES USING NEAR-SURFACE ARGO OBSERVATIONS

Uncertainties in validation of SST analyses using Argo

Emma Fiedler, Alison McLaren

Key Points

- Argo observations are not assimilated in any SST analyses (by agreement through GHRSSST) so they are independent, and also highly accurate: ideal for validation
- A recommendation of this work is that all validation statistics using Argo (or other in situ observations) as a reference should be presented with uncertainty estimates

This work was funded by the E-AMS (Euro-Argo Improvements for the GMES Marine Service) project

1. Matchup sampling requirements for mean difference

Methods

OSTIA is the Met Office Operational Sea surface Temperature and Ice Analysis system.

Matchups between near-surface Argo and the OSTIA analysis were obtained for January 2007 to December 2013.

Shallowest Argo observations between 3-5 m depth were used, good estimate of foundation temperature (Fiedler et al., 2014).

Globe split into 50 grid boxes (36x36 degrees). Sample standard deviation (σ_s) of matchups calculated for each grid box where observations available.

Number of Argo observations (n) needed for each grid box to give standard errors (σ) of 0.02 K was calculated using:

$$\hat{\sigma} = \frac{\sigma_s}{\sqrt{n}}$$

Results

Number of Argo observations required to achieve standard error (sampling uncertainty) of 0.02 K for each grid box

Number of matchups, Dec 2013 - ideal

Difference between ideal numbers above and actual numbers of observations for example month December 2013.

Actual sampling uncertainties for December 2013

Assumes standard deviation independent of n and representative of the region (calculated from full 7 year set)

Sampling Uncertainty (K) Dec 2013

Conclusions

- The current distribution of Argo floats (nominally 3x3°) should be maintained for use in validation of SST analyses to continue.
- Monthly total number of near-surface Argo observations (3-5 m depth) is suitable for sampling uncertainty of ~0.03 K for most major ocean regions.
- Number of floats in high variability regions should be increased to reduce sampling uncertainty.
- For sampling uncertainty of Falklands/Malvinas region to match Gulf Stream (next highest globally) an increase of ~300 observations a month needed.
- To achieve sampling uncertainty of 0.02 K across whole ocean, number of observations in the high variability regions need to be increased by up to 1300 observations a month.
- Recommend all statistics be presented with uncertainty estimates to reflect regional variations in sampling uncertainty.

2. Matchup sampling requirements for standard deviation

Is the number of available Argo matchups (n) sufficient that regional standard deviations are not dependent on n when calculating monthly statistics?

Methods

Sample standard deviation of differences between OSTIA and Argo was calculated directly from the full set of matchups for February 2014 for each ocean region (as defined by MyOcean).

For each region, standard deviation recalculated for Argo observations reduced in increments of 10, and resampled from the full group each time.

Results

Standard deviation for different numbers of matchups (n), for February 2014.

Three example regions shown.

Conclusions

- Number of matchups affects reliability of standard deviation produced.
- Monthly number of Argo observations available is sufficient that a reliable standard deviation can be calculated for major ocean regions (possibly excepting North Atlantic). Number needed for convergence towards this value varies with ocean region.
- Repeated runs of the same experiment show similar results.
- Weekly (or daily) matchup numbers would be in more erratic range (see plots). Increase in number of Argo observations available would therefore be required to validate on a frequency greater than monthly or over smaller regions than the major ocean areas defined by MyOcean.

3. Routine assessment of SST analyses – with uncertainty estimates

Regular monthly validation of OSTIA and other analyses included in GMPE (GHRSSST Multi-Product Ensemble) using Argo has been set up.

Quality-controlled Argo observations are extracted from the EN4 database (Good et al., 2013).

Results freely available at:

ghrssst-pg.metoffice.com/pages/blast_analysis/sst_monitor/argo

Statistics are presented as timeseries and are updated monthly.

Includes global comparisons to Argo for all near-real-time analyses included in GMPE.

Includes regional comparisons to Argo (MyOcean regions) for OSTIA and GMPE median, which also include uncertainty estimates on mean and standard deviation of the differences to Argo.

Example regional rolling 1-year timeseries for OSTIA compared to Argo

North Atlantic

Temperature difference (K)

• Bars show 95% confidence intervals calculated using a bootstrap method

• Importance of showing uncertainties for interpretation of results is clear

Global comparisons to Argo for all GMPE NRT analyses

Available timeseries extended each month

(Uncertainty estimates not shown for clarity but statistics are available)

Legend:

- OSTIA
- GAMSSA_38km
- K10_SST
- AWIPF_OI
- MyO_OI
- FNMOC
- MGSST
- CMC
- RTG
- SWI_amsr_OI
- GMPE_median


References

Fiedler, E. R., A. McLaren and G. Mac (2014). SST: Results and Parameterisations. Euro-Argo Improvements for the GMES Marine Service, DA3.3, 23pp.


Good, S. A., Marin, M. J. and Roman, R. A. (2013). EN4: quality controlled ocean temperature and salinity profiles and monthly objective analyses with uncertainty estimates. J. Geophys. Res., 118, 4796-4811. DOI: 10.1002/joc3600

© Crown copyright | Met Office and the Met Office logo are registered trademarks

POSTER 9: FIDUCIAL REFERENCE MEASUREMENTS FOR CEOS (FRM4CEOS)



Fiducial Reference Measurements for Validation of Surface Temperature from Satellites (FRM4STS)



Project Aim:
To establish and maintain SI traceability of global Fiducial Reference Measurements (FRM) for satellite derived surface temperature product validation and help develop a case for their long term sustainability. An ESA funded project on behalf of the international community to establish community agreed best practises and international harmonisation through support of a CEOS WGCV calibration project following on from the 'Miami series of comparison experiments'

What are Fiducial Reference Measurements?

"The suite of independent ground measurements that provide the maximum return on investment for a satellite mission by delivering, to users, the required confidence in data products, in the form of independent validation results and satellite measurement uncertainty estimation, over the entire end-to-end duration of a satellite mission" (Sentinel-3 Validation Team)

An FRM must:

- Have documented evidence of its degree of consistency for its traceability to SI through the results of round robin inter-comparisons and calibrations using formal metrology standards
- Be independent from the satellite geophysical retrieval process
- Have a detailed uncertainty budget for the instrumentation and measurement process for the range of conditions it is used over.
- Adhere to community agreed measurement protocols, and management practises.

Requirements for Project Objective:

- Comparisons to ensure consistency between measurement teams
- Common descriptions and evaluation of uncertainties
- Robust links to SI
- Experiments to evaluate sources of bias/uncertainty under differing operational conditions
- Provision of guidance and best practises and access to standards and comparisons
- Evidence and publicity of benefits to ensure resources needed to maintain collection of global FRM is forthcoming

Project Breakdown

Task 1: Communication, Outreach and Promotion

Promote and coordinate the FRM4STS project in collaboration with CEOS and the wider sea, land and ice surface temperature (SST/LST/IST) validation community

Task 2: Requirements Review and Preparation for Technical Implementation

Practically plan all aspects of FRM4STS experimental activities for later implementation

Task 3: CEOS SI Inter-Comparison Experiment for TIR Radiometers and Reference Blackbody Calibrators

Perform controlled inter-comparison of FRM thermal infrared (TIR) field radiometers and reference black body sources to SI standards

Task 4: TIR FRM Field Inter-Comparison Experiments


Coordinate and demonstrate field inter comparison activities for TIR FRM

Task 5: International Workshop and Final Reporting

Consolidate the project outcomes and promote findings at an open international workshop





Key Deliverables




- Laboratory-based comparison of the results of participants' calibration processes for FRM TIR radiometers (SST, LST, IST).
- Laboratory-based comparison to verify TIR blackbody sources used to maintain calibration of FRM TIR radiometers.
- Field inter-comparisons of SST using pairs of FRM TIR radiometers on board ships to build a database of knowledge over a several years.
- Conduct field-campaigns for FRM TIR of LST.
- Best practise protocols for the calibration, operation and performance of FRM of Surface temperatures.
- Full data analysis, derivation and specification of uncertainties, following agreed NMI protocols on all data collected as part of FRM4STS.
- All outcomes published to promote benefits of Cal/Val.
- Option to perform a study of means to establish traceability and potential benefits to satellites validation and CDRs of high accuracy Ocean temperature measurements using buoys and similar floating systems.




Mobile radiometric measurements across the gravel plains at Gobabeb, Namibia


Further Information
 Contact: Nigel Fox (nigel.fox@npl.co.uk)
 Earth Observation, Climate & Optical Group,
 National Physical Laboratory
 Hampton Road, Teddington, TW11 0LW, UK
 Or visit: www.frm4sts.org
*available soon




POSTER 11: PATTERN RECOGNITION ENHANCEMENTS TO CLEAR SKY MASK FOR VIIRS SST



Toward improved VIIRS SST imagery for fronts detection and enhanced clear sky mask in ACSPO

Irina Gladkova^{1,2}, Yuri Kihai^{1,3}, Alexander Ignatov¹, Fazlul Shahriar^{2,4}, Boris Petrenko^{1,3}

¹ NOAA STAR, ² CUNY/CREST, ³ SST Inc., ⁴ Graduate Center, CUNY

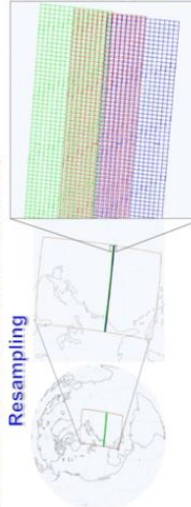


The previously introduced automated SST Pattern Test (SPT; Gladkova et al., 2015) first identifies ocean fronts and adjacent contiguous areas with uniform SSTs, and then makes ocean vs. cloud decision based on the statistics of the whole regions.

Recent enhancements include improved

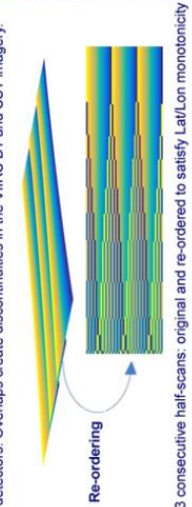
- Brightness temperature (BT) and SST imagery in the full VIIRS swath, using special resampling algorithms to minimize geometrical distortions and fill in the bow-tie deleted pixels;
- front detection, using gradient behavior of the SST field, connectivity of the fronts, and bimodality of SST distribution in their vicinity;
- clustering, using the statistics of the BTs and derived SSTs over large regions.

These enhancements will be incorporated in the future versions of the NOAA Advanced Clear-Sky Processor for Oceans (ACSPO) SST system, to a) generate a new product – ocean fronts (which can be used to validate the gradients in various L4 analyses); and b) improve VIIRS clear-sky mask, especially in the dynamic areas of the ocean, in coastal zones, and in the high-latitude regions).



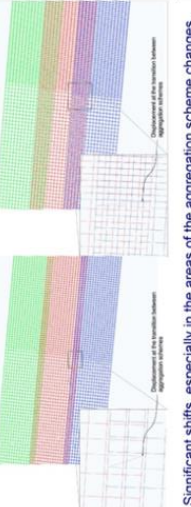
Resampling

Three consecutive VIIRS scans (shown in green, red, blue) each including 16 detectors. Overlaps create discontinuities in the VIIRS BT and SST imagery.



Re-ordering

3 consecutive half-scans: original and re-ordered to satisfy Lat/Lon monotonicity

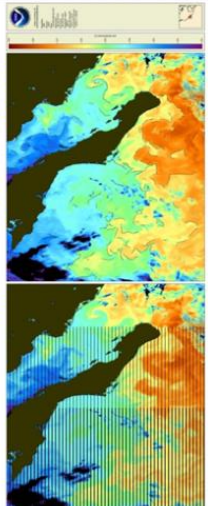


Significant shifts, especially in the areas of the aggregation scheme changes.

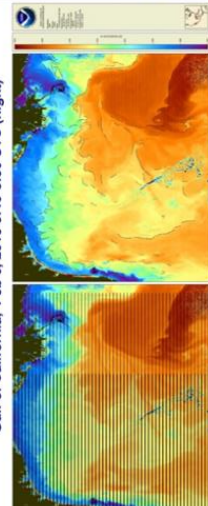
Future ACSPO Enhancements

- Improve BT and SST imagery: resample ("de-bowtize"), and restore pixels in bow-tie areas deleted onboard
- Thermal fronts saved as a bitmask
- Improve clear sky mask in dynamic, coastal, and high-latitude areas

Original SST Imagery with bow-tie deletions



Improved SST Imagery & Frontal Product



Gulf of California, Feb 6, 2015 8:40-8:50 UTC (night)

Gulf of Mexico, Feb 19, 2015 18:40-18:50 UTC (day)

Identification of Thermal Fronts

- Resampling & de-bowtizing
- Liberal thresholds to reduce search domain
- Gradient Field
- Log-enhancement of gradient magnitude
- Eigenvalues of Hessian
- Bilateral Filtering at different scales
- Front Index (logistic function)
- Connecting fragments
- Bimodality check
- Thinning based on gradient field

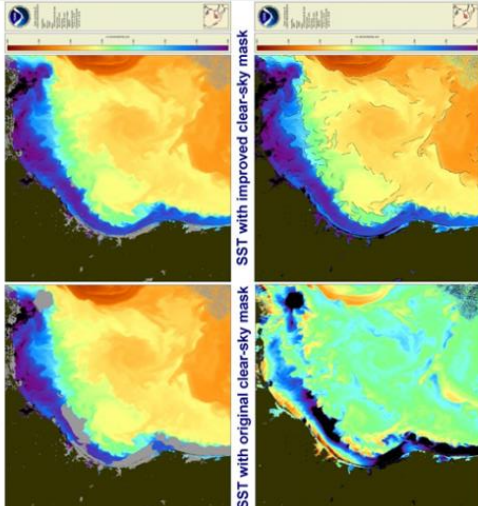
Standard functions from optimized openCV library:

- gradient filter
- range filter
- median filter
- standard deviation filter
- Gaussian filter
- Laplacian of Gaussian (LoG) filter
- bilateral filter
- zero crossing filter
- erosion/dilation morphological function
- connected components

Current limitations of the ACSPO clear-sky mask

- Misclassifications ("false alarms") mostly occur in dynamic areas (currents, eddies, upwellings), coastal zones, and sea-ice transitions
- They are often persistent from one overpass to another
- Result in loss of data in interesting areas and day/night inconsistency

Improvements in ACSPO Clear-Sky Mask



ACSPO – CMC SST

SST with thermal fronts overlaid

Future Work

- Comparisons with other available front detection algorithms
- Comprehensive tests and evaluation with ACSPO clear-sky mask
- Implementation in ACSPO

Acknowledgment

This work is conducted under the JPSS and NOAA ORS Programs. The views, opinions, and findings contained in this presentation are those of the authors and should not be construed as an official NOAA or US Government position policy or decision.

Reference

Gladkova, I., Y.Kihai, A.Ignatov, F.Shahriar, B.Petrenko, 2015: SST Pattern Test in ACSPO clear-sky mask for VIIRS. *Remote Sens. Env.*, **160**, 87-98.

16th GHRSSST Meeting, ESA/ESTEC, The Netherlands, 20-24 July 2015

Correspondence: Irina V Gladkova <gladkova@cs.cuny.cuny.edu>

POSTER 14: IMPLICATIONS OF DIURNAL WARMING EVENTS ON ATMOSPHERIC MODELLING

Implications Of Diurnal Warming Events On Atmospheric Modelling

Ioanna Karagali ^{*1}, Jacob L. Høyer², Jian Ting Du ¹, Xiaoli Guo Larsén ¹

¹DTU-Technical University of Denmark, Risø Campus, Roskilde.
²Climate and Arctic Research, Danish Meteorological Institute, Copenhagen.

DTU Wind Energy
 Department of Wind Energy

Introduction

The diurnal variability of SST is an important mode of variability, modulating air-sea interactions with direct impact on heat and gas fluxes. Low enough winds and sufficient solar heating lead to a diurnal warm layer, typically constrained in the upper few meters of the water column. Diurnal warming is most intense within the first few cm, as the largest percentage of infra-red radiation is absorbed there. This part is observable by infra-red and microwave radiometers, mounted on either satellites or ships. The increased availability of SST retrievals from space has led to the identification of diurnal warming events, occurring at all latitudinal bands in coastal and open ocean conditions [4, 5, 6]. While there is an impact of not properly resolving the diurnal cycle in the estimation of surface heat fluxes [2, 1] and the exchange of CO₂ between the ocean and the atmosphere, most operational atmospheric and oceanic models up to day still do not account for the daily SST variability.

The ESA funded project on the diurnal variability of SST, its regional extend and the implications in atmospheric modelling (SSTDV: R.EX-IM.A.M.) will be finalized by the end of 2015. During its last part, the largest diurnal warming events were identified for a region covering parts of the North and Baltic Sea, using 6 years of SEVIRI data. These events mostly occurred in spring and summer and the peak daily anomaly reached up to 6 degrees in some cases. The hourly SST fields retrieved during those events will be used as boundary conditions in the Weather Research & Forecasting (WRF) model, thus increasing the temporal resolution of SST in the model from the typical daily SST update. With this mode, the surface wind field and the heat fluxes will be modelled and compared to the outputs without the hourly SST update. In addition, 10-meter winds will be compared to in situ measurements from meteorological masts and Synthetic Aperture Radar (SAR) retrieved winds, when available. Heat flux estimates will be compared to the SEVIRI Surface Solar Irradiance (SSI) and Downward Long-wave Irradiance (DLI) products.

Challenges

- ▶ Impact on air-sea fluxes, atmospheric stability
- ▶ Complications for multi-sensor SST
- ▶ SST time-series
- ▶ Atmospheric model outputs
- ▶ SST retrieval algorithms
- ▶ Wind retrieval algorithms

Figure 1: Near surface temperature gradients [7].

Identification of large DW events from SEVIRI

- ▶ Domain: 52-60°N, 2-16°E
- ▶ For warming > 1°
- ▶ In more than > 7 neighbouring cells
- ▶ Top warmest cases
 - ▶ June, July 2006
 - ▶ April, May 2008
 - ▶ April 2009, 2010

Figure 2: The largest warming event identified, 12/06/2006. Top: SST 4, 18, 11. Bottom: QuikSCAT U at 6, 18

Figure 3: The warming event of 08/05/2008. Top: SST 4, 18, 15. Bottom: QuikSCAT U at 6, 18

Optimal Interpolation of Hourly SST

- ▶ Hourly SST: gaps due to clouds
- ▶ Use OI scheme to fill gaps [3]
- ▶ Complementary data:
 - ▶ Pathfinder AVHRR
 - ▶ ENVISAT AATSR (CCI ARC dataset)

Figure 4: Example of the OI SST for the largest warming event identified, occurring on June 12, 2006

Figure 5: Example of the OI SST for the warming event occurring on May 8, 2008

WRF

- ▶ 3 domains: 27, 9 and 3 km
- ▶ ERA Reanalysis
- ▶ PBL schemes to be tested
- ▶ Update SST hourly vs daily
- ▶ Model runs for 3 day periods centred around the day of max warming
- ▶ Model skill tested for wind and heat fluxes

Figure 6: WRF domain set-up

Conclusions

Some preliminary steps required for the implementation of hourly, gap-free SST fields in the atmospheric model WRF are presented in this study. A small domain covering the coastal areas around Denmark has been selected for the analysis. Large diurnal warming events, both in terms of peak warming and spatial extent have been identified and the hourly SEVIRI SST fields were optimally interpolated. The WRF domain is selected, while still pending are the sensitivity tests regarding the selection the PBL schemes and the model boundary conditions.

Acknowledgements

European Space Agency (ESA) Support To Science Element (STSE), SSTDV: R.EX-IM.A.M project, Danish PSO X-WiWa project. SEVIRI data: Centre de Météorologie Spatiale, Météo France & OSI-SAF project.

References

- [1] Bernie, D. J., Galyard, E., Madec, G., Slingo, J. M., Woolnough, S. J., and Cole, J.: Impact of resolving the diurnal cycle in an ocean-atmosphere GCM. Part 2: a diurnally coupled CGCM. *Clim. Dyn.* 31, 909-925, 2008.
- [2] Clayson, C. A., and Bogdanoff, A. S.: The effect of diurnal sea surface temperature warming on climatological air-sea fluxes. *J. Clim.* 20, 2546-2556, 2007.
- [3] Høyer, J. and Shi, J.: Optimal interpolation of sea surface temperature for the North Sea and Baltic Sea. *J. Mar. Sys.* 65 (1-4), 176-189, 2007.
- [4] Karagali, I. and Høyer, J.: Characterisation and quantification of regional diurnal SST cycles from SEVIRI. *Ocean Science* 10, 745-758, 2014.
- [5] Karagali, I. and Høyer, J.: Observations and modelling of the diurnal SST cycle in the North and Baltic Seas. *J. Geophys. Res.-Oceans* 118 (9), 4488-4903, 2013.
- [6] Karagali, I., Høyer, J., and Hasager, C. B.: SST diurnal variability in the North Sea and the Baltic Sea. *Remote Sens. Environ.* 112, 159-170, 2012.
- [7] Minnett, P., and Kaiser Weiss, A.: Near surface oceanic temperature gradients, GHRSSST Discussion document, 2012.

www.vindenergi.dtu.dk

*ioka@dtu.dk

Page 180 of 225

POSTER 15: VALIDATION, ERROR ANALYSIS AND THE EFFECT OF CLOUD CONTAMINATION ON THE QUALITY OF VIIRS SST RETRIEVALS FOR VARIOUS ALGORITHMS



Error analysis and the effect of cloud detection on the quality of VIIRS SST retrievals using various algorithms

Prabhat Koner and Andy Harris

NOAA/ESSIC, 5830 University Research Ct. College Park, MD 20740, USA



INTRODUCTION

There are two distinct schools of thought for scientific parameter estimation from measurement: deterministic and stochastic. Any deterministic must require a physical model as contrary stochastic methods either incorporate physical model (e.g. OEM) or without physical model (e.g. regression). Geophysical parameter estimation for many cases from satellite measurement are severely constrained by the number of measurement as compared to the number of parameters supposed to be retrieved as one example of satellite SST retrieval. As result, many stochastic methods are dominating in operational SST retrieval. Despite of the fact that there are many advantages to use deterministic method for any science problem. Thus, we first attempt to use a deterministic method in operational SST retrieval to understand the advantages even using many parameters from model data, which are not truth. However, the current practice to report operational SST error are basically sum of the two errors (the errors of cloud detection and retrieval methods). To understand the error due to inverse method, we have made a study using two different operational products (OSPO and NAVO) with our deterministic algorithms.

Deterministic Inverse Method

The form of the latest version MTLs method (Koner et al. 2015) is:

$$x_{min} = x_{reg} + (K^T K + \frac{\lambda}{2} \sigma_{reg}^2 I)^{-1} K^T \Delta T_e \quad (1)$$

The analytical error calculation using (Koner and Drummond, 2008 & Koner et al. 2015)

$$\sigma_{reg} = \left[\frac{M_{reg}}{M_{reg} + \frac{\lambda}{2} \sigma_{reg}^2} \right] \sigma_{reg} \quad (2)$$

Where, T_e is a measurement vector, $M_{reg} = (K^T K + \frac{\lambda}{2} \sigma_{reg}^2 I)^{-1} K^T$ is the model resolution matrix, I is the identity matrix, σ_{reg} is assumed true parameter, K is the Jacobian, σ_{reg} is lowest singular value of $[K \Delta T_e]$, λ is the condition number of Jacobian, and $x = \begin{bmatrix} s \\ w \end{bmatrix}$ is used, where, s is SST and w is total column water vapor (TCWV).

Data and Software Used

We have downloaded NAVO and OSPO 1.2P SST data for several months from http://podas-oc2.sci.gsfc.nasa.gov/oc2/podas/Data/oc2/1.2P/VIIRS_NPP/NAVO/1.1/ and http://podas-oc2.sci.gsfc.nasa.gov/oc2/podas/Data/oc2/1.2P/VIIRS_NPP/OSPO/1.2.2/, respectively. The quality flag of 3 and above of NAVO data are assumed to be navy cloud mask (NCM) and the quality flag of 5 of OSPO data is assumed to be opo cloud mask (OCM) for this study. We have collocated the satellite SST (NAVO & OSPO), buoy SST <http://www.met.rdg.ac.uk/~met/naoq/naoq.html>, GPS <http://normaly.met.rdg.ac.uk/GPS/Gps4/>, VIIRS LIB BT and VIIRS geo-location data based on point match for this study. The match-up window of this monthly matchup database (MMDb) was set to ± 30 minutes for buoys coincident with satellite pixels point. *In situ* data are quality controlled using corresponding quality flags from NOAA Aqua Community Radiative Transfer Model (CRTM 2.1) <http://ftp.rem.sci.gsfc.nasa.gov/oc2/crtm/crtm2-1/> is used to calculate simulated Brightness temperatures (BT).

MTLS Suite

MTLS suite includes the deterministic SST retrieval and quasi-deterministic cloud and error masking (CEM) algorithm package. MTLs retrieval method includes two extra features: a) quality flags (QF) using total error calculation (Eq. 2) and b) additional cloud detection (shown in last bin). The binning of QF based on the fixed value of analytical error ($0 < |e| < 1$) into 10 bins evenly spaced in a logarithmic scale. If a bin does not get at least 10% of cloud-free data, then it is combined with the subsequent bin. For each bin, the percentage of total matches is based on the cumulative analytical errors. The last bin is likely to contain a substantial population of "bad" retrievals, i.e. caused by cloud-leakage or other errors in ancillary information including WV profile shape error. This is implemented using appropriate threshold conditions based on physical understanding of the problem on the output of SST and TCWV from MTLs retrieval. Our CEM is hybrid detection algorithm (Koner & Harris 2015a, Koner et al. 2015b) using spectral differences and radiative transfer model (RTM). Our implementation is based on normalized spectral differences and includes TCWV as a functional parameter. We use the double differences technique between the channels of 4 and 11 μm as well as between the simulated and observed BT with appropriate threshold. Employing the single channel TCWV retrieval with a threshold, we discard the cloudy and/or erroneous measurement.

Experimental Cloud Detection

The most challenging task is the quantitative performance analysis of a cloud detection algorithms in the operational environment on a daily basis. Thus, we developed a new concept to quantify the performance of the cloud algorithms. A collocated match-up database with satellite and in-situ buoy measurements is routinely generated in our near real time (NRT) operational sea surface temperature (SST) retrievals and it is true for any operational environments. It is easy to understand the quality of cloud detection algorithm from the collocated measurement of surface and top of the atmosphere (t_{top}) measurements. This has been done as the satellite measured brightness temperature of 410 (T4) channel can be transformed to the surface by single channel retrieval using RT calculated brightness temperature (BT4) and its SST Jacobian and compare with surface measurement (SSTs).

$$rt4 = (T4 - BT4) K(2,1) \quad (3)$$

$$abs(SSTg - rt4 - SSTb) < 1 \quad (4)$$

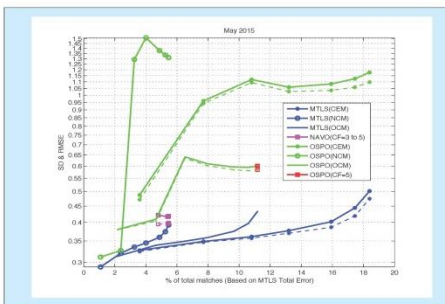


FIGURE 1: RMSE and SD values of three different SST retrievals (MTLS, OSPO, NAVO) for the daytime matches only with three different cloud detection schemes (CEM, OCM, NCM). MTLs and OSPO errors in cross cloud detection schemes.

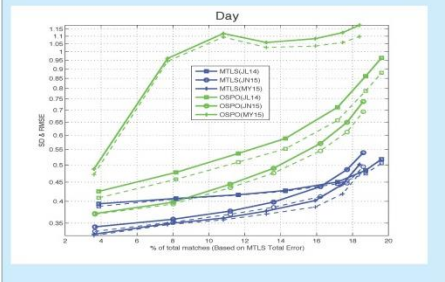


FIGURE 2: RMSE and SD values for OSPO and MTLs for three different months (July 2014, January 2015 and May 2015) under experimental cloud detection filter. (Day only).

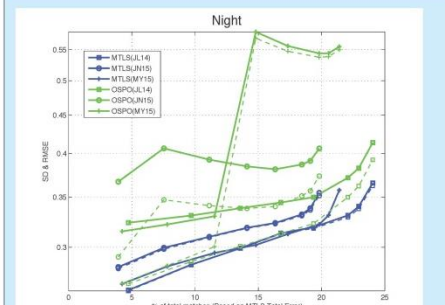


FIGURE 3: RMSE (solid line) and SD (dashed line) values of OSPO and MTLs for three different months (July 2014, January 2015 and May 2015) under experimental cloud detection filter (Night only).

Results & Discussions

Fig. 1 shows that the RMSE values of MTLs, OSPO, NAVO are 0.45 (except last bin), 0.6 (QF=5) and 0.42 (QF=5) and corresponding data coverage of 17.5%, 11% and 4.8% respectively. Even though MTLs suite is performing well above than other two operational products in terms of retrieval error or RMSE and data coverage, we have extended this study in new direction. We have observed that three cloud detection schemes identify three distinct different set of measurement as a cloud free for the same match ups. For example, pixel X is cloud free for A cloud detection scheme, where as same pixel is cloudy for B cloud detection scheme. To understand the ambiguities of mutual consistency between retrieval method and associated cloud detection scheme, we have compared retrieval results with cross platform cloud detection scheme. NAVO retrieval is excluded for cross platform study because this database reports a huge number of SST retrieval is "NAV" and not possible to do proper statistical analysis using other cloud detection schemes. The OSPO and MTLs results under cross platform cloud detection schemes shown in Fig. 1 are grouped using QF of MTLs. It is interesting observation that MTLs retrieval significantly improves as an inversely proportional to the values of data coverage under other two cloud detection schemes. The additional cloud detection and QF of MTLs, which is based on the calculated total error, are also trustworthy with other cloud detection schemes. On the other hand, the OSPO results are severely degraded with other cloud detection schemes, which implies that there may be mutual dependency between their retrieval method and cloud detection scheme. To directly compare the retrieval error due to inverse method, we propose an experimental filter, which can be only used in match up database and trustworthy detection scheme for cloud free measurement. MTLs and OSPO retrievals for three different months (July 2014, January 2015 and May 2015) are compared in Fig. 2 and Fig. 3. It seems from this study that both day and night of OSPO retrievals for the month of May 2015 are degraded due to some other reason apart from the inverse method. MTLs method shows superior performance both day and night according to the total error (RMSE). However, the SD of OSPO for some months is comparable with MTLs for the night (Fig. 3), but the difference of SD and RMSE is high, which implies that bias is high. The bias is the inherent problem for any regression based SST retrieval method. On the other hand, the bias of OSPO retrieval for the day time (Fig. 2) is low, but the RMSE of OSPO is significantly higher than the same of MTLs. The main disadvantage of MTLs suite is that the product error, which is combination of cloud detection and inverse are dependent on the error in ancillary data (profile data of GPS) and approximation error of fast forward RT model. With present available resources, we presented here that the deterministic method can produce better results than stochastic method. Both the errors of forecast model and measurement will be reduced in future due to advancement measurements and forecast model capability.

CONCLUSIONS

Current practice to compare different SST products are based on the total error analysis. Breaking the cloud detection and inverse method errors will be help to improve understanding product quality.

MTLS suite will be a better alternative for VIIRS SST retrieval using present available resources. The QF and additional cloud detection capabilities of MTLs packages make worthwhile to use in operational environment.

References

Koner, P.K., & Drummond, J.R. (2008). A comparison of regularization techniques for atmospheric trace gases retrievals. *J. Quant. Spectrosc. Radiat. Transfer*, 109, 214-226.
Koner, P.K., Harris, A.R. and Maturi, E. (2015). A physical deterministic inverse method for operational satellite remote sensing: an application for SST retrievals. *IEEE Trans. Geosci. & Remote Sens.*, in press.
Koner, P.K., and Harris, A.R. (2015a). A deterministic inversion technique for sea surface temperature retrieval from MODIS radiances. *Proc. SPIE 9459*, Ocean Sensing and Monitoring VII, 94590F (19 Mar 2015), doi: 10.1117/12.2179608.
Koner, P.K., Harris, A.R., and Maturi, E.M. (2015b). Hybrid cloud and error masking to improve the quality of deterministic satellite sea surface temperature retrieval and data coverage, submitted to *Rem. Sens. Environ.*, under review.

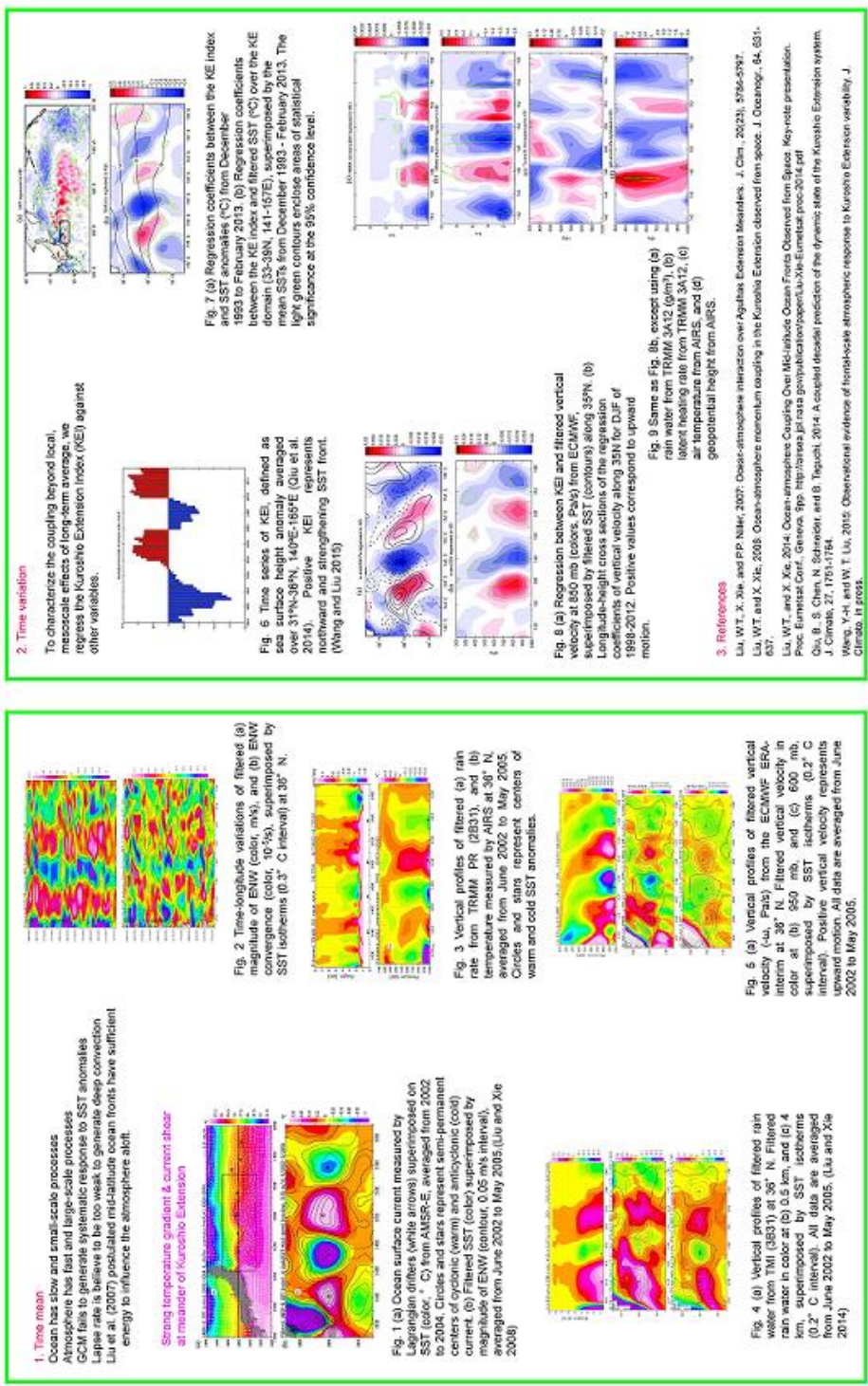
Acknowledgement

This work was funded under NASA Grant number NNX14AP44A. The views, opinions, and findings contained in this report are those of the authors and should not be construed as an official NOAA or US Government position, policy, or decision.

POSTER 16: EFFECTS OF LOW-FREQUENCY FRONTAL SCALE SEA SURFACE TEMPERATURE ON OCEAN-ATMOSPHERE COUPLING

Effect of Low-frequency Frontal Scale Sea Surface Temperature on Ocean-atmosphere Coupling

W. Timothy Liu, Xiaosu Xie, and Yi-Hui Wang
 Jet Propulsion Laboratory, California Institute of Technology, Pasadena, CA
 Email: w.timothy.liu@jpl.nasa.gov



POSTER 17: THE UNCERTAIN HIGH LATITUDE SST SAMPLING ERRORS AND THE REDUCED ERRORS IN SST SEASONAL ANOMALY

UNIVERSITY OF MIAMI
ROSENSTIEL
SCHOOL OF MARINE & ATMOSPHERIC SCIENCE



Seasonal and High Latitude Characteristics of Sampling Errors in IR SST Fields

Yang Liu and Peter J. Minnett

Meteorology and Physical Oceanography, Rosenstiel School of Marine and Atmospheric Science, University of Miami, Miami, Florida, USA



1. Introduction

Clouds and inter-swath gaps are the primary reasons for incomplete coverage of satellite measurements causing sampling errors in averaged satellite SST fields. Previously (Liu & Minnett, 2015) we found that the MODIS monthly sampling error referenced to MUR SSTs is up to 0.13 K, which far exceeds the error threshold needed for climate research. The largest sampling error (> 5 K) is found in the Arctic. The 30°N-30°S zonal band has the smallest errors; a notable exception is the persistent negative errors found in the Tropical Instability Wave area, where the mesoscale ocean-atmosphere interaction leads to a more frequently satellite sampling above the cold sections. The global mean sampling error is generally positive and increases approximately exponentially with missing data fraction, while error variability is mainly controlled by SST variability.

Two questions remain to be explored. First, since the MODIS sampling error was initially calculated based on MUR (Multi-scale Ultrahigh Resolution) SST data (Chin et al. 2010), whether the different SST variability embedded in a different SST reference field causes different sampling error patterns is unknown. Second, can the sampling errors be predicted, for example in terms of the local SST difference from a reference, cloud persistence (the number of consecutive days during which a location is detected to be cloudy), or region and season? That is, can additional, readily-available information be used to predict the sampling errors, and be used to reduce them?

2. Methods and Data

Reference



Mask



1. MUR
2. HYCOM

MUR/HYCOM Sampled by MODIS

$N_{\text{SST}} = \lfloor 1 \text{ day}, 0.25^\circ \text{map} \rfloor$ \rightarrow **Temporal: 3d, 1w, 2w, 1m** $N_{\text{SST}}(K)$
 $N_{\text{SST}} = \lfloor \text{Base resolution} \rfloor$ \rightarrow **Spatial: 0.25°, 0.5°, 1°, 2°, 2.5°, 5°** $N_{\text{SST}}(K)$
 For a grid box L , which has a size represented by the resolution R : $R < L < 5 \cdot R$

Sampling errors: $e_{\text{MUR}}(K) = \sum_{i=1}^{N_{\text{SST}}(K)} \text{SST}_i^{\text{MUR}} - \text{SST}_i^{\text{HYCOM}}$

Reference SST fields:
1. HYCOM reanalysis SST, 1/12° and daily, (HYC)
2. MUR SST, 1km and daily, (MUR)
 IR Mask:
MODIS Terra 4km day and night masks
 Climatology:
OISST, 0.25° and daily (Banzon et al. 2014)
 Study Period:
 Winter: 2010/12/28 - 2011/01/25 Spring: 2011/04/07 - 2011/05/06
 Summer: 2011/07/21 - 2011/08/19 Fall: 2011/10/01 - 2011/10/30

3. Results

3.1 Sampling Error Difference VS Reference SST Difference

• Sampling errors (ERR) in spatial averaged SSTs have a very similar pattern, regardless of the largely different reference fields.

• At low- and mid-latitudes, SST spatial variation represented by HYCOM and MUR are quite similar, thus the sampling error difference (dERR) is small.



Fig. 2 Sampling errors generated from HYCOM and MUR spatial averaged SSTs (upper row). HYCOM-MUR difference of the sampling errors and SSTs (lower row). Note that the dERR is negligible globally except in the polar regions. Boreal winter is shown as an example. Patterns for the HYC_ERR, MUR_ERR, and dERR in other seasons are similar.

3.2 The dependence of dERR

• The persistent pattern exists in the 4-month-mean dERR of [0.25°, mon], even though weakened (Fig. 6).

• The high latitude dERR of spatial averaging remains in the 4-month mean.

• HYC_ERR is generally smaller than MUR_ERR, since dERR is negative skewed while ERRs are both positive skewed.

We also studied the correlated and non-cancelable sampling error on gap fraction (Gap_F, missing data fraction), standard deviation (SD), and cloud persistence (CLD_PST) in Fig. 7.



Fig. 7 The dependence of dERR on HYC_ERR in the (25-mon) averaging case. The color of scatter shows the range of the HYC_SST, Gap_F, HYC_SD, and CLD_PST respectively. The 30°N-50°N boreal winter is shown. Note that the narrower scatter exists at warmer HYC_SST or at larger HYC_SD.

3.3 The reduced sampling error in seasonal anomaly fields.

• The sampling errors are largely reduced in both HYCOM and MUR spatial averaged seasonal anomalies.

• Subtracting the seasonal cycle barely reduces the sampling error in polar regions.



Fig. 8 The sampling errors in seasonal anomalies HYCA (first column) and MURA (second column), and their difference (third column). Spatial averaging case is shown.

• The sampling errors in monthly averaged seasonal anomalies are still large, and are due to daily variations.

• The dERR resembles the previous results of monthly averaged HYCOM and MUR SST.



Fig. 9 Similar to Fig. 10. The monthly averaging case is shown.

• In both spatial and temporal averaging of seasonal anomaly, ERR and dERR increase with latitude in both hemispheres.

• The polar region displays large ERR and dERR, especially when averaging size is one month, 2.5° or 5°.

• The annual sampling error in the SST seasonal anomaly is small at low- and mid-latitudes.



Fig. 10 Zonal mean sampling error of HYCA (first row), MURA (second row), and their difference (third column). Color denotes the resolution.

4. Conclusions

• At low and mid latitudes, the sampling error caused by the seasonal cycle of SST dominates in the annual total sampling error, and displays in a generally consistent geographical pattern between different reference SST fields. This component of the sampling error can be quantified by sampling a climatology reference.

• At high latitudes, the sampling errors remain large in seasonal anomalies and are different when different reference fields are used. These errors are the most uncertain.

• Compared with HYCOM, MUR generates larger sampling errors. This relationship is demonstrated in regions besides the polar area, where the sampling error is not primarily due to the seasonal cycle. This can be caused by the noisier seasonal variation represented by MUR.

• Daily scale variations dominate the sampling errors at high latitudes, because of more robust eddy activity, and also affect sampling errors in regions of low- and mid- latitudes, where the eddy variability is important especially when considering monthly averaging. Therefore, the characteristics of the reference SST field does matter in eddy regions.

4. Acknowledgement

The initial stages of this research were supported by a grant from the NASA Physical Oceanography Program (NNX11AF26G) and then by a NASA graduate fellowship to Y. Liu (NNX14AL28H). This work has benefited from discussions with colleagues, including R. H. Evans, K.A. Kilpatrick, S. Walib, and Mike Chin.

Reference

Banzon, V.F., Reynolds, R.W., Stokes, D., & Xie, Y. (2014). A 1/4° Spatial-Resolution Daily Sea Surface Temperature Climatology Based on a Blended Satellite and in-situ Analysis. *Journal of Climate*, 27, 8221-8224.

Chin, T.M., Jorg, V., & Armstrong, E. (2010). Algorithm Theoretic Basis Document: Multi-scale, multi-composited analysis of sea surface temperature. Version 1.1.

Liu, Y. & Minnett, P. J. (2015). Global Sampling Errors and Error Variability of MODIS Sea-Surface Temperatures. *Remote Sensing of Environment*. (in revision)

POSTER 18: VALIDATION OF MET OFFICE OSTIA DIURNAL ANALYSIS USING ARGO FLOATS

Validation of Met Office OSTIA Diurnal Analysis Using Argo Floats

Chongyuan Mao⁽¹⁾, James While⁽¹⁾, Matthew Martin⁽¹⁾ and Alison McLaren⁽¹⁾

Introduction

The Met Office has developed a new analysis product of the diurnal cycle of skin sea surface temperature (SST, While et al., *in prep*), made freely available through the Copernicus Marine Environment Monitoring Service (CMEMS): <http://marine.copernicus.eu/> (formerly known as MyOcean). This product is a combination of the Operational Sea surface Temperature and Ice Analysis (OSTIA; also available from CMEMS) foundation SST, a warm layer model and a cool skin component. Observations from the satellite instruments SEVIRI, GOES-W, MTSAT2 and NOAA-AVHRR are assimilated into the warm layer model using a 4DVar like scheme.

In this study, satellite SSTs and Argo Near-Surface Temperature (NST) profiles with high vertical resolution were used to validate the OSTIA and diurnal cycle analyses. A standard procedure for adjusting the un-pumped Argo NST profiles against calibrated pumped measurements was set up (Carse et al. 2012), to maximise the accuracy of the validation. The study focused on the Atlantic Ocean during September – November 2014, as the geostationary satellite used (SEVIRI) covered mainly the Atlantic Ocean and southwest Indian Ocean.

Schematic of Diurnal Analysis System

Comparisons between satellite data and the diurnal analysis system

Daily time series of the mean error (dashed lines) and root mean square (RMS, solid lines) over the global ocean for the two satellites that were assimilated in the warm layer model: SEVIRI (actual domain is Atlantic Ocean and southwest Indian Ocean) and NOAA-AVHRR. Note, here we focused on validating the warm layer component, where observations were assimilated into the system, thus foundation SSTs were calculated for each satellite and removed from original SST observations.

The tables show the average statistics and number of observations for O-B (warm layer SST before data assimilation) and O-A (after data assimilation) over the global ocean and main domains (based on MyOcean domains) covered by SEVIRI and NOAA-AVHRR. Bold numbers indicate the statistics improved for the O-A field. It is clear that data assimilation has improved the performance of the warm layer model in all domains.

¹MTSAT2 and GOES-W experienced issues receiving correct data during Sep – Nov 2014 and were not assimilated over this period

Area Name	Mean Error		RMS		Correlation		Number of Observation
	O-B	O-A	O-B	O-A	O-B	O-A	
Global Ocean	0.08	0.04	0.41	0.38	0.27	0.42	242583
North Atlantic	0.07	0.04	0.40	0.38	0.27	0.39	43913
Tropical Atlantic	0.05	0.02	0.38	0.35	0.19	0.40	79837
South Atlantic	0.11	0.05	0.42	0.38	0.31	0.45	59455
Indian Ocean	0.10	0.06	0.44	0.40	0.28	0.42	44594

Area Name	Mean Error		RMS		Correlation		Number of Observation
	O-B	O-A	O-B	O-A	O-B	O-A	
Global Ocean	0.22	0.12	0.47	0.39	0.30	0.51	193974
North Atlantic	0.15	0.08	0.44	0.39	0.31	0.49	20844
Tropical Atlantic	0.28	0.15	0.45	0.36	0.23	0.49	14191
South Atlantic	0.30	0.14	0.54	0.43	0.33	0.53	16258
Indian Ocean	0.25	0.13	0.49	0.39	0.34	0.56	30522

Standard pre-processing of un-pumped Argo NST profiles

Some Argo floats (e.g. APEX) switch off the CTD pump at 5 dbar and the sensors continues to collect data every 6 seconds up to the surface. These un-pumped values need to be calibrated against pumped values

Original profile including pumped (red star, calibrated) and un-pumped (blue circle) values

Adjust un-pumped values against pumped values using linear interpolation

Remove mixed air/water temperature values where $\Delta p < 0.5$ dbar

Final Argo NST profile with Foundation SST and Foundation SST + warm layer SST

Comparisons between Argo NST and OSTIA SSTs

Mean error, standard deviation and standard error of Argo-OSTIA matchups (Argo minus OSTIA SST_{10d}) were calculated for each 1 dbar layer (0-1, 1-2, ... 10-11) using daytime profiles that showed significant diurnal signal.

Argo NST values agree best with OSTIA SST_{10d} close to 4 dbar (~3 meters), which is consistent with previous studies (e.g. Carse et al., 2012).

Argo SST_{10d} = Argo SST₀₋₁ minus Argo SST₄ (closest to 4 dbar within 3-5 dbar range).

Argo SST_{10d} is warmer than warm layer SST, suggesting the current system underestimates the diurnal cycle.

Data assimilation improves the overall statistics of the matchups (Argo SST_{10d} minus warm layer SST).

Statistics	Foundation SST (3-4 dbar)		Warm Layer Background (dSST)		Warm Layer Analysis (dSST)	
	DW	All	DW	All	DW	All
Mean Error	-0.07	0.08	0.31	0.004	0.26	-0.007
Standard Deviation	0.37	0.78	0.55	0.15	0.51	0.15
Standard Error	0.06	0.02	0.093	0.004	0.096	0.004

²DW = Diurnal Warming. Statistics obtained using Argo floats showing diurnal warming

Conclusions & Future Work

- Argo NST proves to be a very useful tool to validate OSTIA SSTs. OSTIA foundation SST agrees best with Argo NST at 4 dbar (~ 3 meters) and OSTIA warm layer SST agrees best with Argo NST 0-1 dbar bin.
- Data assimilation improves the RMS and mean error of the diurnal analysis system, as well as the statistics of the 0-1 dbar for warm layer dSST.
- Current diurnal analysis potentially underestimates the range of the diurnal cycle.
- Future plan is to validate the final product, skin SST, potentially using ship-board radiometer.

Acknowledgements:

The authors would like to thank Fiona Carse (Met Office) and Justin Buck (BOCC) for their advice on obtaining Argo data and associated data processing.

Reference:
 Carse, F., J. Buck and J. Turton (2012). Near-surface temperature profiles from pumped and un-pumped Argo measurements. poster at Argo Science Workshop, Venice, September 2012
 While, J., C. Mao, M. Martin, J. Roberts-Jones, A. McLaren and P. Sykes, An operational analysis system for the global diurnal cycle of sea surface temperature: implementation and validation, *in preparation*.

¹Met Office FitzRoy Road, Exeter, Devon, EX1 3PB United Kingdom
 Tel: +44 1392 885008 Fax: +44 1392 885681
 Email: chongyuan.mao@metoffice.gov.uk

POSTER 20: BIAS AWARENESS IN OPTIMAL ESTIMATION OF SEA SURFACE TEMPERATURE



www.esa-sst-cci.org

Biases in Optimal Estimation of Sea Surface Temperature

Chris Merchant and Jon Mittaz
 University of Reading

Problem addressed:

Optimal estimation techniques implicitly assume zero prior bias and zero bias of measured radiances relative to the forward model. These assumptions are rarely valid at ~0.1 K accuracy levels. Off-line parameterisation of biases is possible, but can bias estimation be done better within the retrieval itself?

Key points:

1. Simulation study of bias-aware optimal estimation, in which we know the truth and can assess results
2. Problem is ill-posed for a single retrieval, but bias parameters can be estimated over many orbits
3. Approach shows promise, but doesn't dispense with need to understand the form of systematic errors

BACKGROUND: OPTIMAL ESTIMATION

The classic OE equation is:

$$\hat{x} - x_o = S_o K^T (K S_o K^T + S_e)^{-1} (y - F[x_o]) = G(y - F)$$

The estimated SST will be unbiased if there are no prior or radiance biases, but in practice there are:

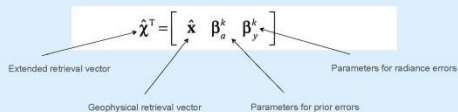
$$\hat{x}' + e_x - (x_o' + e_o) \cong G(y' + e_y - (F[x_o'] + Ke_o))$$

and there is a corresponding systematic error in retrieval of

$$e_x = Ge_y + (I - GK)e_o$$

INVESTIGATED SOLUTION

Extend the retrieved vector to include parameters that represent the biases. Since there will then be many more retrieved quantities than measured radiances, the bias parameters need to be estimated progressively over many observations.



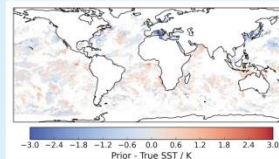
PRECEDENT FOR THIS APPROACH

Bias-aware data assimilation is already widely implemented for numerical weather prediction. The equations for bias-aware optimal estimation are entirely analogous.

Dee, D. P., 2005: Bias and data assimilation. *Quarterly Journal of the Royal Meteorological Society*, **131**, 3323-3343. 10.1256/qj.05.137

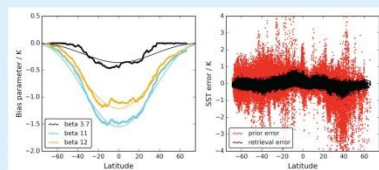
CASE STUDY: AVHRR & PINATUBO AEROSOL

Data: from a simulator of AVHRR observations informed by true orbit geometry and cloud cover, with full simulation of instrument and calibration errors.



The radiance bias is caused by latitude dependent "stratospheric aerosol", as followed the Pinatubo eruption, which is not simulated in the forward model for the retrieval.

No prior knowledge of the relative impact of such aerosol on different thermal channels is assumed.



The smooth curves are the imposed aerosol biases, the thick lines are the retrieved radiance biases. The bias aware OE provides significant insight into the relative aerosol impact. SST retrieval errors have some latitudinal structure, since the bias estimation is not perfect.


CONCLUSION

Progressive estimation of radiance biases has been demonstrated in a realistic simulation study.

Although not a "black-box" solution, bias aware OE should be explored for other OE SST bias problems.





POSTER 21: INFRARED RADIOMETERS ON SHIPS OF OPPORTUNITY FOR SATELLITE-DERIVED SEA-SURFACE TEMPERATURE VALIDATION



An Update on MODIS and VIIRS Sea-surface Temperatures

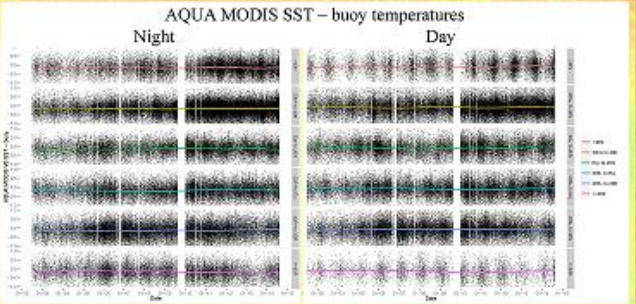
Peter J Minnett, Kay Kilpatrick, Gui Podestá and Elizabeth Williams
 Rosenstiel School of Marine and Atmospheric Science, University of Miami, Miami, USA

The clear-sky atmospheric correction algorithms for the retrieval of skin sea-surface temperature from the top-of-atmosphere brightness temperatures from the Terra and Aqua MODIS's and the S-NPP VIIRS are based on the traditional Non-Linear SST formulation. They continue to be refined, primarily through the analysis of the Match-up Data Bases with in situ measurements from drifting buoys, taken from NOAA's iQuam data set and ship radiometers. Matchups are within 30 minutes and 10 km. About 18% of all available night-time matchups pass acceptance tests and of these, ~20% are used for determining the coefficients for the NLSST algorithm and ~10% are used to assess errors and uncertainties.

MODIS

Both Terra and Aqua MODISs continue to perform very well despite both being far beyond the planned lifetimes. Plots show matchups between buoys and SST (11, 12 μm) for the Aqua mission, segregated into latitude zones. These are for Collection 6 which has just been released. A problem with cloud screening has been identified and will be corrected in the next release.

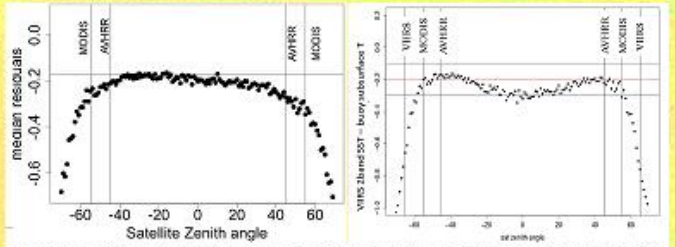


VIIRS

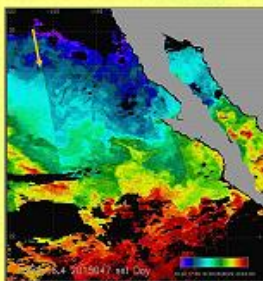
To improve the accuracy of the VIIRS SSTs at high zenith angles (θ) two extra terms, in θ and θ^2 are included in the atmospheric correction algorithm:

$$SST = a_0 + a_1 T_{11} + a_2 (T_{11} - T_{12}) T_{sfc} + a_3 (\sec(\theta) - 1) (T_{11} - T_{12}) + a_4(\theta) + a_5(\theta^2)$$

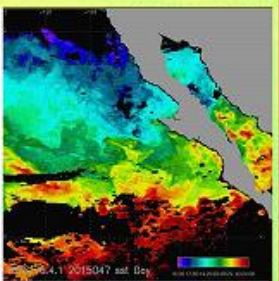
The accuracy at high zenith angles has improved, but still shows a significant negative deviation. The θ terms reduces the asymmetry in the errors, which is indicative of a response vs scan angle effect (r_{vs}) which in VIIRS would be caused by the half-angle mirror. An unwanted consequence of the θ^2 term is a negative bias in the retrievals in the center of the swath. The asymmetry in the errors has also been reduced by the linear term in the zenith angle. However, even though an improvement in the errors follows from adding the additional terms, these were empirically derived, and a more robust algorithm will be sought based on the physics behind the retrievals.




Dependence of VIIRS skin SST errors as a function of satellite zenith angle (standard NLSST; left). The zenith angle limits for the SST retrievals for AVHRR Pathfinder (45°) and MODIS (55°) are also shown. The median residual error (K) shows a marked increase with large satellite zenith angles. The asymmetry of the errors is indicative of an r_{vs} effect. The expected offset due to the mean skin effect is shown by the grey horizontal line at -0.17K. At right, the atmospheric correction algorithm includes the additional terms



The linear feature (arrow) is believed to be from an r_{vs} effect, and is apparent at swath overlaps. The feature is reduced (right), when the atmospheric correction algorithm includes the additional θ and θ^2 terms.




Poster 23



16th International Science Team Meeting (GHRSSST XVI)
 20th-24th July 2015
 European Space Agency ESTEC, The Netherlands.


Acknowledgements: Funding from NASA
 Physical Oceanography Program and
 NOAA NESDIS STAR

POSTER 22: AN UPDATE ON MODIS AND VIIRS SEA-SURFACE TEMPERATURES





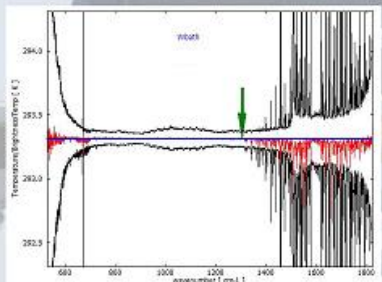
Infrared radiometers on ships of opportunity for satellite-derived sea-surface temperature validation

Peter J Minnett, Goshka Szczodrak, Miguel Izaguirre, Elizabeth Williams, & Michael Reynolds*
 Rosenstiel School of Marine and Atmospheric Science, University of Miami, Miami, USA
 *Remote Measurement & Research Co, Seattle,

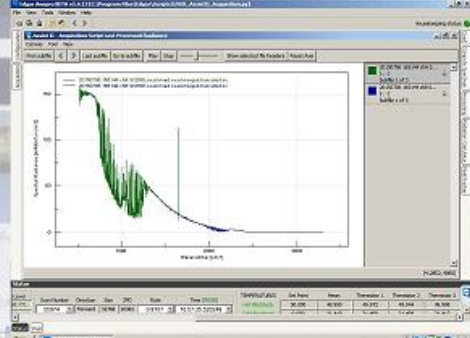


Two Marine-Atmospheric Emitted Radiance Interferometer (M-AERI) Mk2s have been installed on two cruise ships of Royal Caribbean Cruise Lines, the *Allure of the Seas* and *Celebrity Equinox*. These instruments are capable of autonomous operation, and are monitored and controlled from RSMAS through a satellite internet link. The limited bandwidth allows a remote desktop to function and for housekeeping data and a subset of data to be transmitted to shore in real-time. Raw data are written to external disks that are periodically exchanged when the ships are in port.

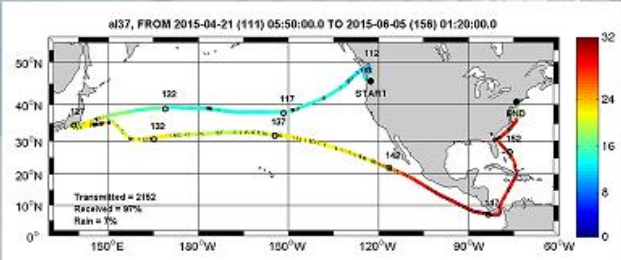


Before deployment the M-AERIs undergo a rigorous laboratory calibration against a NIST-traceable water-bath blackbody target. The figure shows the mean spectrum measured by the M-AERI (red) with the envelope of one standard deviation (black). The blue line is the target temperature, and the green arrow shows the wavenumber at which the skin SST is derived. The calibration error is <10 mK.




An example of the infrared spectrum of atmospheric emission at zenith taken by an M-AERI Mk2 on the *Celebrity Equinox* at 16:51:44 UTC on July 6, 2015. This is a screen capture from a computer at RSMAS connected to the computer on the *Celebrity Equinox* that is controlling the M-AERI Mk2.

An Infrared SST Autonomous Radiometer (ISAR) is running on the commercial ship *M/V Andromeda Leader* that plies between Japan and the USA. ISAR data are reported in real-time via an Iridium data link.



A recently completed track of the *M/V Andromeda Leader*, colored by the skin SST measured by an ISAR according to the temperature scale at right, in °C.




Within the framework of GHRSSST and ISSI Study Group, a consistent format for radiometer data and metadata has been defined to facilitate data exchange. A data archive has been identified,

16th International Science Team Meeting (GHRSSST XVI)
 20th-24th July 2015
 European Space Agency ESTEC, The Netherlands.

Acknowledgements: Funding from NASA Physical Oceanography Program and support from Royal Caribbean Cruise Lines.

Poster 22



Page 187 of 225

POSTER 25: SST USER WORKSHOP ON UNCERTAINTIES

SST user workshop on uncertainties

Nick Rayner, Chris Merchant, Gary Corlett, Jon Mittaz, Claire Bulgin, Chris Atkinson, Simon Good and John Kennedy

Two-way discussion between SST data providers and users to create a common understanding of:

- where this uncertainty comes from;
- how to talk about it;
- how well the uncertainty information that is provided addresses users' needs;
- and how to practically use such uncertainty information.

It achieved this through a mixture of oral and poster presentations, activities and group discussions.

Consistent Terminology is important

Error: Difference of the measured value from the true value, from both random and systematic effects

Uncertainty: Doubt in the measurement

Correction: Some errors can be corrected, but there will always be an unknown residual error adding to the uncertainty

Traceability: Chain to the reference

Practical sessions

A series of short practical sessions – full, worked solutions are available with the workshop report

- working with prepared subsets of the SST CCI data
- allowed users to get to grips with the data
- allowed the organisers to see users getting to grips with the data

What would you like to do now (ignoring technical challenges)?

Example: Assessment of climate model simulations

- Compare different versions of model to observations
- Currently, observational uncertainty assessed using two different data sets
- Would like to make use of well validated uncertainty estimates and full error covariances. (But need to expand CF naming convention.)

Future landscape

- Resolution and timeliness
 - Real time processing; information about the daily cycle
 - Smaller grids e.g. 1km
- Diverse and better characterised observing system
 - Better metadata; wider variety of instruments: Argo, gliders, etc; citizen measurements
- More computing power
- Better treatment of uncertainty, treat analytically
- Easier to send and process lots of data
- Coupled reanalyses using observational error correlation
- NWP: ensemble systems, diurnal SST variability, coupled

Current applications of uncertainty information

- Reanalyses using ensembles of SST as forcing
- Detection and attribution
- High-resolution ensembles to investigate air-sea interactions
- Ocean analyses for seasonal forecasting
- Characterise uncertainty and error in situ
- Assessment of climate model simulations
- Ensembles of gridded global surface temperature
- Sensitivity of ensemble-weather forecasts to different analyses
- Creation of gap-filled SST analyses
- Reanalyses of regional and global oceans

Uncertainty verification

- Verification maps were welcomed by users
- Traceability also thought important
- Reputation of producers key to confidence in uncertainty estimates

Provision of Covariance Information

- Ensembles not always best
- Explicitly forming covariance matrix can be prohibitive
- Parameterise covariance instead
- Provide guidance and clear examples, e.g. What shape are the error distributions?
- Parameterize the distribution shapes, provide examples
- Guidance on the strengths, limitations and characteristics of the methods is needed as well as how to interpret 'features'.

Provision of Ensembles

- Ensemble size 10-1000
 - A single central member, preferred by the data producer
 - A randomly-ordered set of ensemble members so that users can pick at random
- Start ensemble generation from Level 1 (radiances) in order to include structural uncertainties
- Clearly stated underlying assumptions
- Ensemble produced on 0.05 degrees and coarser
- An operationally available ensemble or an operationally available best estimate with the ensemble later
- Updates must truly belong to the same ensemble member
- Clear, non-confusing terminology e.g. are members "equally likely"?

Outcomes

- Draft user requirements will be analysed and incorporated, as appropriate, into the next revision of the SST CCI User Requirements Document, due late 2015



The full workshop report is on the SST CCI web site <http://www.esa-sst-cci.org/PLUS/workshop.htm>

A summary was published: Rayner, N. A., C. J. Merchant, and G. K. Corlett (2015). Communicating uncertainties in sea surface temperature, *Eos*, 96, doi:10.1029/2015EO030286. <https://eos.org/news-reports/communicating-uncertainties-in-sea-surface-temperature>

POSTER 27: PREPARING OSI-SAF SEVIRI/MSG SST REPROCESSING 2004-2012

Preparing OSI-SAF MSG/SEVIRI SST reprocessing 2004-2012

S. Saux Picart, C. Merchant, S. Péré, A. Marsouin

Introduction

The Ocean and Sea-Ice Satellite Application Facility (OSI-SAF) of the European Organisation for the Exploitation of Meteorological Satellites (EUMETSAT) is currently planning for the reprocessing of Sea Surface Temperature (SST) from Spinning Enhanced Visible and Infrared Imager/Meteosat Second Generation (SEVIRI/MSG) archive (2004-2012). Many scientific decisions have to be made regarding the methods and algorithms used for the reprocessing. The objectives of this study are to assess the current OSI-SAF operational processing of SST, to provide a reference for the reprocessing and to help make the right decisions in the implementation of the reprocessing. The current OSI-SAF processing chain is in operation since 2011. It runs a non-linear split-window algorithm and includes the algorithm correction scheme developed by Le Borgne et al. (2011). We have analysed one year of collocation between the OSI-SAF SST Meteosat 09 product and drifting buoys. Results are also compared to those obtained by optimal estimation (OE) following Merchant et al. (2013).

Overview

Characteristics of the reprocessing:

- Covers 2004-2012 (Climate SAF reprocessed cloud mask)
- Region -60 to +60° N and E (final product)
- Regular 0.05° latitude/longitude grid
- Methods of retrieval: Algorithm correction (Le Borgne et al., 2011) and/or Optimal Estimation (Merchant et al., 2013)

Input data to the reprocessing are as follow:

- Level 1.5 MSG/SEVIRI data reprocessed by EUMETSAT (the main difference is the calibration of infrared channels)
- The radiative transfer model RTTOV is used to perform brightness temperature for each pixel. It requires:
 - ECMWF ERA-interim temperature and water vapour profiles
 - OSTIA SST
- Climate SAF reprocessed cloud mask (based on Nowcasting SAF)
- ERA CLIM *in situ* dataset for validation purpose

Methods

Two methods for SST retrieval are being tested for the reprocessing: 1) The algorithm correction suggested by Le Borgne et al. (2011) and 2) the Optimal estimation (triple, smooth) suggested by Merchant et al. (2013). For that purpose we use the matchup dataset collected operationally for Meteosat09 in 2012.

Algorithm correction (Le Borgne et al., 2011): Determine algorithm systematic errors using simulation of brightness temperature from radiative transfer model forced by NWP output.

Optimal Estimation (Merchant et al., 2013):

$$\hat{x} = x_n + (K^T S_e^{-1} K + S_x^{-1})^{-1} K^T S_e^{-1} (y_0 - F(x_n))$$

where $\hat{x} = \begin{bmatrix} x \\ \bar{x} \\ \bar{y} \end{bmatrix}$. Here we also retrieve the averaged SST surrounding the point in consideration. This is a modification from Merchant et al. (2013) which seem to provide better results.

Chi-square statistic:

$$\chi^2 = (K\hat{x}' - y')^T (S_e (K S_n K^T + S_e)^{-1} S_e)^{-1} (K\hat{x}' - y')$$

where $y' = y_0 - F(x_n)$ and $\hat{x}' = \hat{x} - x_n$.

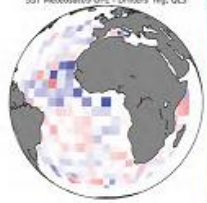
Results

Statistics of comparison against drifting buoys (2012):

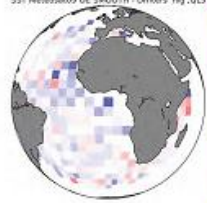
Day			OE			Night			OE			
Quality level	N	bias Std	bias Std	bias Std	Quality level	N	bias Std	bias Std	Quality level	N	bias Std	bias Std
3-4-5	176764	-0.01 0.53	-0.00 0.49		3-4-5	119064	-0.04 0.54	-0.06 0.51				
3	39806	-0.02 0.65	-0.03 0.60		3	26252	-0.05 0.67	-0.10 0.62				
4	53010	-0.01 0.54	-0.01 0.50		4	38045	-0.02 0.56	-0.06 0.52				
5	83948	0.01 0.44	0.02 0.42		5	54767	-0.04 0.45	-0.05 0.44				

Maps of binned average difference (2012):

Algorithm correction



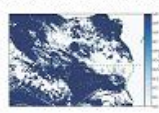
Optimal estimation



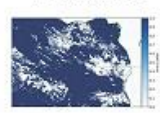
Cloud mask comparison:

Comparison of Climate SAF reprocessed cloud mask against OSI SAF cloud mask control used in MSG/SEVIRI operational chain.


Climat SAF: best quality level



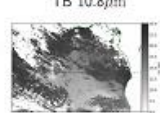
Operational MSG



Difference



TB 10.8µm



Conclusion

Where we are in the reprocessing:

- Level 1.5 reprocessed by EUMETSAT have been downloaded.
- Simulated brightness temperature are being computed using RTTOV.
- Tests for Saharan Dust Index (SDI) are being performed.
- Make more tests on OE and algorithm correction comparison (can we use the chi-square statistic to assign quality level?).
- Set up a procedure for cloud mask control.
- Exploit ERA CLIM *in situ* dataset.

Le Borgne, P., Roguet, H. and Merchant, C. Estimation of Sea Surface Temperature from the Spinning Enhanced Visible and Infrared Imager, improved using auxiliary weather prediction. Remote Sensing of Environment, 2011, 115, 50-65.
 Merchant, C., Le Borgne, P., Roguet, H. and Legendre, G. Extended optimal estimation techniques for sea surface temperature from the Spinning Enhanced Visible and Infra-Red Imager (SEVIRI). Remote Sensing of Environment, 2011, 131, 287-297.

GHRSSST XVI - 20-24 July 2015
stephane.sauxpicart@meteo.fr

POSTER 29: UPWELLING CHARACTERISTICS FROM SST GRADIENTS IN THE PERU/CHILE COASTAL SYSTEM

INTRODUCTION/METHODOLOGY

Mean SST gradient magnitudes were calculated from Oct-Nov 2011 in an area off the South American Coast between 35°S to 0°S and 90°W to 70°W. Data sets included the 0.25 degree Reynolds NCDC data set, and the 1km gridded Multi-Scale Ultra-High Resolution (MUR) SST data set. The model simulation is based on a Latitude/Longitude/pole-Cap (LLC) configuration of the MIT general circulation model. The LLC grid has 13 square tiles with 4320 points on each side (hereafter called LLC4320). Two primary goals were to determine the relationship between the magnitude of the SST gradients and upwelling intensity as identified by the vertical velocity, along with a comparison of upwelling scales identified by the different data sets. The primary goal was to determine if the magnitude of the SST gradients were related to upwelling strength over the intraseasonal to seasonal time scales.

To determine the relationship over the intraseasonal time scales eigenmodes were extracted for LLC4320, MUR, and NCDC gradients, along with the vertical velocity, over the period Oct-Nov, of 2011. SST gradients using only MUR and NCDC were calculated over the time period from 2003-2014 and the annual cycle extracted. Results for the annual cycle were compared with the know historical results off the Peru Chile Coast.

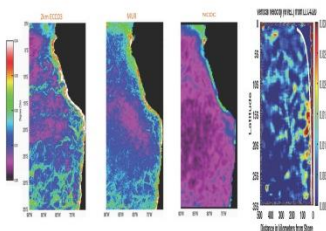


Figure 1: Mean SST Gradients (left three panels) and Vertical Velocity (right panel) for the 2km LLC4320, MUR, and NCDC for Oct.-Nov

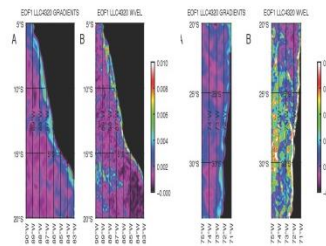


Figure 2: First EOF of the magnitude of the SST gradients and vertical velocity for LLC4320 for the Northern (left panels) and Southern (right panels) Regions for LLC4320.

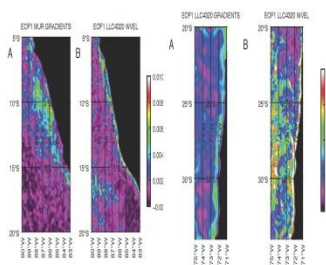


Figure 3: First EOF of the magnitude of the SST gradients and vertical velocity for MUR and vertical velocity for LLC4320 for the Northern (left panels) and Southern Hemispheres (right panels).

UPWELLING CHARACTERISTICS FROM SST GRADIENTS IN THE PERU/CHILE COASTAL SYSTEM

Jorge Vazquez-Cuervo *Jet Propulsion Laboratory/California Institute of Technology*
 jorge.vazquez@jpl.nasa.gov
 Boris Dewitte *LEGOS, Toulouse, France*
 Dimitris Meemenlis *Jet Propulsion Laboratory/California Ins*
 Toshio M. Chin *Jet Propulsion Laboratory/California Ins*
 Edward M. Armstrong *Jet Propulsion Laboratory/California Ins*

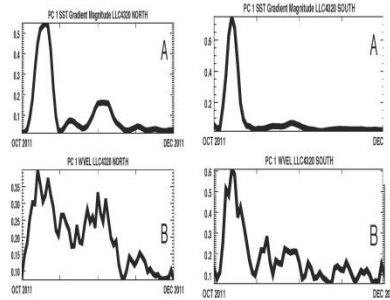


Figure 4: First principal component of the magnitude of the SST gradient and the vertical velocity for LLC4320 for the top panel (Northern Region) and the bottom panel (Southern Region).

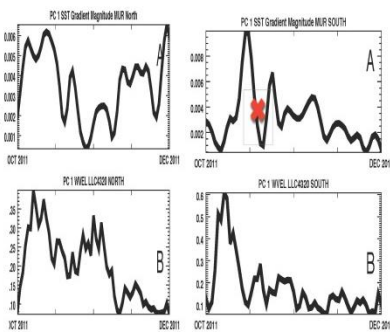


Figure 5: First principal component of the magnitude of the SST gradient from MUR and the vertical velocity for LLC4320 for the top panel (Northern Region) and the bottom panel (Southern Region).

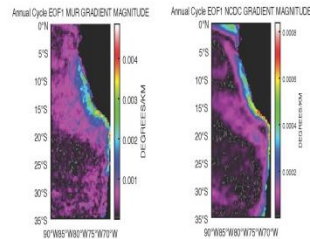


Figure 6: First EOF showing the annual cycle for MUR (left) and NCDC (right)

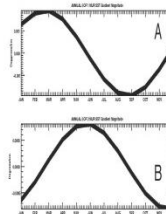


Figure 7: First (top) and second (bottom) principal components of the annual cycle of the magnitude of the SST gradients from MUR.

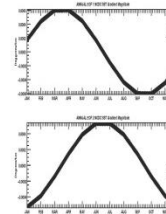


Figure 8: First (top) and second (bottom) principal components of the annual cycle of the magnitude of the SST gradients from NCDC

Parameter/Data Set	Latitude Band	Upwelling Scale
Theory	35°S-25°S	16km
Theory	25°S-15°S	25km
Theory	15°S-5°S	45km
MUR	35°S-25°S	14km
MUR	25°S-15°S	37km
MUR	15°S-5°S	38km
LLC4320	35°S-25°S	16km
LLC4320	25°S-15°S	28km
LLC4320	15°S-5°S	26km
NCDC	35°S-25°S	51km
NCDC	25°S-15°S	50km
NCDC	15°S-5°S	47km
WSAT	35°S-25°S	158km
WSAT	25°S-15°S	200km
WSAT	15°S-5°S	62km
WVEL	35°S-25°S	15km
WVEL	25°S-15°S	23km
WVEL	15°S-5°S	10km

Table 1: Upwelling Scales based on Gaussian fit to offshore SST gradients

CONCLUSIONS

A comparison of derived upwelling scales off the South American Coast is done using output from a high-resolution 2km run of the MIT general ocean circulation model (LLC4320) and satellite derived observations of SSTs. Observations based on the NOAA National Climatic Data Center (NCDC) SST data and NASA's Multi-Scale Ultra High Resolution (MUR) SST data are used. Spatial correlations between LLC4320 and MUR were 0.6 while between LLC4320 and NCDC the correlation was 0.4. Thus even at the higher resolution, with respect to the model, the correlation with MUR was greater. The correlation between the principal components of the magnitude of the SST gradients from both LLC4320 and MUR and the vertical velocity are statistically significant above 0.5. Over the seasonal time scale maximum gradients in the Austral Fall time frame were consistent with historical results. Based on the relationship with vertical velocity as measured by the LLC4320 the magnitude of the SST gradients are a good indicator of upwelling intensity from the intraseasonal to the seasonal time scale.

POSTER 30: THE IMPACT OF THE OCEAN THERMAL SKIN LAYER ON AIR-SEA INTERFACIAL HEAT FLUXES

The Impact of the Ocean Thermal Skin Layer on Air-Sea Interfacial Heat Fluxes

UNIVERSITY OF MIAMI
 ROSENSTIEL SCHOOL of MARINE & ATMOSPHERIC SCIENCE

Air-Sea Interfacial Heat Fluxes

Elizabeth Wong; Peter J. Minnett,
 University of Miami, Rosenstiel School of Marine and Atmospheric Science,
 4600 Rickenbacker Causeway, Miami, FL, 33149

Introduction

Upper ocean heat content (OHC) (0-700 m) has been increasing at a rate of 0.27 W/m² with an average warming of 0.18°C from year 1955-2010 (Levitus et al., 2012). This warming is largely attributed to anthropogenic effects of an increase in atmospheric greenhouse gases which absorb and re-emits much of the longwave radiation (LW_o) back to the Earth's surface. However, the penetration depth of LW_o extends to micrometer scales (fig. 1), where the thermal skin layer (TSL) exists, and does not directly heat the upper few meters of the ocean.

This study aims to answer the conundrum of the mechanism as to how absorption of incident LW_o causes an increase in upper OHC.

We hypothesize the heat lost through the air-sea interface which is controlled by the TSL, modulates the amount of heat stored in the upper few meters of the ocean and is a key component to this study.

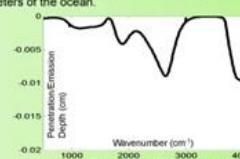


Fig 1. Plot of penetration depth with wavenumber (Bertie and Lan, 1999).

Methods and Data

An infrared (IR) spectrometer called the Marine-Atmospheric Emitted Radiation Interferometer (MAERI) (fig. 2) is used to obtain radiance spectra measurements of the total radiation emitted by the sea surface, $I_m(\nu)$ (ν):

$$I_m(\nu) = - \int_0^{\infty} B(\nu, T(z)) \frac{d\tau}{dz} dz, \quad \tau = e^{-\alpha z}$$

Planck's function

The TSL vertical profile is retrieved from $I_m(\nu)$ through the use of the Truncated Singular Value Decomposition technique with the inclusion of an iteration to obtain better estimates of the end-points of the first-guess profile (fig. 3). This is to enable convergence to occur and obtain a physically reasonable monotonic TSL temperature profile which increases with depth.

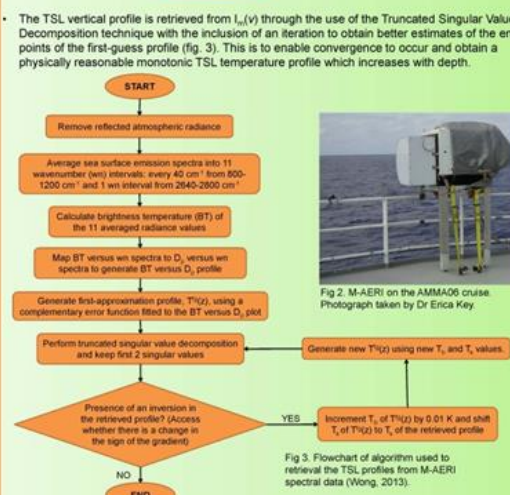


Fig 3. Flowchart of algorithm used to retrieve the TSL profiles from MAERI spectral data (Wong, 2013).

Two cruises are analyzed. The R/V Mirai during the Nauru 1999 expedition which sailed in the tropical Pacific ocean from June to July 1999 and the R/V Ron Brown cruise during the African Monsoon Multidisciplinary Analysis 2006 (AMMA06) campaign which sailed in the sub-tropical Atlantic Ocean from May to June 2006.

- Effects of solar radiation, precipitation and high winds of > 10 m/s are filtered out such that the focus would be on the effects of the TSL and longwave radiative fluxes.
- The temperature difference, ΔT , derived from 5 viscous layer models will also be analyzed and compared with the field results.

References

Bertie, J., and Z. Lan (1999). Infrared intensities of liquids XX. The intensity of the OH stretching band of liquid water revisited, and the best current values of the optical constants of H₂O. *Applied Spectroscopy*, 53(8), 1047-1055.

Donlon, C. J., P. J. Minnett et al. (2002). "Toward improved validation of satellite sea surface skin temperature measurements for climate research." *Journal of Climate* 15, 353-369.

Farrell, C., E. Bradley, et al. (1998). "Cool-skin and warm-layer effects on sea surface temperature." *Journal of Geophysical Research*, 103(C1): 1295-1308.

Levitus, S., J. I. Antonov, T. P. Boyer, O. K. Baranova, H. E. Garcia, R. A. Locantini, A. V. Mishonov, J. R. Reagan, D. Seidel, E. S. Yarosh, M. M. Zwarg, (2012). World ocean heat content and thermosteric sea level change (0-2000 m), 1955-2010. *Geophysical Research Letters*, 39(10), L10603.

Liu, W. T., K. Kubota, et al. (1978). "Sub-penetration of air-sea exchanges of heat and water vapor including the molecular components at the interface." *J Atmos Sci*, 35, 1722-1738.

Saunders, P. M. (1967). "The temperature at the ocean-air interface." *J Atmos Sci*, 24, 205-214.

Soloviev, A. V. and P. Schissel (1994). "Parameterization of the cool skin of the ocean and of the air-ocean gas transfer on the basis of modeling surface renewal." *Journal of Physical Oceanography* 24, 1330-1346.

Wong, E. (2013). Retrieval of the skin sea surface temperature using hyperspectral measurements from the Marine-Atmospheric Emitted Radiation Interferometer. MSc. Thesis, University of Miami, Miami.

Zhang, Y. and X. Zhang (2012). "Ocean thermal skin layer and turbulent surface convection." *J Geophys Res*, 117(C04017): 15.

Results

An increase in LW_o is found to be associated with a decrease in net flux (fig. 4) at low winds (WS < 2 m/s) and decrease in net longwave (not shown).

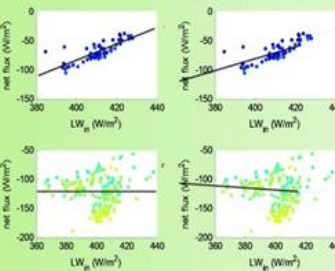


Fig 4. Plot of net flux versus LW_o, binned into wind speed bins of 0-2 m/s, 2-4 m/s, 4-6 m/s and 6-10 m/s. R² values of 0.65, 0.26, 8*10⁻⁴, 0.04 respectively. Gradients are 1.48, 0.801, 0.018 and -0.58 respectively.

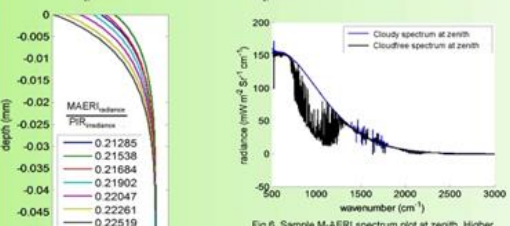


Fig 6. Sample MAERI spectrum plot at zenith. Higher MAERI_{cloud-free} value implies a cloudy spectrum and a closure in the atmospheric window thereby indicating an increase in LW_o.

Fig 5. Plot of binned retrieved profiles at WS < 2 m/s. Bins are performed at a MAERI_{cloud-free}/PIR_{cloud-free} ratio of 0.01.

Fig 5 shows an unexpected observation where this increase is associated with a larger $\Delta T_{skin-subskin}$ and smaller linear temperature gradient near the surface.

- At low winds, the TSL is expected to be thicker due to minimized wind-driven shear effects (Donlon, 2002).
- Because the maximum IR emission depth is < 0.1 mm (fig. 1), the accuracy of the retrievals are limited to the top 0.1 mm. The absence of measurements beyond 0.1 mm may hinder our analysis.
- Evidence of a thicker TSL is observed in plots of $\Delta T_{skin-subskin}$ versus $\Delta T_{skin-5m}$ where significant deviation between both values are found at low winds. We expect $\Delta T_{skin-subskin} = \Delta T_{skin-5m}$ as our data is restricted to low wind, night-time conditions.
- Analysis of 5 viscous layer models (excludes radiative effects) shows ΔT decreasing with LW_o at WS < 2 m/s.

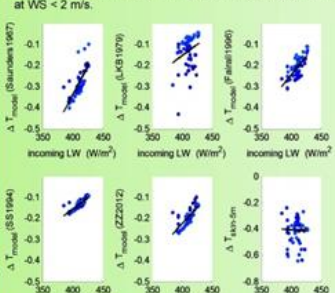


Fig 7. Plot of ΔT derived from 5 viscous layer models using NAURU99 and AMMA06 data at WS < 2 m/s. R² values for Saunders 1967 (Saunders1967), Liu et al. 1979 (LKB1979), Fairall et al. 1996 (Fairall1996), Soloviev and Schissel 1994 (SS1994), Zhang and Zhang 2012 (ZZ2012). $\Delta T_{skin-5m}$ are 0.56, 0.08, 0.51, 0.86, 0.52 and 7*10⁻⁷ respectively.

Conclusions

- NAURU99 and AMMA06 data showed a significant relation of a higher LW_o corresponding to a lower net flux and net LW at low wind speeds implying a mechanism present for retaining OHC.
- Retrieved TSL profiles at WS < 2 m/s shows a larger gradient and higher $\Delta T_{skin-subskin}$ as the atmospheric window closes (i.e. increase in LW_o).
- At low WS, the TSL is thicker due to increased molecular effects and decreased wind-driven shear effects. However, the accuracy of the retrievals are limited by the IR emission depth (< 0.1 mm).
- ΔT from viscous layer models shows a decrease with increasing LW_o.
- Ability to show that a higher LW_o results in a lower ΔT which results in a lower gradient and lower net heat flux implying more OHC retained.

POSTER 31: INVESTIGATING SEA SURFACE TEMPERATURE DIURNAL VARIATION OVER THE TROPICAL WARM POOL USING MTSAT-1R



Investigating Sea Surface Temperature Diurnal Variation over the Tropical Warm Pool Using MTSAT-1R Data



Haifeng Zhang¹, Helen Beggs², Leon Majewski², Xiao Hua Wang¹, Andrew Kiss¹

¹The Sino-Australian Research Centre for Coastal Management, School of Physical, Environmental and Mathematical Sciences, University of New South Wales Canberra at the Australian Defence Force Academy, Canberra, Australia

²Bureau of Meteorology, Docklands, Melbourne, Australia

1 Introduction

Fig. 1. Annual average SST in 2010. Black box indicates the Tropical Warm Pool study region (usually annual mean SST > 28°C).

- A better understanding of SST diurnal variation (DV) events (e.g. Gousses et al., 2008) is essential to better represent the air-sea interaction in weather/climate models.
- Tropical Warm Pool (TWP) region is considered to be an ideal area to conduct DV studies because of its: (1) globally highest annual average SST, (2) calm winds, (3) strong solar insolation, and (4) frequent, large-amplitude DV events.

2 Data & Method

Data sets temporal coverage for Jan - Apr, 2010:

- Bureau of Meteorology reprocessed hourly, 0.05° resolution, v3 MTSAT-1R geostationary satellite SST data (Beggs et al., 2013), https://www.bmco.gov.au/remote_data_and_data_delivery.aspx
- Drifting buoy SST data - obtained from the Global Telecommunications System;
- ABC (ATSR Processing for Climate) v1.1 Advanced Along-Track Scanning Radiometer (AATSR) satellite SST data (Embrey et al., 2012);
- Hourly, 0.375° resolution, wind speed and Solar Shortwave Insolation (SSI) data from ACCESS-R 24-hour forecasts (Pari et al., 2013).

Methods:

- Statistical parameters with respect to drifting buoy/AATSR SST: Bias, Standard Deviation (STD) of the bias, Scatter Index (SI), correlation coefficient (R) and the Median Absolute Difference (MAD).

3 Validation

3.1 In-situ validation

Fig. 2. In-situ validation results: (a) density plot of the daytime (7-19 LST) collocations within each 0.2°C - 0.2°C bin; (b) same as (a) but for nighttime (19-24, 0-7 LST) collocations; (c) same as (a) but for all collocations; (d) collocation numbers, bias and STDs over each SST 1°C range (divided based on in-situ SSTs); (e) same as (d) but over each local hour; (f) quality-controlled MTSAT-1R data coast distribution over each local hour.

- Overestimation/Underestimation is found at low-high SST conditions with an amplitude of 0.5-1°C/1.5-2.5°C.
- Minimal day/night bias is revealed by: (1) average values of -0.064°C/0.08°C respectively; (2) constant bias over 24 hour period (within the order of ± 0.25°C).
- Around local sunrise/sunset times, MTSAT-1R data are largely missing; data quality shortly after sunrise is also damaged.

3.2 Cross-validation

Fig. 3. MTSAT-1R vs AATSR cross-validation: (a) and (b) density plots of the local daytime and nighttime collocations; (c) and (d) collocation numbers, bias and STDs over different SST 1°C ranges (based on AATSR SSTs) of the daytime (-19 LST) and nighttime (-22 LST) collocations.

Fig. 4. The spatial distribution of (a) bias, (c) STD, (e) collocation number for daytime collocations of MTSAT-1R SSTs with AATSR SSTs in 2° × 2° bins; (b), (d), (f), and (f) are the same as (a), (c), (e) respectively, but for nighttime collocations.

- Some overestimation/underestimation is again found at low-high SST conditions but with small amplitude of -0.5°C/1.5-2°C.
- Spatially, over most of the study domain, the bias (grey areas in Fig. 4a and b) is within -0.2°C to 0.2°C and STD (dark and light blue areas in Fig. 4c and d) is within 0°C to 0.4°C.

4 DV events investigation

4.1 Whole domain study

Concepts: (1) SST_{thd}: foundation SST, average value of the 00:30 - 05:30 (LST) SSTs; (2) ΔSST: difference between an SST within a day and SST_{thd} of the same LST day; (3) ΔSST_{max}: maximum ΔSST of the day, i.e. the maximum DV event amplitude.

Fig. 5. (left top) For all four months in 2010: (a) monthly mean ΔSST_{max} for January; (b) frequency (days in a month) of ΔSST_{max} > 1°C for January; (c) monthly mean wind speed for January; (d) monthly mean SSI for January. The second, third, and fourth rows are for February, March, and April, respectively.

Fig. 6. (left bottom) For four months: (a) pixel number distribution over different ΔSST_{max} values; (b) distribution of pixels with ΔSST_{max} over local hours; (c) monthly shape of the diurnal cycle; (d) monthly shape of the STDs of the calculated ΔSST values. Note that in (c) and (d), to highlight the curves, only pixels with ΔSST_{max} > 2°C are selected, and all the 24 ΔSST values at that pixel of the day are then included in the calculation.

- Large amplitude DV events are generally consistent with a combination of low wind and high SSI, like over the north-west Australian coast in March.
- In 0.002% of the cases, DV amplitudes are larger than 3°C.
- Most (22.58%) of the maximum DV amplitudes are observed at 15-16 LST.
- The abnormal jumps at 6-7, 18-19 LST in Fig. 6c and d are also because of the sunrise and sunset effects.

4.2 Regional study

Fig. 7. (left top) Case study: Relationship between ΔSST_{max} (left column) and daily mean wind speed (middle column) and SSI (right column) for four consecutive days (from 5th March 2010) over the north-western Australian coast.

Fig. 8. (left bottom) Case study: Relationship between ΔSST_{max} and SSI/wind speed is investigated by pixels in the selected region and time period (four days from 5th March).

Fig. 9. (right bottom) Correlation coefficients (a) between ΔSST_{max} and the wind speed, and (b) between ΔSST_{max} and the SSI.

- Large DV events are in more consistency with low wind than with high SSI.
- Wind speed, with -0.7 negative correlation coefficients (R_{WS}) with ΔSST_{max}, plays a dominant role in DV events over SSI, with R_{WS} values smaller than 0.5.


5 Conclusions

- The Bureau reprocessed v3 MTSAT-1R data have minimal day/night bias (-0.064°C/0.08°C) and are suitable for DV studies over the TWP region.
- The effects of sunlight near sunrise and sunset times are revealed from both the reduced data amount and the damaged quality.
- Good consistency is found between the large DV events and the low wind speed/high SSI conditions, while as proved both qualitatively and quantitatively, wind plays a dominant role.

6 References

- Beggs, H., Majewski, L., Griffin, C., Verain, R., Sakov, P., Huang, X., Garde, L. & Tingwell, C. (2013). Report to GHRSSST4 from Australia - BlueLink and DMOS. In: *Proceedings of the GHRSSST XIV Science Team Meeting, Woods Hole, USA, 17 - 21 June 2013* (accessed from http://www.ghrssst.org.au/public_html/2July2013/)
- Embrey, G., Merchant, C. J. & Corlett, G. K. (2012). A reprocessing for climate of sea surface temperature from the along-track scanning radiometers: initial validation, accounting for skin and diurnal variability effects. *Remote Sensing of Environment*, 116, 62-78. doi:10.1016/j.rse.2011.02.028.
- Gousses, C. L., Misonnet, P. J., Le Boeuf, P. & Merchant, C. J. (2008). Multi-satellite measurements of large diurnal warming events. *Geophysical Research Letters*, 35(22). doi: 10.1029/2008gl035730
- Pari, K., et al. (2013). Implementation of the initial ACCESS numerical weather prediction system. *Australian Meteorological and Oceanographic Journal*, 63, 265-284.

POSTER 32: IN SITU SST QUALITY MONITOR VERSION2 (IQAM2)




In situ Quality Monitor Version 2 (iQuam2)

www.star.nesdis.noaa.gov/sod/sst/iquam/v2

Xinjia Zhou^{1,2}, Alexander Ignatov¹, Feng Xu^{1,4}

¹NOAA STAR; ²Colorado State University/CIRA; ³GST Inc. ⁴Fudan University, China



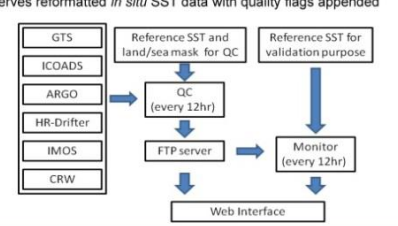
Motivation and Objective

- NOAA is responsible for a wide range of satellite SST products from polar and geostationary satellites, including swath, gridded and blended SSTs
- As part of our GHRSSST responsibilities, we evaluate various community SST products in the NOAA SQUAM www.star.nesdis.noaa.gov/sod/sst/squam/
- "In situ standard" is required for consistent Cal/Val results which
 - Covers full satellite era (from ~1980 – on)
 - Includes all available high-quality in situ SSTs suitable for satellite Cal/Val (drifters, moorings, ARGO floats, ships, in situ radiometers)
 - Uniformly processes all in situ data using state-of-the-art QC, consistent with wider communities such as UK MO, NCEP, ICOADS
 - Provide data in community consensus, user friendly format, via web interface with minimal latency, to support NRT Cal/Val applications
- The iQuam was developed to initially support NOAA SST applications, but has evolved into a community GHRSSST resource

Functionality and Data Flow

The iQuam is a web-based near-real time system. It performs 3 major functions

- Ingests various in situ SSTs, and performs a uniform Quality Control (QC)
- Monitors QCed in situ SSTs online
- Serves reformatted in situ SST data with quality flags appended



Enhancements in iQuam2

- Extend time series to full satellite era (Sep 1981 – on), using ICOADS 2.5
- Improve QC by adding to iQuam files
 - The 2nd reference SST (CMC)
 - Performance history check (iQuam check similar to the UKMO/CMS "black lists")
 - CMS black list; and individual QFs from data producers (ICOADS, ARGO, IMOS)
- Improve web interface
 - Redesign web engine (from flash player to High Charts)
 - Add daily statistics
 - Enhance graphics (interactive display, and print/save functions)
- Change output data files to NetCDF4, maximally reconcile with GDS2
- Add new in situ data
 - ARGO Floats (in NRT and post-processing modes)
 - High-Resolution Drifters
 - IMOS Ships
 - Coral Reef Watch buoys

Quality Control

Category	Check	Type of error handled	Physical basis
Preprocessing	Duplicate Removal	Duplicates arise from multiple transmission or data set merging	Identical space/timeID
Plausibility	Geolocation checks	Unreasonable Geolocation	Range of single fields & Relationships among them
Internal consistency	Tracking	Points falling out of track	Travel speed exceeds limit
Internal consistency	Spike check	Discontinuities in SST time series along track	SST gradient exceeds limit
External consistency	Reference Check	Measurements deviating far away from reference	Bayesian approach (Ref. SST: daily Or SST v2)
Mutual consistency	Cross-platform Check	Mutual verification with nearby measurements ("buddy checks")	Bayesian approach based on space/time correlation of SST field
Performance consistency*	Performance history check	Bad performance of single platform ID	Outlier rate exceeds limit (50% in single platform)

* The Performance History check was added in iQuam2 (similar to CMC / UKMO black lists)

Interface




Fig. 1: Global distribution of in situ data and corresponding statistics of "in situ minus reference SST"




Fig. 2: Monthly in situ number of unique platform IDs and observations (normalized at Max = 100%)




Fig. 3: Monthly in situ time series of mean biases and standard deviations




Fig. 4: Daily in situ Time series of platform ID number (left) and standard deviation (right)




Fig. 5: iQuam file list for user download

Future Work

- Collect users' feedback and implement iQuam2. Retire iQuam1
- Archive w/GHRSSST (PO.DAAC/NODC). Document in literature
- Transition to iQuam2 in all NOAA Cal/Val applications including SQUAM
- Work towards iQuam3
 - Add data from (1) SAMOS Ships; (2) Profilers from NOAA World Ocean Database
 - Test 3-way error analysis, to determine errors in individual in situ data

Acknowledgments & Disclaimer

This work is supported by JPLR, ODSER, and NOAA (PO.DAAC/CORS) Programs. We thank P. Chou, Y. Wang, J. Stapper, K. Lang, S. Perrenin, J. Strou, E. Matou, A. Harris, J. Metz (NOAA/STAR), S. Woodruff, E. Freeman, K. Casey, T. Boyer (NOAA/NGO), S. Worley (NOAA), P. LeBlond, A. Maroulis, S. Parre (Météo France), J.-F. Royer and D. Foster (IFREMER/IFREX), E. Fisher, J. Roberts-Jones, J. Kennedy, R. Rappin (CSIRO), E. Keen (Southampton Oceanography Centre), B. Evans, P. Menemen, K. Kibrikov, E. Williams (U. Miami), G. Cornet (U. Leicester), H. Breggs (IMOS), M. Chou, E. Armstrong (JPL) and for help and collaboration. The views and findings are those of the authors and should not be construed as an official NOAA or US Government position, policy, or decision.

GHRSSST XVI Science Team Meeting, 20-24 July 2015, ESA/ESTEC, the Netherlands
Xinjia.Zhou@noaa.gov / Tel: 301-683-3370
Alex.ignatov@noaa.gov / Tel: 301-683-3379

Page 195 of 225

POSTER ABSTRACTS

POSTER 2: FORECAST OF SST: CALIBRATION OF OCEAN FORCING WITH SATELLITE FLUX ESTIMATES (COFFEE)

Charlie N. Barron⁽¹⁾, Jan M. Dastugue⁽¹⁾, Jackie May⁽¹⁾, Clark Rowley⁽¹⁾, Scott R. Smith⁽¹⁾, Peter L. Spence⁽²⁾, and Silvia Gremes-Cordero⁽³⁾

(1) Naval Research Laboratory, Code 7321, Stennis Space Center, MS, 39529, (USA),
Email: charlie.barron@nrlssc.navy.mil

(2) Vencore, Stennis Space Center, MS, 39529, (USA)

(3) University of New Orleans, Stennis Space Center, MS, 39529, (USA)

ABSTRACT

While satellite observations provide a solid basis to form a global analysis of recent sea surface temperature (SST), they are only part of the solution to ensure accurate SST forecasts. These observations can re-center SST from ocean models at the start of each forecast cycle, but subsequent evolution depends on estimates of surface heat fluxes and upper-ocean processes over the forecast period. A more complete application of satellite remote sensing not only informs the initial ocean state but also anticipates errors in surface heat flux and model representations affecting the distribution of heat in the upper ocean. The COFFEE project (Calibration of Ocean Forcing with satellite Flux Estimates) endeavors to correct ocean forecast bias through a responsive error partition among surface heat flux and ocean dynamics sources. A suite of experiments in the southern California Current demonstrates a range of COFFEE capabilities, showing the impact on forecast error relative to a baseline three-dimensional variational (3DVAR) assimilation using Navy operational global or regional atmospheric forcing. COFFEE addresses satellite-calibration of surface fluxes to estimate surface error covariances and links these to the ocean interior. Experiment cases combine different levels of flux calibration with different assimilation alternatives. The cases may use the original fluxes, apply full satellite corrections during the forecast period, or extend hindcast corrections into the forecast period. Assimilation is either baseline 3DVAR or standard strong-constraint 4DVAR, with work proceeding to add a 4DVAR expanded to include a weak constraint treatment of the surface flux errors. Covariance of flux errors is estimated from the recent time series of forecast and calibrated flux terms. While the California Current examples are shown, the approach is equally applicable to other regions. These approaches within a 3DVAR application are anticipated to be useful for global and larger regional domains where a full 4DVAR methodology may be cost-prohibitive.

1. Introduction

Inaccuracies in forecast SST can be attributed to errors in the initial state and errors in the forecast after the initial state. In the present standard operational approach, recent observations of SST are assimilated within the Navy Coupled Ocean Data Assimilation System (NCODA; Cummings, 2005) using 3D variational assimilation (3DVAR; Smith et al., 2012) to correct the initial state each day, taken to be at 00:00 UTC. A more flexible adjustment of the model is possible with 4DVAR assimilation (Smith et al., 2015), which enables the model trajectory to be also adjusted over the hindcast period leading to the nowcast state. Errors introduced into the forecast evolving from its initial state arise from two sources: (1) errors in the heat flux at the ocean surface, and (2) errors in the redistribution of heat within the ocean model.

The potential impact of errors during the forecast is evident from long non-assimilative, alternatively called free-running, multiyear ocean forecasts using the global Hybrid Coordinate Ocean Model (HYCOM; Chassignet et al., 2007). Evaluation of SST after multiple years of integration using forcing from the real-time operational atmospheric model NOGAPS (Navy's Operational Global Atmospheric Prediction System), reveals

a mean annual bias exceeding $\pm 3^{\circ}\text{C}$ in places. This could be attributed to a proportional bias in the mean surface heat flux, where a mean flux bias of 45 W m^{-2} leads to a mean temperature bias of approximately 1°C . This implies that the net annual heat flux bias is as much as $\pm 150\text{ W/m}^2$, similar in magnitude to the annual mean of the flux itself.

This simple adjustment has been applied in the past, thereby attributing all of the error in estimating the annual mean SST to mean errors in the incoming heat flux. Such an approach is unrealistic, as it does not allow for variation in time, differentiation among flux terms, or errors in the ocean model. It also requires cumbersome reevaluation periods to account for shifting bias due to changes in components of the atmosphere or ocean prediction systems such as a change from NOGAPS to NAVGEM (Navy Global Environmental Model) or subsequent NAVGEM reformulations (Metzger et al., 2013). COFFEE represents a paradigm shift from this monolithic approach and instead endeavors to determine the time-dependent partition of error contributions among surface heat flux and ocean model contributions. If these errors can be measured and corrected in the hindcast period, then the error covariance should allow a projection and correction of errors into the forecast period. Such an approach is responsive both to changing local conditions and to updates in the overall modeling and assimilation system.

New advances in remote sensing and ocean data assimilation are leveraged to determine appropriate balances between errors in surface heat flux and other ocean factors affecting redistribution of heat. Our first hypothesis is that satellite observations can be used to calibrate heat flux values and determine flux error covariance. This is implemented within the NRL Ocean Surface Flux (NFLUX) system. Our second hypothesis is that variational assimilation can relate mismatches with ocean observations to errors in surface flux and the ocean state. This leads to an approach in which satellite observations enable NFLUX to estimate corrected surface fluxes and error covariance, while ocean observations and error covariances allow variational assimilation to balance error contributions among surface flux and ocean processes. We will extend 4DVAR to have a weak-constraint treatment of the surface flux terms. These will be tested in a matrix of experiments in regional cases of interest, spanning a range of cloud conditions and dominant features. Finally these approaches will be extended to global and broader regional applications where the expense of 4DVAR may be prohibitive. Section 2 reports on NFLUX, while section 3 lays out a set of experiments to diagnose alternate methods to determine and balance error contributions related to the distribution of heat within NCODA and the Navy Coastal Ocean Model (NCOM; Barron et al., 2006). Section 4 summarizes our conclusions to date and projects future developments under the COFFEE project.

2. NFLUX

NFLUX offers a system to process and quality control measurements related to the air/ocean boundary layer in order to provide more accurate satellite-corrected estimates of heat flux over hours prior to the present analysis. Consider mean January surface heat flux from the U.S. Navy's global atmospheric model (Figure 1). Solar, strictly non-negative, is direct warming by shortwave, primarily visible radiation from the sun. The other three terms are mixed but primarily negative: longwave thermal radiation between the ocean and clouds, sensible heating where contact with the air directly warms or cools the ocean, and latent heating where evaporation or condensation produces a heat flux.

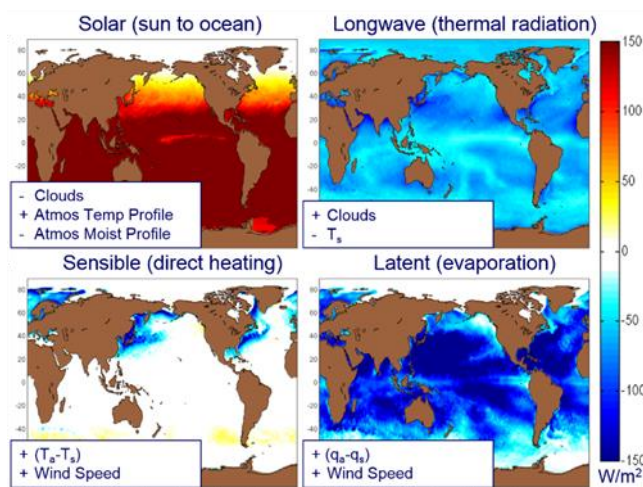


Figure 1: Mean January heat flux from NOGAPS defined such that positive values warm the ocean. Flux values and errors are proportional to ocean and atmospheric properties as indicated in each field's southwest corner.

Consider the downward sensible heat flux, proportional to wind speed and the air-sea temperature difference. Satellite observations tell us about wind speed, air temperature, and sea surface temperature over the hindcast period. These are passed to the COARE 3.0 bulk flux algorithm (Fairall et al., 2003; Wallcraft et al., 2008) for coupling with ocean models. Satellite data from the hindcast period can be assimilated into a model background to make satellite-corrected estimates of the terms in the bulk formulae or, for radiant fluxes, terms in radiative transfer models. Radiant heat flux components are estimated using the Rapid Radiative Transfer Model for Global circulation models (RRTM-G; Iacono et al., 2000) using a variety of inputs (Table 1). Preparation and validation of these terms within NFLUX is covered in Van de Voorde et al., 2015, and May et al., 2014.

RRTM-G Input	Data Source for NFLUX
Temperature and moisture profiles	MIRS (satellite swath)
In-cloud liquid and ice water paths	MIRS (satellite swath)
Albedo	Function of solar zenith angle, wind speed, and MIRS clouds
Cloud water drop and ice effective radius	10, 30 microns
Aerosol optical depth profile	NAAPS 3 hr global field
O ₃ profiles	SMOBA daily global field
CO ₂ , CH ₄ , N ₂ O, CFC-11, CFC-12, HCFC-22, CCl ₄ profiles	WMO 2010 assessment + growth rate (constant profile)
O ₂ profile	.21 mol/mol (constant profile)
SST	HYCOM 3 hr global field
Emissivity	0.99
Solar Constant	1367 W m ⁻²

Table 1: RRTM-G inputs and data sources. MIRS is NOAA's Microwave Integrated Retrieval System; NAAPS is Navy Aerosol Analysis and Prediction System; SMOBA is NOAA's Stratosphere Monitoring Ozone Blended Analysis; WMO is the World Meteorological Organization.

NFLUX and global/regional forecast NAVGEM/COAMPS (Coupled Ocean/Atmosphere Mesoscale Prediction System) turbulent fluxes and their components are evaluated relative to ship and buoy observations, with the flux validation considering only complete matching sets of data. The COARE 3.0 algorithms are used with NFLUX, the atmospheric models, and the validating observations to calculate the turbulent heat flux components. Radiant fluxes calculated with RRTM-G are evaluated relative to independent benchmark observations automatically logged by vessels participating in the Shipboard Automated Meteorological and Oceanographic Systems (SAMOS) initiative. The green cells on Table 2 highlight the flux or constituent predictors that are in closer agreement with the independent observations (i.e., is satellite-corrected NFLUX

better than the NAVGEM forecast). NFLUX provides improved flux estimation overall, particularly when a spatial averaging is applied to the MIRS cloud fields used in RRTM-G. The evaluations with NAVGEM are global; similar regional evaluations are underway using COAMPS as the control estimate.

Flux or Constituent		Bias	RMSE	St. Dev.	R ²	N
Air temp T _a	NFLUX	0.241	1.245	1.222	0.979	199,944
	NAVGEM	-0.304	1.249	1.212	0.979	
Humidity Q _a	NFLUX	0.327	1.246	1.202	0.958	128,086
	NAVGEM	-0.490	1.277	1.180	0.958	
Wind speed U	NFLUX	0.214	2.067	2.056	0.644	194,649
	NAVGEM	-0.326	2.167	2.142	0.626	
Latent Flux Q _L	NFLUX	-9.17	60.33	59.63	0.453	81,510
	NAVGEM	16.69	64.82	62.64	0.470	
Sensible Flux Q _s	NFLUX	-0.80	24.06	24.05	0.386	81,510
	NAVGEM	3.63	24.42	24.15	0.446	
Shortwave	NFLUX ^{AVG}	23.98	151.90	150.00	0.74	10,066
	NFLUX ^{ORIG}	40.08	158.08	152.92	0.73	
	NAVGEM	25.58	165.96	163.98	0.69	
Longwave	NFLUX ^{AVG}	-5.41	29.25	28.75	0.75	17,138
	NFLUX ^{ORIG}	-12.70	31.95	29.32	0.74	
	NAVGEM	-10.72	34.75	33.05	0.72	

Table 2: Model-observation bias, standard deviation, root mean square error, squared correlation, and number of matchups over 13 months from April 2013 to April 2014. For the radiant fluxes, the superscript indicates whether MIRS clouds were used as their ORIGINAL value at each time, location or whether spatial AVeraging was applied.

3. Experiments

Regional NCOM California Current experiments start in April 2013, the beginning of the MIRS data, and after a one-month spin-up enter a 12-month validation period from May 2013 through April 2014. The forecasts cycle with a daily 3DVAR or 4DVAR (Smith et al., 2012; 2015) assimilation of satellite SST (GOES, AVHRR, VIIRS), altimeter (Jason, AltiKa), and in situ temperature and salinity profile observations. Surface-only in situ data are not assimilated; these are a means of independent validation. Other observations are independent when used to evaluate the forecast period, as the daily assimilation includes no data measured after the 00:00 UTC analysis.

Fluxes		Assimilation Type		
		3DVAR	4DVAR standard	4DVAR with flux
COAMPS	unmodified	■	■	□
	NFLUX-full use during forecast	□	□	
	NFLUX-extended from hindcast			
NAVGEM	unmodified	■	■	□
	NFLUX-full use during forecast	□	□	
	NFLUX-extended from hindcast			

Table 3: Planned COFFEE experiments in each region. The rectangle symbols track progress in the California Current region, solid symbols indicating completed runs while open symbols indicate cases in preparation.

Eighteen experiments are envisioned for each of the COFFEE regions, distributed as shown in Table 3. The cases differ on the background atmospheric forcing, the modification applied to heat fluxes, and the assimilation methodology. The International Satellite Cloud Climatology Project reveals the range of conditions within the various regions. Over the California Current, mean cloud cover decreases from annual highs above 80% toward the northern central Pacific to lows below 50% along the coast and toward the Gulf of California. Such variations in cloud distribution are one challenge in predicting heat flux and SST.

In situ observations from buoys, whether fixed or drifting, provide the most reliable estimate of SST at a particular time and location. However, both sets of buoy observations poorly sample the whole domain. Drifting buoys are concentrated in a small number of trajectories while fixed buoys oversample the shelf nearest the

coast. Satellite observations offer more complete coverage with vastly more observations than in situ, but the accuracy of the retrievals may be subject to the same uncertainty sources affecting flux determination.

Figure 2 shows results of an evaluation of the monthly and annual averages of forecast-observation bias and RMS errors. Bias is small relative to AVHRR but up to 1.0°C warm relative to in situ and 1.0°C cool relative to GOES. Comparisons with GOES and fixed buoys give the largest RMS errors. The error and bias trends shown here are representative of those found in the nowcast and other forecast intervals in the various experiments run to date. Work to diagnose such discrepancies and their relation to surface forcing or assimilation continues.

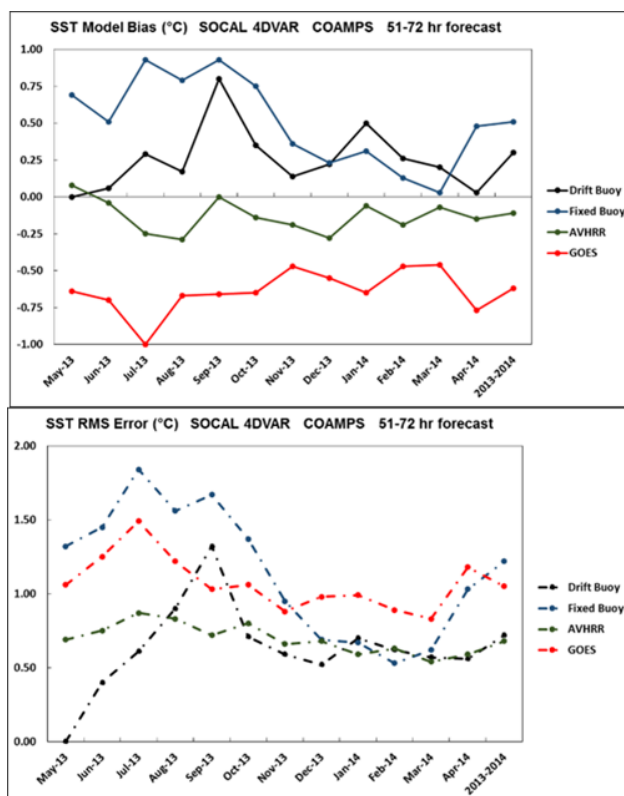


Figure 2: Monthly and annual average forecast-obs SST bias (top) and RMS errors (bottom) for the 51-72 hour forecast from the standard 4DVAR California Current experiment using unmodified NAVGEM forcing.

4. Conclusion

COFFEE demonstrates a capability using satellite-based estimates of heat flux and variational balancing of uncertainties among surface heat flux and ocean dynamics sources to provide more accurate forecasts of SST and boundary layer conditions. The NFLUX satellite-corrected estimates of turbulent and radiative heat exchange at the ocean surface have smaller errors than the operational forecast fields, enabling calculation of a flux error covariance that extends into the short-term forecast. Parallel efforts have evaluated the baseline performance of 3DVAR and 4DVAR ocean forecasts in the California Current. Work is proceeding on evaluating the impact of satellite-corrected fluxes in a hindcast scenario and extending them in short term forecasts, providing a capability that is responsive to environmental and forecast system changes. Demonstration of these capabilities in the California Current is a first step in establishing their applicability in other regions and globally. Such a capability is envisioned to play a role in mediating imbalances between components of regional and global coupled modeling systems.

5. Acknowledgements

Work under the Calibration of Ocean Forcing with satellite Flux Estimates (COFFEE) project was supported by the Naval Research Laboratory and the Office of Naval Research, which further supported participation in GHRSSST XVI and preparation of these through the Multisensor Improved Sea Surface Temperature for Integrated Ocean Observing System (MISST-IOOS) project.

6. References

- Barron, C.N., A.B. Kara, P.J. Martin, R.C. Rhodes, and L.F. Smedstad, 2006: Formulation, implementation and examination of vertical coordinate choices in the global Navy Coastal Ocean Model (NCOM). *Ocean Modelling* **11**(3-4), 347-375, doi:10.1016/j.ocemod.2005.01.004.
- Chassignet, E.P., H.E. Hurlburt, O.M. Smedstad, G.R. Halliwell, P.J. Hogan, A.J. Wallcraft, R. Baraille, and R. Bleck, 2007: The HYCOM (HYbrid Coordinate Ocean Model) data assimilative system. *J. Mar. Sys.*, **65**, 60-83.
- Cummings, J.A., 2005: Operational multivariate ocean data assimilation. *Quart. J. Roy. Met. Soc.* **131**, 3583-3604.
- Fairall, C.W., E.F. Bradley, J.E. Hare, A.A. Grachev, and J.B. Edson, 2003: Bulk parameterization of air sea fluxes: updates and verification for the COARE algorithm. *J. Climate*, **16**, 571-591.
- Iacono, M.J., E.J. Mlawer, S.A. Clough, and J.J. Morcrette, 2000: Impact of an improved longwave radiation model, RRTM, on the energy budget and thermodynamic properties of the NCAR community climate model, CCM3. *J. Phys. Oceanography*, **105**(D11), 14,873-14,890.
- May, J., N. Van de Voorde, and C. Rowley, 2014: Validation test report for the NRL ocean flux (NFLUX) quality control and 3d variational analysis system. NRL Memorandum Report, NRL/MR/7320--14-9524.
- Metzger, E.J., A.J. Wallcraft, P.G. Posey, O.M. Smedstad, and D.S. Franklin, 2013: The switchover from NOGAPS to NAVGEM 1.1 atmospheric forcing in GOFS and ACNFS. NRL Memorandum Report NRL/MR/73-8677-03-5.
- Smith, S.R., M.J. Carrier, H.E. Ngodock, J. Shriver, and P. Muscarella, 2015: Validation Testing Report for the Navy Coastal Ocean Model Four-Dimensional Variational Assimilation (NCOM 4DVAR) System, Version 1.0. NRL Memorandum Report NRL/MR/7320-15-9574.
- Smith, S.R., J.A. Cummings, P. Spence, S.N. Carroll, C. Rowley, O.M. Smedstad, P. Chu, B. Lunde, J. Shriver and R. Helber, 2012. Validation Test Report for the Navy Coupled Ocean Data Assimilation 3D Variational Analysis (NCODA-VAR) System, Version 3.43. NRL Memorandum Report, NRL/MR/7320-12-9363.
- Van de Voorde, N.E., J. May, and C. Rowley, 2015: NFLUX PRE: Validation of new specific humidity, surface air temperature, and wind speed algorithms for ascending/descending directions and clear or cloudy conditions. NRL Memorandum Report, NRL/MR/7320-15-9611.
- Wallcraft, A.J., A.B. Kara, H.E. Hurlburt, E.P. Chassignet, and G.H. Halliwell, 2008: Value of bulk heat flux parameterizations for ocean SST prediction. *J. Mar. Sys.*, **74**, doi:10.1016/j.marsys.2008.01.009.
- WMO (World Meteorological Organization), 2010: Scientific Assessment of Ozone Depletion. Global Ozone Research and Monitoring Project, Report No. 52, Geneva, Switzerland, 516 pp.
-

POSTER 17: THE UNCERTAIN HIGH LATITUDE SST SAMPLING ERRORS AND THE REDUCED ERRORS IN SST SEASONAL ANOMALY

Yang Liu⁽¹⁾ and Peter J. Minnett⁽²⁾

(1) University of Miami, Miami, FL, USA, yliu@rsmas.miami.edu

(2) University of Miami, Miami, FL, USA, pminnett@rsmas.miami.edu

1. Introduction

Clouds and inter-swath gaps are the primary reasons for incomplete coverage in satellite measurements cause sampling errors in averaged satellite SST fields. Previously quantified sampling errors in MODIS monthly SSTs are substantial especially in regions that are continuously cloudy for weeks. Two questions remain to be explored. First, since the MODIS sampling error was initially calculated based on MUR (Multi-scale Ultrahigh Resolution) SST data (Chin et al. 2010), whether the different SST variability embedded in a different SST reference field causes different sampling error patterns is unknown. Second, given that the seasonality of SSTs and clouds yield seasonal changes of sampling errors, and that the seasonality of SSTs is sampled the most sparsely in extremely cloudy regions, we would like to ask: can sampling error be reduced in those extremely cloudy regions, assuming that we can estimate the seasonal changes of SSTs below the clouds? In this study, we address the first question by quantifying the MODIS sampling errors using HYCOM reanalysis data as the reference, and the second question by calculating the sampling errors in MODIS SST seasonal anomaly.

2. Data and Methods

We used thermal IR daytime and mid-IR nighttime Level 3 fields of Terra MODIS SSTs. Global day and night cloud masks (i.e., quality masks) were acquired by considering the grids with quality flags greater than 1 as

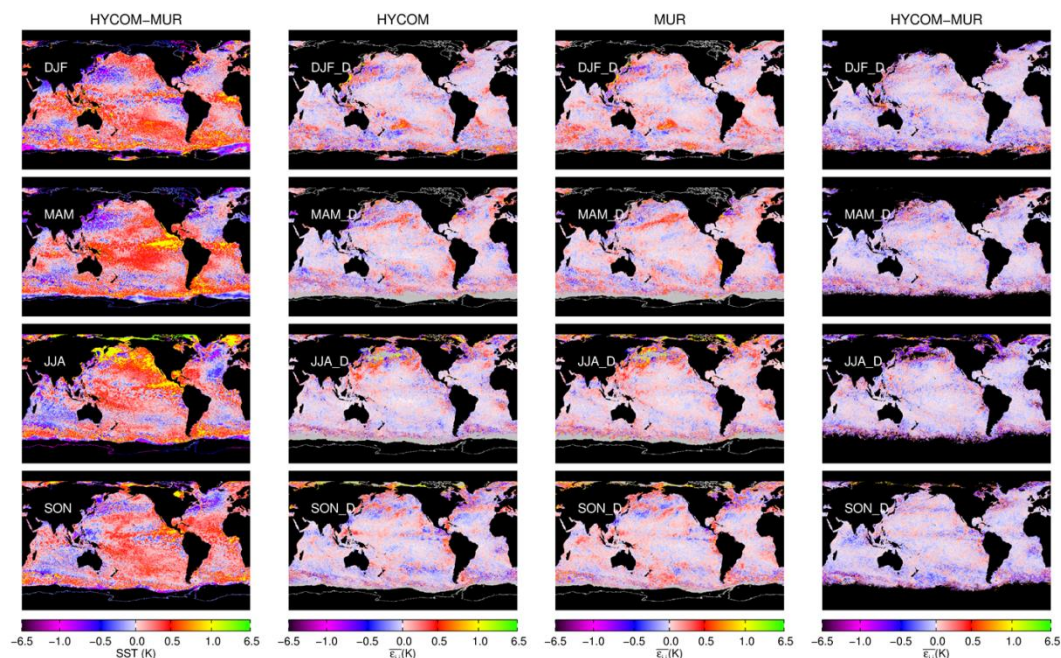


Figure 1: From the left column to the right: Difference in the monthly mean SST of MUR and HYCOM; Sampling errors in the temporal averaged HYCOM SSTs; Sampling errors in the temporal averaged MUR SSTs; The difference in SST sampling errors between HYCOM and MUR.

missing data primarily due to cloud cover or gaps between successive orbits. The MODIS sampling process is represented by superimposing daily cloud masks on daily reference fields. Two reference SST data sets are used: 1) HYCOM + NCODA (Hybrid Coordinate Ocean Model + Navy Coupled Ocean Data Assimilation) Global 1/12° reanalysis; 2) MUR SST anomaly calculated by subtracting OISST daily climatology (Banzon et al. 2014).

3. Results

The differences between HYCOM and MUR SSTs are systematic (Figure.1), and show seasonal patterns. Sampling error patterns calculated from the HYCOM data resemble the results of MUR to a large extent. The differences between the sampling errors calculated from the two reference fields are generally small in the tropics and mid-latitudes, and the differences do not show apparent seasonal patterns. Zonal mean sampling error distributions (not shown) show there are large differences around Antarctica, regardless of the averaging dimension (spatially or temporally). Where the disagreement in temporal averaging cases of both reference data exists are in coincidence with previously identified long cloud persistence regions. Therefore, we argue that the sampling error magnitudes in regions with extremely sparse measurements (around Antarctica) are uncertain and may be determined by the quality of the input reference SSTs.

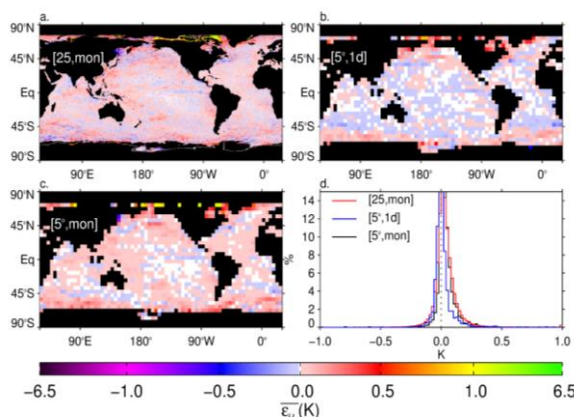


Figure 2: Sampling errors in SST seasonal anomalies. a., b. and c. show temporal averaging, spatial averaging, and spatiotemporal averaging respectively. d. shows the histograms of the errors.

Although there is a large amount of uncertainty in SSTs in regions of long cloud persistence, we can at least confidently assume the seasonal variability of those SSTs, by using a seasonal climatology of SSTs. MODIS sampling errors in SST seasonal anomalies are shown in Figure.2. Compared with the sampling errors SSTs (not shown), errors in the seasonal anomalies are smaller, especially in the regions identified with persistent clouds.

4. Summary

By using HYCOM reanalysis as the sampling error reference, we found that the error distribution resembles the previous result calculated from MUR SSTs. Although there are substantial disagreements between the two SST data sets, the sampling error fields of both basically agree to a large extent, except for those around Antarctica and the Arctic, which are the least sampled regions. Therefore, we argue that sampling errors in the high latitude regions remain large and uncertain and need to be clarified in aspects of the different uncertainty sources. Sampling errors in SST seasonal anomalies can be reduced, except for the polar regions. However, whether the SST climatology field has sampling errors remains unknown. Future work will include the exploration of uncertainties in the high sampling errors, such as difference in the input data sets of the reference, sampling errors in SST climatology, and the high latitude SST data reliability.

5. References

- Banzon, V.F., Reynolds, R.W., Stokes, D., & Xue, Y. (2014). A 1/4°-Spatial-Resolution Daily Sea Surface Temperature Climatology Based on a Blended Satellite and in situ Analysis. *Journal of Climate*, **27**, 8221-8228
- Chin, T.M., Jorge, V., & Armstrong, E. (2010). Algorithm Theoretic Basis Document: Multi-scale, motion-compensated analysis of sea surface temperature Version 1.1

POSTER 20: BIAS AWARENESS IN OPTIMAL ESTIMATION OF SEA SURFACE TEMPERATURE

Chris Merchant⁽¹⁾, Jon Mittaz^(1, 2)

(1) *University of Reading, Reading, UK Email: c.j.merchant@reading.ac.uk*

(2) *National Physical Laboratory, Teddington, Email: j.mittaz@reading.ac.uk*

ABSTRACT

The classic formulations of optimal estimation (OE) return retrievals that minimize estimated retrieval error variance or maximize retrieval likelihood in some way, provided certain assumptions are made. These assumptions include two relating to bias in the observation/retrieval system: (1) the prior information (often also used as the linearization point for forward simulation) is assumed to be unbiased (zero mean error); (2) the forward simulation of the observations and their partial derivatives is assumed also to be unbiased. Neither assumption is generally true in practice, and our experience in sea surface temperature (SST) retrieval using OE is, as with other variables, that bias correction is necessary. Bias awareness has been worked on extensively within data assimilation, and by analogy, OE can be made bias aware. To explore this, the case of AVHRR retrieval of SST has been simulated in detail, and it is shown that various bias problems can be addressed through bias-aware techniques: include prior bias and unmodelled effects of stratospheric volcanic aerosol.

1. Introduction

The classic formulations of optimal estimation (OE) return retrievals that minimize estimated retrieval error variance or maximize retrieval likelihood in some way, provided certain assumptions are made. These assumptions include two relating to bias in the observation/retrieval system: (1) the prior information (often also used as the linearization point for forward simulation) is assumed to be unbiased (zero mean error); (2) the forward simulation of the observations and their partial derivatives is assumed also to be unbiased. Neither assumption is generally true in practice, and our experience in sea surface temperature (SST) retrieval using OE is, as with other variables, that bias correction is necessary.

A difficulty is that these two forms of bias need different treatment. We do not want to correct the simulation system to compensate for the prior information bias, because then the bias in the prior will persist in the retrieval: improving on the prior is the purpose of the retrieval, after all. We do want to correct the simulation system for the forward model bias. However, it is not generally possible from the results of a single retrieval to partition the retrieval error to distinguish sources of bias, and thereby correct only the forward model.

Over many retrievals, the two forms of bias may have different spatio-temporal scales. Separation by scale is attempted, for example, within the OSI-SAF forward simulation system, using a method based on running average differences over a certain space-time scale. However, this doesn't necessarily capture the true form of systematic error in the simulation, which may have a complex state dependence.

Theory for bias-aware retrieval methods exists, in classic retrieval texts and also adaptable from the literature on bias-aware data assimilation. In essence, biases must be modelled/parameterized and the parameters describing the bias retrieved. This should be done progressively over many retrievals.

2. Exploration in simulation world

Progressing such ideas in a retrieval system is therefore a question of addressing practical decisions in how to go about applying bias-aware theory. However, assessing different approaches using real-world data can be complex and ambiguous (there is never perfect validation data for the task).

It is beneficial, therefore, to use an Earth observation simulation system (EOSS) experimentally created by NPL and University of Reading to synthesize data that can be used to learn about bias-aware strategies. The

EOSS simulates instruments from radiance field, through detector, amplifier, digitization and on-board calibration system, to geophysical product retrieval and validation match-ups. All this is done using real-world orbit geometries and cloud distributions. Two simulation streams run: the true-world of a perfectly calibrated noise-free instrument and perfectly known atmospheric conditions; and the available-world of an imperfectly calibrated, noisy instrument with simulations run on numerical weather prediction fields that are imperfect estimates of the real atmosphere. The true-world and available-world differences are of realistic magnitudes given instrumental, forward model and NWP uncertainties.

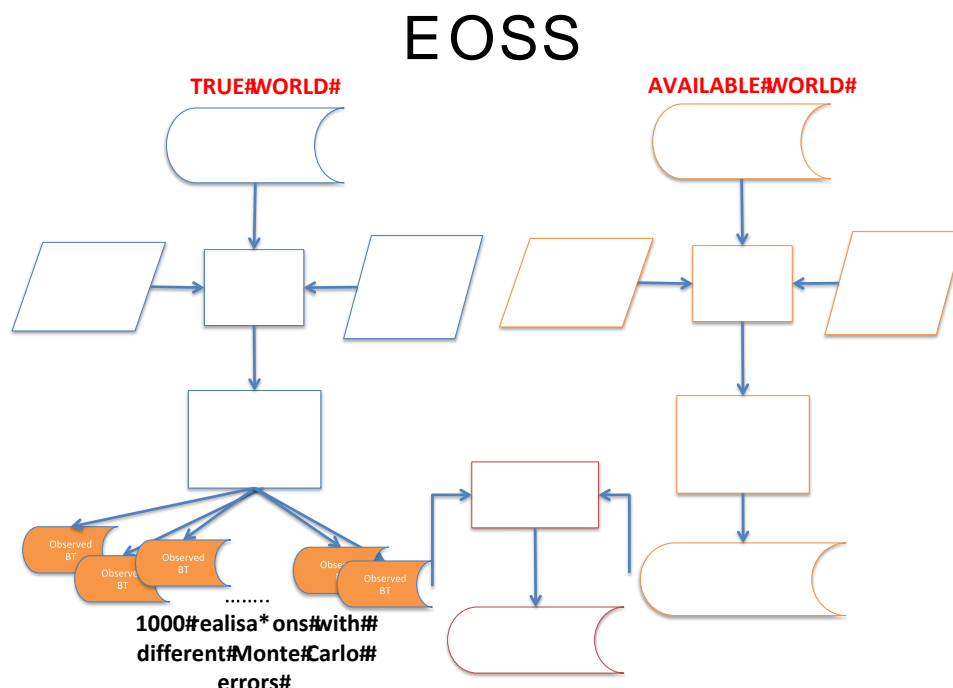


Figure 1: Earth observation simulation system. The outputs include “true world” simulations (blue), that provide a truth value, allowing retrieval errors to be fully characterised. The “available world” simulations (orange) mimic the restricted information available to an investigator in the real world attempting SST retrieval from AVHRR.

With the true-world and available-world outputs of this system (Figure 1), it is possible to run informative retrieval experiments using different bias-correction strategies. One can assume various levels of ignorance about the nature of available-world errors, and test whether different bias correction strategies are successful.

3. Radiance bias example: post-Pinatubo aerosol

OE is neutral about the source of radiance bias: it cannot distinguish between instrument calibration bias, forward model errors, or effects absent in the forward simulation of observations. An example of the latter is using OE to retrieve SST during a period of elevated stratospheric aerosol, such as post-Pinatubo, when using a model that doesn't represent this aerosol. In this case, a bias aware formulation of OE can be used to retrieve the bias (brightness temperature change) arising from this source, having added aerosol effects to the EOSS outputs. The bias aware formulation essentially tries to retrieve the aerosol related effect over many retrievals. Figure 2 shows that useful estimates of the aerosol effects can be obtained, simultaneously to the SST retrieval.

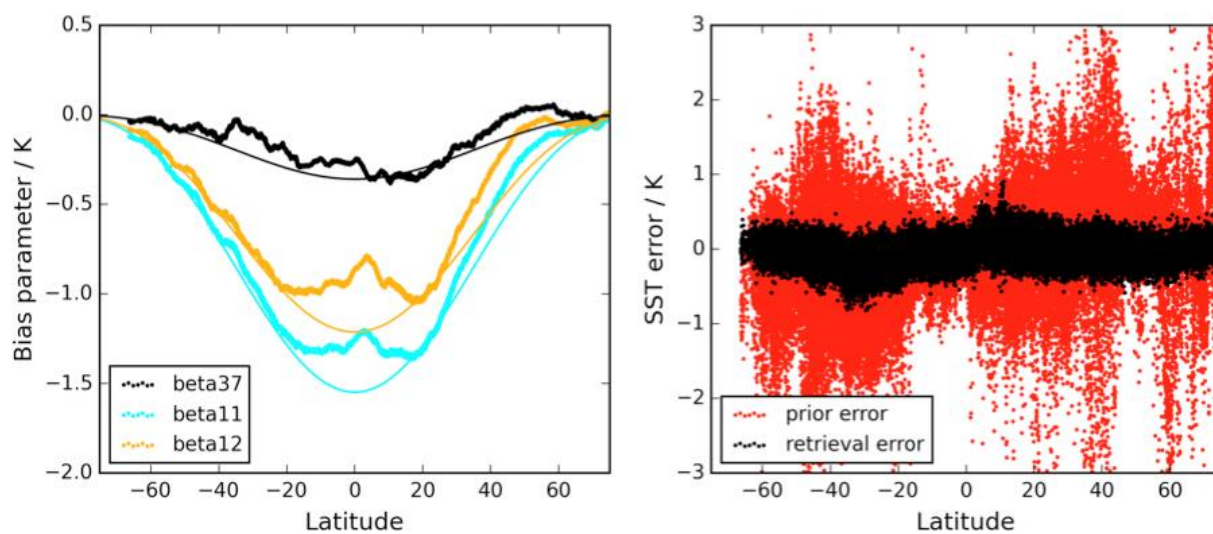


Figure 2: Left: imposed aerosol biases as a function of latitude (thin lines, coloured as legend); bias-aware estimate of bias parameter capturing aerosol effect (thick lines). The aerosol parameter retrieved is good except at the equatorial latitudes where water vapour is highest. Right: prior SST error (red) and retrieved SST error using bias awareness.

4. Conclusion

The main limitation of OE is bias, and bias awareness needs to be further developed for further progress in applying OE to SST retrieval. Testing bias awareness strategies in a “simulated world” is useful.

POSTER 29: UPWELLING CHARACTERISTICS FROM SST GRADIENTS IN THE PERU/CHILE COASTAL SYSTEM

Jorge Vazquez⁽¹⁾, Dimitris Menemenlis⁽¹⁾, Boris Dewitte⁽²⁾, Toshio M. Chin⁽¹⁾, and Edward M. Armstrong⁽¹⁾

(1) Jet Propulsion Laboratory/California Institute of Technology 4800 Oak Grove Dr., Pasadena, California, United States, Email: jorge.vazquez@jpl.nasa.gov

(2) LEGOS/IRD, Toulouse, France

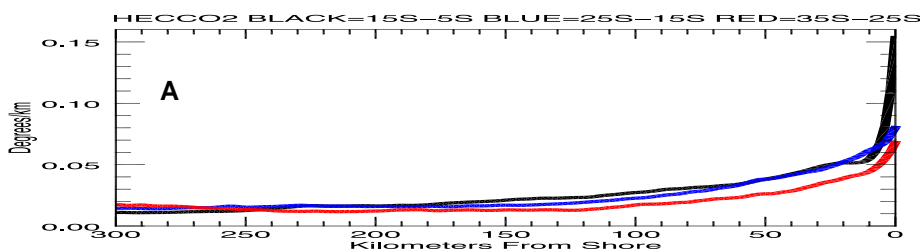
ABSTRACT

1. Introduction

The South American Coast along Peru and Chile is one of the most productive fisheries of the world's oceans due to upwelling of cold water from depth. Dynamically, it is unique among other Eastern Boundary Current regions, such as the California Coast and the Benguela region off Africa, because off Peru and Chile the upwelling is not only influenced by local wind forcing due to Ekman Pumping and Ekman Transport but also by remote forcing from the Equatorial Pacific. The remote forcing can be due to both annual and interannual Kelvin Waves that propagate and become coastally trapped (Clarke and Shi, 1991). Variability also exists at the intraseasonal time scale forced by local winds (Illig et al., 2014). Other factors can influence the upwelling scales, including the cross-shelf topography and geostrophic adjustment due to the Humboldt Current (Marchesiello et al., 2010). Although the forcing that creates upwelling regions has been well understood (Pedlosky, 1979), the response of the upwelling on intraseasonal, seasonal, and interannual scales is still an area of active research (e.g., Dewitte et al., 2011; Echevin et al. 2008; Macias et al., 2012). Recent attention has focused on understanding the impacts of climate variability and change on these coastal areas (Melillo et al., 2014).

2. Upwelling Scales

We estimated upwelling scales by applying a Gaussian filter to the magnitude of SST gradients from three data sets: the Multi-scale Ultra-high Resolution (MUR) SST, the National Climatic Data Center (NCDC) SST analysis gridded on 0.25° grid, and a high resolution internal-tide and upwelling resolving ocean simulation called LLC4320. Figure1(a,b,c,d) shows the mean of the magnitude of the SST gradients for MUR, NCDC, LLC4320, and WindSat for Oct.-Nov. 2011.



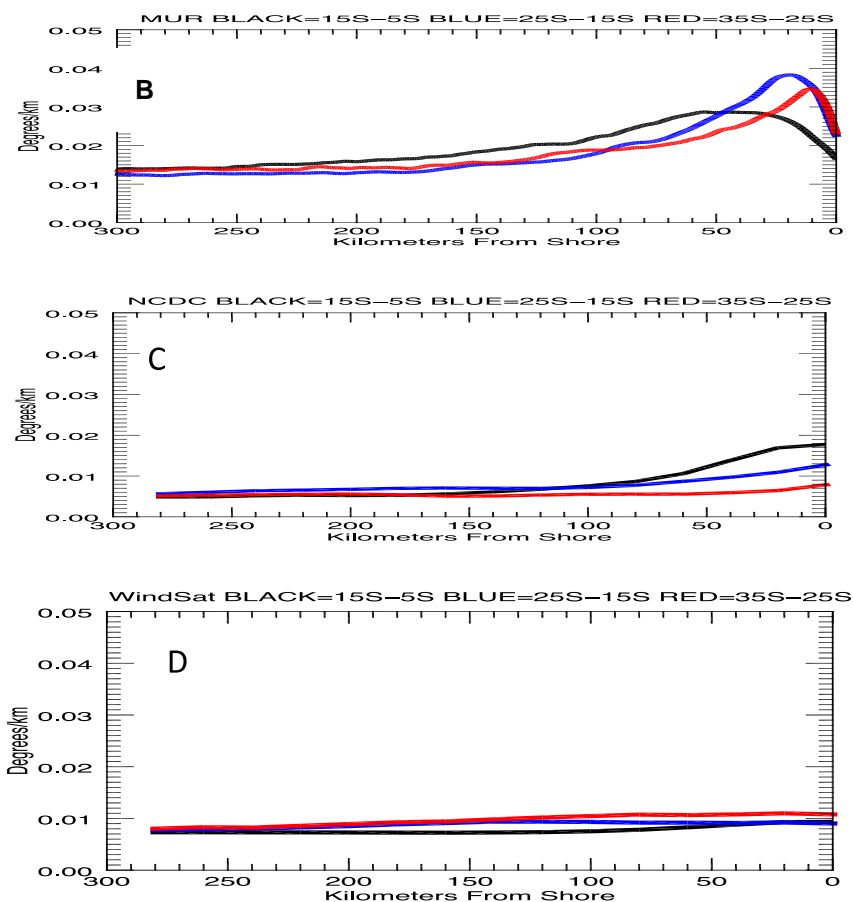


Figure 1 (a,b,c,d): Magnitude of SST gradients versus cross-shore distance for a) LLC4320, b) MUR c) NCDC and d) WindSat

The table below summarizes the upwelling scales based on Figure 1.

Parameter/Data Set	Latitude Band	Upwelling Scale
MUR	35°S-25°S	14km
MUR	25°S-15°S	37km
MUR	15°S-5°S	38km
LLC4320	35°S-25°S	10km
LLC4320	25°S-15°S	20km.
LLC4320	15°S-5°S	20km
NCDC	35°S-25°S	51km
NCDC	25°S-15°S	50km.
NCDC	15°S-5°S	47km
WSAT	35°S-25°S	158km
WSAT	25°S-15°S	200km
WSAT	15°S-5°S	62km

Table 1: Comparison of cross-shore upwelling scales from LLC4320, MUR, NCDC, and WindSat

3. Conclusion

A simple methodology based on the magnitude of SST gradients is used to derive a cross-shore upwelling scale. Results indicate that a decrease in the cross-shore upwelling scale is observed in the MUR and LLC4320 data sets with distance South of Equator. Using the methodology both LLC4320 and MUR show cross-shore upwelling scales that decrease to less than 50km with increasing latitude South. MUR and vertical velocities from LLC4320 compare best with theory in showing a decrease in cross-shore upwelling scale with distance South from the equator, as well as cross-shore upwelling scales of approximately 15km between 35°S and 25°S. Both NODC and WindSat show larger cross-shore upwelling scales, most likely due to the lower gridding resolution. Results are consistent with derivations of the cross-shore upwelling scale based on using the vertical velocity output from the LLC4320 model. In general both NODC and gradients-derived SSTs from the microwave WindSat satellite, indicate that lower resolution data sets are not resolving the cross-shore upwelling scales. South of 20° both NODC and WindSat have limitations in identifying the coastal upwelling. Comparisons with only SST gradients from WindSat results indicate high resolution infrared derived SSTs are adding critical information for identifying the coastal upwelling, especially as the cross-shore upwelling scale decreases to less than 50 kilometers, the Nyquist wavelength of the microwave derived SSTs (WindSat).

4. References

- Clarke, A. J. and C. Shi, Critical (1991), Frequencies at Ocean Boundaries, *Journ. of Geophys. Res.* **90** (C6), 10731-10738.
- Dewitte, B., S. Illig, L. Renault, K. Goubanova, K. Takahashi, D. Gushchina, K. Mosquera and S. Purca (2011), Modes of covariability between sea surface temperature and wind stress intraseasonal anomalies along the coast of Peru from satellite observations (2000-2008). *Journal of Geophysical Research-Oceans*, **116**, pp.16. <10.1029/2010jc006495>. <hal-00994325>
- Echevin, V., O. Aumont, J. Ledesma, and G. Flores (2008), The seasonal cycle of surface chlorophyll in the Peruvian upwelling system: A modeling study, *Progress in Oceanography*, **79**, (2-4), 167-176, doi:10.1016/j.pocean.2008.10.02.
- Illig, S., B. Dewitte, K. Goubanova, G. Cambon, J. Boucharel, F. Monetti, C. Romero, S. Purca, and R. Flores (2014), Forcing mechanisms of intraseasonal SST variability off central Peru in 2000-2008, *J. Geophys. Res. Oceans*, **119**, 3548-3573, doi:10.1002/2013JC009779. 3189-3196DOI: 10.1002/2014GL059589.
- Macias, D., M. R. Landry, A. Gershunov, A.J. Miller and P.J.S. Franks (2012), Climatic Control of Upwelling Variability along the Western North-American Coast, *PLOS/One*, DOI: 10.1371/journal.pone.0030436.
- Marchesiello P., and P. Estrade, 2010: Upwelling limitation by geostrophic onshore flow, *Journal of Marine Research*, **68** (1), 37-62.
- Melillo, Jerry M., Terese (T.C.) Richmond, and Gary W. Yohe, Eds. (2014), *Climate Change Impacts in the United States: The Third National Climate Assessment*. U.S. Global Change Research Program, 841 pp. doi:10.7930/J0Z31WJ2.
- Pedlosky, J. (1979), *Geophysical Fluid Dynamics*, Spring-Verlag, New York, pp. 671.

POSTER 30: THE IMPACT OF THE OCEAN THERMAL SKIN LAYER ON AIR-SEA INTERFACIAL HEAT FLUXES

Elizabeth Wong⁽¹⁾, Peter J. Minnett⁽²⁾

(1) University of Miami, Rosenstiel School of Marine and Atmospheric Science, 4600 Rickenbacker Causeway, Miami, FL, 33149-1031, USA, Email: ewong@rsmas.miami.edu

(2) University of Miami, Rosenstiel School of Marine and Atmospheric Science, 4600 Rickenbacker Causeway, Miami, FL, 33149-1031, Email: pminnett@rsmas.miami.edu

ABSTRACT

The upper ocean heat content has been observed to be increasing over the past few decades much of which has been attributed to anthropogenic effects resulting in an increase in greenhouse gases thereby increasing the amounts of incoming longwave (LWin) radiation impinging onto the ocean's surface. However, the penetration depth of LWin extends to micrometer scales, where the thermal skin layer (TSL) exists, and does not directly heat the upper few meters of the ocean. We hypothesize the heat lost through the air-sea interface which is controlled by the TSL, modulates the amount of heat stored in the upper few meters of the ocean. An analysis on properties of the retrieved TSL profiles with heat fluxes (specifically LWin) and wind speeds from two cruises limited to night-time data are presented. We also present a comparison between these properties with current published TSL models. The results show that the data have an inherent wind speed dependence with net flux thereby requiring a segregation of the data into wind speed bins such that shear effects may be segregated in the analysis. The temperature differences derived from the TSL models indicates the TSL profile's gradient is potentially decreasing with increased LWin which leads to a lowered net flux and is in agreement with our hypothesis.

1. INTRODUCTION

The ocean's thermal skin layer (TSL), exists at micrometer scales on the aqueous side of the air-sea interface, and consists of a strong temperature gradient that sustains the upward heat flux by molecular conduction. Most, if not all of the heat that leaves the ocean is conducted through the TSL, thus knowledge of the physics of the TSL and its behavior with environmental variables (such as wind speeds and fluxes) is an important research area in air-sea heat exchanges. Furthermore, the penetration depth of impinging infrared (IR) radiation lies within TSL depths, thereby implying that the response of the upper ocean to variations in incident IR radiation, such as those caused by variations in clouds, water vapor and greenhouse gases, takes place within the TSL. We postulate that the amount of heat lost through the interface, which is controlled by the non-linear gradient of the TSL, modulates the storage of heat in the upper few meters of the ocean. Heat content in the upper few meters of the ocean is largely a product of the absorption of incoming solar radiation. Thus, analysis of the TSL gradient may provide an answer to the observed increase in upper ocean heat content with increasing greenhouse gases over the past few decades (Levitus, 2012).

This study presents an analysis on properties of retrieved TSL profiles obtained from the Marine-Atmospheric Emitted Radiance Interferometer (M-AERI) with heat fluxes and wind speeds. Comparisons between data from two cruises are also performed with published TSL models.

2. METHODS/BACKGROUND

To retrieve the TSL, we utilized high spectral resolution measurements obtained from the M-AERI which measures radiance ($\text{mWm}^{-2}\text{Sr}^{-1}(\text{cm}^{-1})^{-1}$) emitted across the wavenumber range $500\text{-}3000\text{cm}^{-1}$. Details of the M-AERI are given in Minnett *et al.*, 2001. The total radiance, $I_m(\nu)$, emitted by the sea surface with respect to wavenumber, ν in cm^{-1} , is defined by:

$$I_m(v) = \int_0^{\infty} B(v, T(z)) \frac{d\tau}{dz} dz, \text{ where } \tau = -e^{-\alpha z} \quad (1)$$

where α is the absorption coefficient and $B(v, T(z))$ is Planck's function with a temperature-depth profile of $T(z)$. We would like to obtain $T(z)$ given $I_m(v)$ which is difficult given that Equation (1) is ill-conditioned and the profile, $T(z)$, is highly non-linear. Wong and Minnett (2015) demonstrated the use of the truncated singular value decomposition technique (TSVD) to perform a retrieval of the TSL vertical profile using M-AERI spectra with knowledge that the TSL approximates to a complementary error function structure (Liu and Businger, 1975). They used an iterative method to estimate the skin and subskin temperatures of the resulting profile such that a smooth and continuous function is obtained.

This retrieval technique was performed on M-AERI spectra obtained from 2 cruises: the *R/V Ron Brown* cruise during the AMMA campaign from May to June 2006 and the *R/V Mirai* cruise during the NAURU'99 expedition from June to July 1999. The effects of solar radiation, precipitation and high winds of > 10 m/s are filtered out so that we can concentrate on the effects of the TSL and fluxes.

Five models were used to analyze the difference between the skin and subskin temperature derived from the retrieved profiles, $\Delta T_{\text{skin-subskin}}$, and the difference between the temperature at 5 m and the skin temperature, $\Delta T_{\text{skin-5m}}$: Saunders1967 (Saunders 1967), LKB1979 (Liu et al. 1979), Fairall1996 (Fairall 1996), SS1994 (Soloviev and Schluessel 1994) and ZZ2012 (Zhang and Zhang 2012). Comparisons were also made with Donlon's (2002) parameterization of $\Delta T_{\text{skin-5m}}$, hereinafter Donlon2002.

3. RESULTS

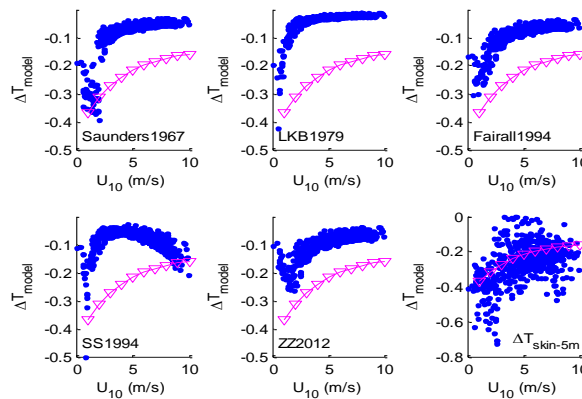


Figure 1: Plot of ΔT_{model} with U_{10} . Inverted magenta triangles denote Donlon's 2002 parameterization.

Figure 1 shows plots of ΔT_{model} and $\Delta T_{\text{skin-5m}}$ with measured wind speed at 10 m, U_{10} . $\Delta T_{\text{skin-subskin}}$, is not shown nor analyzed due to the high scatter observed and it is better to compare Donlon's parameterization with $\Delta T_{\text{skin-5m}}$. All plots follow Donlon2002 exponential decay of ΔT with increasing wind speed except for SS1994. Unfortunately, all calculated ΔT_{model} is relatively lower than $\Delta T_{\text{skin-5m}}$. This may be because the models are modelling the viscous sublayer which is much shallower than the 5 m depth resulting in a smaller ΔT . The discrepancy at higher winds for SS1994 is because for the data, higher winds happen to correspond to higher net fluxes which results in ΔT of SS1994 to increase with U_{10} .

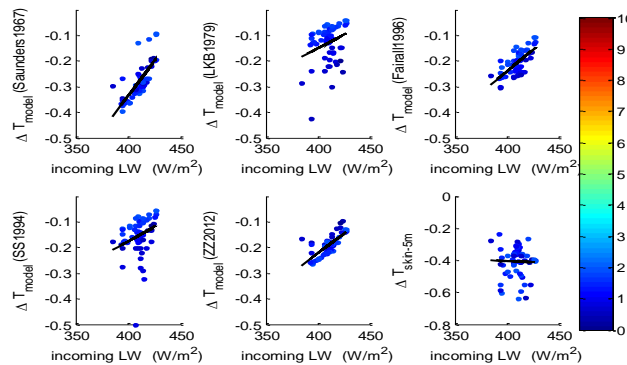


Figure 2. Plot of ΔT_{model} and $\Delta T_{skin-5m}$ with incoming longwave for wind speed < 2 m/s. R^2 values for Saunders1967, LKB1979, Fairall1996, SS1994, ZZ2012 are 0.56, 0.08, 0.51, 0.66, 0.52 and $7 \cdot 10^{-7}$ respectively.

No clear relationship is observed between the incoming longwave, LWin, and ΔT . However, if U_{10} is held relatively constant by binning into 2 m/s bins such that the effects of wind speed variations are minimized, a significant trend is found between ΔT and LWin. This significance is observed to decrease at higher winds, with the most significant range found at $U_{10} < 2$ m/s (fig. 2). This is likely due to the higher shear rates produced by higher U_{10} values resulting in a near constant ΔT . For $U_{10} < 2$ m/s, the effects of buoyancy surpasses that of surface shear and fig 2 shows that an increase in LWin lowers ΔT thereby suggesting the linear thermal gradient, $\frac{dT}{dz}$, will likely decrease. This also agrees with plots of ΔT with net flux (not shown) in which ΔT is observed to decrease with decreasing net flux thereby suggesting that less heat escapes the interface as LWin increases.

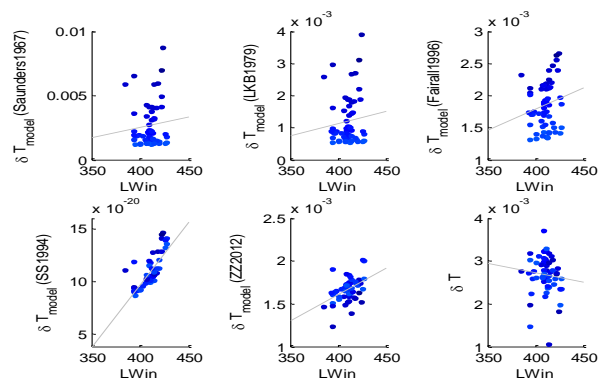


Figure 3. Plot of ΔT_{model} and $\Delta T_{skin-5m}$ with LWin for wind speed < 2 m/s.

Since the profile of the TSL is non-linear, it is worthwhile to look at the depth of the viscous sublayer, δT_{model} , and δT of the retrieved data which is defined to be the depth in which the temperature profile decays to 98% of $\Delta T_{skin-subskin}$. Figure 3 plots this relationship for $U_{10} < 2$ m/s and δT_{model} is observed to increase with LWin. This indicates that an increase in LWin lowers ΔT but thickens the TSL. As U_{10} becomes higher, the significance of the relationship between δT_{model} and LWin is observed to decrease (similarly with ΔT_{model}) showing the increased effects of surface shear as U_{10} increases.

Unfortunately, no significance is observed for $\Delta T_{skin-5m}$ and δT which is likely due to the large scatter observed for both variables thereby indicating a continued need to improve the accuracy in deriving ΔT and δT . The lack of data at low wind speeds may have also hindered the ability in obtaining a good correlation, thus there is also a need for further field or experimental data involving the M-AERI and heat fluxes.

4. CONCLUSION

Despite a lack of dependency between the observed $\Delta T_{\text{skin-5m}}$ and δT with LWin, we see a significant dependence between ΔT and δT of the models at low winds. At $U_{10} < 2$ m/s, an increase in LWin decreases ΔT and increases δT indicating that the gradient of the thermal skin layer decreases but extends deeper thus creating a more gradual TSL. A TSL with a more gentle curvature is indicative that less heat flux escapes from the ocean to the atmosphere (increase in net flux is observed to result in an increase in ΔT and decrease in δT) thereby retaining the upper ocean heat content, which is produced by the absorption of insolation during the day, and subsequently causing a warming of the ocean.

5. REFERENCES

- Bertie, J.E. and Z. Lan, Infrared intensities of liquids XX: the intensity of the OH stretching band of liquid water revisited and the best current values of the optical constants of H₂O (l) at 25C between 15,000 and 1cm⁻¹, *Applied Spectroscopy*, **50** (8), pp. 1047-1057, 1996.
- Donlon, C. J., P. J. Minnett, et al., Toward improved validation of satellite sea surface skin temperature measurements for climate research. *J. of Climate* **15**: pp. 353-369, 2002
- Fairall, C.W., E.F. Bradley, J.S. Godfrey, G.A. Wick, J.B. Edson, and G.S. Young, Cool-skin and warm-layer effects on sea surface temperature', *J. of Geophys Res. C. Oceans*, **101** (1), pp. 1295-1308, 1996
- Levitus S., J. I. Antonov, et al., World ocean heat content and thermosteric sea level change (0-2000 m), 1955-2010. *Geophys Res Letters*, **39**(10), pp. L10603, 2012
- Liu, W.T. and J.A. Businger, Temperature profile in the molecular sublayer near the interface of a fluid in turbulent motion, *Geophys. Res. Letters*, **2** (9), pp. 403-404, 1975
- Liu, W.T. and J.A. Businger, Bulk Parameterization of air-sea exchanges of heat and water vapor including the molecular constraints at the interface, *J. Atmos. Sci*, **36**, pp. 1722-1735, 1979
- Minnett, P.J., R.O. Knuteson, F.A. Best, B.J. Osborne, J.A. Hanafin and O.B. Brown, The Marine-Atmosphere Emitted Radiance Interferometer (M-AERI): a high-accuracy, sea-going infrared spectroradiometer, *Journal of Oceanic and Atmospheric Technology*, **18**, pp. 994-1013, 2001
- Saunders, P. M., The temperature at the ocean-air interface. *J. Atmos. Sci.* **24**, pp. 269-274, 1967
- Soloviev, A. V. and P. Schlüssel, Parameterization of the cool skin of the ocean and of the air-ocean gas transfer on the basis of modeling surface renewal. *J. Phy Oceanography* **24**, pp. 1339-1346, 1994
- Wong, E. and P.J. Minnett, Retrieval of the ocean skin temperature profiles from measurements of infrared hyperspectral radiometers. Part I: Evaluation of the truncated singular value decomposition technique. Manuscript submitted for publication, 2015
- Zhang, Y. and X. Zhang, Ocean haline skin layer and turbulent surface convections. *J. Geophys Res.* **117** pp. C04017, 2012

POSTER 31: INVESTIGATING SEA SURFACE TEMPERATURE DIURNAL VARIATION OVER THE TROPICAL WARM POOL USING MTSAT-1R

Haifeng Zhang⁽¹⁾, Helen Beggs⁽²⁾, Leon Majewski⁽³⁾, Xiao Hua Wang⁽⁴⁾, Andrew Kiss⁽⁵⁾

(1) *The Sino-Australian Research Centre for Coastal Management, UNSW Canberra @ ADFA, ACT, Australia, Email: haifeng.zhang@student.adfa.edu.au*

(2) *Bureau of Meteorology, Docklands, VIC 3008, Australia, Email: h.beggs@bom.gov.au*

(3) *Bureau of Meteorology, Docklands, VIC 3008, Australia, Email: l.majewski@bom.gov.au*

(4) *The Sino-Australian Research Centre for Coastal Management, UNSW Canberra @ ADFA, ACT, Australia, Email: X.Wang@adfa.edu.au*

(5) *The Sino-Australian Research Centre for Coastal Management, UNSW Canberra @ ADFA, ACT, Australia, Email: A.Kiss@adfa.edu.au*

ABSTRACT

Diurnal variation (DV) of sea surface temperature (SST) plays an important role in air-sea interaction. The parameterization of DV events is potentially useful in air-sea coupled models for weather, seasonal and climate scales. The Tropical Warm Pool (TWP) in the Eastern Indian and Western Pacific Oceans experiences particularly high diurnal warming of the sea surface temperature, exceeding 5°C under low wind speed and high solar insolation conditions. It is therefore considered to be an ideal region for a coordinated study of DV using observations and models. The dataset used in this study is the four months (January – April 2010) Australian Bureau of Meteorology (BoM) reprocessed version 3 Multi-functional Transport Satellite-1R (MTSAT-1R) data with 4 km resolution. This data set is a contribution to the “TWP+ data set”, a comprehensive dataset (1 January to 30 April 2010) used to quantify DV events and test DV models as part of the Group for High Resolution SST (GHRSSST) Tropical Warm Pool Diurnal Variability (TWP+) Project. Further information on the TWP+ project and data set can be found at <https://www.ghrsst.org/ghrsst/tags-and-wgs/dv-wg/twp/>.

The work includes the validation, including both in-situ validation and cross-validation using Advanced Along-Track Scanning Radiometer (AATSR) data, of the v3 MTSAT-1R SST data. Results show that this data set is of fine quality and suitable for SST DV investigations. In addition the quantification of the amplitude, frequency and spatial coverage of DV events over the TWP domain is conducted with special focus on a selected region over the north-western coast of Australia where the densest available measurements exist.

1. Data

The dataset used in this study is the four months (January – April 2010) Australian Bureau of Meteorology (Bureau) reprocessed version 3 (v3) Multi-functional Transport Satellite-1R (MTSAT-1R) data with 4 km resolution (Beggs et al., 2013). This data set is a contribution to the “TWP+ data set”, a comprehensive dataset (1 January to 30 April 2010) used to quantify DV events and test DV models as part of the Group for High Resolution SST (GHRSSST) Tropical Warm Pool Diurnal Variability (TWP+) Project. Further information can be found at <https://www.ghrsst.org/ghrsst/tags-and-wgs/dv-wg/twp/>.

Before the v3 MTSAT-1R data are used for characterization of the DV events, the validation, including both in-situ validation and cross-validation, is first conducted. For in-situ validation, drifting buoy data within the same period, also obtained from the TWP+ data set, are used. For the cross-validation, the Advanced Along-Track Scanning Radiometer (AATSR) data are utilised. The exact version used in this study is the ARC (ATSR Reprocessing for Climate) v1.1 (Embury et al., 2012).

Other data sets, including the wind speed data and the solar shortwave insolation (SSI) data, are obtained from the Bureau's ACCESS-R (Australian Community Climate and Earth System Simulator-Regional) model.

2. Validation

In general, validation results show that this v3 MTSAT-1R data set is of fine quality and suitable for SST DV investigations. In the in-situ validation, a 0.003°C bias and a 0.727°C standard deviation (STD) are found (Table 1). Minimal day-night biases are revealed by the constant biases (within $\pm 0.25^\circ\text{C}$) over the local 24-hour time period. In the meanwhile, in both validation works, an overestimation at low SST conditions (in-situ SST < 27°C) and underestimation at high SST conditions (in-situ SST > 31°C) are discovered.

		Num	Bias (°C)	STD (°C)	SI	R	MAD (°C)
INSITU	Day	1138	-0.064	0.712	0.026	0.845	0.410
	Night	988	0.080	0.737	0.026	0.902	0.410
	All	2126	0.003	0.727	0.026	0.883	0.410
AATSR	Day	292489	-0.045	0.48	0.017	0.944	0.287
	Night	236639	0.063	0.48	0.017	0.934	0.300
	All	529128	0.003	0.483	0.017	0.940	0.293

Table 1. Parameters of both in-situ validation and cross-validation. Num represents the number of collocations, STD the standard deviation of the bias, SI the scatter index, R the correlation coefficient and MAD the Median Absolute Difference. In the in-situ validation, daytime is defined from 7:00 to 19:00 Local Solar time (LST) and night-time from 19:00 to 7:00 LST, while in the cross-validation day/night times refer to 10:00/22:00 LST, i.e. local equator crossing times of the AATSR sensor.

3. Characterisation of SST DV Events

Using the validated four months v3 MTSAT-1R data, the SST DV events (i.e. the SST rise and fall within a local 24-hour period) over the TWP region are studied. Several concepts should be illustrated first:

(1) SST_{nd}: a concept defined by the Group for High Resolution SST (GHRSSST) which refers to the temperature free of diurnal temperature variability. In this study, it is calculated as the average value of the values from 0:30 to 5:30 LST.

(2) dSST: the daily SST variation at a given time within a solar day, calculated as the difference between that SST value and the SST_{nd}.

(3) dSST_{max}: the maximum dSST at one grid point within one solar day.

The monthly mean dSST_{max}, the occurrence of dSST_{max} larger than 1°C, monthly mean wind speed, and monthly mean SSI are seen in Figure 1. It is shown that generally, large DV events occur where the wind speed is low and SSI is high.

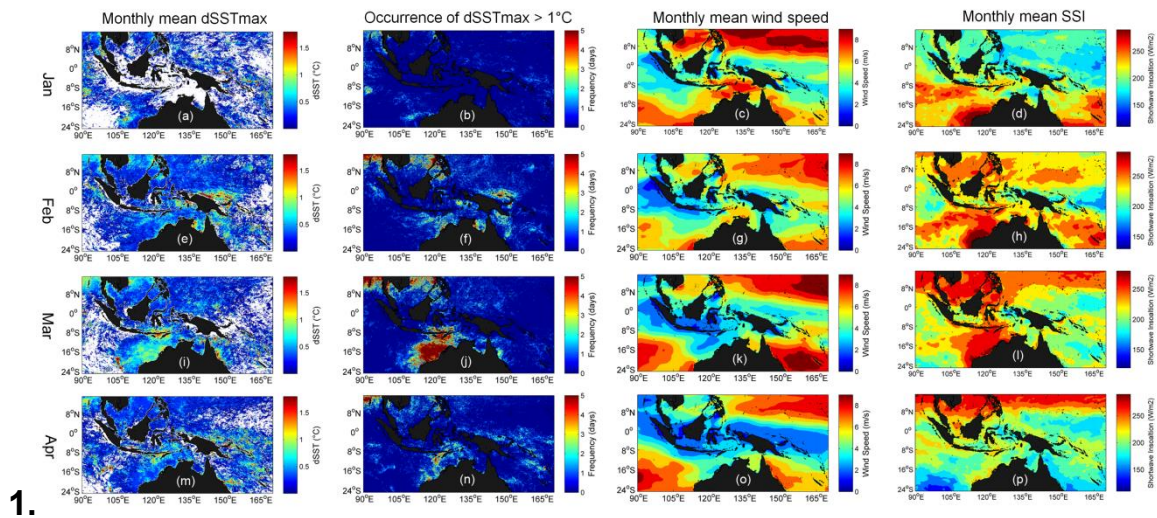


Figure 1. Spatial distribution of all four months in 2010: (a) monthly mean $dSST_{max}$ for January; (b) frequency (days in a month) of $dSST_{max} > 1^{\circ}C$ for January; (c) monthly mean daytime (7:00-19:00 LST) wind speed for January; (d) monthly mean daytime (7:00-19:00 LST) SSI for January. The second, third, and fourth rows are the same as the first but for February, March, and April respectively.

The SST DV amplitudes under different wind speed conditions are shown in Figure 2. For wind speeds smaller than 3 ms^{-1} , the monthly mean DV amplitudes are between $1^{\circ}C - 1.2^{\circ}C$. The values reduce to $0.4^{\circ}C - 0.6^{\circ}C$ when the wind speed is higher than 3 ms^{-1} but smaller than 6 ms^{-1} . If the wind speed is even higher (larger than 6 ms^{-1}), the diurnal cycles are no longer evident.

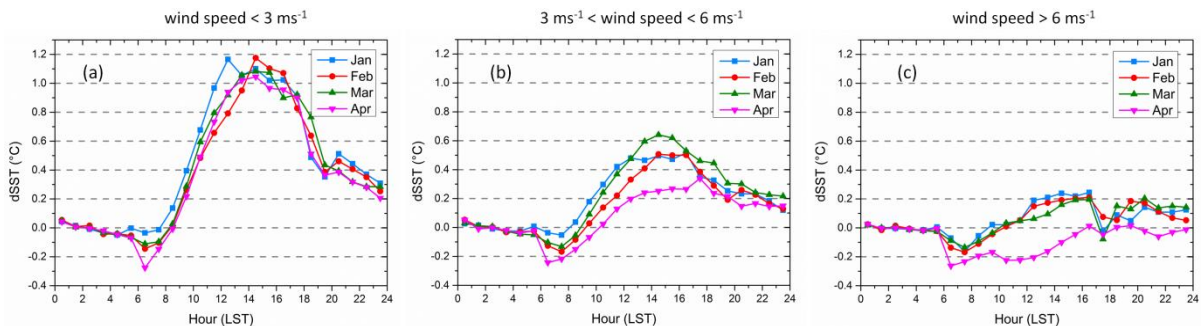


Figure 2. Monthly shape of the diurnal cycles under different wind speed conditions: (a) wind speed $< 3 \text{ ms}^{-1}$; (b) $3 \text{ ms}^{-1} < \text{wind speed} < 6 \text{ ms}^{-1}$; (c) wind speed $> 6 \text{ ms}^{-1}$. Wind speeds are the mean daytime (7:00-19:00 LST) values. The $dSSTs$ at each hour is the average of all measurements calculated.

The relationship between the DV amplitudes and wind speed/SSI values is also investigated. Results show that DV amplitudes are the largest when the wind speed is low and SSI is high (Figure 3). The dominant role of wind speed is revealed by its larger correlation coefficient with $dSST_{max}$ (a negative 0.7) than the correlation coefficient between SSI and $dSST_{max}$ (a positive 0.4).

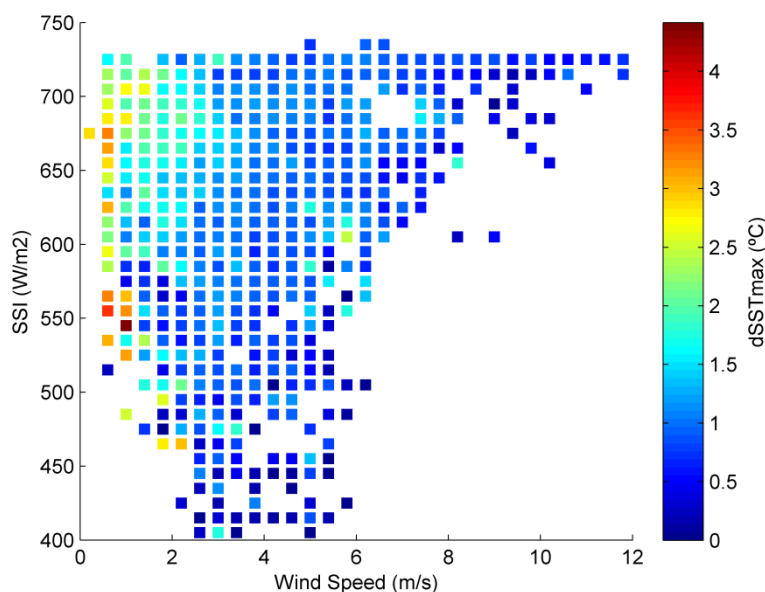


Figure 3. Relationship between $dSST_{max}$ and the daily mean SSI and wind speed is investigated by pixels in the selected region and time period (four days from 5-8th March). Shown in the figure are the average $dSST_{max}$ values over each $10 \text{ Wm}^{-2} \times 0.4 \text{ ms}^{-1}$ bin. Note that the SSI starts at 400 Wm^{-2} as there are few pixels falling below this value which are therefore cancelled. Also the daily mean wind speed and SSI are the average values of 7:00 to 19:00 LST.

4. Conclusion

The validation results indicate that the v3 MTSAT-1R data set is suitable for SST DV investigations and validation of DV models. Plausible relationships are found between DV events and low wind and high SSI conditions, respectively. The dominant role of wind speed in SST DV events over the SSI is also revealed.

5. References

Beggs, H., L. Majewski, C. Griffin, R. Verein, P. Sakov, X. Huang, L. Garde, and C. Tingwell, Report to GHRSSST14 from Australia - Bluelink and IMOS, In: Proceedings of the GHRSSST XIV Science Team Meeting, Woods Hole, USA, 17 - 21 June 2013, 104-121, 2013. <https://www.ghrsst.org/documents/q/category/ghrsst-science-team-meetings/ghrsst-xiv-woods-hole-ma-usa/>

Embury, O., C. J. Merchant, and G. K. Corlett, A reprocessing for climate of sea surface temperature from the along-track scanning radiometers: initial validation, accounting for skin and diurnal variability effects. *Remote Sens. Environ.*, 116, 62–78, 2012. doi:10.1016/j.rse.2011.02.028.

SECTION 5: APPENDICES

APPENDIX 1 – LIST OF PARTICIPANTS

First Name	Family name	Email Address	Country
Andrew	Acreman	Andy.acreman@npl.co.uk	United Kingdom
Ed	Armstrong	edward.m.armstrong@jpl.nasa.gov	United States
Eleanor	Barber	eleanor.barber@stfc.ac.uk	United Kingdom
Charlie	Barron	charlie.barron@nrlssc.navy.mil	United States
Helen	Beggs	h.beggs@bom.gov.au	Australia
Maurice	Borgeaud	Maurice.Borgeaud@esa.int	Italy
Silvia	Bragaglia-Pike	s.bragagliapike@reading.ac.uk	United Kingdom
Claire	Bulgin	c.e.bulgin@reading.ac.uk	United Kingdom
Kenneth	Casey	kenneth.casey@noaa.gov	United States
Sandra	Castro	sandrac@colorado.edu	United States
Jean-François	Cayula	j.cayula@ieee.org	United States
T. Mike	Chin	mike.chin@jpl.nasa.gov	United States
Carol Anne	Clayson	cclayson@whoi.edu	United States
Gary	Corlett	gkc1@le.ac.uk	United Kingdom
Peter	Cornillon	pcornillon@me.com	United States
Erik	Crosman	erik.crosman@utah.edu	United States
Prasanjit	Dash	prasanjit.dash@noaa.gov	United States
Craig	Donlon	craig.donlon@esa.int	Netherlands
Owen	Embury	o.embury@reading.ac.uk	United Kingdom
Emma	Fiedler	emma.fiedler@metoffice.gov.uk	United Kingdom
Gutenberg	França	gutenberg@lma.ufrj.br	Brazil
Rishi Kumar	Gangwar	rgphybhu@gmail.com	India
Chelle	Gentemann	gentemann@remss.com	United States
Irina	Gladkova	gladkova@cs.cuny.cuny.edu	United States
Simon	Good	simon.good@metoffice.gov.uk	United Kingdom
Lei	Guan	leiguan@ouc.edu.cn	China
Andrew	Harris	andy.harris@noaa.gov	United States
Masakazu	Higaki	m-higaki@naps.kishou.go.jp	Japan
Alexander	Ignatov	Alex.Ignatov@noaa.gov	United States
Misako	Kachi	kachi.misako@jaxa.jp	Japan
Alexey	Kaplan	alexeyk@ldeo.columbia.edu	United States
Ioanna	Karagali	ioka@dtu.dk	Denmark

First Name	Family name	Email Address	Country
Hugh	Kelliher	hugh.kelliher@spaceconnexions.com	United Kingdom
Prabhat	Koner	prabhat.koner@noaa.gov	United States
Yukio	Kurihara	kurihara.yukio@jaxa.jp	Japan
Arrow	Lee	arrow.lee@stfc.ac.uk	United Kingdom
Chung-Chi	Lin	Chung-Chi.Lin@esa.int	Netherlands
W. Timothy	Liu	w.t.liu@jpl.nasa.gov	United States
Yang	Liu	yliu@rsmas.miami.edu	United States
Chongyuan	Mao	chongyuan.mao@metoffice.gov.uk	United Kingdom
Salvatore	Marullo	salvatore.marullo@enea.it	Italy
Eileen	Maturi	eileen.maturi@noaa.gov	United States
David	Meldrum	dtm@sams.ac.uk	United Kingdom
Chris	Merchant	c.j.merchant@reading.ac.uk	United Kingdom
Rolv	Midthassel	rolv.midthassel@esa.int	Netherlands
Peter	Minnett	pminnett@rsmas.miami.edu	United States
Jonathan	Mittaz	j.mittaz@reading.ac.uk	United Kingdom
Tim	Nightingale	tim.nightingale@stfc.ac.uk	United Kingdom
Anne	O'carroll	Anne.Ocarroll@eumetsat.int	Germany
Rosa Cristhyna	Paes	rosa@lma.ufrj.br	Brazil
Kevin	Pearson	k.j.pearson@reading.ac.uk	United Kingdom
Boris	Petrenko	boris.petrenko@noaa.gov	United States
Jean-François	Piollé	jfpiolle@ifremer.fr	France
Andrea	Pisano	andrea.pisano@artov.isac.cnr.it	Italy
Nick	Rayner	nick.rayner@metoffice.gov.uk	United Kingdom
Hervé	Roquet	Herve.Roquet@meteo.fr	France
Korak	Saha	korak.saha@noaa.gov	United States
Rosalia	Santoleri	rosalia.santoleri@artov.isac.cnr.it	Italy
Stéphane	Saux Picart	stephane.sauxpicart@meteo.fr	France
Rodrigo	Sousa	rodrigo@lma.ufrj.br	Brazil
Dorina	Surcel Colan	dorina.surcel-colan@ec.gc.ca	Canada
Evangelos	Theocharous	e.theo@npl.co.uk	United Kingdom
Cristina	Tronconi	c.tronconi@isac.cnr.it	Italy
Jorge	Vazquez	jorge.vazquez@jpl.nasa.gov	United States
James	While	james.while@metoffice.gov.uk	United Kingdom
Gary	Wick	gary.a.wick@noaa.gov	United States

First Name	Family name	Email Address	Country
Keith	Willis	Keith.D.Willis@navy.mil	United States
Ruth	Wilson	ruth.wilson@spaceconnexions.com	United Kingdom
Werenfrid	Wimmer	w.wimmer@soton.ac.uk	United Kingdom
Elizabeth	Wong	ewong@ersmas.miami.edu	Singapore
Xiaosu	Xie	xiaosu.xie@jpl.nasa.gov	United States
Xinjia	Zhou	xinjia.zhou@noaa.gov	United States
Victor	Zlotnicki	victor.zlotnicki@jpl.nasa.gov	United States

APPENDIX 2 –PARTICIPANTS PHOTO



APPENDIX 3 – SCIENCE TEAM 2015/16

Peter Minnett (Chair)	RSMAS, University of Miami, USA
Ed Armstrong	NASA JPL, USA
Viva Banzon	NOAA/NESDIS, USA
Helen Beggs	Bureau of Meteorology, Melbourne, Australia
Kenneth S Casey	NOAA/NODC, USA
Sandra Castro	University of Colorado, Boulder, USA
Mike Chin	NASA JPL, USA
Carol Anne Clayson	WHOI, USA
Peter Cornillon	University of Rhode Island, USA
Prasanjit Dash	NOAA, USA
Craig J Donlon	European Space Agency, The Netherlands
Steinar Eastwood	Met.no, Norway
Owen Embury	University of Reading, UK
Emma Fiedler	MetOffice, UK
Gutemberg França	Federal University of Rio de Janeiro - UFRJ, Brazil
Chelle Gentemann	Remote Sensing Systems Inc., USA
Simon Good	MetOffice, UK
Robert Grumbine	NOAA/NWS/NCEP, USA
Lei Guan	Ocean University of China, China
Andrew Harris	NOAA/NESDIS, USA
Simon Hook	NASA JPL, USA
Jacob Høyer	Danish Meteorological Institute, Denmark
Alexander Ignatov	NOAA/NESDIS/STAR, USA
Misako Kachi	Japan Aerospace Exploration Agency (JAXA), Japan
Alexey Kaplan	Lamont–Doherty Earth Observatory of Columbia University, USA
Ioanna Karagali	Technical University of Denmark, Denmark
W Timothy Liu	NASA JPL, USA
Eileen Maturi	NOAA/NESDIS, USA
Doug May	Naval Oceanographic Office, USA
Christopher Merchant	University of Reading, UK
Jonathan Mittaz	University of Reading, UK
Tim Nightingale	Rutherford Appleton Laboratory, UK
Anne O'Carroll	EUMETSAT, Darmstadt, Germany
Jean–François Piollé	IFREMER, France
David Poulter	Pelamis Scientific Software Ltd, UK
Nick Rayner	MetOffice Hadley Centre, UK
Ian S Robinson	National Oceanography Centre, UK
Hervé Roquet	Météo-France, France
Jorge Vazquez	NASA JPL, USA
Christo Whittle	CISR, South Africa
Gary Wick	NOAA ETL, USA
Keith Willis	Naval Oceanographic Office, USA
Werenfrid Wimmer	University of Southampton, UK

LAST PAGE